New Design Approach of Antennas with Integrated Coupled Resonator Filters

Ekasit Nugoolcharoenlap

A thesis submitted to the University of Birmingham for the degree of Doctor of Philosophy

School of Electronic, Electrical and System Engineering
The University of Birmingham

March 2015

UNIVERSITY OF BIRMINGHAM

University of Birmingham Research Archive

e-theses repository

This unpublished thesis/dissertation is copyright of the author and/or third parties. The intellectual property rights of the author or third parties in respect of this work are as defined by The Copyright Designs and Patents Act 1988 or as modified by any successor legislation.

Any use made of information contained in this thesis/dissertation must be in accordance with that legislation and must be properly acknowledged. Further distribution or reproduction in any format is prohibited without the permission of the copyright holder.

Abstract

In the majority of microwave receiving and transmitting systems, a requirement is to have a filter immediately adjacent to the antenna or antenna array. Conventionally the filter and antenna are designed as separate components and a matching circuit is used in order to get maximum power transfer between them. This thesis presents a new methodology for antenna design where a filter is either fully or partially integrated with the antenna elements. The design of this antenna-filter follows the well-established coupled-resonator filter design theory, in which each resonator can not only be used as a filter element but also as a radiator.

In order to verify the concept, dipole antennas have been employed as antenna elements, and in addition to their radiating properties they are treated as the resonators in the filter circuit. For this purpose, an inductor has been integrated with each dipole antenna forming the resonator circuit. A two-port bandpass filter designed using dipole antennas is the first work in this thesis to verify the use of dipole antennas as resonators; this confirms the design concepts. The coupling matrix has been used to obtain the filter response. Further work demonstrates one-port antenna-filters made out of one, two and three dipoles; in these cases the designed filtering response uses the dipoles as resonators as well as radiating elements. The simulation and measurement results are in good agreement.

The method has also been utilised to implement X-band waveguide antenna components, here the radiation is from the open end of a waveguide. An antenna-filter, antenna-power divider and an antenna-diplexer are all demonstrated. The antenna-filter is designed for improve the selectivity. The other two components are three-port components and designed using the coupling matrix. The antenna power divider is designed so that the radiation pattern can be controlled in addition to providing the filtering. The antenna-diplexer

is designed in order to include the radiation element into a structure which also provides power splitting at two different frequencies. These three variations of the waveguide antenna-filter has been designed, simulated, fabricated and measured. The results are in good agreement. They have provided verification of the method, showing the antenna and filter theories and can be applied to miniaturise these components. The results have application in the wireless communication and radar systems.

Acknowledgements

I am extremely grateful for the guidance and support of my supervisors Prof. Michael Lancaster and Dr. Frederick Huang. They gave me many important advices and helpful suggestions during my study.

My appreciation also goes to my colleagues in the Emerging Device Technology for their support and friendship (EDT) Research Group at the University of Birmingham. Especially, I would like to thanks Dr. Xiaobang Shang for many helpful suggestions during my study, Wenlin Xia for helpful discussion on the filter design, Rashad Hassan Mahmud for helpful discussion on the antenna theory and David Glynn for helpful discussion on thesis writing. I am also thankful Mr. Warren Hay for fabricating all the waveguide devices presented in this thesis.

I appreciate Dr. Ghaith Elsanosi M. Mansour and Dr. Zhen Hua Sampson Hu. They gave many advices for the antenna measurement technique. Thanks to Dr. Khurram Saleem Alimgeer in many suggestions for doing the research work during his visited time.

Finally, my sincere gratitude goes to my parents for their invaluable support and encouragement. I also appreciate the Royal Thai Government for financial and general supports until course end.

Table of Contents

Chapter 1: Introduction..... 1

1.1 Overview of Integration of the Antenna and Bandpass Filter Components..... 1

1.2 Literature review..... 4

1.3 Thesis Motivation..... 8

1.4 Thesis Overview..... 10

References..... 11

Chapter 2: Fundamental Theory..... 16

2.1 Antenna Theory..... 16

2.1.1 Overview of Antennas..... 16

2.1.2 Dipole Antennas..... 21

2.1.2.1 Equivalent Circuit of Dipole Antenna..... 25

2.1.2.2 Quality Factor of Dipole Antenna..... 31

2.1.3 Waveguide Aperture Antennas..... 33

2.2 Microwave Filter Theory..... 34

2.2.1 Overview of Microwave Filters..... 34

2.2.2 Microwave Resonators..... 39

2.2.3 Rectangular Waveguide Cavity Resonator..... 41

2.2.4 Coupled Resonator Filters..... 44

2.2.5 Coupling Matrix for Coupled Resonator Filters..... 45

2.3 Coupling Matrix for Antenna-Filters..... 53

2.4 CST Microwave Studio®..... 55

2.4.1 CST Microwave Studio® Overview..... 56

2.4.2 Instruction for using CST Microwave Studio® 56

References 64

Chapter 3: Two-Port Dipole Bandpass Filter 66

3.1 Introduction 66

3.2 Resonator Design 67

3.2.1 Equivalent Circuit of Dipole Antenna in Simulation 67

3.2.2 Design of Dipole Antenna with Inductor 70

3.2.3 Unloaded Quality Factor 73

3.3 Design of Two-Port Dipole Bandpass Filter 73

3.4 Realisation of Two-Port Dipole Bandpass Filter 76

3.4.1 Air Coil Inductor Design 76

3.4.2 Extraction of External Quality Factor 79

3.4.3 Extraction of Coupling Coefficient 81

3.4.4 Simulation Results 82

3.4.5 Fabrication and Measurement 85

3.5 Conclusions 87

References 88

Chapter 4: One-Port Dipole Antenna-Filter 89

4.1 Introduction 89

4.2 One-Resonator Dipole Antenna-Filter 90

4.2.1 Antenna-Filter Design 90

4.2.2 Extraction of Design Parameters from Physical Structure 91

4.2.3 Calculation and Simulation Results 95

4.2.4 Fabrication and Measurement 96

4.3 Two-Resonator Dipole Antenna-Filter..... 100

4.3.1 Antenna-Filter Design..... 100

4.3.2 Calculation and Simulation Results..... 104

4.3.3 Fabrication and Measurement..... 106

4.4 Three-Resonator Dipole Antenna-Filter..... 109

4.4.1 Antenna-Filter Design..... 109

4.4.2 Calculation and Simulation Results..... 113

4.4.3 Fabrication and Measurement..... 114

4.5 Conclusions..... 125

References..... 126

Chapter 5: Waveguide Antenna-Filters..... 127

5.1 Introduction..... 127

5.2 Quality Factors of Cavity Resonators..... 129

5.2.1 Extraction of the External Quality Factor from Physical Structure..... 130

5.3 Waveguide Aperture Antennas..... 133

5.4 Coupling Coefficient Extraction from the Physical Structure..... 135

5.5 Coupling Matrix Synthesis for Multiple Port Antenna-Filters..... 137

5.6 X-Band 5-Resonator Waveguide Antenna-Filter..... 139

5.6.1 Waveguide Antenna-Filter Design..... 139

5.6.2 Fabrication and Measurement..... 143

5.7 X-band 3-Resonator Antenna Power Divider..... 146

5.7.1 Waveguide Antenna Power Divider Design..... 146

5.7.2 Fabrication and Measurement..... 149

5.8 X-Band 3-Resonator Antenna-Diplexer..... 153

5.8.1 Waveguide Antenna-Diplexer Design..... 153

5.8.2 Fabrication and Measurement..... 157

5.9 Conclusions..... 161

References..... 162

Chapter 6: Conclusions and Future Work..... 163

6.1 Conclusions..... 163

6.2 Future Work..... 165

References..... 168

Appendix A: *Q*-calculation for the one-port component..... 169

References..... 173

Appendix B: Publications ……..... 174

Chapter 1

Introduction

1.1 Overview of Integration of Antenna and Bandpass Filter Components

Recently attention in the design of microwave circuits has been directed towards miniaturisation and low profile for components in wireless communication systems. An antenna and a bandpass filter are essential components employed at the front-ends. Examples of the use of an antenna and a bandpass filter at the front-end of Radio Frequency (RF) transmitter and receiver are shown in Figure 1.1. For the transmitter shown in Figure 1.1(a), a bandpass filter follows a power amplifier and used for selecting a transmission frequency and rejecting out of band frequency before being sent to an antenna for broadcasting the RF signal. On the other hand, an antenna is the first device of the receiving system as shown in Figure 1.1(b). The antenna is placed at the front of the receiver to receive the RF signal and sent to a bandpass filter. It also acts as a pre-selector for the reception carrier frequency to the input of a low-noise amplifier. This arrangement of the antenna and filter reduces noise and interference before converting lower frequency by mixer and oscillator [1]. However, a degradation of the front-end performance is caused by mismatched impedance of an antenna and a bandpass filter. A matching network [1] is therefore needed for the front-end circuit to match impedance between antenna and filter. The matching network may improve the performance of the systems, but the circuit size may also be increased. In general, bandpass filters are designed based on coupled resonator circuits. This bandpass filter is named a *coupled resonator filter* [2]. Figure 1.2 shows an example diagram of nth order coupled-

resonator bandpass filter, where white circles represent resonators, and the solid lines linking resonators represent coupling.

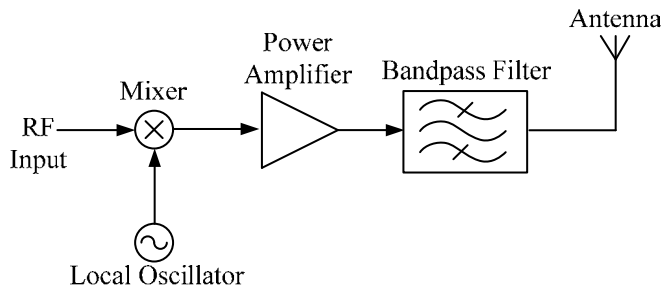

(a)

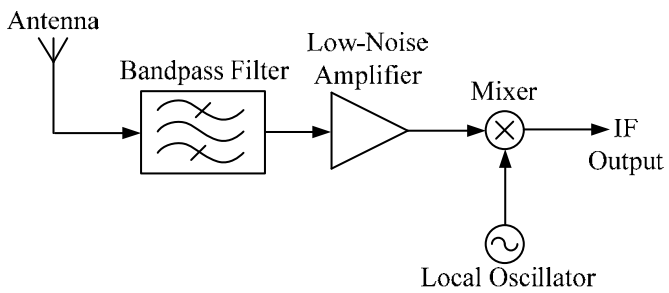

(b)

Figure 1.1 Block diagram of (a) An RF transmitter and (b) Block diagram of an RF receiver [1].

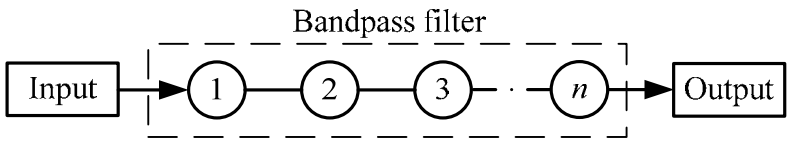

Figure 1.2 An example diagram of nth order coupled-resonator bandpass filter.

As mentioned above, the main function of an antenna is to radiate the RF signal to free space. It can also act as a resonator of the filter when it resonates at the operating frequency. It is possible to demonstrate the relation of antenna and resonator by analysing and comparing the resonant antenna circuit (i.e. the reactance (X) or the susceptance (B) of the reactive element is

zero) with the conventional resonant circuit. Two examples of the equivalent circuits of resonant antennas are a dipole antenna and a patch antenna from [3]. The structure of dipole and patch antennas are shown in Figure 1.3(a) and 1.3(c), respectively. The equivalent circuits of both antennas are represented as lossy resonant circuits and shown in Figure 1.3(b) and 1.3(d); where R_r is the radiation resistance of an antenna, L_a is the antenna inductance, C_a is the antenna capacitance, X_a is the antenna reactance and B_a is the antenna susceptance.

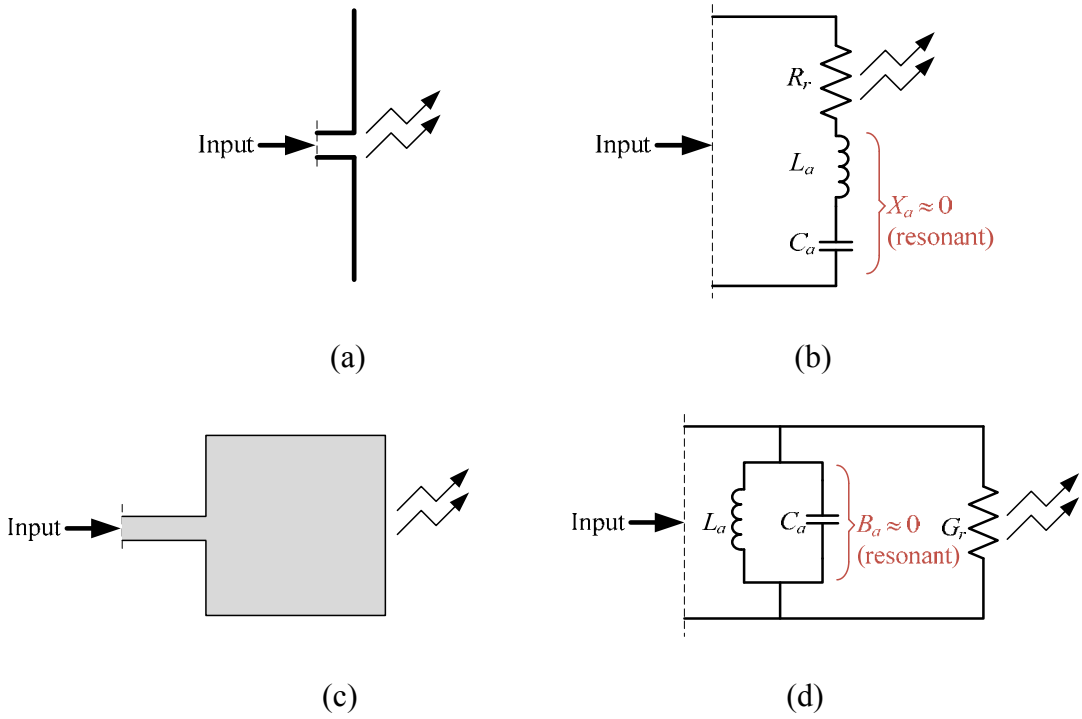

Figure 1.3 Antenna examples and their equivalent circuits. (a) Dipole antenna. (b) Dipole antenna's equivalent circuit. (c) Patch antenna. (d) Patch antenna's equivalent circuit [3].

These examples show that the resonant antenna can be treated as one of resonators in coupled resonator filters. This allows the design of antenna and filter integration to be a single component named an *antenna-filter* by following the coupled resonator filter theory [2]. The advantage is that the matching network is eliminated, reducing the circuit size and the

problem of a connection between antenna and bandpass filter. This is the main work and will be discussed in this thesis.

1.2 Literature Review

This section presents a literature review of antenna-filter approaches. In general, the antenna-filter is usually designed using a matching network to cascade between an antenna and a bandpass filter as described in the previous section. The design approaches using the matching network were presented in [4], [5]. The advantage of the method is to enhance the bandwidth of the microstrip antenna. A design approach of the antenna and filter integration without the matching network has been firstly presented in [6] with the use of the filter synthesis. The method was to consider an antenna as equivalent to a last resonator in the filter circuit. This has been used to implement a slot-line dipole antenna with a coplanar filter. The approached design can improve the filtering response by tuning the radiation resistance of the resonant antenna to match the load resistance of filter circuits at the resonant frequency. In addition, the filter synthesis has been implemented on the various structures for size reduction, e.g. [7], [8] which show a microstrip filter integrated with a patch antenna, an E-plane waveguide filter integrated with a patch antenna [9]. A multilayer technology is of interest to RF circuit designer and can be employed to miniaturise the RF circuits and integrate RF components into a single module. In [10], a composite ceramic-foam substrate with the multilayer technology has been implemented to design a microstrip patch antenna integrated with a filter. A similar concept in [6] is employed to design the antenna-filter component. Moreover, the approach [10] has firstly introduced the design of antenna-filter using the principle of the coupled-resonator filter design. The design method was simple by

considering the quality factor of the antenna as the same external quality factor of the last resonator of filter circuits. The circuit diagram of the approach in [10] is shown in Figure 1.4.

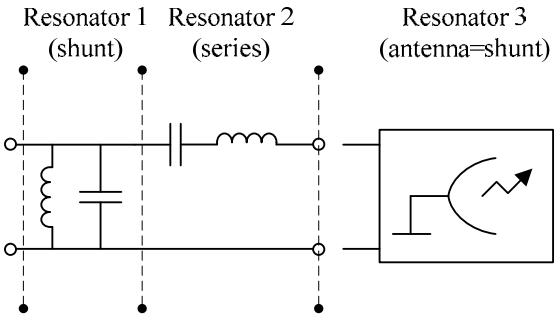

Figure 1.4 The diagram of the antenna integrated in the bandpass filter circuits [10].

A cavity filter integrated into a horn antenna has been presented in [11]. This work exhibited a good two-pole filter response and radiation pattern shape. The integration of ultra-wide band (UWB) antenna with a filter was presented in [12], [13]. These approaches have been implemented on the planar structure in order to miniaturise the size. In [14], the design of a patch antenna integrated with the folded step-impedance resonator (SIR) filter can be applied to reject the unwanted harmonic response. In [15], multi-layer circuit technology has been used to implement a multi-layer antenna-filter structure. The approach [15] has been used to design a hairpin filter positioned at the bottom layer combined with the patch antenna placed on the top layer of the component. This work exhibited a two-pole response and well-shaped radiation pattern. In [16], the design approach presented the dual-band filter integrated with the dual-band patch antenna. This component was designed for use in the modern wireless system, e.g. the wireless LAN system. The concept of filter design has again been utilised with the co-design of antenna and filter integration. The co-design approaches were implemented on the microstrip filter with an inverted-L antenna [17], the microstrip filter with Γ-shaped antenna [18], the substrate-integrated waveguide (SIW) filters with patch antenna

[19], the waveguide slot antenna with integrated filters [20], the aperture evanescent waveguide antenna with filter [21], [22], and the integration of aperture antenna and filter for the SIW structure [23].

Antenna arrays can be used to improve radiation performance compared with single antennas. The antenna array has been incorporated with the antenna-filter design for various structures. For example, four-slot antenna arrays integrated with cavity filters [24], Yagi antenna combined with a high *Q*-resonator [25] and four-patch antenna array integrated with power dividers and filters [26]. In addition, it is possible to design the antenna and filter with multi-band response. Previously, a dual-band antenna has been designed with an integrated diplexer and presented in [27]. The approach exhibited a new combined component for the transceiver of the wireless LAN system with a compact size and good filter performance. In [28], the microstrip patch antenna was designed and combined with two bandpass filters to create a single module.

A type of antenna with filtering function has been presented in [29] and is called a *filtering antenna* or a *filtenna*. This component is designed by integrating a bandpass filter into an antenna in order to enhance the filtering functionality of the antenna. Also cost and size reductions are required for the component. Following the filtenna's design concept, the gain response of filtenna can exhibit flat in-band gain, high out of band gain suppression and high harmonic rejection. The approach presented in [29] aims to show a design technique of filtenna implemented on horn structure by covering a substrate integrated waveguide cavity (SIWC) FSS filter at the aperture of a horn antenna. The SIWC-FSS acts as a frequency selector placed at the aperture to suppress the unwanted frequency from the received signals before being sent to the input of receiver. This component is suitably utilised as a receiving antenna. The planar filtennas have been presented in [30]-[32]. In [30], an SIW filter was

designed with the inductive window structure and integrated with a planar coaxial collinear (COCO) radiation element. The performance of this co-design exhibited a very good return loss response and the best omnidirectional radiation pattern. In [31], a tunable bandpass filter using a varactor was designed and integrated with a wideband Vivaldi antenna. This approach aims to show a design of a reconfigurable filtenna using the tunable filter. The filtenna exhibited the good agreement of frequency response in simulation and measurement for tuning frequencies from 6.16 to 6.6 GHz. In [32], a coplarnar waveguide (CPW) was designed as a compact microstrip resonant cell (CMRC) that is integrated with a patch antenna. This approach exhibited good suppressions for 2nd and 3rd harmonic frequency and high suppressed cross-polarisation. A bandstop filter or a notch filter can be used to design a filtenna implemented on a horn structure. The notch filter was used to block a frequency in order to extend the dual-passband frequency response which is similar to the response of a dual-band filter. The approach was presented in [33] and was designed using an open-ring dual-band-notch filter taken into a horn antenna. The performance of approach [33] exhibited the high gain response with two different notched-bands.

As mentioned above, it can be concluded that the antenna-filter is an RF front-end component designed by integrating an antenna into a filter, where the last resonator of filter is replaced by the antenna. Similarly, the filtenna is also the RF front-end component designed by integrating a filter into an antenna, where the filter is placed before the input of antenna and also is treated as a balun. Both components are the similar components that achieve filtering and radiating functions simultaneously. Almost those approaches have been designed using basic filter design principles. Some approach has been designed without the use of filter synthesis, e.g. a design uses an active component for tuning frequency bandwidth. This thesis aims to present a new design of antenna-filters using the coupling matrix synthesis whilst

those antenna-filter and filtenna approaches have not been designed using this technique. This new design approach using the coupling matrix has significant advantages, which are not only used to design the antenna-filters, but also used to design antennas integrated with different components. For examples, an antenna integrated with two-array antennas and power divider, and an antenna integrated with the diplexer. They have been achieved in designs using the coupling matrix and will be discussed in Chapter 5.

1.3 Thesis Motivation

There have been many designs of integrated antenna and bandpass filter in order to miniaturise the circuit area and improve the performance as described in the literature review of Section 1.2. A diagram of the new antenna-filter approach is shown in Figure 1.5(b) and is compared to a diagram of conventional design shown in Figure 1.5(a). The new combined component (antenna-filter) has no a matching network, because the antenna is matched in the coupled resonator circuit and also treated as the last resonator of the filter.

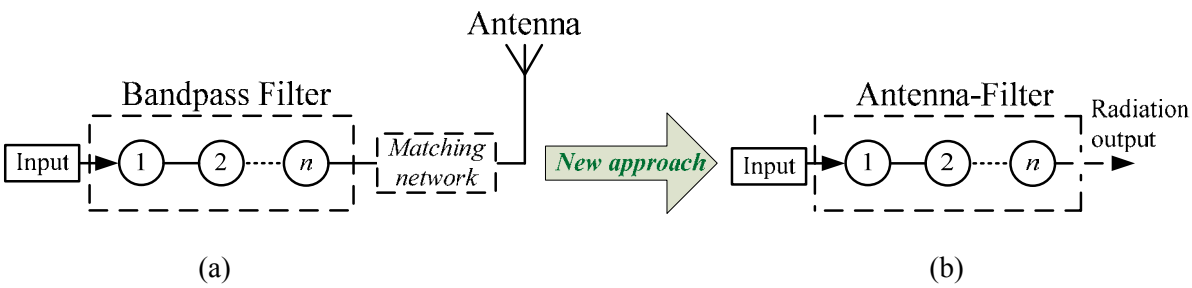

Figure 1.5 A conventional design of antenna and bandpass filter integration using a matching network (a) compared to the new approach (b).

However, the previous approaches presented in the literature review did not show good filtering performance (good skirt selectivity at the passband-edge and high-suppression at out-

of-band) or good radiating performance (high antenna gain and well-shaped radiation pattern). The main reasons for the problems in the antenna-filter approaches are (i) Poor match of antenna to filter (ii) inaccurate values of the coupling coefficient and the external quality factor in the design, and (iii) a small number of antenna elements which cannot enhance the antenna gain.

This thesis addresses the development of a novel antenna-filter design technique based on the coupled resonator filter using the coupling matrix synthesis. This technique will reduce the complexity in the design procedure, enhance the design accuracy and allow more complex antenna-filters to be designed. As a first step, dipole antennas are chosen with inductors completing the resonator circuits. The proposed dipole antennas, integrated with inductors, are employed to design a two-port dipole antenna-filter using the coupling matrix synthesis, as shown in Figure 1.6. This circuit maybe of little application, but it allows the design procedure to be investigated. The proposed dipole antennas can then be employed to design a one-port dipole antenna-filter as shown in Figure 1.7. It can be seen that the layout of the dipole antenna-filter can be represented as the structure of coupled resonators as well as a multi-element array for the requirement of both the filtering and radiating efficiency.

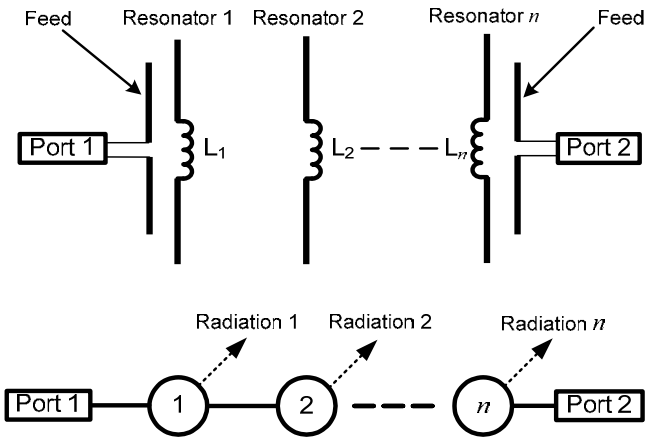

Figure 1.6 A two-port dipole antenna-filter.

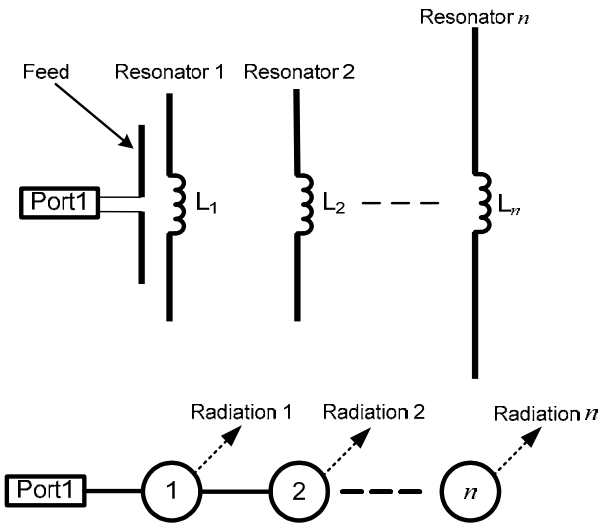

Figure 1.7 A one-port dipole antenna-filter.

A directional antenna such a waveguide antenna (e.g. aperture, slot and horn antennas) is one of the most popular antennas due to it providing a very good performance in terms of the antenna efficiency, bandwidth and radiation pattern. A waveguide aperture antenna will be discussed in this thesis and employed in the novel design of the waveguide filter-antennas with the use of coupling matrix synthesis for the antenna-filter component.

1.4 Thesis Overview

This thesis consists of six chapters which have been organised as follows:

Chapter 1 provides an introduction to the thesis. The overviews of the antenna-filter and the literature review are discussed. Thesis motivation and thesis overview are presented.

Chapter 2 provides the fundamental theories required for this research. It includes the theory of antennas (i.e. dipole and waveguide antennas, antenna array), theory of microwave filter based on the coupled resonator circuit, and the integration of antenna and filter using the coupling matrix synthesis.

Chapter 3 presents a new design technique of resonators using dipole antennas. The technique is based on the antenna theory utilised to analyse the equivalent circuit of dipole antennas [3]. Inductors are employed with dipole antennas in order to complete to the resonator circuit. It can be achieved by designing a bandpass filter using dipole antennas with inductors based on the design of a direct-coupled resonator filter [34]. The coupling matrix is employed for this approach with the comparison of *S*-parameters. The fabrication and measurement are also provided.

Chapter 4 uses a similar design technique to that described in Chapter 3. This is intended to design an antenna-filter as a single-port component with new coupling matrix synthesis. The synthesis was derived from the equivalent circuit of the antenna-filter as described in Chapter 2. The approach for the work in this chapter has completed in fabrication for the single, two and three resonator dipole antenna-filters.

Chapter 5 is the continuation of the work presented in chapter 4 which is employed to design a waveguide antenna integrated with a cavity filter. This work is presented to show different coupling topologies of the antenna-filter integrated with the physical structure of the rectangular waveguide. The approach for this work has been used to implement three new designs, which consist of five-resonator antenna-filter, three-resonator antenna power divider and three-resonator antenna-diplexer.

Chapter 6 concludes the thesis with inclusion of the future work.

References

[1] Pozar D. M. Microwave Engineering. 3rd ed. USA: John Wiley & Sons; 2005.

[2] Hong J. S. and Lancaster M. J. Microstrip Filters for RF/Microwave Applications. New York, USA: John Wiley & Sons; 2001.

[3] Balanis C. A. Antenna Theory Analysis and Design. 3rd ed. New Jersey, USA: John Wiley & Sons; 2005.

[4] Pues, H.F., Van de Capelle, AR., An impedance-matching technique for increasing the bandwidth of microstrip antennas. IEEE Trans. Antennas Propag., 1989 Nov., 37(11): 1345–1354.

[5] An H., Nauwelaers B., Van de Capelle A., A new approach of broadband microstrip antenna design. in IEEE Antennas & Propag. Soc. Int. Symp., 1992 Jun. 18–25: 475–478.

[6] Le Nadan T., Coupez J.P., Toutain S., C. Person, Integration of an Antenna/Filter Device, using a Multi-Layer, Multi-Technology Process. in 28nd Eur. Microw. Conf., 1998 Oct.: 672–677.

[7] Abbaspour-Tamijani A., Rizk J., Rebeiz G., Integration of Filters and Microstrip Antennas. in IEEE Int. Antennas Propag. Symp. Dig., 2002 Jun.: 874–877.

[8] Queudet F., Pele I., Froppier B., Mahe Y., and Toutain S., Integration of pass-band filters in patch antennas. in Proc. 32nd Eur. Microw. Conf., 2002 Sep. 23–26: 685–688.

[9] Goussetis G. and Budimir D., Antenna filter for modern wireless systems. in Proc. 32nd Eur. Microw. Conf., 2002 Sep. 23–26: 1–3.

[10] Le Nadan T., Coupez J.P., Person C., Optimization and miniaturization of a filter/antenna multi-function module using a composite ceramic-foam substrate. in Microwave Symp. Dig., 1999 Jun. 13–19: 219–222.

[11] Froppier B., Mahe Y., Cruz E. M. and Toutain S., Integration of a filtering function in an electromagnetic horn. in 33rd Eur. Microw. Conf., 2003 Oct. 7–9: 939–942.

[12] Lee J.N., Yoo J.H., Kim J.H., Park J.K., Kim J.S., The Design of UWB Bandpass Filter-Combined Ultra-Wide Band Antenna. in Vehi. Tech. Conf., 2008 Sep. 21–24: 1–5.

[13] Yilin C. and Yonggang Z., Design of a filter-antenna subsystem for UWB communications. in 3rd IEEE Int. Symp. on Mic., Ant., Prop. and EMC Tech. for Wireless Comm., 2009 Oct. 27–29: 593–595.

[14] Zayniyev D. and Budimir D., An integrated antenna-filter with harmonic rejection. in 3rd Eur. Conf. on Anten. and Propag., 2009 Mar. 23–27: 393–394.

[15] Jianhong Z., Xinwei C., Guorui H., Li L. and Wenmei Z., An Integrated Approach to RF Antenna-Filter Co-Design. IEEE Antennas and Wireless Propagation Letters, 2009, 8: 141–144.

[16] Zayniyev D. and Budimir D., Dual-band microstrip antenna filter for wireless communications. in IEEE Anten. and Propag. Soc. Int. Symp. (APSURSI), 2010 Jul. 11–17: 1–4.

[17] Chuang C.-T. and Chung S.-J., Synthesis and Design of a New Printed Filtering Antenna. IEEE Trans. Antennas Propag., 2011 Mar., 59(3): 1036–1042.

[18] Wu W.-J., Yin Y.-Z., Zuo S.-L., Zhang Z.-Y., Xie J.-J., A new compact filter-antenna for morden wireless communication systems. IEEE Antennas Wireless Propag. Lett., 2011 Oct., 10: 1131–1134.

[19] Yusuf Y., Cheng H., Gong X., Co-Designed substrate-Integrated Waveguide Filters with Patch Antennas. IET J. Microw., Antennas, Propag., 2013 May., 7(7): 493–501.

[20] Yang Y. and Lancaster M., Waveguide slot antenna with integrated filters. presented at the ESA Workshop on Antennas for Space Applications, Noordwijk, Netherlands, 2010 Oct.: 48–54.

[21] Ludlow P. and Fusco V., Reconfigurable small-aperture evanescent waveguide antenna. IEEE Trans. Antennas Propag., 2011 Dec., 59(12): 4815–4819.

[22] Ludlow P., Fusco V., Goussetis G. and Zelenchuk D. E., Small Aperture Evanescent-mode waveguide antenna matched using distributed s. Electron. Lett., 2013 Apr., 49(9): 580–581.

[23] Yusuf Y., Gong X., Integration of three-dimensional high-*Q* filters with aperture antennas and bandwidth enhancement utilising surface waves. IET J. Microw., Antennas, Propag., 2013 May, 7(7): 468–475.

[24] Cheng H. T., Yusuf Y., and Gong X., Vertically integrated three-pole filter/antennas for array applications. IEEE Antennas Wireless Propag. Lett., 2011, 10: 278–281.

[25] Wang Z., Hall P. S., Gardner P., Yagi antenna with frequency domain filtering performance. in IEEE Antennas & Propag. Soc. Int. Symp., 2012 Jul.: 1–2.

[26] Lin C.-K. and Chung S.-J., A filtering microstrip antenna array, IEEE Trans. Microw. Theory Tech. 2011 Nov., 59(11): 2856–2863.

[27] Demir V., Huang C. P., Elsherbeni A., Novel Dual-Band WLAN Antennas with Integrated Band-Select Filter For 802.11 a/b/g WLAN Radios In Portable Devices. Microw. & Opt. Technol. Lett., 2007 Aug., 49(8): 1868–1872.

[28] Zayniyev D., AbuTarboush H. F., Budimir D., Microstrip Antenna Diplexers for Wireless Communications. in Proc. 39th Eur. Microw. Conf., 2009 Sep. 29–Oct. 1: 1508–1510.

[29] Luo G.-Q., Hong W., Tang H.-J., Chen J.-X., Yin X.-X., Kuai Z.-Q., Wu.K. Filtenna Consisting of Horn Antenna and Substrate Integrated Waveguide Cavity FSS. IEEE Trans. Antennas Propag., 2007 Jan., 55(1): 92–98.

[30] Yu C., Hong W., Zhenqi K., Wang H. Ku-Band Linearly Polarized Omnidirectional Planar Filtenna. IEEE Antennas and Wireless Propagation Letters, 2012, 11: 310–313.

[31] Tawk Y., Costantine J., Christodoulou, C.G. A Varactor-Based Reconfigurable Filtenna. IEEE Antennas and Wireless Propagation Letters, 2012, 11: 716–719.

[32] Ma Z., Vandenbosch, G.A.E. Wideband Harmonic Rejection Filtenna for Wireless Power Transfer. IEEE Trans. Antennas Propag., 2014 Jan., 62(1): 371–377.

[33] Barbuto M., Trotta F., Bilotti F., Toscano A. Horn Antennas With Integrated Notch Filters. IEEE Trans. Antennas Propag., 2015 Feb., 62(2): 781–785.

[34] Cohn S. B. Direct-Coupled-Resonator Filters. Proceedings of the IRE. 1957 Feb.; 45(2): 187–196.

Chapter 2

Fundamental Theory

This chapter presents a review of the relevant theory in three topic areas, firstly basic antenna theory, secondly microwave filter theory and the thirdly integration of antenna and filter. Each will be studied ready for the new design approaches presented in this thesis. Section 2.1 reviews the antenna theory used in the proposed design for the dipole antenna and aperture antenna. Section 2.2 reviews the microwave filter theory to introduce the filter concept. Both antenna and filter theories can be applied in the design of an antenna-filter presented in this thesis. Section 2.3 presents the coupling matrix for antenna-filter utilised for the design approaches in this thesis. CST microwave studio software instruction is also provided and is presented in Section 2.4.

2.1 Antenna Theory

2.1.1 Overview of Antennas

An antenna is a passive device used for transmitting or receiving radio frequency (RF) signals used in wireless communication systems. Figure 2.1 illustrates the functions of antennas in a wireless communication link. For the transmitting function, the transmitting antenna delivers the EM wave from the feeding source, and radiates the EM wave into the free-space. For the receiving function, the receiving antenna receives the EM wave from the space and sends it into the receiver.

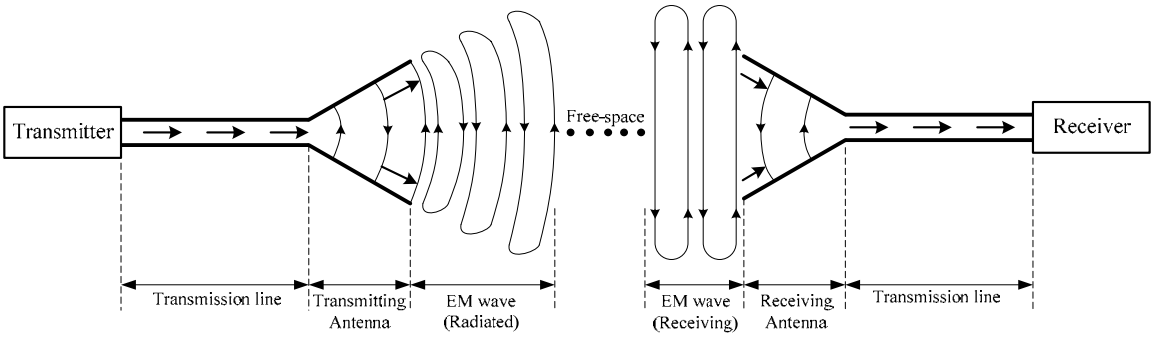

Figure 2.1 An example showing the antennas function in a wireless communication link [1].

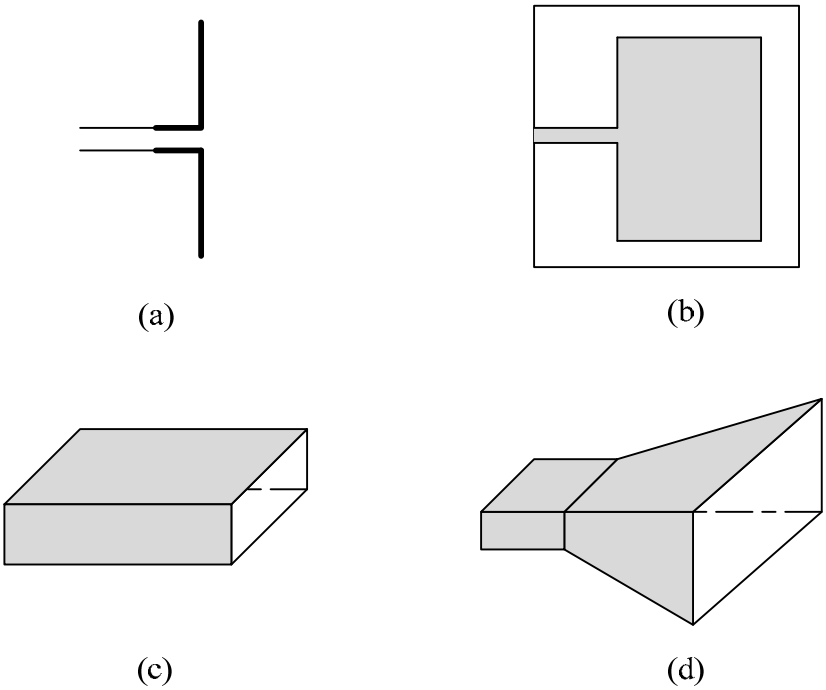

Figure 2.2 Examples of typical antennas. (a) Dipole antenna, (b) Rectangular patch antenna, (c) Waveguide aperture antenna, (d) Horn antenna [2].

Figure 2.2 illustrates examples of typical antennas. A dipole antenna, shown in Figure 2.2(a), is a wire antenna and is widely used in basic applications such as television, FM radio, etc.. The rectangular patch antenna, in Figure 2.2(b), is a microstrip antenna and consists of a rectangular flat sheet on top of a ground plane, connected with a feed line. This antenna is simple, low cost and can be fabricated using the printed circuit board (PCB) technology. An

open-ended waveguide antenna shown in Figure 2.2(c), is Type of aperture antenna and is configured so the direction of EM radiation direction is based on the orientation of the waveguide propagation mode (normally TE_{10} mode). This antenna is simple, efficient and can also be installed on the surface of the spacecraft or aircraft [2]. A horn antenna, shown in Figure 2.2(d), is also a waveguide aperture antenna that has a large aperture at the end for improving the antenna gain and radiation patterns.

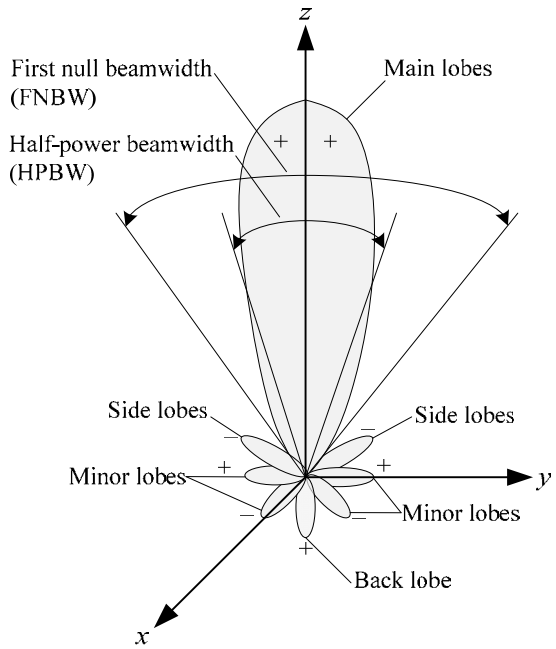

(a)

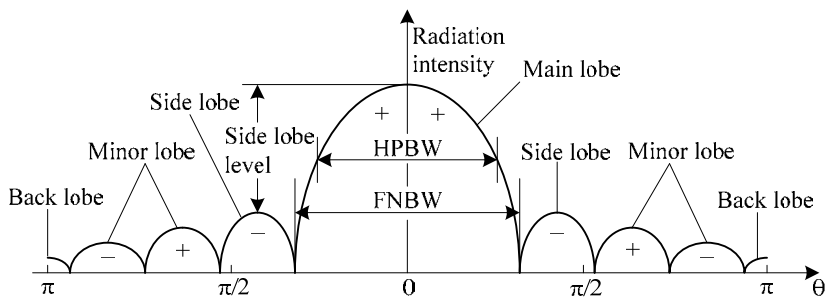

(b)

Figure 2.3 (a) Three-dimensional radiation pattern of an antenna. (b) Two-dimensional radiation pattern of an antenna [2].

The performance of antennas can be described in terms of bandwidth, radiation patterns, directivity, efficiency and gain. Figure 2.3 illustrates a typical radiation pattern of an antenna. The lobes of the radiation pattern have different shapes, and can be divided into: main, minor, side and back lobes [2]. The main lobe represents direction of the maximum radiation intensity of an antenna. The half-power beam width (HPBW) can be calculated from the main lobe. The HPBW is the angular width of the main lobe, as measured at the half-power points. The zero level of the main lobe introduces the first null of the radiation pattern. The angular distance between two first nulls is called the first-null beamwidth (FNBW). The FNBW can also be used to estimate the HPBW of an antenna with a uniform distribution by FNBW/2 ≈ HPBW [2]. A side lobe is close to the main lobe and is usually expressed as a ratio of the radiation intensity between main lobe and side lobe. This is called the *side lobe level*. A back lobe is in the opposite direction (180°) from the main lobe. A minor lobe is any lobe except for the main lobe, side lobe and back lobe and represents the radiation in an undesired direction [2].

The radiation performance of an antenna can be expressed in terms of directivity. The directivity of an antenna is defined as [2]

$$D = \frac{U}{U_0} = \frac{4\pi U}{P_{\text{rad}}} \tag{2.1a}$$

In decibels;

$$D(\text{dB}) = 10\log_{10}\left[D\right] \tag{2.1b}$$

where D is the directivity.

U is the radiation intensity (W/unit solid angle).

U_0 is the radiation intensity of isotropic source (W/unit solid angle).

P_{rad} is the total radiated power (W).

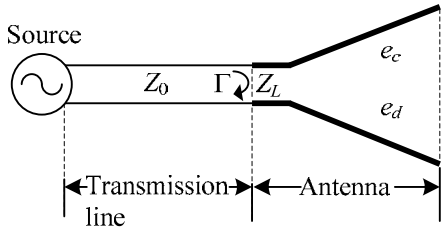

Figure 2.4 A basic diagram of antenna usage [2].

A diagram of antenna usage shown in Figure 2.4 is used to describe the antenna efficiency which is related to the antenna gain and directivity. Antenna gain is an antenna parameter used to describe the transmitted power in the maximum radiation direction. It is associated with the directivity and antenna efficiency, defined as [2]

$$G = e_0 D \tag{2.2}$$

where G is the gain of the antenna.

e_0 is the total efficiency of the antenna.

The total efficiency of an antenna is defined as [2]

$$e_0 = e_r \cdot e_c \cdot e_d \tag{2.3}$$

Where $e_r = 1 - |\Gamma|^2$ is the reflection or mismatch efficiency.

Γ is the voltage reflection coefficient at the input terminals of the antenna by $\Gamma = (Z_L - Z_0)/(Z_L - Z_0)$ where Z_L is the load impedance at input terminals of an antenna, Z_0 is the characteristic impedance of the transmission line.

e_c is the conduction efficiency.

e_d is the dielectric efficiency.

VSWR = $(1 + |\Gamma|)/(1 - |\Gamma|)$ is the voltage standing wave ratio.

Essential background for antennas presented in this thesis is described in Section 2.1.2 for dipole antennas and Section 2.1.3 for waveguide aperture antenna.

2.1.2 Dipole Antennas

A dipole antenna is a basic simple antenna with a good closed form expression available to describe its properties. The structure of a dipole antenna consists of two identical straight wires being positioned along the *z*-axis and is shown in Figure 2.5.

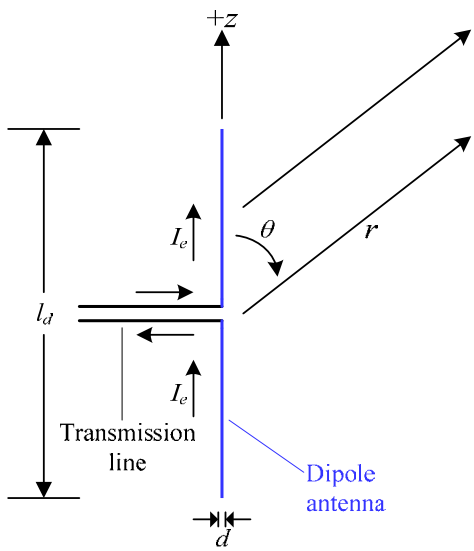

Figure 2.5 The geometry of a dipole antenna [3].

The dipole antenna is usually fed at the centre with a transmission line. The currents on each wire are opposite in direction and can be obtained from the geometry of the dipole antenna. The current distribution along a dipole antenna for a small diameter *d* (thin wire dipole) can be defined as [2]

$$I_e(z) = \begin{cases} I_m \sin\left[k\left(\frac{l_d}{2} - z\right)\right], & 0 \le z \le \frac{l_d}{2} \\ I_m \sin\left[k\left(\frac{l_d}{2} + z\right)\right], & -\frac{l_d}{2} \le z \le 0 \end{cases} \tag{2.4}$$

where I_e is the current distribution along a thin wire dipole antenna.

I_m is the maximum current magnitude.

$k = 2\pi/\lambda$ is the propagation constant.

l_d is the total dipole length.

The radiation pattern of the dipole antenna can be obtained from the line integral of the current along the *z*-axis, given by [3]

$$E_\theta = j\omega \sin\theta \cdot A_z = j\omega \sin\theta \cdot \frac{\mu e^{-jkr}}{4\pi r} \int_{-l_d/2}^{l_d/2} I_e(z) \cdot e^{jkz\cos\theta} dz \tag{2.5}$$

$$H_\phi = \frac{E_\theta}{\eta} \tag{2.6}$$

where E_θ is the electric field in the far field.

H_ϕ is the magnetic field in the far field.

A_z is the potential vector of the current along *z*-axis.

$\omega = 2\pi f$ is the radian frequency (rad/s).

μ is the permeability (H/m).

$\eta = \sqrt{\frac{\mu_0}{\varepsilon_0}} = 376.73\ \Omega \approx 120\pi\ \Omega$ is the intrinsic impedance of free-space (ohms)

Substituting the current equation from (2.4) to (2.5) gives

$$E_\theta = j\omega \sin\theta \cdot \frac{\mu e^{-jkr}}{4\pi r} \left[\int_{-l_d/2}^{0} I_m \sin\left[k\left(\frac{l_d}{2} + z \right) \right] \cdot e^{jkz\cos\theta} dz + \int_{0}^{l_d/2} I_m \sin\left[k\left(\frac{l_d}{2} - z \right) \right] \cdot e^{jkz\cos\theta} dz \right] \tag{2.7}$$

Solving the integral equation (2.7) gives

$$E_\theta = j\eta \frac{I_m e^{-jkr}}{2\pi r} \cdot \frac{\cos\left[\left(kl_d/2\right)\cdot\cos\theta\right] - \cos\left(kl_d/2\right)}{\sin\theta} \tag{2.8}$$

The magnetic field can be obtained as

$$H_\phi = \frac{E_\theta}{\eta} = j\frac{I_m e^{-jkr}}{2\pi r} \cdot \frac{\cos\left[\left(kl_d/2\right)\cdot\cos\theta\right] - \cos\left(kl_d/2\right)}{\sin\theta} \tag{2.9}$$

The current distribution and the normalised radiation pattern (E-field) for different dipole lengths l_d are obtained using equations (2.4) and (2.8), and shown in Table 2.1.

Table 2.1 The current distribution and the normalised radiation for different length dipoles

Dipole length (l_d)	Current distribution [Equation 2.4]	Normalised radiation pattern (E-field) [Equation 2.8]
0.1λ	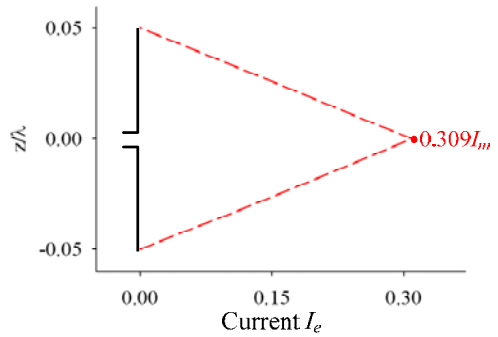	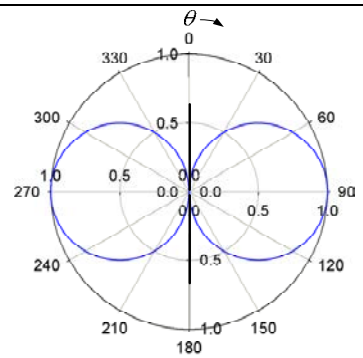
0.25λ	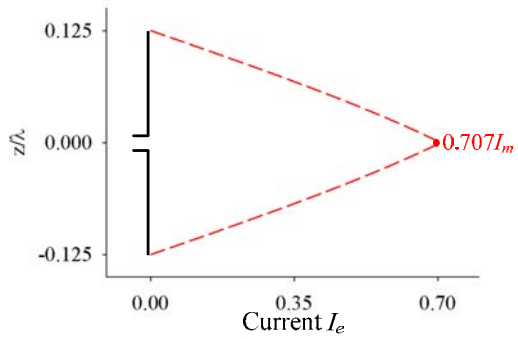	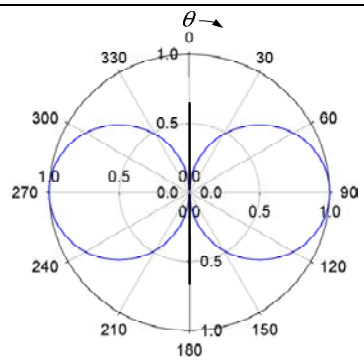
0.5λ	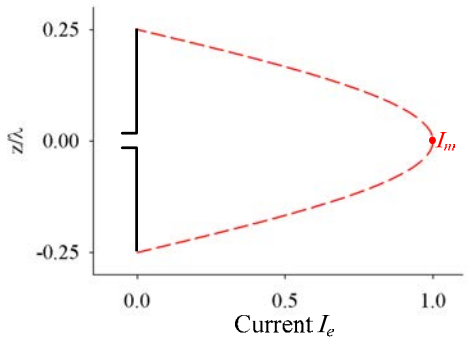	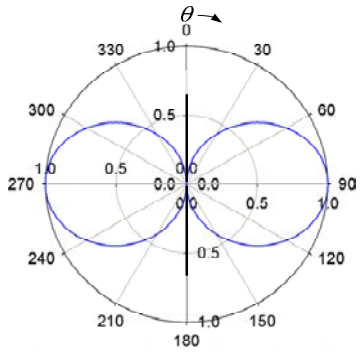
λ	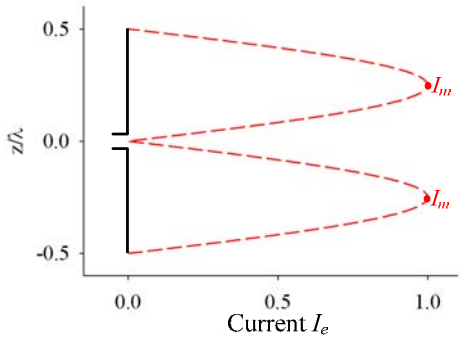	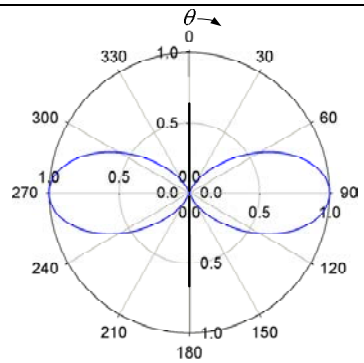

2.1.2.1 Equivalent Circuit of Dipole Antenna

This section is to study an equivalent circuit of a dipole antenna, which is initially analysed from an antenna impedance (Z_A). The antenna impedance Z_A is the ratio of voltage (V) to current (I) at a pair of terminals. It is corresponded to a diagram of the use of dipole antenna in transmitting mode, as shown in Figure 2.6(a). The dipole antenna shown in Figure 2.6(a), is equivalent to a series circuit of an antenna resistance (R_A) and an antenna reactance (X_A), as illustrated in Figure 2.6(b).

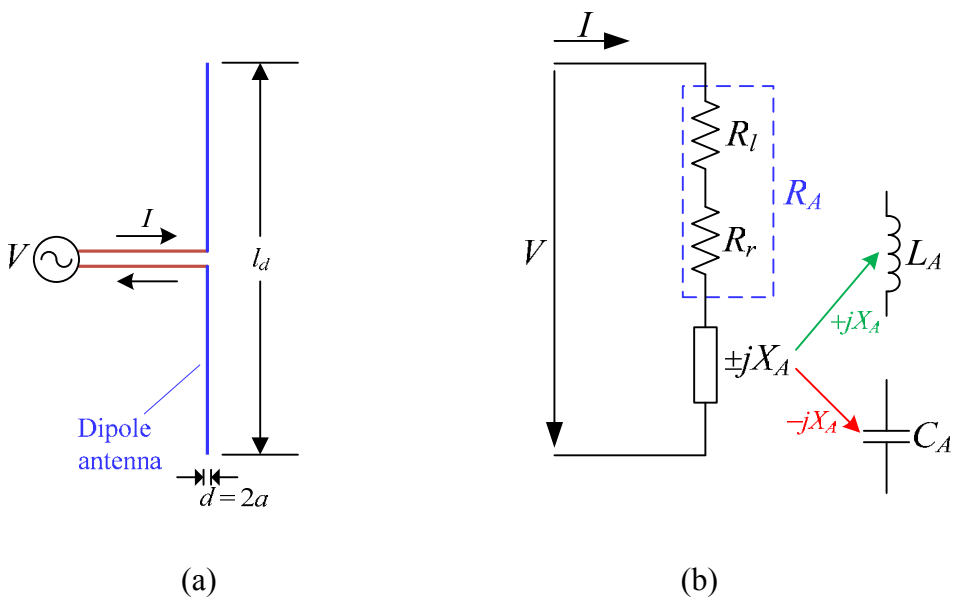

Figure 2.6 (a) Dipole antenna usage. (b) Equivalent circuit.

Referring to Figure 2.6(b), the impedance of the dipole antenna is defined as

$$Z_A = \frac{V}{I} = R_A \pm jX_A \tag{2.10}$$

where Z_A is the antenna impedance (ohms).

R_A is the antenna resistance (ohms).

X_A is the antenna reactance (ohms).

For the resistive part of Z_A, it represents R_A by

$$R_A = R_r + R_l \tag{2.11}$$

where R_r is the radiation resistance (ohms).

R_l is the loss resistance (ohms).

For the reactive part of Z_A, it represents X_A, which can be a positive or a negative value. For positive X_A, it is equivalent to an antenna inductance (L_A). For negative X_A, it is equivalent to an antenna capacitance (C_A).

The equations used to calculate R_r and X_A element values for finite length dipoles are derived using the induced EMF method, given by [2]

$$\begin{aligned} R_r(l_d) = \frac{\eta}{2\pi}\Big\{ & C + \ln(kl_d) - C_i(kl_d) + \frac{1}{2}\sin(kl_d)\left[S_i(2kl_d) - 2S_i(kl_d)\right] \\ & + \frac{1}{2}\cos(kl_d)\left[C + \ln(kl_d/2) + C_i(2kl_d) - C_i(kl_d)\right]\Big\} \end{aligned} \tag{2.12}$$

and

$$\begin{aligned} X_A(l_d) = \frac{\eta}{4\pi}\Big\{ & 2S_i(kl_d) + \cos(kl_d)\left[2S_i(kl_d) - S_i(2kl_d)\right] \\ & - \sin(kl_d)\left[2C_i(kl_d) - C_i(2kl_d) - C_i\left(\frac{2ka^2}{l_d}\right)\right]\Big\} \end{aligned} \tag{2.13}$$

where l_d is the length of the dipole antenna, a is the wire radius, k is the propagation constant ($k = 2\pi/\lambda_0$), $C = 0.5772$ (Euler's constant) and $C_i(x)$ and $S_i(x)$ are the cosine and sine integrals and given by

$$C_i(x) = \int_{\infty}^{x} \frac{\cos y}{y}\, dy \tag{2.14}$$

$$S_i(x) = \int_{0}^{x} \frac{\sin y}{y}\, dy \tag{2.15}$$

An example of R_r and X_A calculation using equations (2.12) and (2.15) for a half-wavelength (0.5λ) lossless dipole antenna (R_l = 0 Ω), the results shows that R_r is 73 ohms and X_A is 42.5 ohms, which corresponded to the antenna theory.

The loss resistance R_l of wire dipole antenna represents the conductor loss and is considered in a case of lossy dipole. R_l is calculated based on the current distribution, given by [3]

For a uniform current distribution,

$$R_l = \frac{l_d}{4\pi a}\sqrt{\frac{\pi f \mu_0}{\sigma}} \tag{2.16}$$

For a triangular current distribution,

$$R_l = \frac{l_d}{6\pi a}\sqrt{\frac{\pi f \mu_0}{\sigma}} \tag{2.17}$$

where a is the wire radius of dipole antenna.

f is the frequency (Hz).

μ_0 is the permeability of free-space (4πx10^{-7} H/m).

σ is the conductivity of the metal (S/m).

For example, a loss resistance R_l of an half wave length dipole antenna made from the copper (σ = 5.7x10^7 S/m), wire radius a is 3x10^{-4}λ. The R_l is calculated at f of 100 MHz using equation (2.16) that is equal to 0.349 ohms. For equation (2.17), it is used to calculate R_l for a short dipole antenna (l_d << λ).

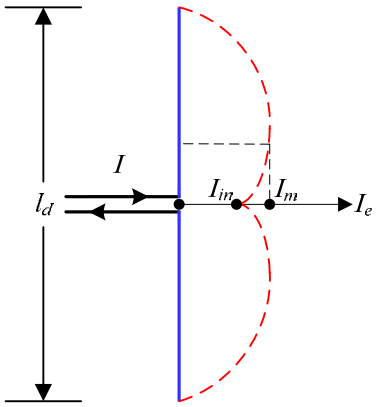

Figure 2.7 The current distribution of a wire dipole antenna in a case of $I_{in} \neq I_m$ [2].

Previously, the radiation resistance R_r and the antenna reactance X_A of dipole antennas were obtained using equations (2.12) and (2.13). These equations are only valid for some dipole lengths (l_d = λ/4, 3λ/4, λ, etc.), that the maximum current (I_m) is equal to the current (I_{in}) at input terminals. It should be noted that the maximum current I_m may not be equal to the current I_{in} for a particular length l_d. It can be considered from a diagram shown in Figure 2.7. Assuming the input power (P_{in}) is equal to the radiated power (P_r) as

$$\frac{|I_{in}|^2}{2} R_{in} = \frac{|I_m|^2}{2} R_r \tag{2.18a}$$

or

$$R_{in} = \left[\frac{I_m}{I_{in}}\right]^2 R_r \tag{2.18b}$$

where R_{in} is the radiation resistance at input (feed) terminals.

R_r is the radiation resistance at current maximum obtained from equation (2.12).

I_m is the current maximum.

I_{in} is the current at input terminals.

Referring to Figure 2.7, the current I_{in} is related to the maximum current I_m for a length l_d and is given by [2]

$$I_{in} = I_m \sin\left(\frac{kl_d}{2}\right) \tag{2.19}$$

Substituting equations from (2.20) to (2.19), thus equation (2.19) can be written as

$$R_{in} = \frac{R_r}{\sin^2\left(\frac{kl_d}{2}\right)} \tag{2.20}$$

Also the antenna reactance (X_{in}) at input terminals of dipole antenna can be written as [2]

$$X_{in} = \frac{X_A}{\sin^2\left(\frac{kl_d}{2}\right)} \tag{2.21}$$

Substituting equations from (2.12) to (2.21) and from (2.13) to (2.22) thus,

$$\begin{aligned} R_{in}(l_d) = \frac{\eta}{2\pi \sin^2\left(\frac{kl_d}{2}\right)} \Big\{ & C + \ln(kl_d) - C_i(kl_d) + \frac{1}{2}\sin(kl_d)\left[S_i(2kl_d) - 2S_i(kl_d)\right] \\ & + \frac{1}{2}\cos(kl_d)\left[C + \ln(kl_d/2) + C_i(2kl_d) - C_i(kl_d)\right]\Big\} \end{aligned} \tag{2.22}$$

and

$$\begin{aligned} X_{in}(l_d) = \frac{\eta}{4\pi \sin^2\left(\frac{kl_d}{2}\right)} \Big\{ & 2S_i(kl_d) + \cos(kl_d)\left[2S_i(kl_d) - S_i(2kl_d)\right] \\ & - \sin(kl_d)\left[2C_i(kl_d) - C_i(2kl_d) - C_i\left(\frac{2ka^2}{l_d}\right)\right]\Big\} \end{aligned} \tag{2.23}$$

It is concluded that the input impedance (Z_{in}) of a lossless dipole antenna is

$$Z_{in} = \frac{V_{in}}{I_{in}} = R_{in} \pm jX_{in} \tag{2.24}$$

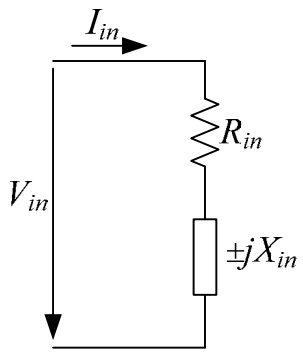

Figure 2.8 Equivalent circuit of a lossless dipole antenna.

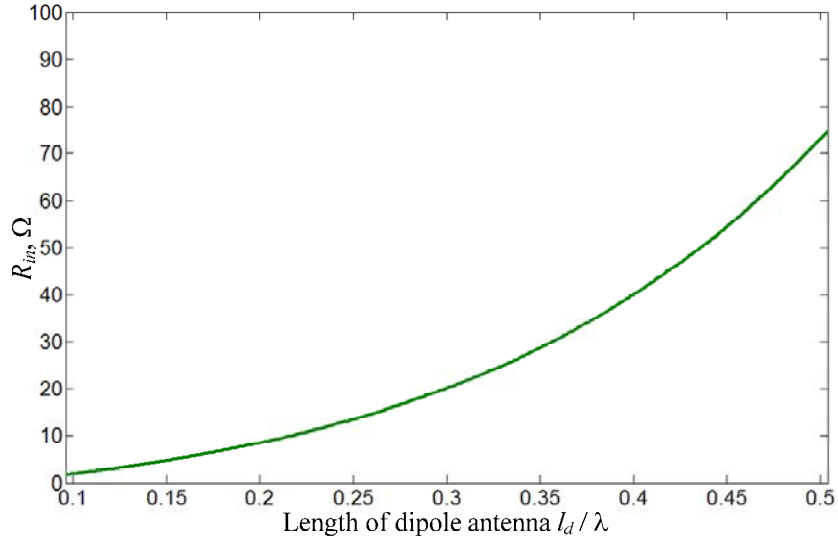

(a)

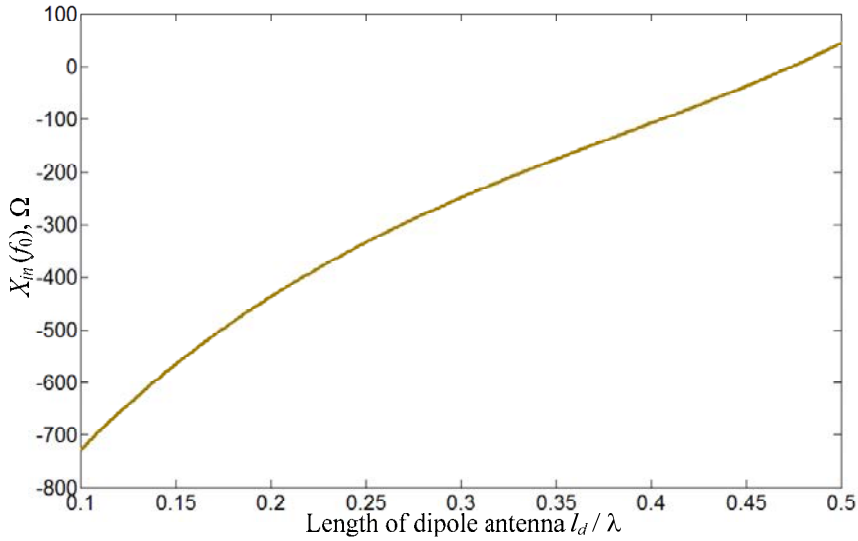

(b)

Figure 2.9 (a) The R_{in} calculated using equation (2.22) for different values of l_d. (b) The X_{in} calculated using equation (2.23) for different values of l_d.

It is represented as an equivalent circuit shown in Figure 2.8. The equivalent circuit of lossless dipole will be used to define its quality factor that is a parameter in order to design a resonator using dipole antenna in Chapter3. Figure 2.9 shows R_{in} and X_{in} calculated using equations (2.23) and (2.24) for the length l_d between 0.1λ and 0.5λ. These R_{in} and X_{in} calculation will then be utilised to calculate the quality factor (Q) of dipole antenna in Section 2.1.2.2.

2.1.2.2 Quality Factor of Dipole Antenna

The equivalent circuit of dipole antenna was analysed for different antenna lengths, as described in Section 2.1.2.1. An antenna element can also be described as a resonator in terms of the quality factor (Q). In this thesis, the dipole antenna will be initially studied and designed for a lossless dipole (R_l = 0 Ω). This is because it is a simple way to determine its quality factor, which is only related to the radiation or is named *the radiation quality factor* Q_r. The Q_r can be obtained from the equivalent circuit of a lossless dipole, which is analysed at the input. As mentioned in Section 2.1.2.1, a lossless dipole was equivalent to a R_{in} and X_{in} series circuit. In this case, Q_r of a lossless dipole can be calculated using the values of R_{in} and X_{in} considering at f_0, given by [4]

$$Q_r(f_0) = \frac{f_0}{2R_{in}(f_0)}\left(\frac{dX_{in}(f_0)}{df} + \frac{|X_{in}(f_0)|}{f_0}\right) \tag{2.25}$$

where f_0 is the centre frequency (Hz), $R_{in}(f_0)$ is the radiation resistance at the centre frequency (Ω), $X_{in}(f_0)$ is the antenna reactance at the centre frequency (Ω), $\frac{dX_{in}(f_0)}{df}$ is the derivative of X_{in} at the centre frequency and can also be defined as

$$\frac{dX_{in}(f_0)}{df} \approx \frac{X_{in}(f_0+\Delta f)-X_{in}(f_0-\Delta f)}{2\Delta f}$$

and Δf is a small change in f

The value of Δf must be small to improve the accuracy of the calculation of Q_r. The value selected is about 1% of the bandwidth or 0.01 for this calculation.

The radiation quality factor Q_r is calculated using equation (2.25) with the calculated values of R_{in} and X_{in} for equations (2.23) and (2.24). A curve of Q_r for the length l_d between 0.1λ and 0.5λ are shown in Figure 2.10. Equation (2.25) will then be utilised for obtaining Q_r of a lossless dipole from CST simulation software [5], which will be presented in Chapter 3.

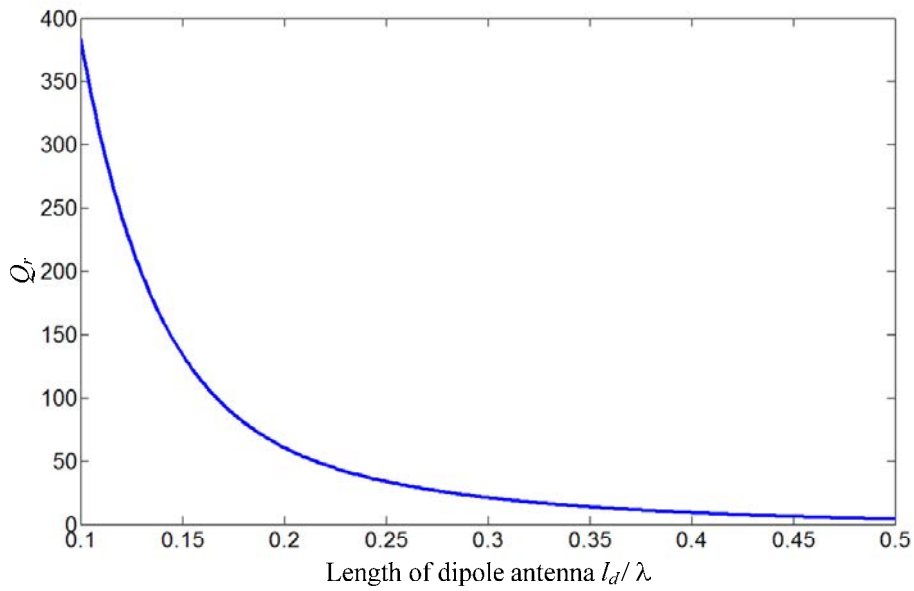

Figure 2.10 The radiation quality factor Q_r calculated using equation (2.25).

2.1.3 Waveguide Aperture Antennas

A waveguide aperture antenna is a simple antenna structure and is usually designed with an opening at the end of a rectangular waveguide. The aperture area of the waveguide is used to radiate the electromagnetic wave. Figure 2.11 shows the structure of the waveguide antenna and the distribution of the E and H fields inside of the waveguide for the dominant TE_{10} mode.

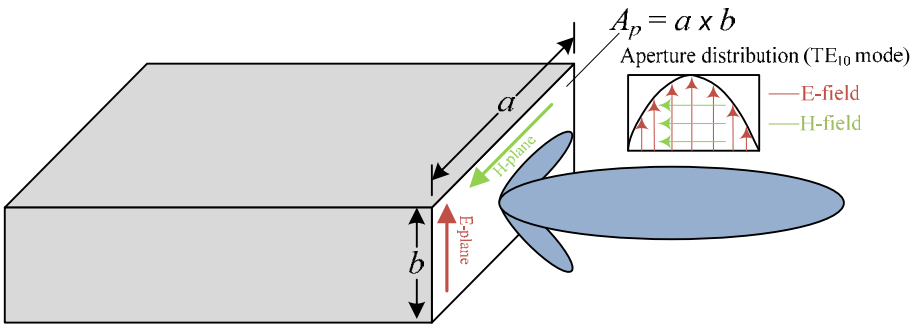

Figure 2.11 The geometry of an open-ended waveguide antenna.

For the open-ended waveguide, the radiated power does not use the full physical aperture (A_p) due to E-fields at the sidewall that becomes zero for TE_{10} propagation mode. Thus, the effective area A_e of the aperture is less than the physical aperture A_p and corresponds to the aperture efficiency ε_{ap} of the antenna as given by [2]

$$\varepsilon_{ap} = \frac{A_e}{A_p} \tag{2.26}$$

The radiated power of the aperture antenna can be obtained by integrating the average Poynting vector W_{av} and is given by [2]

$$P_{rad} = \oiint_S W_{av} \cdot dS = ab\frac{|E_0|^2}{4\eta} \tag{2.27}$$

The maximum radiation intensity $U_{\max}$ at $\theta = 0^{\circ}$ is given by [2]

$$U_{\max} = \frac{8}{\pi^2}\left(\frac{ab}{\lambda}\right)^2 \frac{|E_0|^2}{4\eta} \tag{2.28}$$

The maximum directivity D_0 of the aperture antenna is obtained using equation [2]:

$$D_0 = \frac{4\pi U_{\max}}{P_{rad}} = \frac{8}{\pi^2}\left[ab\left(\frac{4\pi}{\lambda^2}\right)\right] = 0.81\left[ab\left(\frac{4\pi}{\lambda^2}\right)\right] = 0.81A_p\left(\frac{4\pi}{\lambda^2}\right) = A_{em}\left(\frac{4\pi}{\lambda^2}\right) \tag{2.29}$$

where $Ap = a \times b$ is the physical aperture for the open-ended waveguide antenna.

$A_{em} = \varepsilon_{ap} \cdot A_p = 0.81A_p$ is the maximum effective aperture for the open-ended waveguide antenna.

Thus, the aperture efficiency ε_{ap} for the waveguide aperture antenna is equal to 0.81, which indicates 81% efficiency of the physical aperture A_p can be utilised for radiating EM energy. It is noted that the equation (2.29) is only valid for the aperture mounted on the infinite ground plane.

2.2 Microwave Filter Theory

2.2.1 Overview of Microwave Filters

As this project is about combining antennas and filters we now move on the filter theory. A microwave filter is a two-port passive component utilised for selecting a required frequency and rejecting an unwanted frequency in the microwave frequency range (300 MHz–300 GHz) [6]. The microwave filter is represented by a two-port network [7], as shown in Figure 2.12.

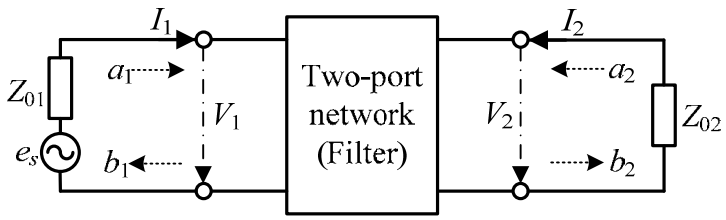

Figure 2.12 Two-port network representation of a microwave filter. V_1, V_2 and I_1, I_2 are the voltage and current at the port 1 and 2, Z_{01} and Z_{02} are the terminal impedances [7].

The input/output transmission and reflection coefficients for the two-port network in Figure 2.12 is represented by the incident waves (a) and the reflected wave (b). These variables are defined from the voltage (V) and current (I) variables, as computed by [7]

$$a_n = \frac{1}{2}\left(\frac{V_n}{\sqrt{Z_{0n}}} + \sqrt{Z_{0n}}I_n\right)$$
$$n = 1,2 \qquad (2.30)$$
$$b_n = \frac{1}{2}\left(\frac{V_n}{\sqrt{Z_{0n}}} - \sqrt{Z_{0n}}I_n\right)$$

The performances of microwave filters are commonly described by S-parameters. The S-parameters for a two-port network are related to the incident waves (a) and the reflected wave (b). Reflected waves in terms of incident waves are presented in matrix form as follows

$$\begin{bmatrix} b_1 \\ b_2 \end{bmatrix} = \begin{bmatrix} S_{11} & S_{12} \\ S_{21} & S_{22} \end{bmatrix} \begin{bmatrix} a_1 \\ a_2 \end{bmatrix} \qquad (2.31)$$

where $S_{11} = \left.\frac{b_1}{a_1}\right|_{a_2=0}$ is the input reflection coefficient with output properly terminated.

$S_{21} = \left.\frac{b_2}{a_1}\right|_{a_2=0}$ is the forward transmission coefficient from port 1 to port 2.

$S_{22} = \left.\frac{b_2}{a_2}\right|_{a_1=0}$ is the output reflection coefficient with input properly terminated.

$S_{12} = \left.\dfrac{b_1}{a_2}\right|_{a_1=0}$ is the reverse transmission coefficient from port 2 to port 1.

The characteristics of filters are shown by the transmission loss L_A and the return loss L_R which are obtained from the magnitude of S-parameters for the two-port network in decibels, as follows

$$L_A = -20\log_{10}\left(\left|S_{21}\right|\right) \text{ dB} \tag{2.32a}$$

$$L_R = -20\log_{10}\left(\left|S_{11}\right|\right) \text{ dB} \tag{2.32b}$$

The transmission and return losses are assumed to have positive values. The relation between the transmission loss L_A and return loss L_R for a lossless network only are given by [7]

$$L_A = -10\log_{10}\left(1-10^{-L_R/10}\right) \text{ dB} \tag{2.33a}$$

$$L_R = -10\log_{10}\left(1-10^{-L_A/10}\right) \text{ dB} \tag{2.33b}$$

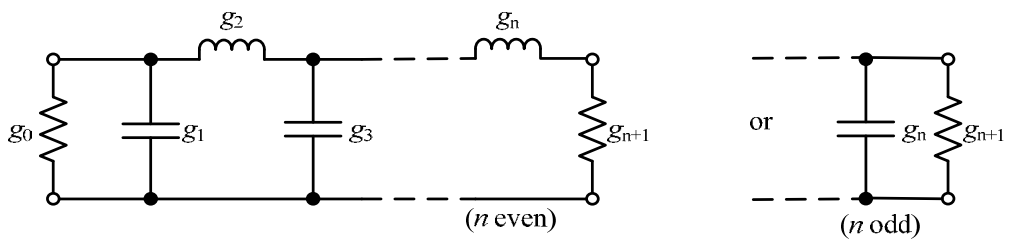

(a)

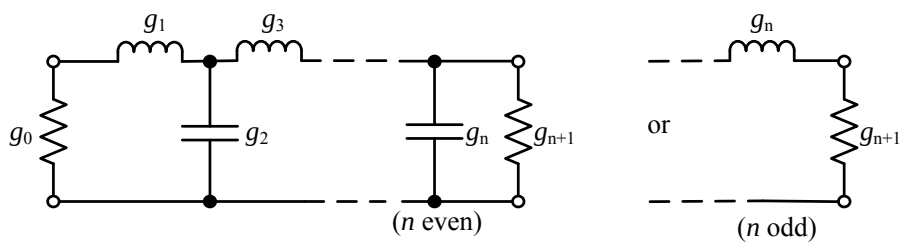

(b)

Figure 2.13 Lowpass prototype filters for all-pole filters with (a) A ladder circuit beginning with a shunt element and (b) A ladder circuit beginning with a series element [7].

In designing a filter, the circuit inside of a two-port filter network is initially assumed to be a lumped element circuit, having the form of a ladder network also known as a *lowpass prototype filter circuit* [7], as shown in Figure 2.13.

The lowpass prototype *g* values can be obtained from the filter response. The Chebyshev filter response is selected for designing the filters in this thesis. The response of Chebyshev lowpass filter has an equal-ripple passband response and maximally flat stopband [7] and as illustrated in Figure 2.14.

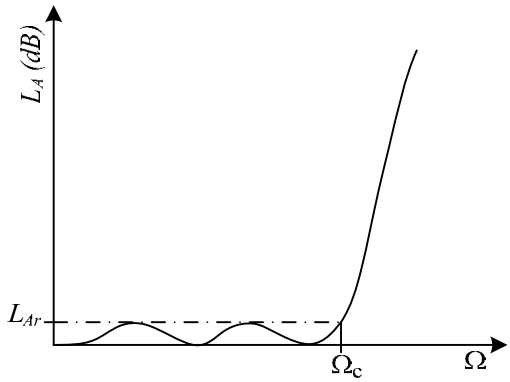

Figure 2.14 Chebyshev lowpass response [7].

The amplitude-squared transfer function for a lossless filter with Chebyshev response is [7]

$$\left|S_{21}\left(j\Omega\right)\right|^2 = \frac{1}{1+\varepsilon^2 T_n^2\left(\Omega\right)} \tag{2.34}$$

and the amplitude-squared input function for a lossless filter with Chebyshev response is

$$\left|S_{11}\left(j\Omega\right)\right|^2 = 1-\left|S_{21}\left(j\Omega\right)\right|^2 = 1-\frac{1}{1+\varepsilon^2 T_n^2\left(\Omega\right)} \tag{2.35}$$

where Ω is the angular frequency, ε is the ripple constant, which is obtained from the passband ripple L_{Ar} in dB by

$$\varepsilon = \sqrt{10^{\frac{L_{Ar}}{10}} - 1} \tag{2.36}$$

A Chebyshev function $T_n(\Omega)$ of the nth order filter can be defined as [7]

$$T_n(\Omega) = \begin{cases} \cos\left(n \ \cos^{-1}\Omega\right) & |\Omega| \le 1 \\ \cosh\left(n \ \cosh^{-1}\Omega\right) & |\Omega| \ge 1 \end{cases} \tag{2.37}$$

The g values for a lowpass prototype filter having the Chebyshev response the passband ripple is L_{Ar} in dB and the cutoff frequency $\Omega_c = 1$ can be calculated using equations below [7]: In these equations

$$g_0 = 1.0$$

$$g_1 = \frac{2}{\gamma}\sin\left(\frac{\pi}{2n}\right)$$

$$g_i = \frac{1}{g_{i-1}} \frac{4\sin\left[\frac{(2i-1)\pi}{2n}\right]\cdot\sin\left[\frac{(2i-3)\pi}{2n}\right]}{\gamma^2 + \sin^2\left[\frac{(i-1)\pi}{n}\right]} \qquad \text{for } i = 2, 3, \cdots n \tag{2.38}$$

$$g_{n+1} = \begin{cases} 1.0 & \text{for } n \text{ odd} \\ \coth^2\left(\frac{\beta}{4}\right) & \text{for } n \text{ even} \end{cases}$$

where

$$\beta = \ln\left[\coth\left(\frac{L_{Ar}}{17.37}\right)\right]$$

$$\gamma = \sinh\left(\frac{\beta}{2n}\right)$$

Using these equations a low pass prototype filters can be calculated and the g element values shown in Figure 2.13 calculated.

2.2.2 Microwave Resonators

Microwave resonators are microwave devices utilised in microwave coupled resonator filters. Examples are microstrip resonators, cavity resonators, dielectric resonators, etc.. The microwave resonator can be modeled as a similar circuit to a lumped-element resonator (i.e. a series or parallel resonant circuit). Figure 2.15 shows the equivalent circuit of several microwave resonators. A lossless resonator is an ideal resonator with no loss, i.e. $R = 0$ in Figure 2.15(a) for a series circuit and Figure 2.15(b) for a parallel circuit.

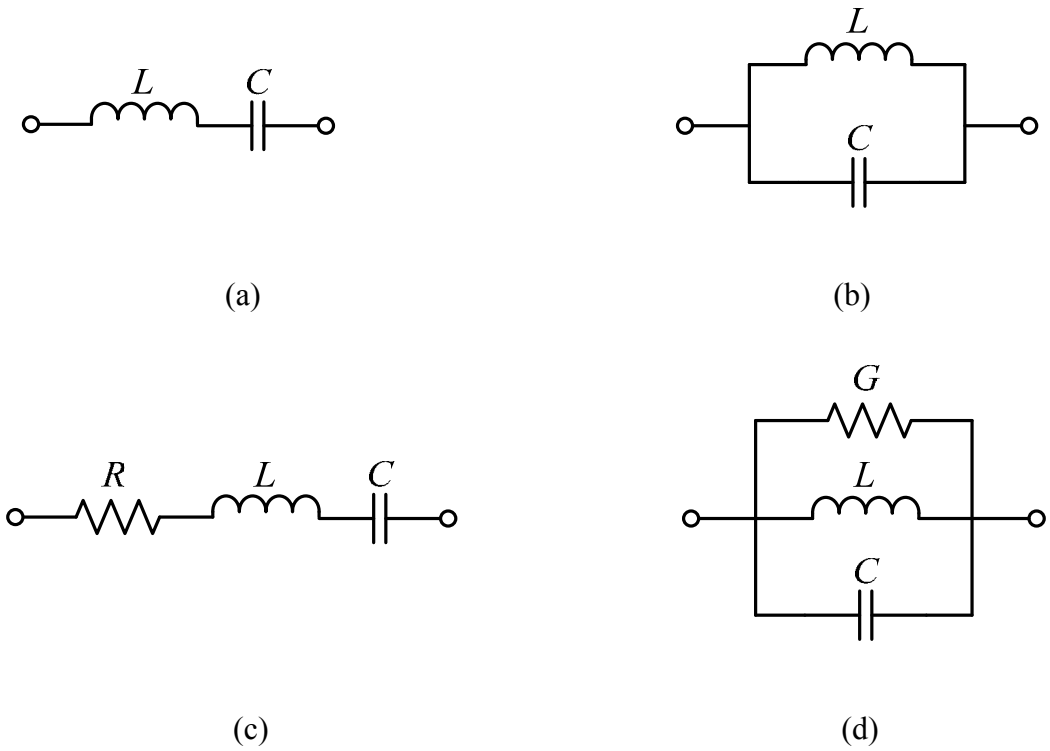

Figure 2.15 The resonant circuits represented as microwave resonators. (a) Series lossless resonant circuit. (b) Parallel lossless resonant circuit. (c) Series lossy resonant circuit. (d) Parallel lossy resonant circuit.

For lossy resonators, the losses in the resonator are conventionally represented by the resistance (R) in the resonant circuit of Figure 2.15(c) or the conductance (G) in the resonant circuit of Figure 2.15(d). The unloaded quality factor (Q_u) is a parameter used to describe the losses of a resonant circuit. For example, a low loss implies a high Q_u, whereas a high loss implies a low Q_u. For the series lossy resonant circuit, the unloaded quality factor Q_u is defined by [7]

$$Q_u = \frac{\omega L}{R} \tag{2.39}$$

For the parallel lossy resonant circuit, The unloaded quality factor Q_u is defined by [7]

$$Q_u = \frac{\omega C}{G} \tag{2.40}$$

In principle, the general definition of the unloaded quality factor Q_u is [7]

$$Q_u = \omega \frac{\text{Time-average energy stored in resonator}}{\text{Average power lost in resonator}} \tag{2.41}$$

The losses in the resonator are usually associated with the conductors, dielectrics in the resonator and radiation from the resonator. Thus, the total unloaded quality factor Q_u can be determined by including these losses together [7]

$$\frac{1}{Q_u} = \frac{1}{Q_c} + \frac{1}{Q_d} + \frac{1}{Q_r} \tag{2.42}$$

where Q_c is the conductor quality factor, Q_d is the dielectric quality factor and Q_r is the radiation quality factor.

In filter design, the passband response of the filters may be distorted due to the losses in the resonators of the filter circuits. The value of unloaded quality factor Q_u can be used to calculate the insertion loss in the bandpass filter design using the resonators with finite Q_u, given by [7]

$$\Delta L_{A0} = 4.343 \sum_{i=1}^{n} \frac{\Omega_C}{FBW \cdot Q_{ui}} g_i \quad \text{(dB)} \tag{2.43}$$

where ΔL_{A0} is the increase of passband insertion loss in dB, FBW is the fractional bandwidth ($FBW = (f_2 - f_1)/2$), $f_2 - f_1$ is the passband bandwidth, Ω_C is the cut-off frequency ($\Omega_C = 1$), g_i is the g values for i elements obtained from the filter response and Q_{ui} is the unloaded quality factor for i resonator.

2.2.3 Rectangular Waveguide Cavity Resonator

A rectangular waveguide cavity resonator can be made from a section of a rectangular waveguide that is terminated at both ends with conducting plates. Figure 2.16 shows the geometry of a rectangular waveguide cavity where a is the width, b is the height and d is the length.

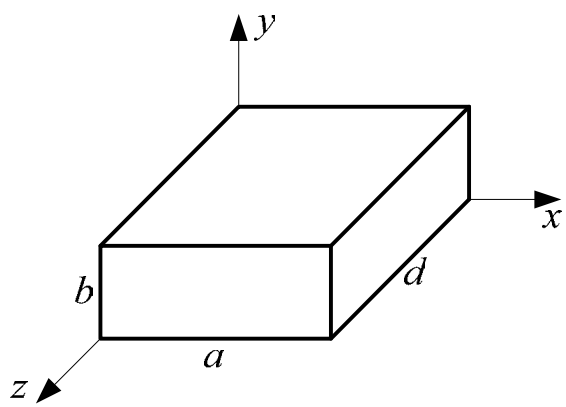

Figure 2.16 A rectangular waveguide cavity [6].

The transverse electric fields (E_x, E_y) of the TE_{mn} and TM_{mn} mode for the rectangular waveguide cavity can be written as [6]

$$\overline{E}_t(x,y,z) = \overline{e}(x,y)\left[A^+ e^{-j\beta_{mn}z} + A^- e^{j\beta_{mn}z}\right] \tag{2.44}$$

where $\overline{e}(x,y)$ are the transverse variations of the mode in the x and y directions, A^+ and A^- are the arbitrary amplitude of the travelling waves in the +z and –z directions and β_{mn} is the propagation constant and is given by [6]

$$\beta_{mn} = \sqrt{k^2 - \left(\frac{m\pi}{a}\right)^2 - \left(\frac{n\pi}{b}\right)^2} \tag{2.45}$$

where $k = 2\pi f_0\sqrt{\mu\varepsilon}$, and μ and ε are the permeability and permittivity of the material filling the waveguide.

For the boundary condition of the waveguide cavity at z = 0 and z = d, it requires $\overline{E}_t(x,y,z) = 0$. Applying the condition $\overline{E}_t = 0$ at z = 0 to equation (2.44) becomes $A^+ = -A^-$. Also, applying the condition $\overline{E}_t = 0$ at z = d, equation (2.44) becomes $d = l\cdot(\pi/\beta_{mn}) = l\cdot(\lambda_g/2)$ where l = 1, 2, 3... This condition means that the cavity length (d) must be an integer multiple of a half-guide wavelength ($\lambda_g/2$) at the resonant frequency [6]. The resonant wavenumber of the rectangular waveguide cavity can be defined as [6]

$$k_{mnl} = \sqrt{\left(\frac{m\pi}{a}\right)^2 + \left(\frac{n\pi}{b}\right)^2 + \left(\frac{l\pi}{d}\right)^2} \tag{2.46}$$

where the indices m, n, l indicate the number of half wavelength variations in the x, y, z directions, respectively. The resonant frequency of the TE_{mnl} or the TM_{mnl} can be defined as [6]

$$f_{mnl} = \frac{ck_{mnl}}{2\pi\sqrt{\mu_r\varepsilon_r}} = \frac{c}{2\pi\sqrt{\mu_r\varepsilon_r}}\sqrt{\left(\frac{m\pi}{a}\right)^2 + \left(\frac{n\pi}{b}\right)^2 + \left(\frac{l\pi}{d}\right)^2} \tag{2.47}$$

where c = 3 x 10^8 m/s is the light speed, and μ_r and ε_r are the relative permeability and permittivity of the material filling the waveguide. In the case of $b < a < d$, the mode with the lowest resonant frequency is known as the dominant mode and will be TE_{101} mode. The electromagnetic-field configuration associated with TE_{101} mode rectangular cavity resonator is shown in Figure 2.17.

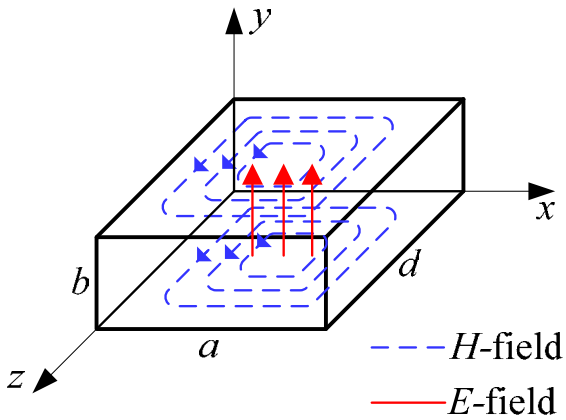

Figure 2.17 Electromagnetic-field configuration of TE_{101} mode [8].

For a design example, a WR-90 rectangular waveguide operates at X-band frequencies (8.2 GHz to 12.4 GHz) and has the width a of 22.86 mm and the height b of 10.16 mm. The guided wavelength of the WR-90 waveguide at the middle band frequency (about 10 GHz) can be calculated using the equation [8], given by

$$\lambda_g = \frac{\lambda_0}{\sqrt{1-(\lambda_0/\lambda_c)^2}} \tag{2.48}$$

where $\lambda_0 = c/f$ is the free-space wavelength, f is frequency (Hz).

$\lambda_c = \dfrac{2}{\sqrt{(m/a)^2+(n/b)^2}}$ is the cut-off wavelength.

Thus, the guide wavelength of a WR-90 waveguide at 10 GHz is calculated using equation (2.48). This yields a value of 39.76 mm. The WR-90 waveguide can be used to design a

cavity resonator terminated at both ends with conducting plates. The resonator is half a guide wavelength long. Using equation (2.47), and assuming that the inside of cavity is filled with air (i.e. $\mu_r = \varepsilon_r = 1$), the calculated resonant frequency (f_{101}) of the TE_{101} mode is 10 GHz.

2.2.4 Coupled Resonator Filters

Microwave bandpass filter is usually designed based on coupled resonator circuit. The filter can be simply designed by combining all resonators using coupling theory, as described in [7].

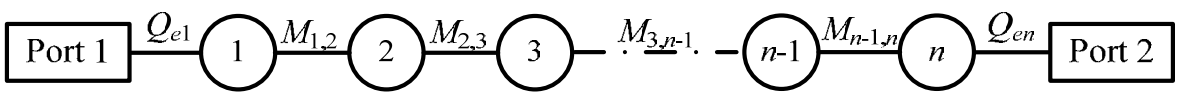

Figure 2.18 The coupling topology diagram of *n*-coupled resonator filter.

Figure 2.18 shows the coupling topology for the nth coupled resonator filter, where the white circles represent resonators and the lines linking resonators represent couplings. For designing an nth coupled resonator bandpass filter, the coupling coefficient ($M_{i,i+1}$) and the external quality factor (Q_{e1} and Q_{en}) are the design parameters. The design parameters can be obtained from the filter specifications with equations [7]:

$$M_{i,i+1} = \frac{FBW}{\sqrt{g_i g_{i+1}}}, \qquad \text{for } i = 1, 2, \ldots, N-1$$
$$Q_{e1} = \frac{g_0 g_1}{FBW} \text{ and } Q_{en} = \frac{g_n g_{n+1}}{FBW} \tag{2.49}$$

In the normalised form,

$$m_{i,i+1} = \frac{M_{i,i+1}}{FBW} = \frac{1}{\sqrt{g_i g_{i+1}}}, \qquad \text{for } i = 1, 2, \ldots, N-1$$
$$q_{e1} = FBW \cdot Q_{e1} = g_0 g_1 \text{ and } q_{en} = FBW \cdot Q_{en} = g_n g_{n+1} \tag{2.50}$$

where $M_{i,i+1}$ is the coupling coefficient between adjacent resonators.

Q_{e1} and Q_{en} are the external quality factors of the input and output resonators.

$FBW = \dfrac{f_2 - f_1}{f_0}$ is the fractional bandwidth.

$f_2 - f_1$ is the design bandwidth.

f_0 is the centre frequency.

$m_{i,i+1}$ is the normalised coupling coefficient between adjacent resonators.

q_{e1} and q_{en} are the normalised external quality factors of the input and output resonators.

g is the g value obtained from the filter response (e.g. Chebyshev filter response from equation (2.38)).

The normalised design parameters will then be utilised with the coupling matrix to calculate the filter response corresponding to filter specifications.

2.2.5 Coupling Matrix for Coupled Resonator Filters

The coupled resonator filters are conventionally designed using the coupling coefficient ($M_{i,i+1}$) and the external quality factors (Q_{e1} and Q_{en}), as described in the previous section. The

coupling matrix is a general technique for analysing the filter response of coupled resonator filters based on the coupling coefficient and the external quality factor with couplings potentially between any every pair of resonators. The coupling matrix is derived from the coupled resonator circuits and can be applicable to design filters for different coupling topologies. The calculated coupling values, from the coupling matrix, can then be utilised for defining the physical dimensions for the filter structure. The coupling coefficient and the external quality factor extraction technique are dependent on the filter structure and will be described in the next chapters. This section derives the coupling matrix equations for coupled resonator filters with the lossy and lossless resonators. Here the lossy resonators are assumed in the filter circuit when deriving the coupling matrix equation in the case of filter circuits with finite Q_u. The n-coupled resonator filter circuits with finite Q_u for the magnetic coupling and the electric coupling circuits are shown in Figure 2.19.

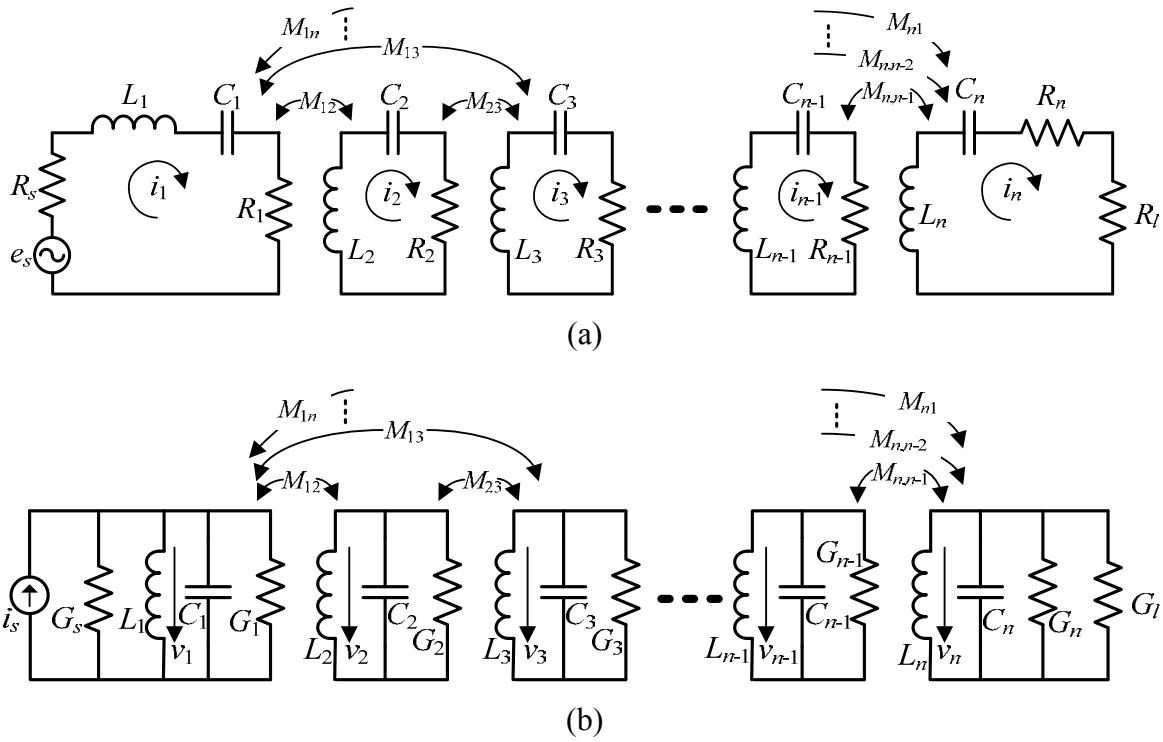

Figure 2.19 Equivalent circuits of n-coupled resonator filters with lossy resonators. (a) Magnetic coupling circuits. (b) Electric coupling circuits.

Figure 2.19(a) illustrates an equivalent circuit of an *n*-coupled resonator filter with lossy resonators for the case of magnetic coupling, where *L*, *C* and *R* are the inductance, capacitance and resistance, respectively; R_s is the source resistance, R_l is the load resistance, *i* represents the loop current and e_s is the voltage source. For this equivalent circuit, the resonators are coupled by mutual inductances (i.e. magnetic couplings). The circuit shown in Figure 2.19(a) is analysed by the loop equations using Kirchhoff's voltage law and can be written is the matrix form as [75]

$$\begin{bmatrix} R_s + R_1 + j\omega L_1 + \dfrac{1}{j\omega C_1} & -j\omega L_{12} & \cdots & -j\omega L_{1n} \\ -j\omega L_{21} & R_2 + j\omega L_2 + \dfrac{1}{j\omega C_2} & \cdots & -j\omega L_{2n} \\ \vdots & \vdots & \ddots & \vdots \\ -j\omega L_{n1} & -j\omega L_{n2} & \cdots & R_l + R_n + j\omega L_n + \dfrac{1}{j\omega C_n} \end{bmatrix} \begin{bmatrix} i_1 \\ i_2 \\ \vdots \\ i_n \end{bmatrix} = \begin{bmatrix} e_s \\ 0 \\ \vdots \\ 0 \end{bmatrix} \quad (2.51)$$

or

$$[Z]\cdot[i]=[e]$$

where [*Z*] is an $n \times n$ impedance matrix. For simplicity, the coupling circuit for this filter is derived on the assumption of synchronous tuning where the resonant frequency of all resonators are the same frequency. The angular resonant frequency $\omega_0 = 1/\sqrt{LC}$, where $L = L_1 = L_2 = ... = L_n$ and $C = C_1 = C_2 = ... = C_n$. For a narrow-band approximation assuming $\omega \approx \omega_0$, equation (2.51) can be simplified as [7]

$$\left[\overline{Z}\right]=\begin{bmatrix} \frac{1}{q_{e1}}+\frac{1}{q_{u1}}+p & -jm_{12} & \cdots & -jm_{1n} \\ -jm_{21} & \frac{1}{q_{u2}}+p & \cdots & -jm_{2n} \\ \vdots & \vdots & \ddots & \vdots \\ -jm_{n1} & -jm_{n2} & \cdots & \frac{1}{q_{en}}+\frac{1}{q_{un}}+p \end{bmatrix} \tag{2.52}$$

where $\left[\overline{Z}\right]$ is the normalised impedance matrix.

$p = j\frac{1}{FBW}\left(\frac{\omega}{\omega_0}-\frac{\omega_0}{\omega}\right)$ is the complex frequency variable.

$q_{e1} = FBW \cdot Q_{e1}$ is the normalised external quality factor of input resonator.

$Q_{e1} = \frac{\omega_0 L}{R_s}$ is the external quality factor of input resonator.

$q_{en} = FBW \cdot Q_{en}$ is the normalised external quality factor of output resonator.

$Q_{en} = \frac{\omega_0 L}{R_l}$ is the external quality factor of output resonator.

$q_{ui} = FBW \cdot Q_{ui}$ (for $i = 1, 2, \ldots, n$) is the normalised unloaded quality factor of resonator *i*.

$Q_{ui} = \frac{\omega_0 L}{R_i}$ (for $i = 1, 2, \ldots, n$) is the unloaded quality factor of resonator *i*.

$m_{ij} = \frac{M_{ij}}{FBW}$ is the normalised coupling coefficient of resonator *i* and *j*.

$M_{ij} = \frac{L_{ij}}{L}$ is the coupling coefficient of resonator *i* and *j*.

All resonators of the circuit of Figure 2.19(a) may have different resonant frequencies in the case of asynchronously tuned coupled-resonator circuits [7]. The normalised self-coupling

coefficient m_{ii} accounts for asynchronous tuning and is related to the self-resonant frequency of each resonator. The m_{ii} can be added into the diagonal entries in $\left[\overline{Z}\right]$, for asynchronous tuning as [7]

$$\left[\overline{Z}\right]=\begin{bmatrix} \frac{1}{q_{e1}}+\frac{1}{q_{u1}}+p-jm_{11} & -jm_{12} & \cdots & -jm_{1n} \\ -jm_{21} & \frac{1}{q_{u2}}+p-jm_{22} & \cdots & -jm_{2n} \\ \vdots & \vdots & \ddots & \vdots \\ -jm_{n1} & -jm_{n2} & \cdots & \frac{1}{q_{en}}+\frac{1}{q_{un}}+p-jm_{nn} \end{bmatrix} \tag{2.53}$$

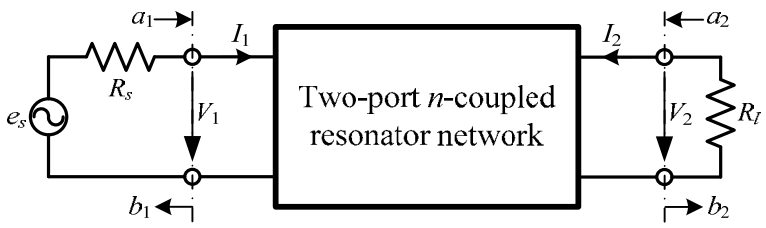

(a)

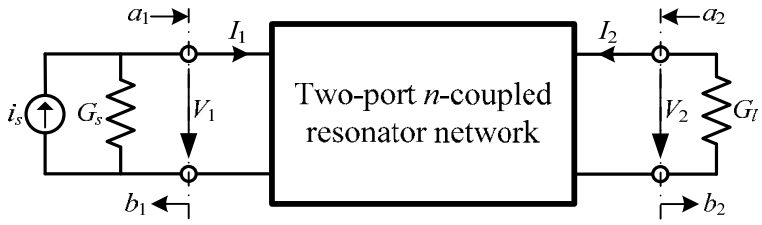

(b)

Figure 2.20 Network representation of two-port circuit in (a) Figure 2.19(a) and (b) Figure 2.19 (b).

The network representation for the circuit of Figure 2.19(a) is shown in Figure 2.20(a), where a_1, b_1 and a_2, b_2 are the wave variables and V_1, I_1 and V_2, I_2 are the voltage and current variables. Port 1 connected to resonator 1 and port 2 is connected to the resonator n.

The wave variables can be defined from the voltage (V) and current (I) variable. The expressions are similar to these given in Section 2.2.1, defined by

$$a_n = \frac{1}{2}\left(\frac{V_n}{\sqrt{R}} + \sqrt{R}I_n\right) \text{ and } b_n = \frac{1}{2}\left(\frac{V_n}{\sqrt{R}} - \sqrt{R}I_n\right) \tag{2.54}$$

where n is the port number, R corresponds to R_s for port 1 and R_l is for port 2. Comparing the circuit in Figure 2.19(a) with the network in Figure 2.20(a) we can calculate that $I_1 = i_1$, $I_2 = -i_n$ and $V_1 = e_s - i_1R_s$. Thus, the wave variables equation (2.54) can be rewritten as

$$\begin{aligned} a_1 &= \frac{e_s}{2\sqrt{R_S}} & b_1 &= \frac{e_s - 2i_1R_S}{2\sqrt{R_S}} \\ a_2 &= 0 & b_2 &= i_n\sqrt{R_l} \end{aligned} \tag{2.55}$$

The S-parameters can be obtained from the wave variables as follows,

$$S_{11} = \left.\frac{b_1}{a_1}\right|_{a_2=0} = 1 - \frac{2R_s i_1}{e_s} \tag{2.56a}$$

$$S_{21} = \left.\frac{b_2}{a_1}\right|_{a_2=0} = \frac{2\sqrt{R_s R_l}\, i_2}{e_s} \tag{2.56b}$$

i_1 and i_2 can be found by solving (2.51),

$$i_1 = \frac{e_s}{\omega_0 L \cdot FBW}\left[\overline{Z}\right]_{11}^{-1} \tag{2.57a}$$

$$i_2 = \frac{e_s}{\omega_0 L \cdot FBW}\left[\overline{Z}\right]_{21}^{-1} \tag{2.57b}$$

Substituting (2.57) into (2.56) gives,

$$S_{11} = 1 - \frac{2R_s}{\omega_0 L \cdot FBW}\left[\overline{Z}\right]_{11}^{-1} \tag{2.58a}$$

$$S_{21} = \frac{2\sqrt{R_s R_l}}{\omega_0 L \cdot FBW}\left[\overline{Z}\right]_{21}^{-1} \tag{2.58b}$$

Rewriting (2.58) in terms of the normalised external quality factors ($q_{e1} = \omega_0 L \cdot FBW / R_s$ and $q_{en} = \omega_0 L \cdot FBW / R_l$). Thus, *S*-parameters become,

$$S_{11} = 1 - \frac{2}{q_{e1}}\left[\overline{Z}\right]_{11}^{-1} \tag{2.59a}$$

$$S_{21} = \frac{2}{\sqrt{q_{e1} \cdot q_{en}}}\left[\overline{Z}\right]_{21}^{-1} \tag{2.59b}$$

Similarly, the equivalent circuit of the resonators coupled by mutual capacitances (i.e. electric couplings) shown in Figure 2.19(b) can be analysed by the node equation using Kirchhoff's current law. The normalised admittance matrix $\left[\overline{Y}\right]$ for the filter of Figure 2.19(b) can be defined as

$$\left[\overline{Y}\right] = \begin{bmatrix} \frac{1}{q_{e1}} + \frac{1}{q_{u1}} + p - jm_{11} & -jm_{12} & \cdots & -jm_{1n} \\ -jm_{21} & \frac{1}{q_{u2}} + p - jm_{22} & \cdots & -jm_{2n} \\ \vdots & \vdots & \ddots & \vdots \\ -jm_{n1} & -jm_{n2} & \cdots & \frac{1}{q_{en}} + \frac{1}{q_{un}} + p - jm_{nn} \end{bmatrix} \tag{2.60}$$

The *S*-parameters for the filter circuit in Figure 2.19(b) can be defined in a similar way to that for the magnetic coupling circuit

$$S_{11} = -\left(1 - \frac{2}{q_{e1}}\left[\overline{Y}\right]_{11}^{-1}\right) \tag{2.61a}$$

$$S_{21} = 2\frac{1}{\sqrt{q_{e1} \cdot q_{en}}}\left[\overline{Y}\right]_{n1}^{-1} \tag{2.61b}$$

It can be concluded that the normalised impedance matrix $\left[\overline{Z}\right]$ and the normalised admittance matrix $\left[\overline{Y}\right]$ are of the same form. Thus, the *S*-parameters for these coupling circuits may be defined as

$$S_{11} = \pm\left(1 - \frac{2}{q_{e1}}\left[A\right]_{11}^{-1}\right) \tag{2.62a}$$

$$S_{21} = 2\frac{1}{\sqrt{q_{e1} \cdot q_{en}}}\left[A\right]_{n1}^{-1} \tag{2.62b}$$

where the matrix [*A*] is

$$\left[A\right] = \begin{bmatrix} \frac{1}{q_{e1}} + \frac{1}{q_{u1}} & 0 & \cdots & 0 \\ 0 & \frac{1}{q_{u2}} & \cdots & 0 \\ \vdots & \vdots & \ddots & \vdots \\ 0 & 0 & \cdots & \frac{1}{q_{en}} + \frac{1}{q_{un}} \end{bmatrix} + p\begin{bmatrix} 1 & 0 & \cdots & 0 \\ 0 & 1 & \cdots & 0 \\ \vdots & \vdots & \ddots & \vdots \\ 0 & 0 & \cdots & 1 \end{bmatrix} - j\begin{bmatrix} m_{11} & m_{12} & \cdots & m_{1n} \\ m_{21} & m_{22} & \cdots & m_{2n} \\ \vdots & \vdots & \ddots & \vdots \\ m_{n1} & m_{n2} & \cdots & m_{nn} \end{bmatrix} \tag{2.63}$$

or $\quad \left[A\right] = \left[q\right] + p\left[U\right] - j\left[m\right]$

where [*A*] is the sum of three *n* x *n* matrices, [*U*] is the *n* x *n* identity matrix, [*q*] is an *n* x *n* quality factor matrix, [*m*] is an *n* x *n* coupling matrix.

In a case of filters with lossless resonators, the coupling matrix equation is derived in a similar way to that for filters with finite Q_u by not considering the loss resistance in the all resonators. Thus, the matrix [*A*] for the lossless filter is defined as [7]

$$[A]=\begin{bmatrix} \frac{1}{q_{e1}} & 0 & \cdots & 0 \\ 0 & 0 & \cdots & 0 \\ \vdots & \vdots & \ddots & \vdots \\ 0 & 0 & \cdots & \frac{1}{q_{en}} \end{bmatrix} + p\begin{bmatrix} 1 & 0 & \cdots & 0 \\ 0 & 1 & \cdots & 0 \\ \vdots & \vdots & \ddots & \vdots \\ 0 & 0 & \cdots & 1 \end{bmatrix} - j\begin{bmatrix} m_{11} & m_{12} & \cdots & m_{1n} \\ m_{21} & m_{22} & \cdots & m_{2n} \\ \vdots & \vdots & \ddots & \vdots \\ m_{n1} & m_{n2} & \cdots & m_{nn} \end{bmatrix} \tag{2.64}$$

The S-parameter equations for the lossless filter circuits are the same as the equations for the filter with finite Q_u (equations (2.62a) and (2.62b)).

2.3 Coupling Matrix for Antenna-Filters

Previously, the antenna and microwave filter theories have been presented and related to the work in this thesis. Both theories will be used for the new design, involving antenna and filter integration based on the coupled resonator filter theory [7]. The antenna theory will then be applied to design the dipole antennas in Chapter 3 and 4, and waveguide aperture antennas in Chapter 5. The antennas will then be designed to perform as resonators integrated into the coupled resonator circuit. As a first step, we will follow the study of the coupled resonator filter theory to design a conventional two-port bandpass filter using all the dipole antennas as resonators presented in Chapter3. The principle of the work will then be used to design an antenna-filter in which all resonators are dipole antennas with the second port replaced as the radiation port. All the designs in this work are presented in Chapter 4 and are designed using the coupling matrix synthesis. Figure 2.21(a) shows a topology of n-coupled resonator antenna-filter; where the white circles represent resonators, the solid lines linking resonators represent couplings and a dashed line with an arrow represents radiation from the antenna. The coupling matrix equation for this topology can be derived in a similar way of to that given in Section 2.2.5, considering the external output as the source of radiation ($q_{en} = q_{rn}$)

and assuming the antenna is lossless. The coupling matrix equation of the topology in Figure 2.21(a) is defined as

$$[A]=\begin{bmatrix} \frac{1}{q_{e1}} & 0 & \cdots & 0 \\ 0 & 0 & \cdots & 0 \\ \vdots & \vdots & \ddots & \vdots \\ 0 & 0 & \cdots & \frac{1}{q_{rn}} \end{bmatrix} + p\begin{bmatrix} 1 & 0 & \cdots & 0 \\ 0 & 1 & \cdots & 0 \\ \vdots & \vdots & \ddots & \vdots \\ 0 & 0 & \cdots & 1 \end{bmatrix} - j\begin{bmatrix} m_{11} & jm_{12} & \cdots & jm_{1n} \\ jm_{21} & m_{22} & \cdots & jm_{2n} \\ \vdots & \vdots & \ddots & \vdots \\ jm_{n1} & jm_{n2} & \cdots & m_{nn} \end{bmatrix} \tag{2.65}$$

or $\quad [A]=[q]+p[U]-j[m]$

where $[A]$ is the sum of three n x n matrices, $[U]$ is an n x n identity matrix, $[q]$ is an n x n quality factor matrix, $[m]$ is an n x n matrix of coupling factors.

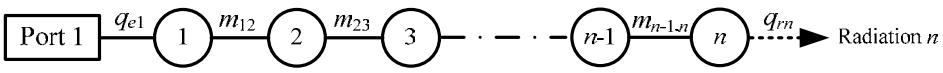

(a)

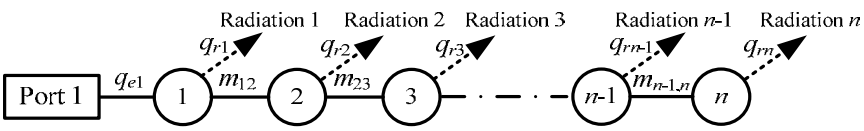

(b)

Figure 2.21 The coupling topology diagram of n-coupled resonator antenna-filter for (a) The last resonator is the antenna (Chapter 5), (b) All resonators are antennas (Chapter 4).

Figure 2.21(b) shows the topology of an n-coupled resonator antenna-filter in which all resonators are antennas, the white circles represent antennas. The coupling matrix equation for this topology can be derived in a similar way to that shown in Section 2.2.5, assuming that the antennas are lossless. The coupling matrix equation of the topology in Figure 2.21(b) is defined as

$$[A]=\begin{bmatrix} \frac{1}{q_{e1}}+\frac{1}{q_{r1}} & 0 & \cdots & 0 \\ 0 & \frac{1}{q_{r2}} & \cdots & 0 \\ \vdots & \vdots & \ddots & \vdots \\ 0 & 0 & \cdots & \frac{1}{q_{rn}} \end{bmatrix}+p\begin{bmatrix} 1 & 0 & \cdots & 0 \\ 0 & 1 & \cdots & 0 \\ \vdots & \vdots & \ddots & \vdots \\ 0 & 0 & \cdots & 1 \end{bmatrix}-j\begin{bmatrix} m_{11} & jm_{12} & \cdots & jm_{1n} \\ jm_{21} & m_{22} & \cdots & jm_{2n} \\ \vdots & \vdots & \ddots & \vdots \\ jm_{n1} & jm_{n2} & \cdots & m_{nn} \end{bmatrix} \quad (2.66)$$

or $\quad [A]=[q]+p[U]-j[m]$

where [*A*] is the sum of three *n* x *n* matrices, [*U*] is the *n* x *n* identity matrix, [*q*] is an *n* x *n* quality factor matrix, [*m*] is an *n* x *n* coupling matrix.

This is a one port component which is considered only the reflection coefficient S_{11}. The magnitude of S_{11}, for this coupling matrix is given by

$$S_{11}=\pm\left(1-\frac{2}{q_{e1}}[A]_{11}^{-1}\right) \quad (2.67)$$

The coupling matrix for equation (2.66) can be utilised to design the antenna-filter using the dipole antennas which will be presented in Chapter 4. Also, the coupling matrix for equation (2.65) can be utilised in the design of waveguide antenna-filters in Chapter 5.

2.4 CST Microwave Studio®

High frequency (HF) components are usually designed and simulated using Electromagnetic (EM) simulators in order to analyse their parameters such as *S*-parameters, radiation patterns,..etc.. The EM simulator uses the Maxwell's equation solver to analyse the modeled structure depending on the boundary conditions. It also uses numerical methods in order to

obtain accurate results. The numerical methods consist of finite element method (FEM), finite different time domain method (FDTD), method of moment (MOM) and integral equation method (IEM). Each method is suitable for specific type of calculation. The main requirements of users for the EM simulator are easy in use, fast simulation and high accurate results. The structures of designed components presented in this thesis have been simulated using CST Microwave studio software [5]. This section provides an overview of CST software in Section 2.4.1 and a few instruction of CST usage.

2.4.1 CST Microwave Studio® Overview

CST Microwave studio [5] is an EM commercial simulation software and can provide those requirements of users. This software includes 3D solver, circuit simulator and optimiser. The solvers in CST software package consist of a transient domain (TD) solver, frequency domain (FD) solver, Eigenmode (EM) solver, Integral equation (IE) solver, Asymptotic (A) solver and TLM solver. The work presented in this thesis is to design an antenna-filter which will be simulated in the open boundary with add space using a solver in CST software package. Here TD solver is a simulation tool for structures designed in the opened boundary using the finite frequency domain (FDTD) method. This solver is suitable for use in this work and shows good agreement between simulation and the measurement results.

2.4.2 Instruction for using CST Microwave Studio®

Figure 2.22 shows a beginning of opened CST software usage. It shows a new project creator which provides the supporting templates for user in order to set up the new project. It can be

used for selecting a appropriate template to design a component. For an example, 'Antenna (Wire)' is for design a wire dipole antenna.

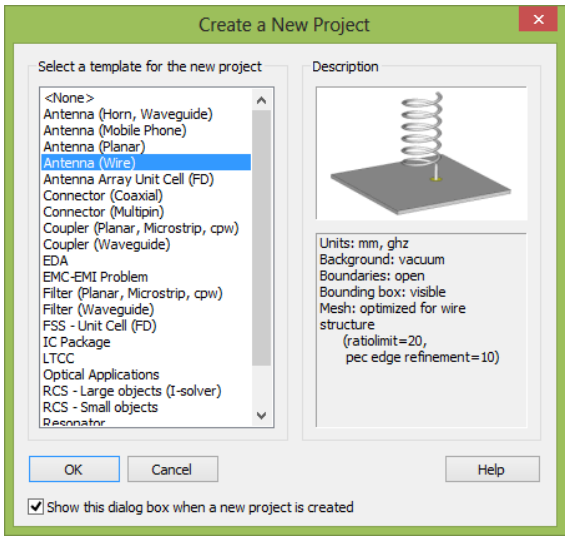

Figure 2.22 Design templates for the new project in CST.

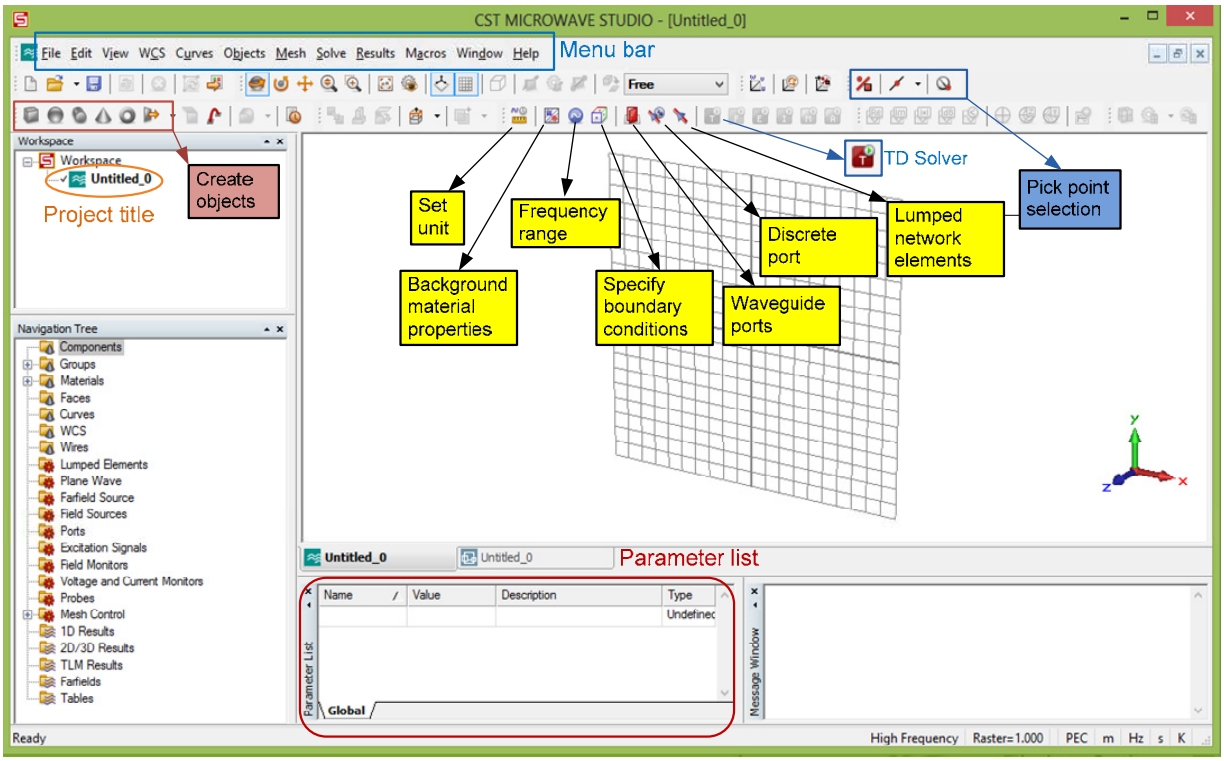

Figure 2.23 First use of CST microwave studio software.

After created the project, the CST microwave studio software will be displayed in Figure 2.23. In the CST software, there are many tools displayed as small icons. It is used for setting up the design project. Here we will describe only the most tools shown in Figure 2.23 for basic users. The tool box usage in CST microwave studio software will be described in step by step as follows:

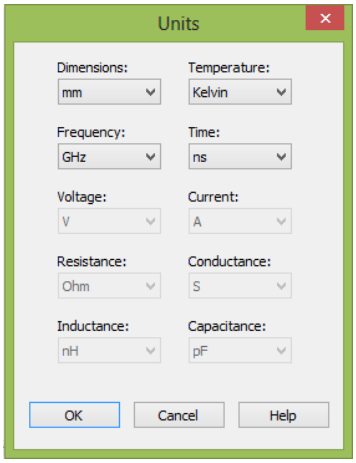

Figure 2.24 Unit setting menu.

Step 1, the units is firstly setting up in a design of component and is shown in Figure 2.24. It can be set the required units that normally include the dimension, frequency, temperature and time units.

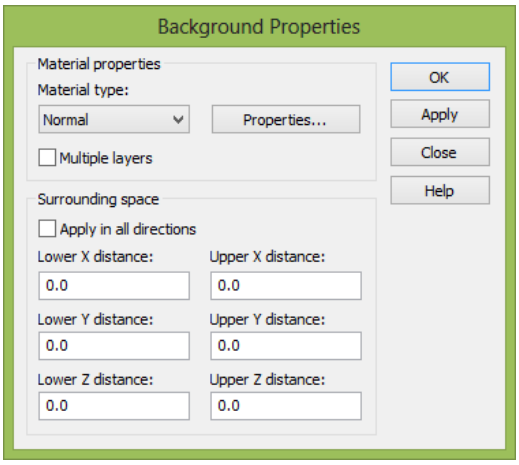

Figure 2.25 Background property setting menu.

Step 2, the background properties in CST are used for setting the material property environment in the simulation, as shown in Figure 2.25. This can be selected the material type that includes normal, PEC, Anisotropic and lossy material depending on the design. In this thesis, a normal material has been chosen to design antenna-filters and is also a lossless material in the free-space.

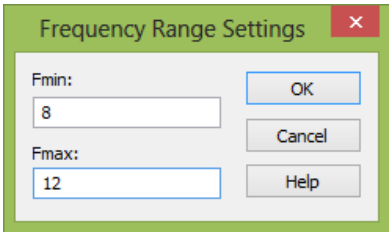

Figure 2.26 Frequency setting menu.

Step 3, the frequency operation for a design component can be set in the CST simulation by selecting a frequency range icon shown in Figure 2.23. Figure 2.26 shows a frequency setting menu and displays Fmin and Fmax, where Fmin is a frequency minimum and Fmax is a frequency maximum (Fmax). For example, an X-band frequency is set for Fmin = 8 GHz and for Fmax = 12 GHz.

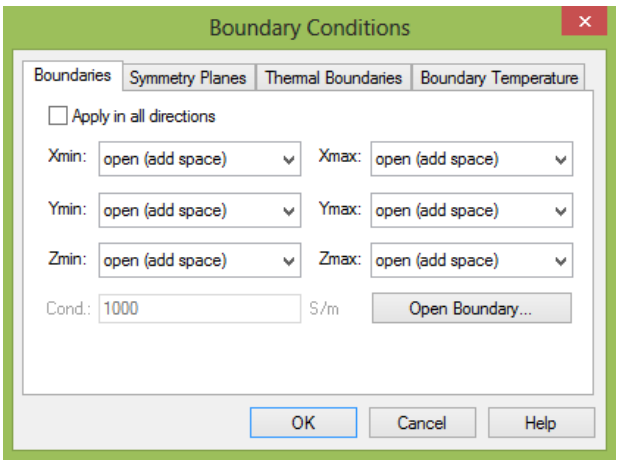

Figure 2.27 Boundary condition setting menu.

Step 4, this step is to describe the use of object tool and boundary condition setting menu for designing the structure. The object tools are used to create the structure by selecting the small icons shown on the left of Figure 2.23. It can be used to create a brick, a sphere, cylindrical, cone and torus shape. Materials of objects can be selected in the object's menu. After created objects, the boundary conditions for the structure need to be set in any direction as shown in Figure 2.27. It is depended on a type of component. For examples, an opened with add space boundary condition in all directions is set for an antenna in simulation, an electric (Et = 0) boundary condition in all directions is set for a waveguide cavity filter in simulation.

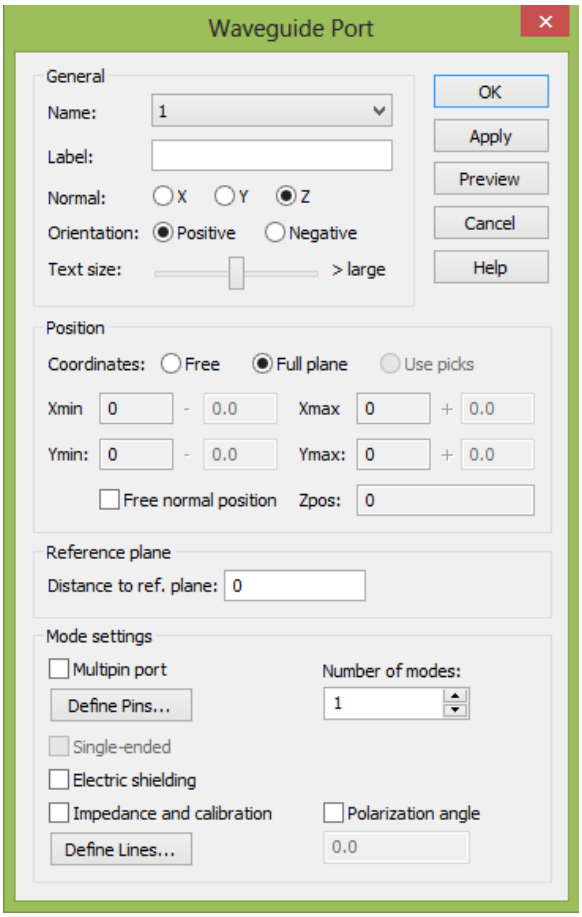

Figure 2.28 Waveguide port setting menu.

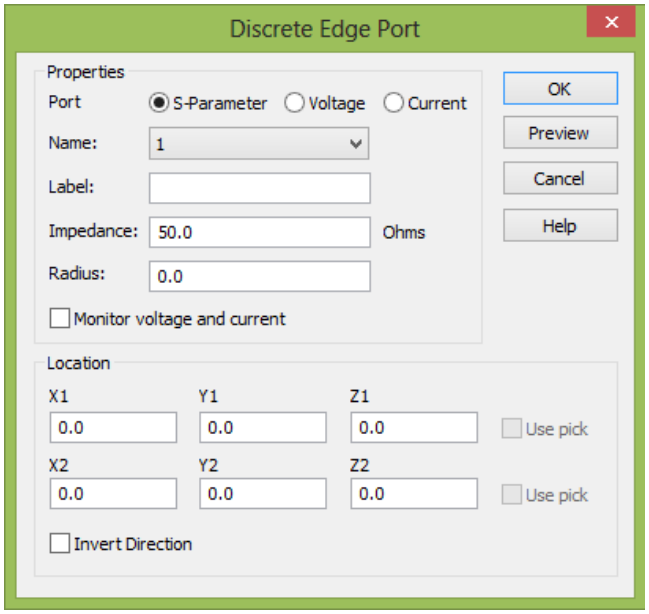

Figure 2.29 Discrete edge port setting menu.

Step 5, ports or input/output terminations of components in CST software is depended on a component type and can be made as a waveguide port and a discrete edge port. Figure 2.28 shows a menu for setting ports that is used to define a waveguide port in simulation. This can be set a label port, orientation in positive or negative, and coordinates in full plane for a waveguide and in free plane for a microstrip. Figure 2.29 shows a menu for setting ports that is used to define a discrete edge port in simulation. This can be set a label port, impedance (default as 50 ohms), radius of the port and location of the port. This port is usually defined for a wire dipole antenna and will be presented in this thesis.

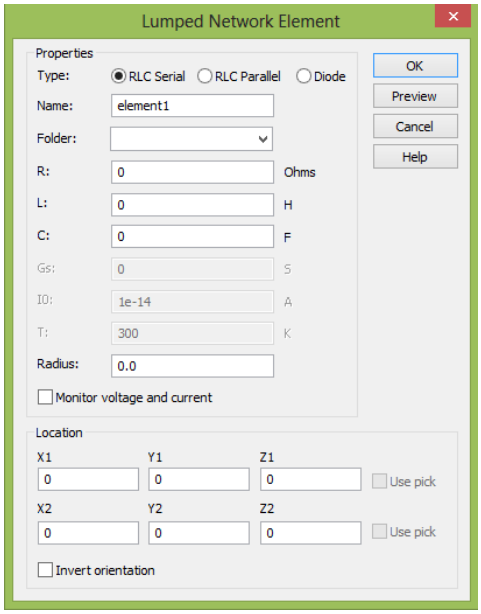

Figure 2.30 Lumped network element setting menu.

Step 6, lumped network element can be set in 3D simulation by choosing the menu shown in Figure 2.30. It can be selected to create three lumped element circuit types which include a RLC serial, RLC parallel and diode circuit. This menu can be used to set the values of each element, radius of element and location of element. The lumped network element will be used to design an inductor presented in Chapter 3 and 4.

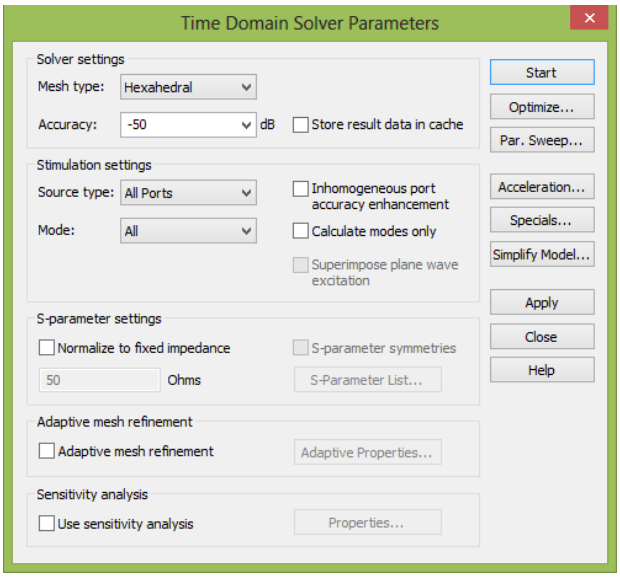

Figure 2.31 TD solver setting menu.

After completed all of those setting, we can simulate the structure using solvers in CST software. Here time domain (TD) solver is only selected for antenna-filter design in this thesis. TD solver has a menu shown in Figure 2.31 and is used to set the accuracy (medium is '-50 dB') before starting to run the simulation. The CST optimiser is shown on the right of the TD solver menu. After opened optimiser, the CST optimiser menu will be displayed in Figure 2.32. Before running optimisation, the optimiser needs to be set the initial dimension parameter values (it is normally set to be vary about 5 %) with algorithm (default is 'Trust Region Framework') to search the best matched values depending on the goals. The goal setting menu is used to set the condition to achieve the desired *S*-parameter values and is shown in Figure 2.33. For an example, the goal is set to achieve the target for the S_{11} < -20dB in the frequency range from 9 GHz to 11 GHz.

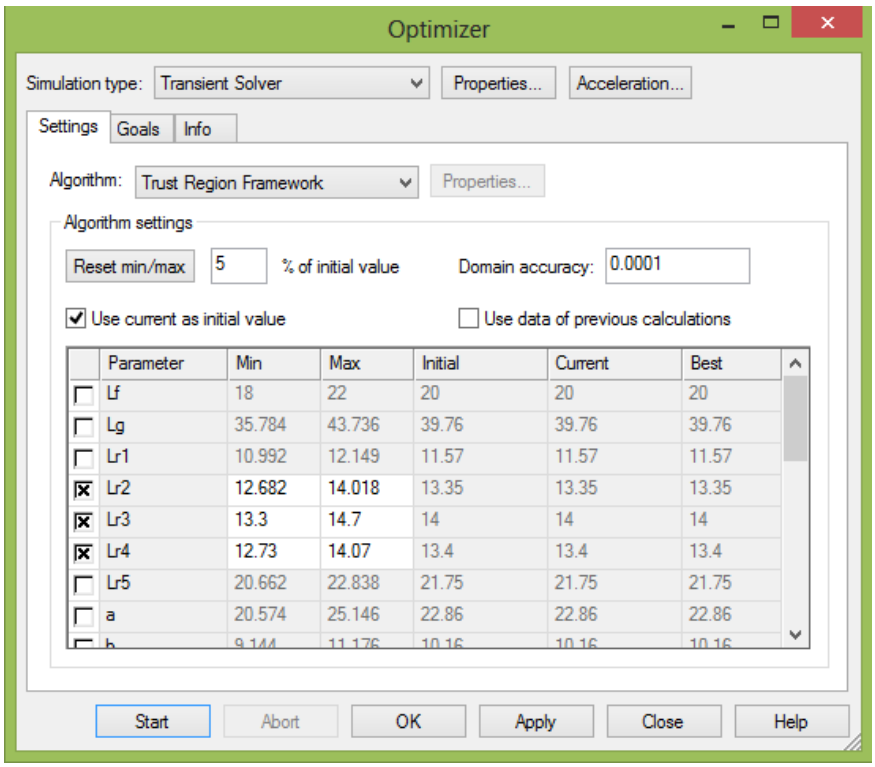

Figure 2.32 CST optimiser setting menu.

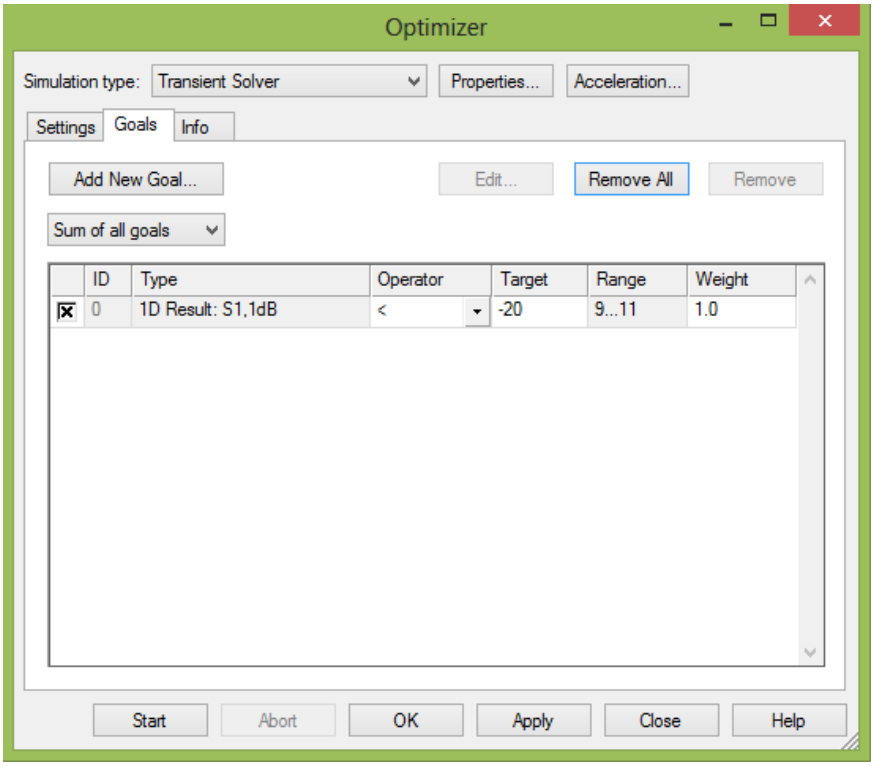

Figure 2.33 Goal setting menu in CST optimiser.

References

[1] Kraus J. D. and Marhefka R. J. Antennas For All Applications. 3rd ed. New York, USA: McGraw-Hill; 2003.

[2] Balanis C. A. Antenna Theory Analysis and Design. 3rd ed. New Jersey, USA: John Wiley & Sons; 2005.

[3] Stutzman W. L. and Thiele G. A. Antenna Theory and Design. 3rd ed. New Jersey, USA: John Wiley & Sons; 2013.

[4] Best S. R. The Foster Reactance Theorem and Quality Factor for Antennas. IEEE Antennas Wireless Propag. Lett. 2004 Dec.; 3(1): 306-309.

[5] Computer Simulation Technology (CST), Microwave Studio [Internet]. 2014 Available from URL: http://www.cst.com.

[6] Pozar D. M. Microwave Engineering. 3rd ed. USA: John Wiley & Sons; 2005.

[7] Hong J. S. and Lancaster M. J. Microstrip Filters for RF/Microwave Applications. New York, USA: John Wiley & Sons; 2001.

[8] Koryu Ishii T. Microwave Engineering. 2nd ed. USA: Oxford University Press; 1995.

Chapter 3

Two-Port Dipole Bandpass Filter

3.1 Introduction

The advantages of integrating RF/microwave components into a single module are to reduce the microwave component count and miniaturise the total circuit area, and additionally improve the noise and interference performance in the system. An antenna and a bandpass filter are essential components employed at the front-end. An antenna is used for transmitting and receiving RF signals [1], whereas a bandpass filter selects the required frequencies and rejects unwanted frequencies. Usually the input impedance of the antenna and the output impedance of the bandpass filter are different. A matching network is therefore required [2] to improve power transfer. The integration of an antenna and a bandpass filter is considered here as a new RF component called an *antenna-filter*.

In this chapter, a new design approach of antenna and filter integration will be started from a bandpass filter designed using the antennas. This work is to demonstrate the antenna elements which can serve as resonators of the filter, as well as performing their role as radiating elements [3]. Here a dipole antenna is selected to design a resonator. The structure of dipole is simple and can be arrayed as a side-by-side structure corresponding to the structure of a coupled resonator filters [4]. The antenna and filter theories in [1] and [4] are used in order to simplify the problem initially and get a good understanding in the design approach. From a filter point of view the radiation from the antennas represent significant source of loss for each resonator. At this stage no account is taken of the radiation pattern. This design describes the initial concepts of an antenna-filter design based on the coupled

resonator filter theory. The proposed component will be called a *Two-port dipole bandpass filter*. The measurements for the fabricated prototype are also presented in this chapter.

3.2 Resonator Design

This section presents a new method in the resonator design based on the structure of dipole antennas. This work is firstly to study an equivalent circuit of a dipole antenna, which is considered as a series resonant circuit [2]. This equivalent circuit will then be considered for extracting the quality factor of antennas [5]. Here the quality factor of dipole is only considered as the radiation quality factor (Q_r), since the antenna is made from a lossless material. This will be described in Section 3.2.1. The dipole antenna will be designed as a resonator with an inductor to control the Q_r and the centre frequency f_0. This will be presented in Section 3.2.2. The unloaded quality factor of resonator dipole antenna is presented in Section 3.2.3.

3.2.1 Equivalent Circuit of Dipole Antenna in Simulation

In this section, a dipole antenna is selected and is designed at the centre frequency (f_0) of 1 GHz [1]. For simplicity in the design, the dipole antenna is assumed to be made from a lossless material (i.e. a Perfect Electric Conductor or PEC) in the CST simulation software [6] and shown in Figure 3.1(a).

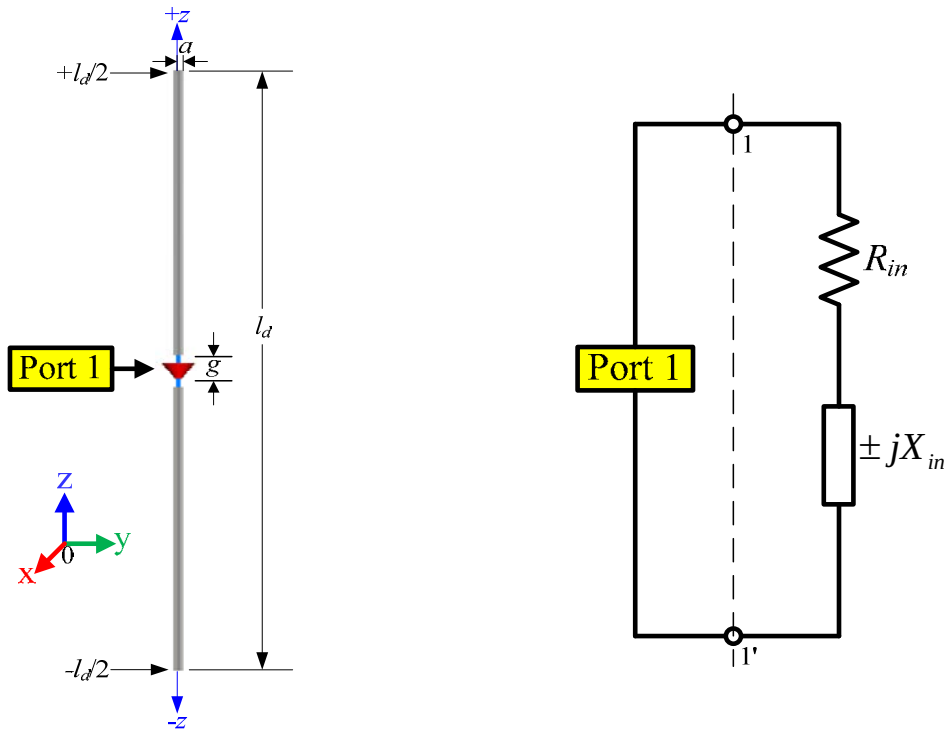

(a) (b)

Figure 3.1 A lossless dipole antenna (a) Geometry of the dipole antenna in CST simulation software [6]. $a = \lambda_0/400$, $g = \lambda_0/60$, $l_d = 0.1\lambda_0 - 0.5\lambda_0$. (b) Equivalent circuit of Figure 3.1(a).

The simulated antenna structure shown in Figure 3.1(a) is designed corresponding to the ideal dipole antenna. The structure is considered as a lossless dipole antenna due to no conductor loss taken in simulation. According to the theory described in Section 2.1.2.1, the equivalent circuit of Figure 3.1(a) is therefore considered as a R_{in} and X_{in} series circuit and is shown in Figure 3.1(b); where R_{in} is the radiation resistance at input terminals, X_{in} is the antenna reactance at input terminals. Here, both R_{in} and X_{in} element values can be extracted from the simulation results of its input impedance (Z_{in}) obtained at 1 GHz (f_0) using CST simulation software [6]. R_{in} is extracted from the simulated real part (Re.) of Z_{in}. X_{in} is extracted from the simulated imaginary part (Im.) of Z_{in}. In this work, both R_{in} and X_{in} values of the simulated dipole will be obtained for different values of dipole length l_d. In this work, we will select the

dipole length l_d from $0.1\lambda_0$ to $0.5\lambda_0$, which are suitable lengths for use to fabricate the devices. These R_{in} and X_{in} will then be used to obtained its quality factor (Q) used to design the resonator in Section 3.2.2. The curves of simulated values of R_{in} and X_{in} versus l_d are shown in Figure 3.2(a) and 3.2(b), respectively. The simulated values of R_{in} and X_{in} show the corresponding results with the calculation results presented in Section 2.1.2.1.

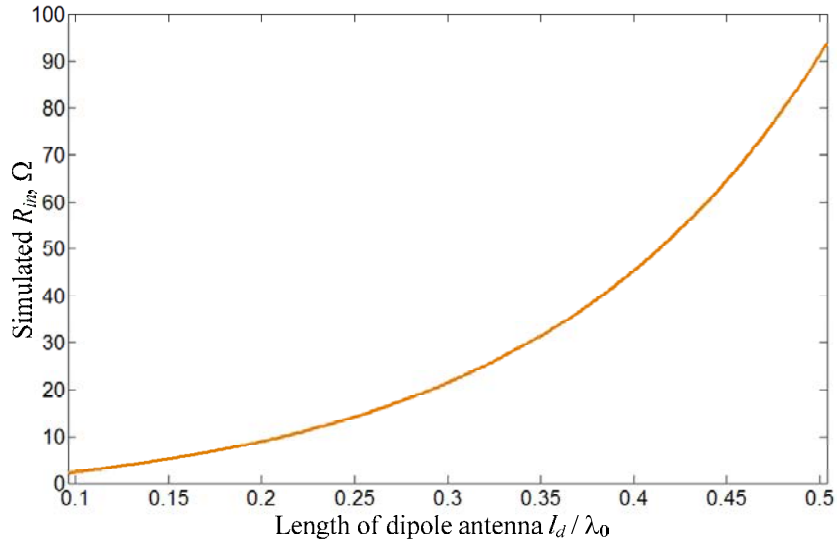

(a)

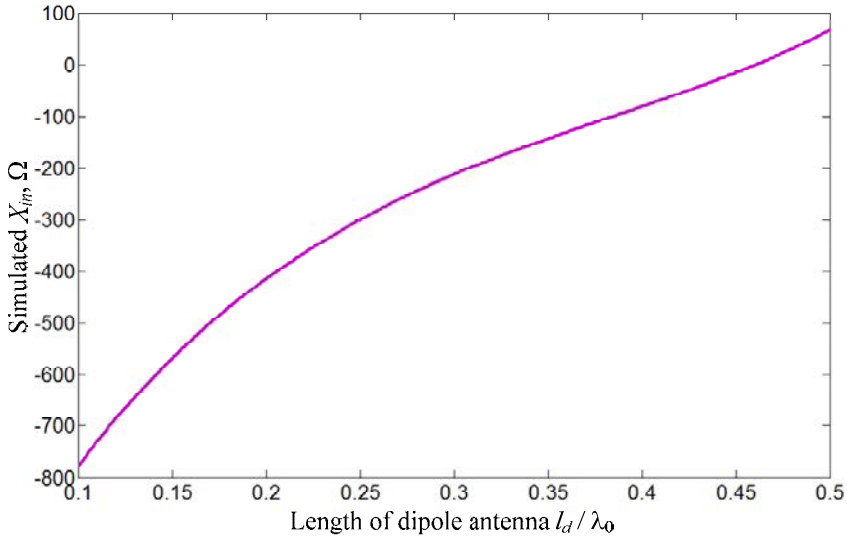

(b)

Figure 3.2 (a) The simulated R_r for different values of l_d. (b) The simulated X_A for different values of l_d.

3.2.2 Design of Dipole Antenna with Inductor

This section presents the resonator design method based on the structure of dipole antenna comparing with its quality factor Q. The quality factor Q is a parameter which is firstly considered and used to design a resonator in this work. It will then be extracted from the simulated structure of lossless dipole antenna in Section 3.2.1. The quality factor of lossless dipole antenna is only considered for the radiation and is defined as *the radiation quality factor* (Q_r). Here Q_r can be extracted in a similar way described in from Section 2.1.2.2 using the simulated values of R_{in} and X_{in} with the use of equation (2.25). A curve of simulated Q_r versus the length l_d is shown in Figure 3.3. The simulated values of Q_r show that it is corresponded to the calculated results presented in Section 2.1.2.2.

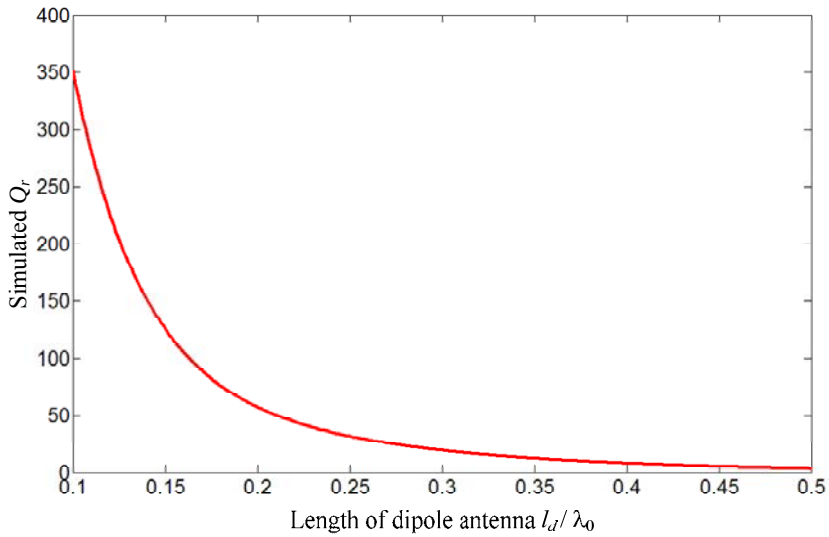

Figure 3.3 The radiation quality factor Q_r obtained from CST simulation.

For designing a dipole antenna to serve as a resonator, the reactive element (X_{in}) of a dipole antenna is considered to analyse the circuit behavior. The dipole behaves as a capacitive element (C_A) for l_d from about $0.1\lambda_0$ to $0.47\lambda_0$. To form a complete *RLC* series resonant circuit [2] an inductor (L) is required in order to complete the resonant circuit. Here this

inductor is integrated with the dipole antenna to achieve a resonant frequency of 1 GHz. Figure 3.4(a) shows a simulation model for a dipole antenna with an inductor *L*. The equivalent circuit of the simulated structure, shown in Figure 3.4(a), can be represented as a *RLC* series resonant circuit, as presented in Figure 3.4(b).

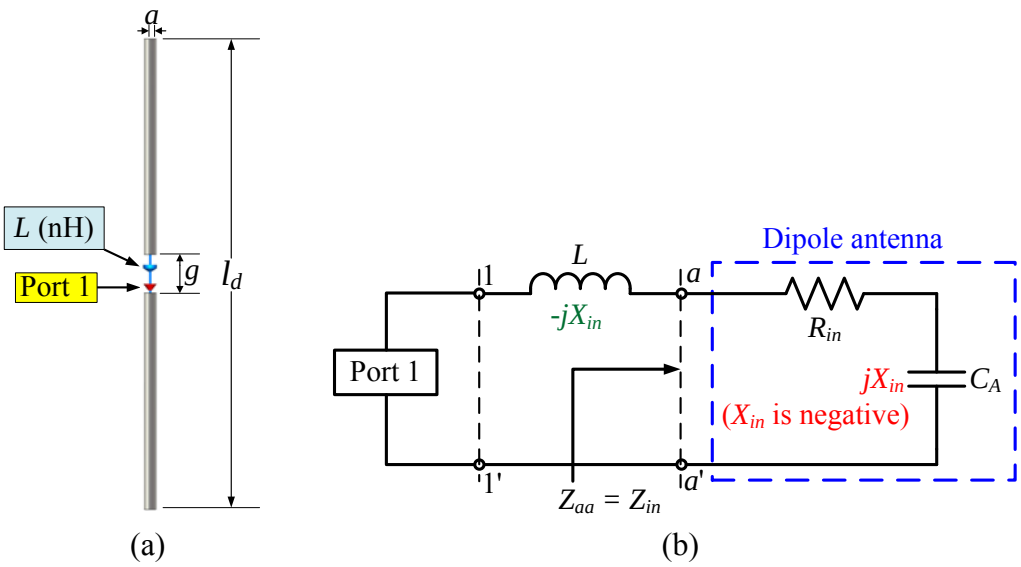

Figure 3.4 (a) The lossless dipole antenna with an inductor (*L*). (b) The equivalent circuit of a lossless dipole antenna with the inductor (*L*).

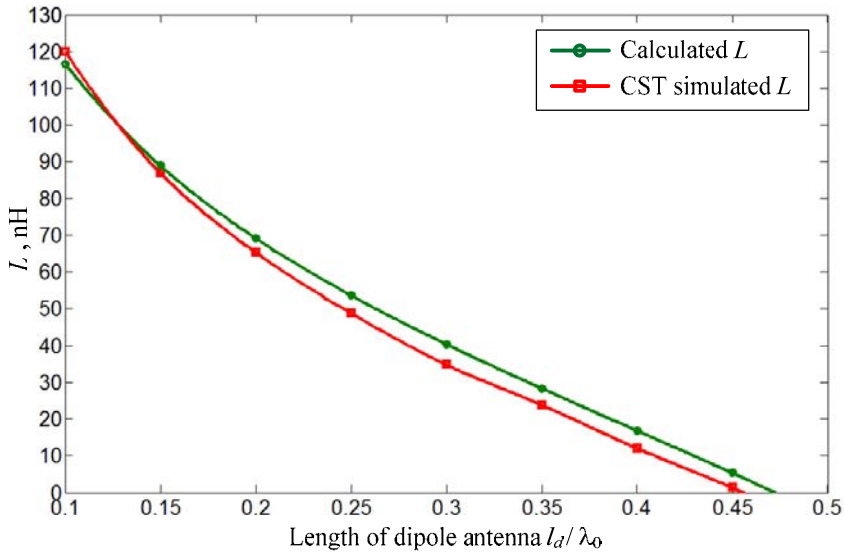

Figure 3.5 The inductance of *L* for different values of l_d, obtained from calculations and CST simulations enabling it to resonate at 1 GHz.

An inductor L, for each l_d value, can be designed using the antenna reactance X_{in} value obtained from calculation and simulation at the centre frequency (f_0) and is defined as

$$L(l_d) = \frac{-X_{in}(f_0)}{2\pi f_0} \tag{3.1}$$

Equation (3.1) can be used to extract the required inductance of L versus the dipole length l_d by using calculated and simulated X_{in} values. Simulation results of inductance variations as a function of length l_d are compared with the calculation results as shown in Figure 3.5. The centre frequency f_0 is taken at 1 GHz. An $0.1\lambda_0$ dipole antenna integrated with an inductor of 120 nH is an example to demonstrate its design. The simulated reflection coefficient (S_{11}) illustrated in Figure 3.6 exhibits a resonant frequency of 1 GHz corresponding to a response of a resonator of filter designed at 1 GHz. This can be confirmed that dipole antenna with an inductor serves as a resonator of filter.

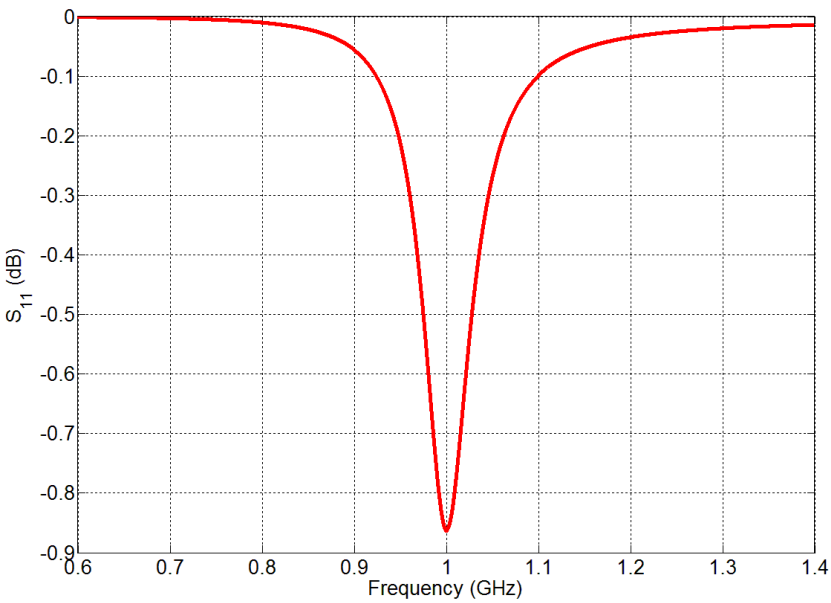

Figure 3.6 An example of simulated response of S_{11} (dB) for the $0.1\lambda_0$ dipole ($a = \lambda_0/400$, $g = \lambda_0/60$) with the inductor of 120 nH conforming resonance at 1 GHz.

3.2.3 Unloaded Quality Factor

The total unloaded quality factor of a resonator (a dipole antenna with an inductor) may be defined by adding these losses as follows [4],

$$\frac{1}{Q_u} = \frac{1}{Q_c} + \frac{1}{Q_r} + \frac{1}{Q_{ind}} \tag{3.2}$$

where Q_c, Q_r, Q_{ind} are the conductor, radiation and inductor quality factors, respectively.

In this work, the dipole antenna is made from copper. This is associated with the loss resistance (R_l) of antennas, which is considered to obtain the quality factor Q_c described in Section 2.1.2.1. The loss resistance R_l of a dipole antenna is calculated using equation (2.17). The R_l value will then be used instead of R_{in} (f_0) in equation (2.25) to obtained Q_c of dipole antenna. For example, the calculated R_l value for a $0.1\lambda_0$ dipole antenna operating at 1 GHz is found using equation (2.17), to be 0.0175 ohms. The calculated R_l is employed to calculate the Q_c value, using equation (2.25). The calculated Q_c is about $4.9\text{x}10^4$. It implies that the Q_c value has negligible effect on the total unloaded Q of resonator. Thus, the total unloaded Q factor of a resonator (a dipole antenna with an inductor) can be defined as

$$\frac{1}{Q_u} = \frac{1}{Q_{ind}} + \frac{1}{Q_r} \tag{3.3}$$

where Q_r obtained from simulation is 380 for a $0.1\lambda_0$ dipole antenna and the Q_{ind} can be obtained from the physical dimensions of the inductor and is 320, which will be described in Section 3.4. Thus, the total Q_u results as 174.

3.3 Design of Two-Port Dipole Bandpass Filter

A new design of a third-order bandpass filter using dipole antennas is presented in this section. The proposed component is designed using the concept of conventional coupled

resonator filter [4]. The structure of the dipole bandpass filter with two electrical ports (not including radiation as a port) is shown in Figure 3.7. It consists of an array of three dipole antennas with inductors (i.e. resonators) and two input/output feeds. The proposed structure corresponds to an inline topology, as shown in Figure 3.8.

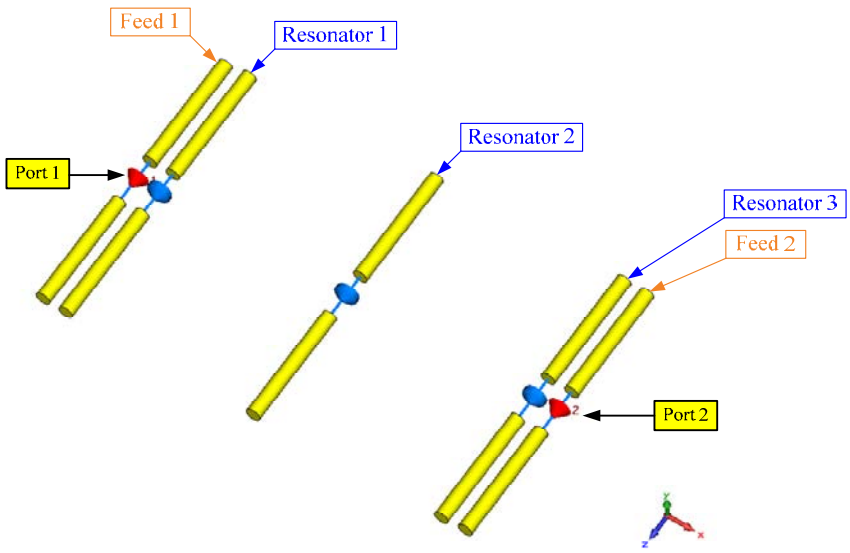

Figure 3.7 The structure of the 3rd dipole bandpass filter in three-dimensions. The blue parts are inductors. The red symbols represent the ports.

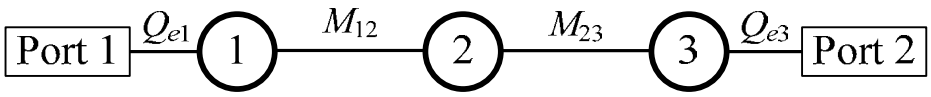

Figure 3.8 The coupling topology of 3rd order dipole bandpass filter.

The third-order dipole bandpass filter is designed to have a 2% fractional bandwidth (FBW = 0.02) at a centre frequency of 1 GHz (f_0 = 1GHz). A third-order Chebyshev lowpass prototype with a return loss of 20 dB is chosen. The corresponding g values for the 3rd order Chebyshev lowpass prototype filter with a 20 dB return loss calculated using equation (2.38) are: g_0 =1.0, g_1 = 0.8516, g_2 = 1.1032, g_3 = 0.8516, and g_4 = 1.0. The g-element values are used to calculate

the external quality factors (Q_e) and coupling coefficients (M) using the equations (2.49) given below

$$Q_{e1} = \frac{g_0 g_1}{FBW},\ Q_{en} = \frac{g_n g_{n+1}}{FBW},\ M_{i,i+1} = \frac{FBW}{\sqrt{g_i g_{i+1}}} \quad \text{for } i = 1 \text{ to } n-1 \tag{3.4}$$

From the bandpass filter's specifications, Q_{e1}, Q_{en} and $M_{i,i+1}$ are calculated to be: $Q_{e1} = Q_{e3} = 42.58$ and $M_{12} = M_{23} = 0.0206$. These Q_e and M values correspond to the coupling topology shown in Figure 3.8. The coupling matrix for a lossless filter, given in Chapter 2, is employed to observe the frequency response of bandpass filter using the obtained values for Q_e and M. Figure 3.9 shows the ideal response of the designed bandpass filter plotted using equations (2.62) from Chapter 2. This calculated response is assumed no losses including in the design for observing the filter performance. It should be noted that the performance of the proposed design might not be realised as similar to the performance of this ideal filter, since it does not take into account losses from the radiation and loss resistance of inductors.

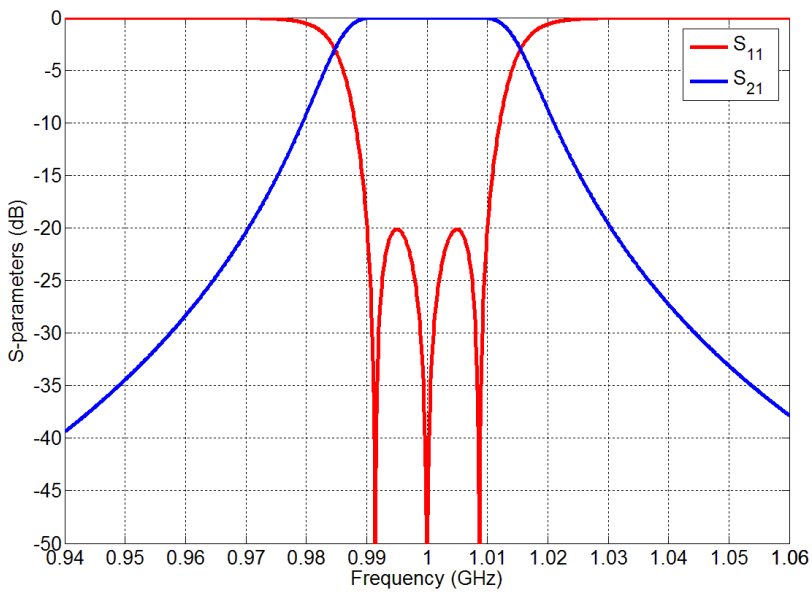

Figure 3.9 Ideal S-parameter response of the 3rd order dipole bandpass filter calculated from the coupling matrix.

3.4 Realisation of Two-Port Dipole Bandpass Filter

This section presents design, simulation and measurement of two-port dipole bandpass filter. In order to realise dipole antennas as resonators, the inductors are firstly considered in the resonator design based on the frequency of operation, size and quality factor. In this work, air coil inductors are chosen in fabrication. The design procedure and fabrication will be described in Section 3.4.1. The inductor parameters (L, Q_{ind}) obtained from Section 3.4.1 will then be taken into the CST simulations to obtain physical dimensions in terms of quality factors (Q) and coupling coefficient (M) in Section 3.4.2 and 3.4.3, respectively. The simulation and measurement results are discussed and presented in Section 3.4.4 and in Section 3.4.5, respectively

3.4.1 Air Coil Inductor Design

This section presents the design procedure of air coil inductor following the conventional design in [7]. The layout in two-dimensions of the air coil is illustrated in Figure 3.10.

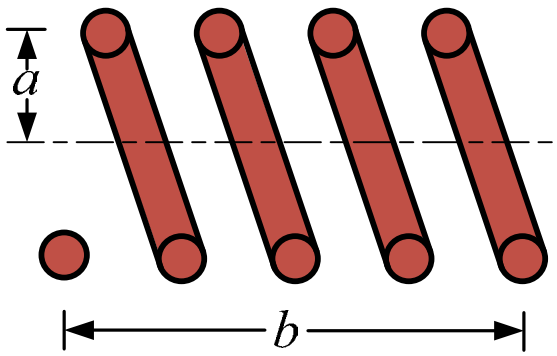

Figure 3.10 Air coil model in the calculation of inductance [7].

The inductance (L) of an air coil can be obtained approximately from the geometry shown in Figure 3.10, given by [7]

$$L = \frac{\mu_0 \pi a^2 n^2}{b + 0.9a} \tag{3.5}$$

where L is coil inductance (H), μ_0 is the permeability of free space ($\mu_0 = 4\pi$ x 10^{-7} H/m), n is total number of turns, a is coil radius (mm), b is coil length (mm).

The inductor presented in this work is designed to exhibit an inductance of 120 nH. Equation (3.5) is used to estimate the air coil dimensions in order to match the inductance of 120 nH. The air coil dimensions are: the coil radius (a) is 0.7925 mm; the coil length (b) is 3.9 mm; and the number of turn (n) is 15 turns. The dimensions are used to fabricate the air coil inductors. Copper wire was employed for this purpose The wire had an American gage number 30 (AWG-30), which is 0.255 mm in diameter. The fabricated inductor was measured using a network analyser, as shown in Figure 3.11. The result is shown in Figure 3.12. It can be seen that the measured inductances corresponded to the desired values.

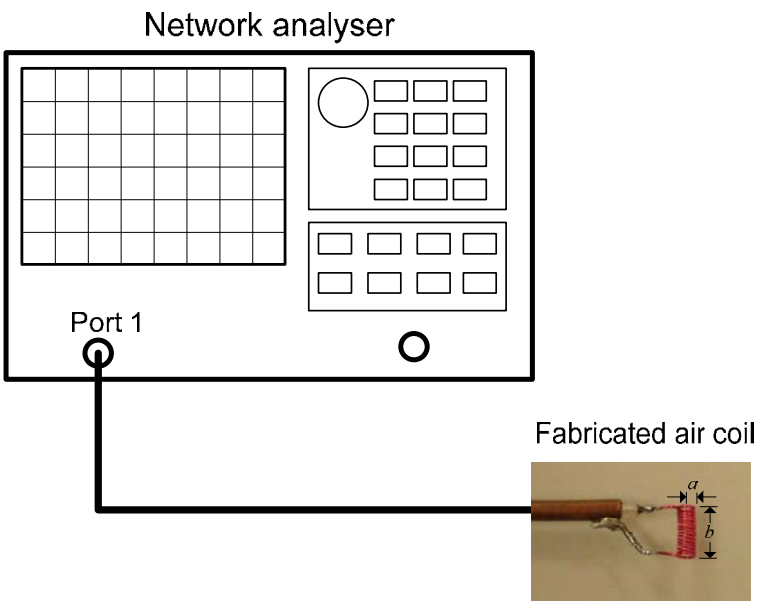

Figure 3.11 The measurement of an air coil inductance using the network analyser.

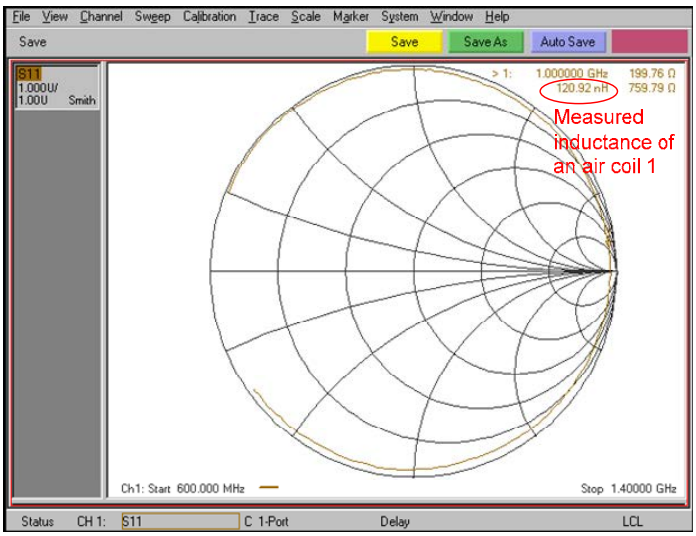

Figure 3.12 The measured inductance of an air coil from the network analyser.

In this work, the inductor will be made from a lossy conductor (i.e. copper wire), which will be considered to obtain the Q value of inductor. Here, the quality factor (Q_{ind}) of an air coil inductor is depended on the conductivity of material and the physical dimension. The quality factor Q_{ind} can be calculated using Wheeler's equation, given by [7]

$$Q_{ind} = \frac{a}{\delta\left(1+0.9\left(\frac{a}{b}\right)\right)} \tag{3.6}$$

where Q_{ind} is the quality factor of air coil inductor, a is the coil radius (mm), b is the coil length (mm), and δ is the skin depth of the metal, given by [7]

$$\delta = \frac{1}{\sqrt{\pi f \mu_0 \sigma}} \tag{3.7}$$

where f is the frequency (Hz), μ_0 is the permeability of free space ($\mu_0 = 4\pi \times 10^{-7}$ H/m), and σ is the conductivity of the metal (S/m).

The inductor quality factor (Q_{ind}) is associated with the loss resistance (R_{ind}) of the inductor, which will be modeled, in the CST simulation [6], using a lumped network element. The

lumped network element in CST simulation is used to model the equivalent circuit of lossy inductor, as shown in Figure 3.13.

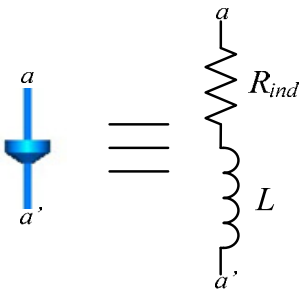

Figure 3.13 A lumped element in CST simulation is equivalent to a lossy inductor.

The inductor quality factor (Q_{ind}) in terms of lumped elements is defined by [4]

$$Q_{ind} = \frac{2\pi fL}{R_{ind}} \tag{3.8}$$

Rearranging equation (3.8),

$$R_{ind} = \frac{2\pi fL}{Q_{ind}} \tag{3.9}$$

where Q_{ind} is the quality factor of the air coil inductor, R_{ind} is the loss resistance of the air coil inductor (ohms), L is the inductance of the air coil (H), f is the frequency (f = 1 GHz)

Thus, the loss resistance R_{ind} can be calculated using equation (3.9). In this work, Q_{ind} calculated using equation (3.6), is 320 and R_{ind}, calculated at 1 GHz, is 2.32 ohms.

3.4.2 Extraction of External Quality Factor

The external quality factor (Q_e) of the input/output resonator, in the arrangement of the dipole antenna structure, shown in Figure 3.14 will be extracted. The input impedance for this pair of coupled dipoles may be changed due to the mutual coupling impedance between the elements [1]. The inductor needs to be recalculated using equation (3.1) with the simulated input reactance at 1 GHz, given as 87 nH. The Q_e value is obtained from the simulated magnitude

of S_{11} using the Q calculation method in [9]. The Q_e values versus the different length of l_f are shown in Figure 3.15.

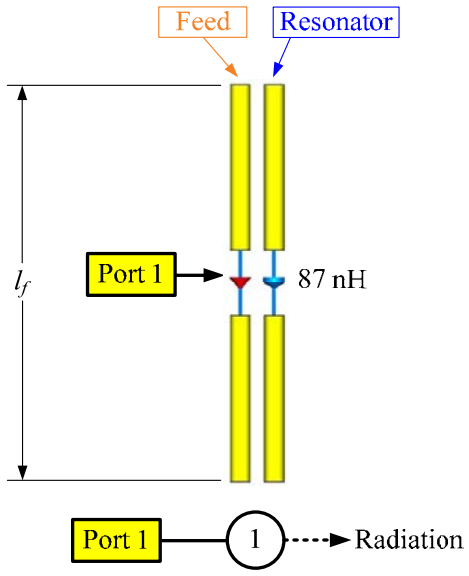

Figure 3.14 An antenna arrangement to extract Q_e.

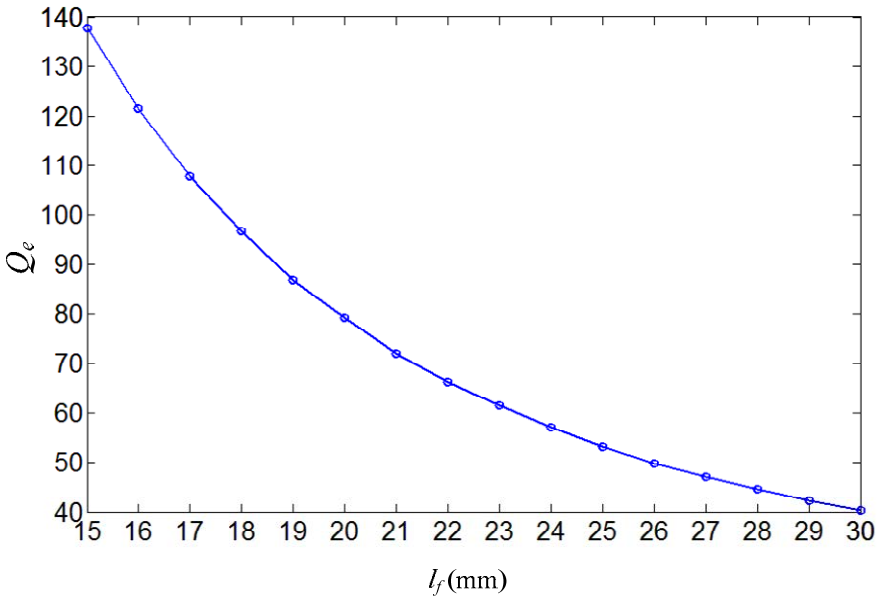

Figure 3.15 External quality factor (Q_e) obtained from CST simulation.

3.4.3 Extraction of Coupling Coefficient

In this section, the coupling coefficient between resonators will be extracted by rearranging two resonator dipole antennas to create weak input/output couplings, as shown in Figure 3.16(a). Simulated S_{21} response for the simulated structure of Figure 3.16(a) is depicted in Fig. 3.16(b). Two peak frequency (f_1 and f_2) are used to calculate the coupling coefficient value (M) using the equation given by [4]

$$M = \frac{f_2^2 - f_1^2}{f_2^2 + f_1^2} \tag{3.10}$$

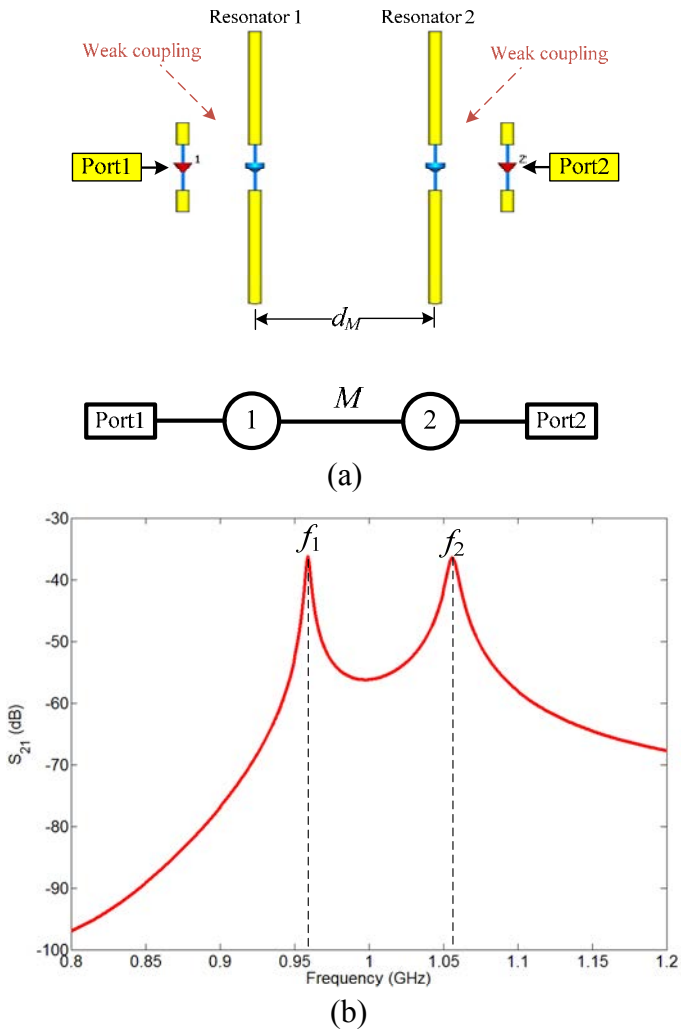

Figure 3.16 (a) Coupling structure of two coupled resonators. (b) Simulated resonant response of two coupled resonators for d_M = 9 mm.

The coupling coefficient (M) for different distances d_M between the two resonant dipole antennas is obtained from the simulated S_{21} with the use of equation (3.10) and is shown in Figure 3.17.

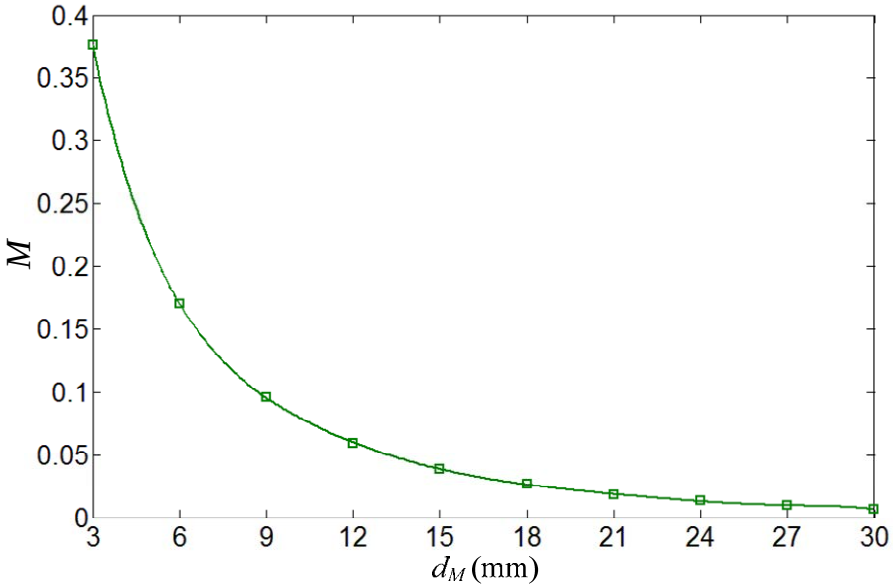

Figure 3.17 Coupling coefficients (M) as a function of d_M obtained from CST simulation.

3.4.4 Simulation Results

All of the dimensions of the 3rd order dipole bandpass filter are defined from the designed values (i.e. $Q_{e1} = Q_{e3} = 42.58$ and $M_{12} = M_{23} = 0.0206$) presented in Section 3.3. These designed values will then be compared with the Q_e values from the curve of Figure 3.15 and M value from the curve of Figure 3.17, in order to obtain the length l_f and the coupling distance d_M values, respectively. The l_f value corresponding with $Q_e = 42.58$ shown in Figure 3.15 is found to be 28.82 mm. Additionally, the d_M value corresponding with $M = 0.0206$ shown in Figure 3.17 is found to be 19.9 mm. These l_f and d_M values are utilised as the initial physical dimensions of the whole structure. The simulated S-parameter responses of the initial structure (before optimisation) are shown in Figure 3.18. The simulated response does not meet the requirement and can be improved with the use of the optimiser in CST software

package [6]. Starting from the initial response, the dipole bandpass filter has been optimised the length l_f of input/output feeds and coupling distance d_M between resonators to meet the goal (i.e. S_{11} <= 20 dB) at the passpand frequency. The final simulated *S*-parameter responses (after optimisation) are shown in Figure 3.18. The optimised structure corresponding to all of the dimensions parameters are depicted in Figure 3.19.

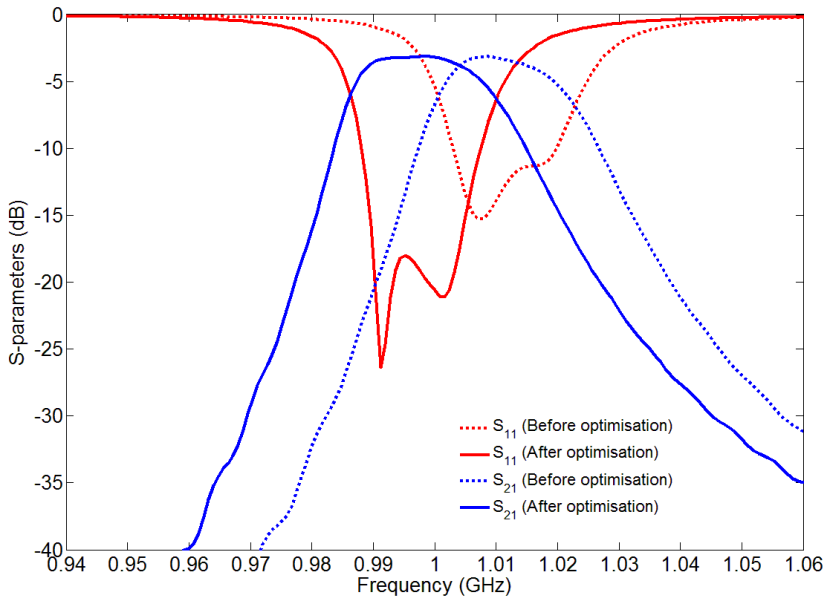

Figure 3.18 Simulated responses of 3rd order dipole bandpass filter before and after optimisation.

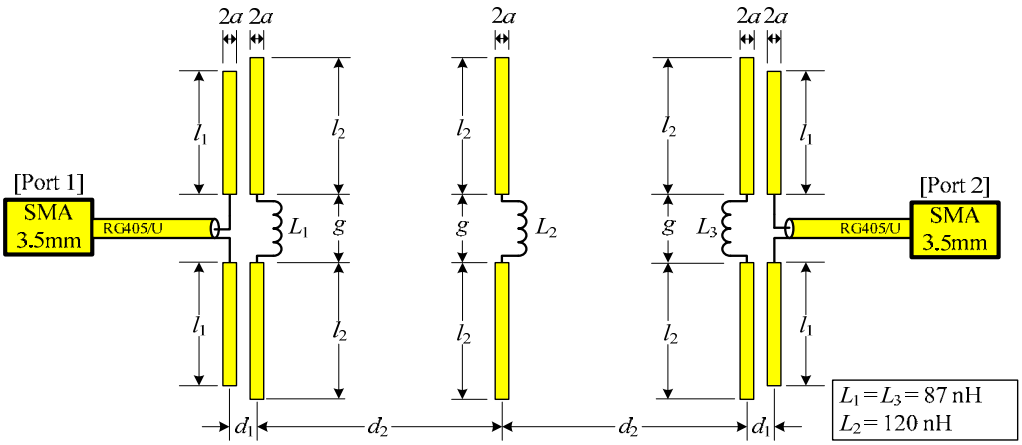

Figure 3.19 The layout of 3rd order dipole bandpass filter. a = 0.75, g = 5, l_1 = 12.4, l_2 = 12.5, d_1 = 2.5, d_2 = 20.2. Unit: mm.

The optimised responses in Figure 3.18 show that the passband has the maximum insertion loss of -3.21 dB and the maximum return loss is -18 dB. A degradation of the passband insertion loss may cause from the loss resistance R_{ind} of inductor included in resonator. This can be proven by comparing the *S*-parameter responses for the filter with R_{ind} and the filter without R_{ind} using the CST simulation software [6].

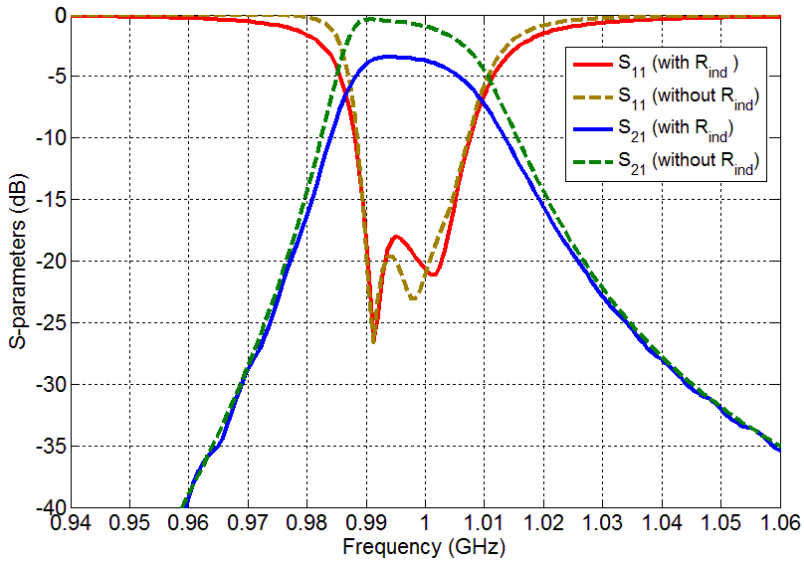

Figure 3.20 Simulated responses of 3rd order dipole bandpass filter with R_{ind} and without R_{ind}.

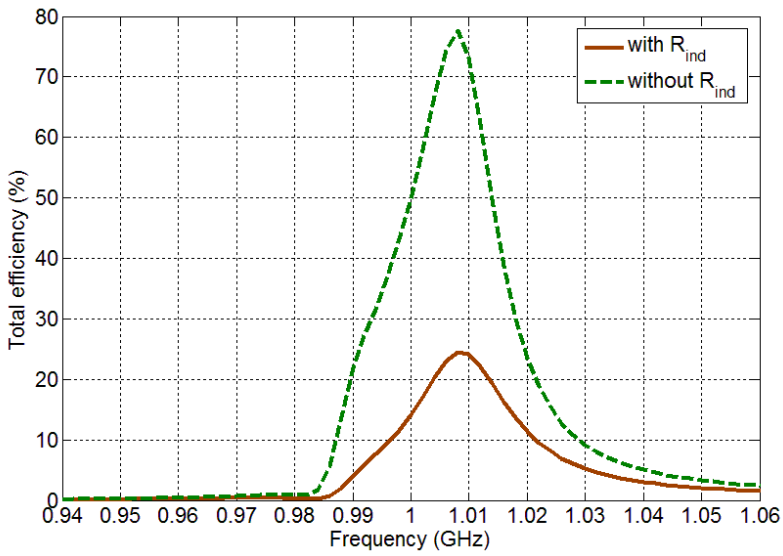

Figure 3.21 Simulated total antenna efficiency of 3rd order dipole bandpass filter with R_{ind} and without R_{ind}.

The responses of the dipole filter with R_{ind} and without R_{ind} are compared and shown in Figure 3.20. It is seen that the S_{21} response of the filter without R_{ind} is higher than the filter with R_{ind}, and it has the maximum value closed to zero at the lower band-edge (0.99 GHz), whereas the S_{21} level around the higher band-edge (1 GHz to 1.01 GHz) is dramatically decreased due to high radiation occurred. The whole device is made using dipole structure, which it can be observed a cause of degradation of the filter performance from the total antenna efficiency (e_t). Figure 3.21 shows the total antenna efficiency for the filter with R_{ind} and without R_{ind}. The total antenna efficiency is also related to the loss resistance R_{ind} which will affect to degrade the antenna conduction efficiency (e_c) when R_{ind} is high. The total antenna efficiency of the filter without R_{ind} at the passband frequency has a maximum value of 77% at 1.008 GHz, whereas the total efficiency of the filter with R_{ind} has a lower value of 25% due to low conduction efficiency (e_c). This might be related to a missing one reflection zero of the S_{11} response at the higher band-edge shown in Figure 3.20.

3.4.5 Fabrication and Measurement

The 3rd order dipole bandpass filter has been fabricated. The photograph of the fabricated two-port dipole bandpass filter is shown in Figure 3.22. The measured *S*-parameter responses are compared with the simulated response, as shown in Figure 3.23. The measurement results are agreed well with the simulation results. The results show that the passband insertion loss for the measurement is -3.44 dB, whereas the simulation is -3.21 dB. From a filter point of view , the degraded performance is occurred due to the loss resistance R_{ind} in the filter circuit, which has been described in Section 3.4.4. Also, R_{ind} is represented as the loss resistance in the resonator, which is associated with the unloaded quality factor (Q_u). In this case, the total Q_u of a dipole with an inductor can be obtained as follows an equation (3.3), given by

$$Q_u = \frac{1}{\frac{1}{Q_{ind}} + \frac{1}{Q_r}} \tag{3.11}$$

Here Q_{ind} is 320 and the simulated Q_r of $0.1\lambda_0$ dipole is 350. Thus, the total Q_u calculated using (3.11) is 167. The total Q_u can be used to estimate the increase of passband insertion loss ΔL_{A0} at the centre frequency f_0 using equation (2.43) for 3rd order bandpass filter, given by [8]

$$\Delta L_{A0} = 4.343\left[\frac{g_1}{FBW \cdot Q_{u1}} + \frac{g_2}{FBW \cdot Q_{u2}} + \frac{g_3}{FBW \cdot Q_{u3}}\right] \text{ (dB)} \tag{3.12}$$

where the g values are $g_1 = 0.8516$, $g_2 = 1.1032$, $g_3 = 0.8516$, the fractional bandwidth FBW is 0.02, and $Q_{u1} = Q_{u2} = Q_{u3} = 167$. Thus, the calculated ΔL_{A0} at f_0 of 1GHz is 3.65 dB, where as the ΔL_{A0} obtained from simulation is 3.21 dB. The ΔL_{A0} obtained from the simulated and measured response are 3.21 dB and 3.44 dB, respectively. As expected the reduction of unloaded Q for the filter designed using dipole antennas causes an increase in the insertion loss at the centre frequency and is accounted by the calculated Q values.

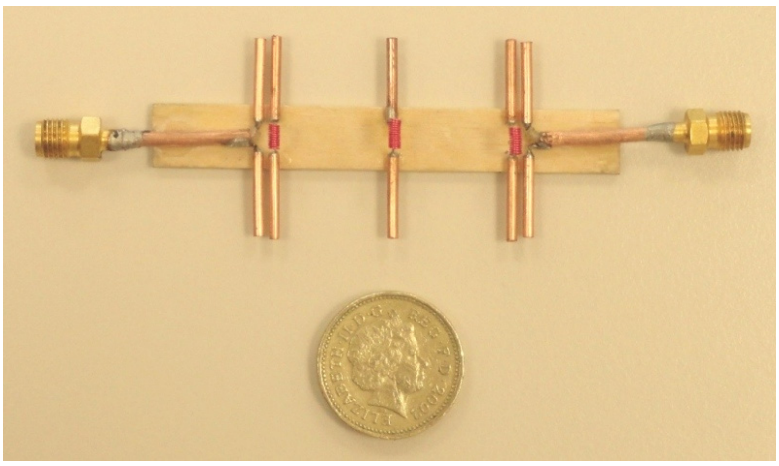

Figure 3.22 Photograph of 3rd order dipole bandpass filter.

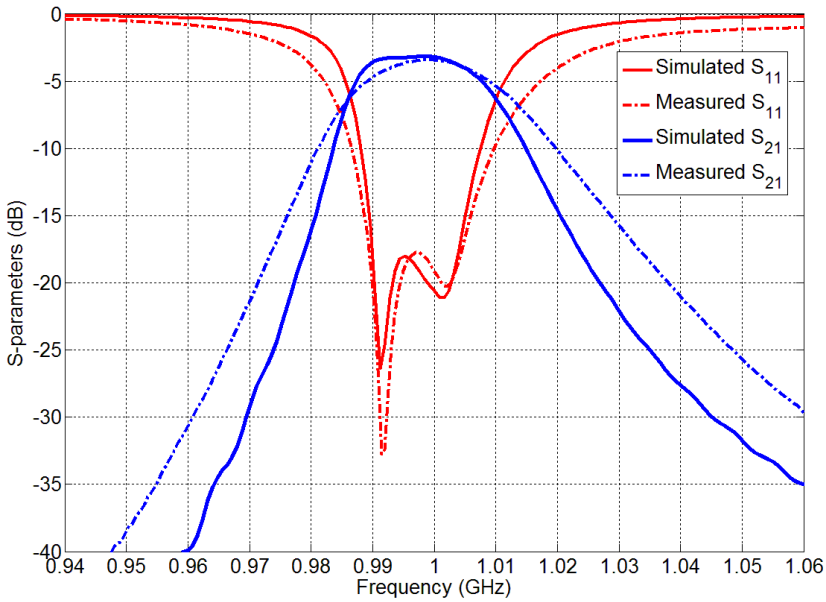

Figure 3.23 The simulated and measured responses of 3rd order dipole bandpass filter.

3.5 Conclusions

A 3rd order bandpass filter designed based on the dipole structure has been simulated and fabricated. The simulated and measured results are in good agreement. The degradation of the filter performance occurred due to a cause of the radiation from the structure which has been made from dipole antennas. Also, the loss resistance R_{ind} of inductors was included in the circuit. The R_{ind} will affect to degrade the antenna efficiency in terms of conduction and also the Q_u value of resonators. The Q_u-factor will be taken into account in the calculation of coupling matrix for the design in Chapter 4. The structure of the proposed bandpass filter is similar to a structure of dipole array which is suite for designing one-port dipole antenna-filters in Chapter 4.

References

[1] Balanis C. A. Antenna Theory Analysis and Design. 3rd ed. New Jersey, USA: John Wiley & Sons; 2005.

[2] Pozar D. M. Microwave Engineering. 3rd ed. USA: John Wiley & Sons; 2005.

[3] Chang K., York R. A., Hall P. S., Itoh T. Active integrated antennas. IEEE Trans. Microw. Theory Techn. 2002 Mar.; 50(3): 937-943.

[4] Hong J. S. and Lancaster M. J. Microstrip Filters for RF/Microwave Applications. New York, USA: John Wiley & Sons; 2001.

[5] Best S. R. The Foster Reactance Theorem and Quality Factor for Antennas. IEEE Antennas Wireless Propag. Lett. 2004 Dec.; 3(1): 306-309.

[6] Computer Simulation Technology (CST), Microwave Studio [Internet]. 2014 Available from URL: http://www.cst.com.

[7] Wheeler H. A. Formulas for the Skin Effect. Proceedings of the IRE. 1942 Sep.; 30(9): 412-424.

[8] Lancaster M. J. Passive Microwave Device Applications of High-Temperature Superconductors. Cambridge, UK: Cambridge University Press; 1997.

Chapter 4

One-Port Dipole Antenna-Filter

4.1 Introduction

In Chapter 3, a two-port dipole bandpass filter was designed based on the concept of coupled resonator filter theory [1]. In this chapter, the design method of the two-port dipole bandpass filter can be applied to the one-port dipole antenna-filter design (with radiation not considered as a port). This chapter presents the three new designs of dipole antennas and bandpass filters integrated into a single module using the coupling matrix synthesis. The coupling matrix can be utilised to optimise design parameters (coupling coefficients and external quality factor) in order to improve the frequency response corresponding to the specifications. The optimised parameters will then be utilised to find the physical dimensions of dipole antenna-filters using standard techniques [1]. The work presented in this chapter has been divided in three sections as follows. Section 4.2 presents a one-resonator dipole antenna-filter in order to understand the basic idea with the simplest antenna-filter. Section 4.3 presents a two-resonator dipole antenna-filter. The two-resonator design provides improved passband return loss S_{11} and the realised gain of the antenna-filter. Section 4.4 presents a three-resonator dipole antenna-filter. Each of these three sections includes the design method using the coupling matrix, the calculation and simulation results, and fabrication and measurement. The conclusion is provided in Section 4.5.

4.2 One-Resonator Dipole Antenna-Filter

4.2.1 Antenna-Filter Design

This section presents a design of a one-resonator dipole antenna-filter using the coupling matrix synthesis. The one-resonator dipole antenna-filter is considered with the topology shown in Figure 4.1; the white circle is the resonator, the dashed line with an arrow is the radiation from the antenna-filter which can be replaced by the radiation quality factor (Q_r) and the solid line is coupling between the port 1 and the resonator replacing the external quality factor (Q_e).

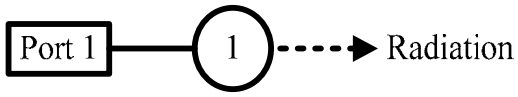

Figure 4.1 Topology of the designed one-resonator dipole antenna filter.

The topology shown in Figure 4.1 is related to the coupling matrix including source [2], and can be expressed as follows;

$$[A] = [R] + p[U] + j[m]$$

$$[A] = \begin{bmatrix} R_s & 0 \\ 0 & 0 \end{bmatrix} + P\begin{bmatrix} 0 & 0 \\ 0 & 1 \end{bmatrix} + j\begin{bmatrix} 0 & m_{s1} \\ m_{s1} & 0 \end{bmatrix} = \begin{bmatrix} R_s & jm_{s1} \\ jm_{s1} & P \end{bmatrix} \tag{4.1a}$$

where

$$\left.\begin{aligned} &R_s = 1\ \Omega \text{ is the source impedance.} \\ &P = \alpha + j\Omega \text{ is the normalised complex frequency.} \\ &\alpha = 1/FBW \cdot Q_{u1} \text{ is the normalised attenuation constant.} \\ &Q_{u1} \text{ is the normalised unloaded quality factor of the resonator 1.} \\ &\Omega = \frac{1}{FBW}\left(\frac{f}{f_0} - \frac{f_0}{f}\right) \text{ is the normalised frequency variable.} \end{aligned}\right\} \tag{4.1b}$$

f is the frequency (Hz).

f_0 is the centre frequency (Hz).

$m_{s1} = \dfrac{1}{\sqrt{FBW \cdot Q_e}}$ is the normalised coupling coefficient between the input source (port 1) and the resonator 1. (4.1b)

Q_{e1} is the normalised external quality factor of the input resonator.

The matrix [A] is used to calculate the frequency response of reflection coefficient (S_{11}), given by [2]

$$S_{11}(f) = 1 - 2R_s [A]_{11}^{-1} \tag{4.2}$$

where R_s = 1 Ω is the source impedance.

The inverse matrix $[A]_{11}^{-1}$ may be determined by

$$[A]_{11}^{-1} = \frac{\left[cof\left([A_{11}]\right)\right]^T}{\det\left([A]\right)} = \frac{P}{m_{s1}^2 + P} \tag{4.3}$$

Substituting (4.3) into (4.2) yields

$$S_{11}(f) = \frac{m_{s1}^2 - P}{m_{s1}^2 + P} = \frac{\left(m_{s1}^2 - \alpha\right) - j\Omega}{\left(m_{s1}^2 + \alpha\right) + j\Omega} \tag{4.4}$$

The equation (4.4) will be used to recalculate the design parameters of the antenna-filter in Section 4.2.3.

4.2.2 Extraction of Design Parameters from Physical Structure

In this work, a dipole antenna and an inductor are chosen to design as a resonator of a one-resonator dipole antenna-filter. The proposed structure is resonator 1 coupled to a feed element, as shown in Figure 4.2. The proposed design corresponds to the coupling topology shown in Section 4.2.1. Here the resonator is designed to operate at 1 GHz using a dipole

antenna with an inductor L. The design methodology of the resonator dipole antenna has been described in Chapter 3. In practice, the losses of the resonator are considered to occur due to radiation, the resistance of the material (i.e. copper) and the loss within the inductor. Here the total unloaded quality factor Q_{u1} of resonator 1 is considered from these losses and is associated with the radiation quality factor Q_r, the conductivity quality factor Q_c and the inductor quality factor Q_{ind} by

$$\frac{1}{Q_{u1}} = \frac{1}{Q_r} + \frac{1}{Q_c} + \frac{1}{Q_{ind}} \tag{4.5}$$

The radiation quality factor Q_r for an antenna length of $0.15\lambda_0$ and is about 127. Q_c is the conductivity quality factor of the copper which is about 16000. Q_{ind} is the quality factor of the 87 nH inductor which is about 313. Thus, the total Q_{u1} is about 90 with the radiation quality factor being dominant. All the Q-factor values can be obtained by following the method described in Chapter 3.

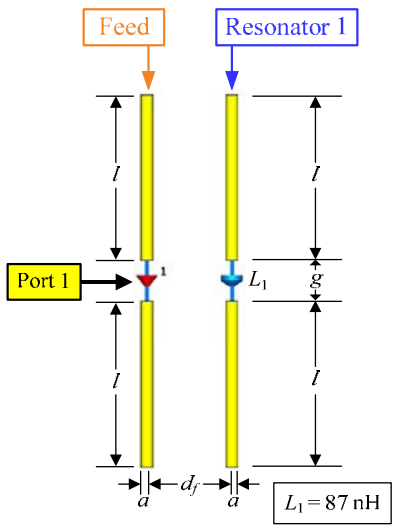

Figure 4.2 The layout of 1st order dipole antenna filter. a = 0.75 mm, g = 5 mm, l = 20 mm.

The parameters of the design for the 1st order dipole antenna-filter consist of the unloaded quality factor Q_{u1}, the external quality factor Q_{e1} and the centre frequency f_0. They are

extracted from the simulated response of S_{11} using CST simulation software [3] with the use of Q-calculation method for the one-port component in [4].

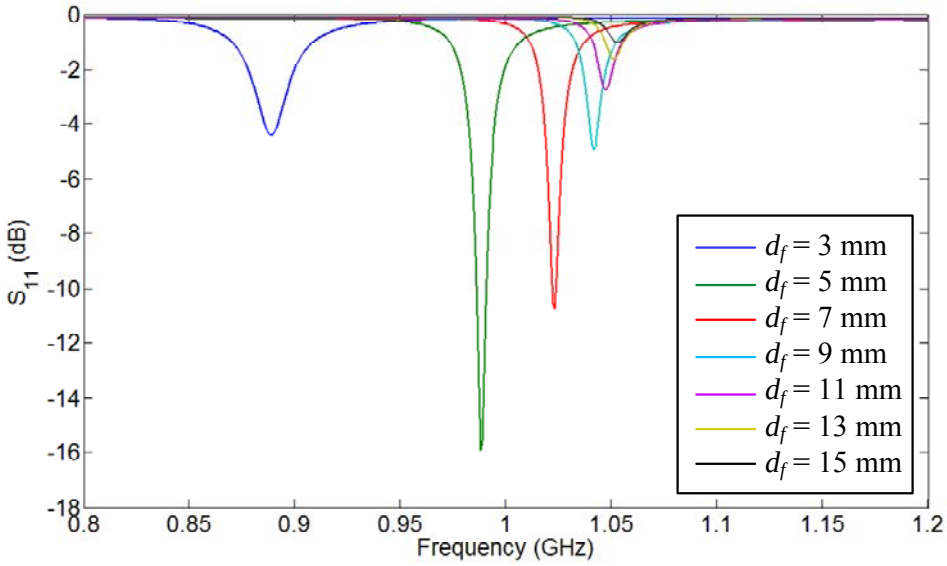

(a)

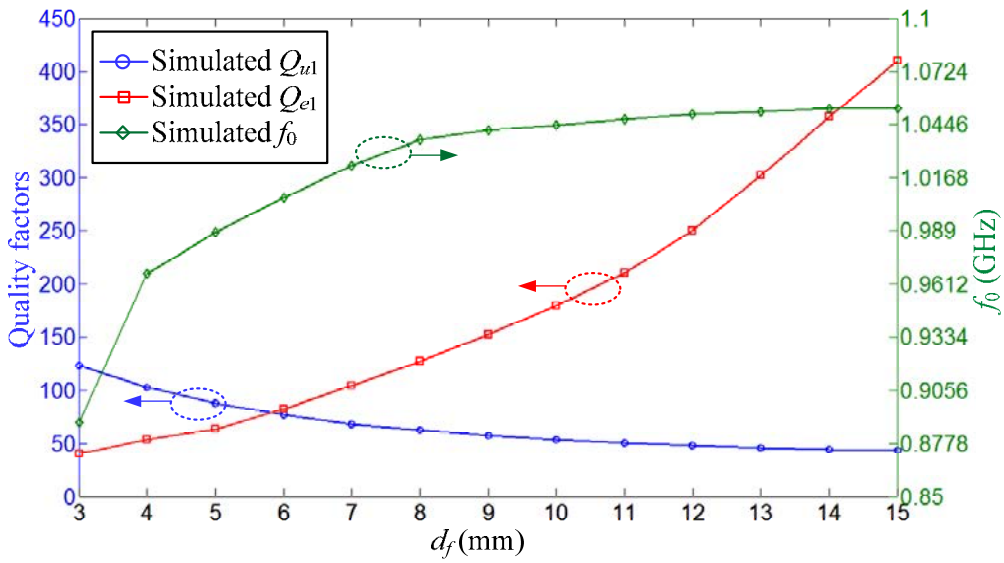

(b)

Figure 4.3 (a) Simulated S_{11} responses of the structure in Figure 4.2 for different values of d_f. (b) Simulated Q_{e1}, Q_{u1} and f_0 values for different values of d_f.

This structure can tune the S_{11} response by moving the feed or adjusting the separation d_f. The simulated S_{11} response of the 1st order dipole antenna-filter for different value of d_f is shown in Figure 4.3(a). At df = 3 mm, the S_{11} response of antenna-filter exhibits a large bandwidth

and the S_{11} magnitude ($|S_{11}(f_0)|$) at f_0 = 0.88 GHz as about -4 dB due to strong coupling occurred between feed and resonator. When d_f is increased to be 5 mm, the bandwidth will be narrower and f_0 will be higher with the lower value of $|S_{11}|$ as about -16 dB due to critical coupling nearly occurred. For d_f is above 5 mm, the bandwidth will be a bit smaller and the f_0 will be higher with the higher value of $|S_{11}|$ due to weak coupling occurred between feed and resonator. As described above, the S_{11} responses tuned following d_f values corresponds to types of coupling between feed and resonator. It is also related to the extracted values of Q_{u1}, Q_e and f_0 from the simulated S_{11}. The simulated values of Q_{u1}, Q_{e1} and f_0 for different values of d_f are plotted in Figure 4.3(b). These parameters correspond to the bandwidth, f_0 and S_{11} magnitude of the S_{11} responses shown in Figure 4.3(a). The plotted values of Q_{u1}, Q_{e1} and f_0 in Figure 4.3(b) will be utilised to define the physical dimensions of the antenna-filter structure. These parameters correspond to the designed parameters obtained from the coupling matrix for the final design in Section 4.2.3.

The simulated values of Q_{u1}, Q_{e1} and f_0 shown in Figure 4.3(b) are corresponded to the coupling theory in [1], which can be described as follows; The strong coupling of an input feed and a resonator is related to a small value of Q_e and a large value of Q_{u1}. This corresponds to the S_{11} response for a small value of coupling distance d_f below 5 mm. On the other hands, a large value of Q_e and a small value of Q_{u1} represent the weak coupling of an input feed and a resonator. This corresponds to the S_{11} response for a large value of coupling distance d_f above 5 mm. The critical coupling of an input feed and a resonator can be occurred when Q_e value is equal to Q_{u1} value. Here the critical coupling for the 1st order dipole antenna-filter corresponds to d_f = 5.8 mm for both Q_e and Q_{u1} values are 79.32. The S_{11} response for the critical coupling will be discussed in Section 4.2.3.

4.2.3 Calculation and Simulation Results

The coupling matrix presented in Section 4.2.1 is employed to design the antenna-filter in this section. Equation (4.4) is utilised to recalculate the values of the designed parameters to meet the required response of the reflection coefficient S_{11}. Equation (4.4) can be rewritten using equation (4.1b) as

$$\left|S_{11}(f)\right| = \left|\frac{(Q_{u1} - Q_{e1}) - jQ_{u1}Q_{e1}\left(\frac{f}{f_0} - \frac{f_0}{f}\right)}{(Q_{u1} + Q_{e1}) + jQ_{u1}Q_{e1}\left(\frac{f}{f_0} - \frac{f_0}{f}\right)}\right| \tag{4.6}$$

The magnitude of the reflection coefficient $\left|S_{11}(f)\right|$ of the 1st order antenna filter can be calculated using the equation (4.6) with the use of simulated values of Q_{u1}, Q_{e1} and f_0. The S_{11} response of 1st order dipole antenna-filter can perfectly be matched at f_0 when a Q_{u1} value is equal to Q_{e1}. In this design, Figure 4.3(b) is used to search for the best matched values of Q_{u1} and Q_{e1}. The values of Q_{u1}, Q_e and f_0 shown in Figure 4.3(b) are varied following the d_f value as described in Section 4.2.2. The best matched values of Q_{u1} and Q_{e1} can be found for both Q values of 79.32, where the Q_{u1} line crosses to the Q_{e1} line at d_f = 5.8 mm that corresponds to f_0 = 1.006 GHz. The simulated S_{11} of the antenna-filter structure for a d_f of 5.8 mm is compared with the calculated S_{11} using equation (4.6) with the use of simulated values of Q_{u1}, Q_{e1} and f_0 for a d_f of 5.8 mm, as shown in Figure 4.4. The simulated S_{11} response shows good agreement with the calculation. However, simulated $|S_{11}(f_0)|$ value at f_0 = 1.006 GHz does not go to the minimum value (not showing the best match) as comparing to calculated $|S_{11}(f_0)|$ value at the same frequency f_0. It might be a cause from the accuracy of CST simulation software [3]. Also a small error occurs from the matched values of Q_{u1} and Q_e at d_f = 5.8 mm which are estimated from the reading values of a curve in Figure 4.3(b).

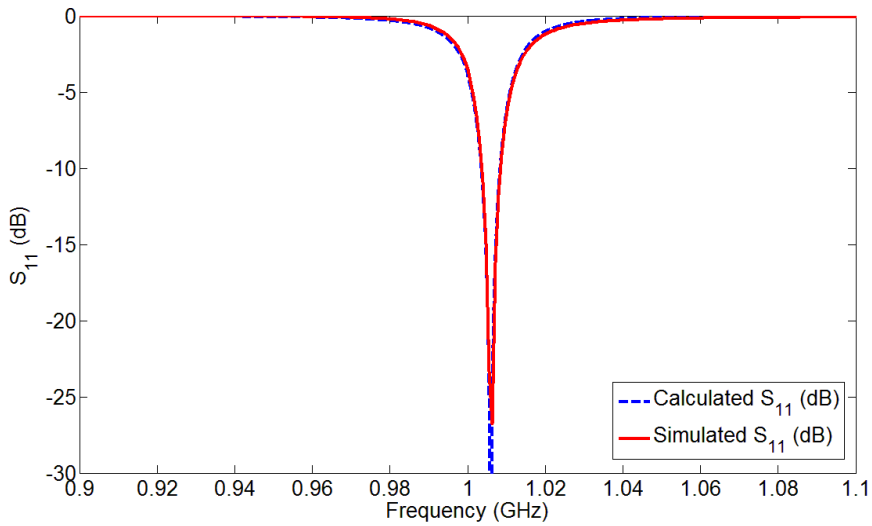

Figure 4.4 The calculated and simulated responses of S_{11} of the designed 1st order dipole antenna-filter.

4.2.4 Fabrication and Measurement

The 1st order dipole antenna-filter has been fabricated. The photograph of the fabricated dipole antenna-filter is shown in Figure 4.5. The rigid foam (ROHACELL 71 HF) can be considered as air and made as the core of the structure (the white material). The cotton wires are used to mount the coaxial cable underneath the rigid foam. The fabricated structure can adjust the separation (d_f) between the feed and the resonator. The fabricated antenna-filter is measured for different positions of the d_f value.

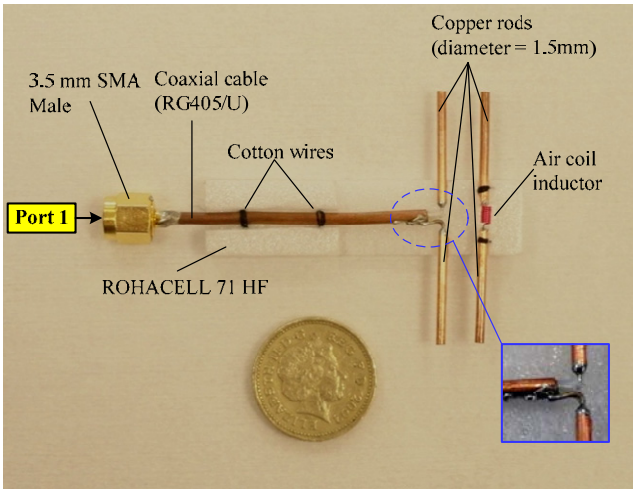

Figure 4.5 The photograph of the fabricated 1st order dipole antenna-filter.

The measured responses of the reflection coefficient S_{11} for different values of d_f are shown in Figure 4.6(a). The measurement Q values are extracted from the measured S-parameters using the calculation technique in [4]. The measurement Q_{u1}, Q_{e1} and f_0 for different value of d_f are shown in Figure 4.6(b).

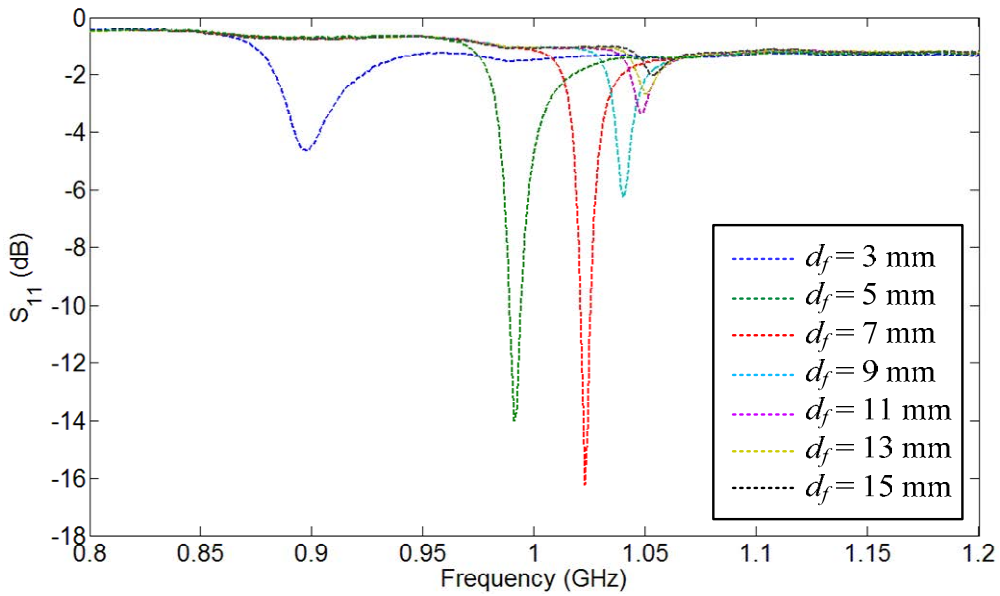

(a)

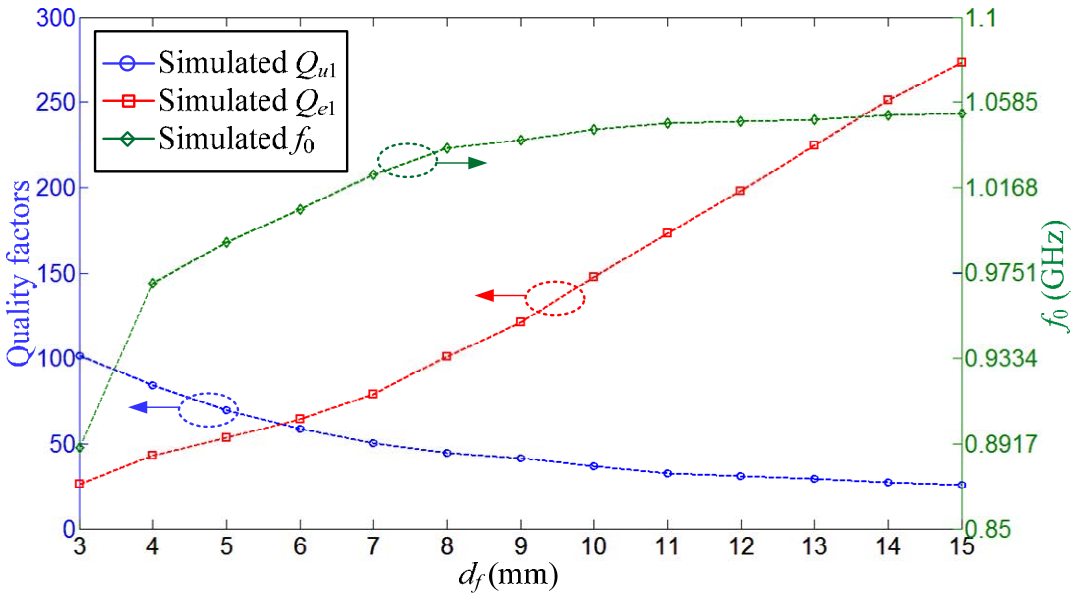

(b)

Figure 4.6 (a) Measured S_{11} responses of the 1st order dipole antenna filter for different values of d_f. (b) Simulated and measured Q_{e1}, Q_{u1} and f_0 curves for different values of d_f.

In this experiment, the response of the fabricated antenna-filter can be matched at the centre frequency f_0 when the values of Q_{u1} and Q_{e1} are the same. Both measurement values of Q_{u1} and Q_{e1} can be found from the plotted graph in Figure 4.6(b). The matched values of Q_{u1} and Q_{e1} are about 62 at the d_f value of 5.8 mm. The measured *S*-parameter response of the fabricated antenna-filter for d_f of 5.8 mm shows good agreement with the simulated response, as shown in Figure 4.7.

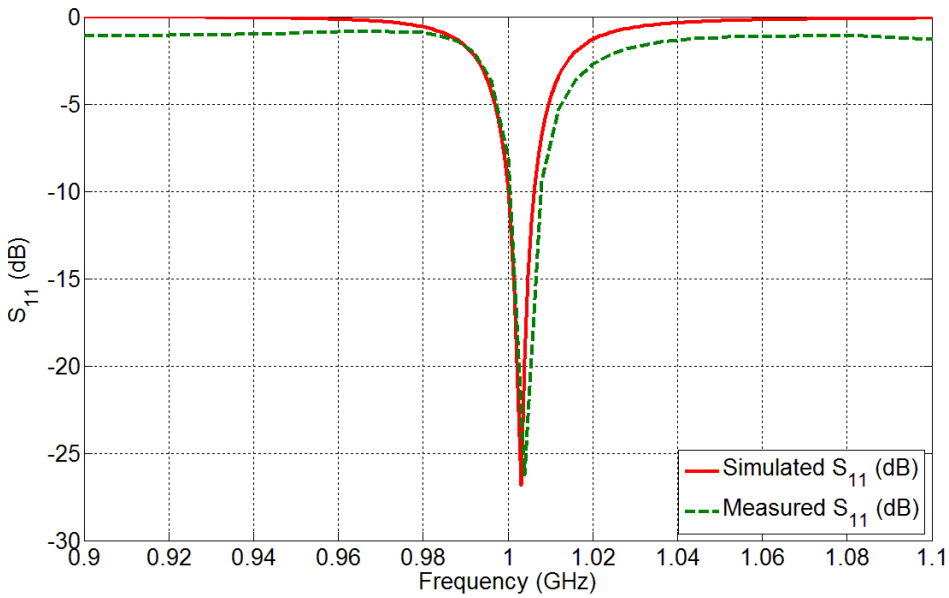

Figure 4.7 The simulated and measured responses of S_{11} of 1st order dipole antenna-filter for $d_f = 5.8$ mm.

The 1st order dipole antenna-filter has been measured inside an anechoic chamber using an HP8722D vector network analyzer (VNA) and a dual polarised horn antenna (3164-03 from ESCO Technology Company, a reference antenna) to obtain the frequency response of the realised gain. The realised gain is an actual gain of antenna used to describe the effective radiated power in the main direction. In this thesis, the frequency response of the realised gain is an important parameter to demonstrate the filtering capability of antenna-filters and can be measured using the comparison method [5]. The measured realised gain is compared with

simulation, as shown in Figure 4.8. The measured realised gain shows a response similar to the 1st order bandpass filter and is in good agreement with the simulation. The maximum measured realised gain is about -1.09 dB, whereas the simulation is about -0.75 dB. The difference between the simulated and measured realised gain is due to the additional losses (materials and inductor) in the fabricated component. The realised gain of the antenna-filter can be improved for the next design which presented in Section 4.3 and 4.4.

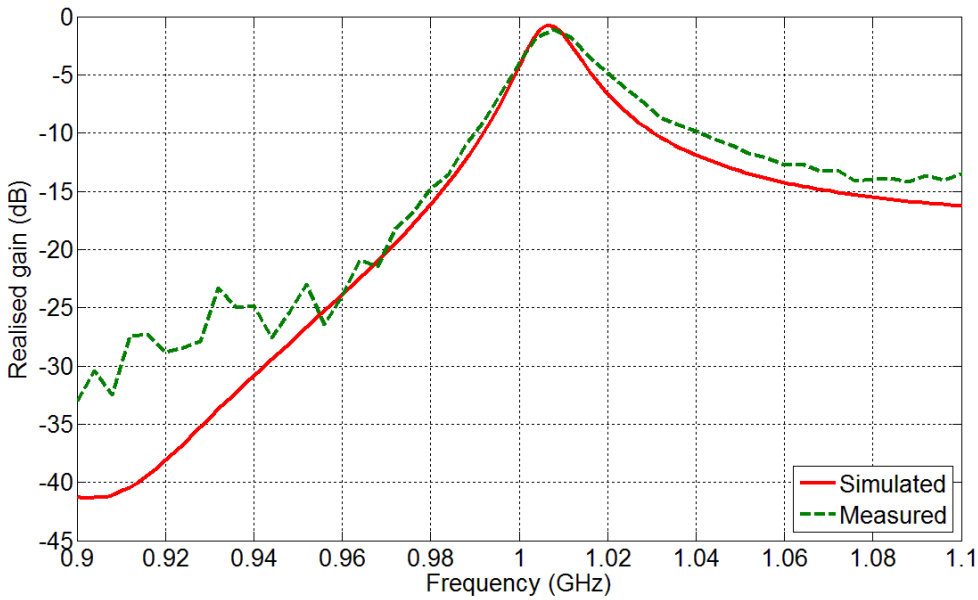

Figure 4.8 Simulated and measured realised gain of 1st order dipole antenna-filter for $d_f = 5.8$ mm.

The simulated and measured radiation patterns of the 1st order dipole antenna-filter are shown in Figure 4.9. The measured radiation patterns in H and E plane are in good agreement with the simulation. The maximum level of the cross polarisation in H-plane is below -10 dB in the simulation and the measurement, whereas the maximum level of the cross polarisation in E-plane are below -6 dB in the simulation and below -10 dB in the measurement. The 3 dB beamwidth in E-plane is 88 degrees in the simulation and 81 degrees

in the measurement, whereas The 3 dB beamwidth in H-plane cannot be estimated due to its radiation pattern that exhibits an omnidirectional pattern in H-plane.

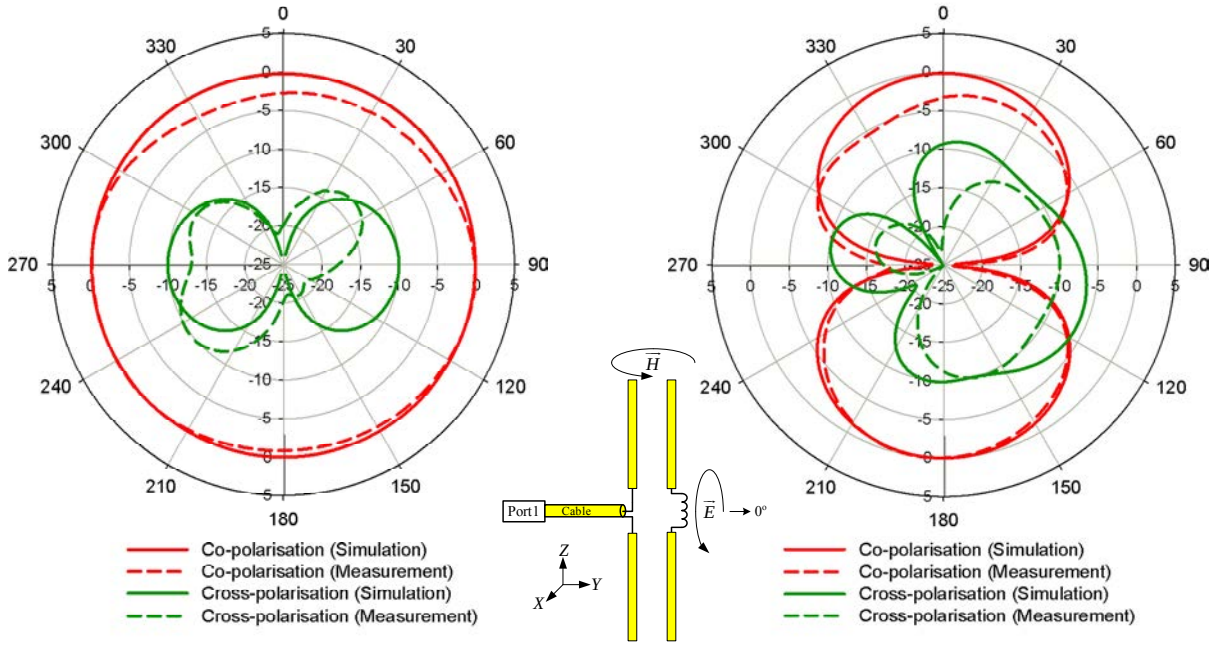

(a) (b)

Figure 4.9 (a) Normalised simulated and measured radiation patterns at 1 GHz for (a) H (XY) plane. (b) E (YZ) plane. (Radial units are dB. Circumferential scale is θ in degrees.)

4.3 Two-Resonator Dipole Antenna-Filter

4.3.1 Antenna-Filter Design

In this section, the antenna-filter is designed based on the structure of a coupled dipole antenna using the coupling matrix, presented in Chapter 2. Figure 4.10 shows the topology of two-coupled resonator antenna-filter; the input is port 1 and radiation occurs from both resonators.

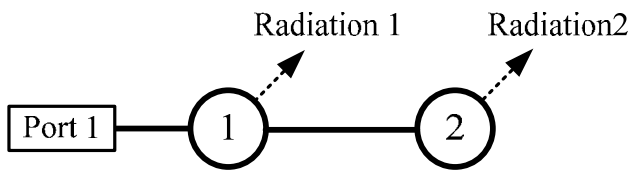

Figure 4.10 Topology of designed two-resonator dipole antenna filter.

The coupling matrix equations for the designed topology, shown in Figure 4.10, are given as

$$[A]=[q]+p[U]-j[m]$$

$$[A]=\begin{bmatrix} \frac{1}{q_{e1}}+\frac{1}{q_{u1}} & 0 \\ 0 & \frac{1}{q_{u2}} \end{bmatrix}+p\begin{bmatrix} 1 & 0 \\ 0 & 1 \end{bmatrix}-j\begin{bmatrix} 0 & m_{12} \\ m_{12} & 0 \end{bmatrix}=\begin{bmatrix} \frac{1}{q_{e1}}+\frac{1}{q_{u1}}+p & -jm_{12} \\ -jm_{12} & \frac{1}{q_{u2}}+p \end{bmatrix} \tag{4.7a}$$

where $q_{e1} = FBW \cdot Q_{e1}$ is the normalised external quality factor of the input resonator.

$q_{ui} = FBW \cdot Q_{ui}$ is the normalised unloaded quality factor of the resonator i;

$i = 1, 2$.

$m_{12} = M_{12}/FBW$ is the normalised coupling coefficient between the resonator 1 and the resonator 2.

$p = \frac{j}{FBW}\left(\frac{f}{f_0}-\frac{f_0}{f}\right)$ is the complex frequency variable. (4.7b)

The reflection coefficient S_{11} is obtained from the matrix $[A]$ given by

$$S_{11}(f)=1-\frac{2}{q_{e1}}[A]_{11}^{-1} \tag{4.8}$$

The inversed matrix $[A]_{11}^{-1}$ may be determined by

$$[A]_{11}^{-1} = \frac{\dfrac{1}{q_{u2}} + p}{p^2 + \left(\dfrac{1}{q_{u1}} + \dfrac{1}{q_{u2}} + \dfrac{1}{q_{e1}}\right)p + \left(m_{12}^2 + \dfrac{1}{q_{u1}q_{u2}} + \dfrac{1}{q_{e1}q_{u2}}\right)} \tag{4.9}$$

Substituting (4.9) into (4.8) yields

$$S_{11}(f) = \frac{q_{e1}p^2 + \left(\dfrac{q_{e1}}{q_{u1}} + \dfrac{q_{e1}}{q_{u2}} - 1\right)p + \left(q_{e1}m_{12}^2 + \dfrac{q_{e1}}{q_{u1}q_{u2}} - \dfrac{1}{q_{u2}}\right)}{q_{e1}p^2 + \left(\dfrac{q_{e1}}{q_{u1}} + \dfrac{q_{e1}}{q_{u2}} + 1\right)p + \left(q_{e1}m_{12}^2 + \dfrac{q_{e1}}{q_{u1}q_{u2}} + \dfrac{1}{q_{u2}}\right)} \tag{4.10}$$

Equation (4.10) is utilised to calculate the reflection coefficient (S_{11}) for only this design. Here the equation (4.10) will be used to recalculate the designed parameters to meet the required S_{11} magnitude at the centre frequency (f_0).

Substituting $f = f_0$ into the equation (4.10) yields

$$\mathrm{Re}\{S_{11}(f_0)\} = \frac{q_{e1}\left(q_{u2}m_{12}^2 + \dfrac{1}{q_{u1}}\right) - 1}{q_{e1}\left(q_{u2}m_{12}^2 + \dfrac{1}{q_{u1}}\right) + 1} \tag{4.11}$$

Rearranging the equation (4.11) and using (4.7b),

$$Q_{e1} = \frac{-\left(\mathrm{Re}\{S_{11}(f_0)\} + 1\right)}{\left(Q_{u2}M_{12}^2 + \dfrac{1}{Q_{u1}}\right)\left(\mathrm{Re}\{S_{11}(f_0)\} - 1\right)} \tag{4.12}$$

where Q_{e1} is the external quality factor, Q_{u1} is the unloaded quality factor of resonator 1, Q_{u2} is the unloaded quality factor of resonator 2, M_{12} is the coupling coefficient between resonator 1 and resonator 2 and $\mathrm{Re}\{S_{11}(f_0)\}$ is the real part of S_{11} magnitude at the centre frequency. The Equation (4.12) will be utilised to find the Q_{e1} value for optimising the return loss S_{11} in this design.

The 2nd order antenna-filter is initially designed with a return loss (L_R) of 20 dB and a fractional bandwidth of 2% (FBW = 0.02) at a centre frequency (f_0) of 1 GHz. The g-values for 2nd order Chebyshev lowpass prototype filter with a return loss of 20 dB (or passband ripple L_{Ar} = 0.04321) are calculated using the equation (2.21) to result in g_0 =1.0, g_1 = 0.6648, g_2 = 0.5445 and g_3 = 1.2210. Initially, the unloaded quality factor (Q_{un}) of the last resonator has to be equal to the external quality factor (Q_{e1}) of the input resonator to be similar to the conventional coupled-resonator filter design. The external quality factors and coupling coefficients of the design are calculated from specifications using equations (2.27), given by

$$Q_{e1} = \frac{g_0 g_1}{FBW},\ Q_{un} = Q_{en} = \frac{g_n g_{n+1}}{FBW},\ M_{i,i+1} = \frac{FBW}{\sqrt{g_i g_{i+1}}} \quad \text{for } i = 1 \text{ to } n-1 \tag{4.13}$$

The values of the designed parameters are calculated using equations (4.13) given as Q_{e1} = Q_{u2} = 33.324 and M_{12} = 0.03324. In this design, all resonators are antennas which are considered as lossy resonators. In this design, the initial Q_{u1} value is assumed above 100. It will then be used to calculate the new Q_{e1} value using equation (4.12) in order to preserve the filter characteristics. Thus, a 0.13λ_0 dipole antenna with an inductor is chosen and has a total unloaded Q value (Q_{u1}) of about 112. The initial design values are used with the equation (4.8) to obtain the initial response of S_{11} as shown in Figure 4.11. The initial response is not matched to the specification due to low Q_{u1} value. The response can be improved with the newly calculated value of Q_{e1} = 26.72, obtained using equation (4.12) as 26.72. Figure 4.11 shows the calculated final response of S_{11} compared with the calculated initial response from the coupling matrix. The calculated final response shows the good result that is obtained from

the new calculated values. These values will be used to get the physical dimensions of the dipole antenna structure using the methods in Chapter 3.

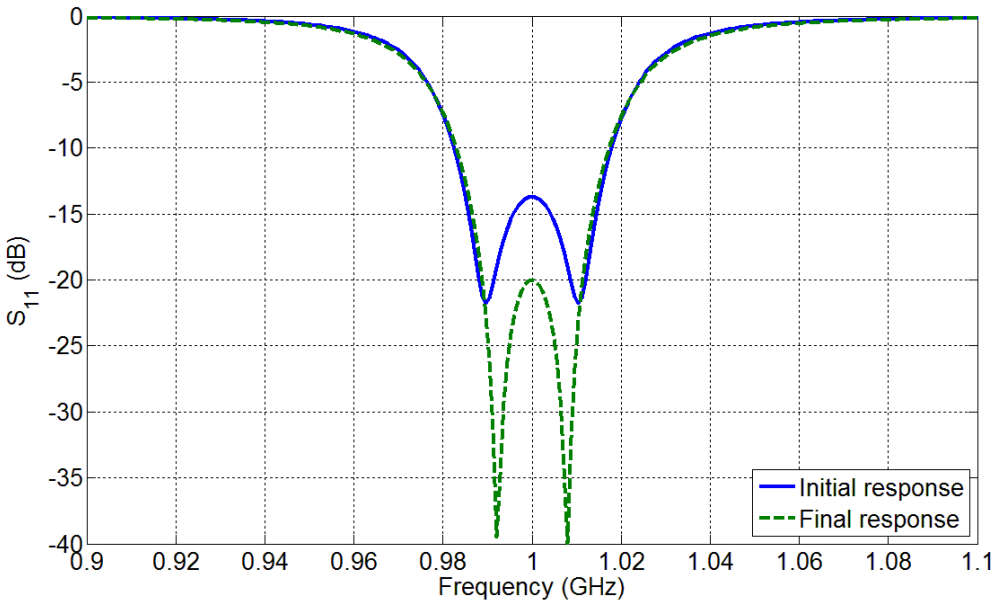

Figure 4.11 Comparison between initial and final responses of S_{11} for the 2nd order antenna-filter calculated from the coupling matrix.

4.3.2 Calculation and Simulation Results

The physical dimensions of the two-resonator antenna-filter are defined from the design parameters given in the previous section. The layout of the designed antenna-filter with all the physical dimensions is shown in Figure 4.12. The structure is similar to an end-fire Yagi-Uda dipole array. This can be gained the benefit from this structure to improve the radiation pattern and realised gain which will be discussed in Section 4.4. The simulated return loss S_{11} curve is compared with the calculation, as shown in Figure 4.13. The simulation result is in reasonable agreement with the calculation result. The simulated passband bandwidth of S_{11} at -20 dB is 16 MHz, whereas the calculated passband bandwidth is 20 MHz. An inaccurate simulated result may occur from a small physical dimension error obtained from the curves of Q_e versus l_f and M versus d_M using CST simulation software [3].

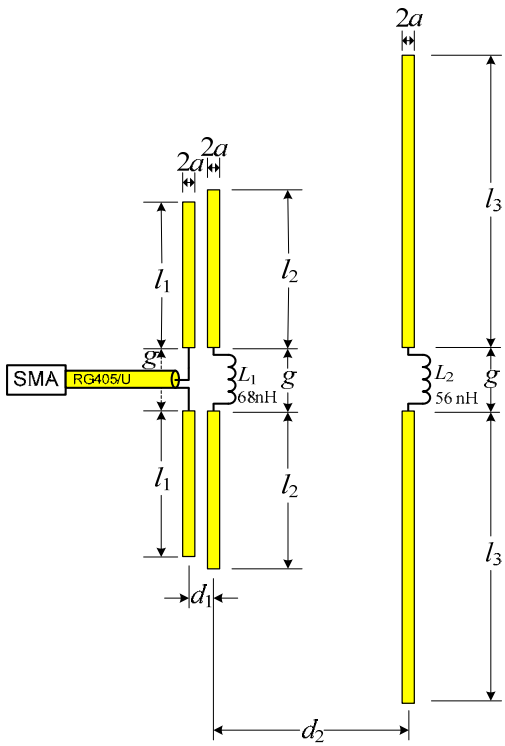

Figure 4.12 Geometry of 2nd order dipole antenna filter are a = 0.75 mm, g = 5mm, l_1 = 16.1 mm, l_2 = 17 mm, l_3 = 32.75 mm, d_1 = 2.5 mm, d_2 = 21.3 mm.

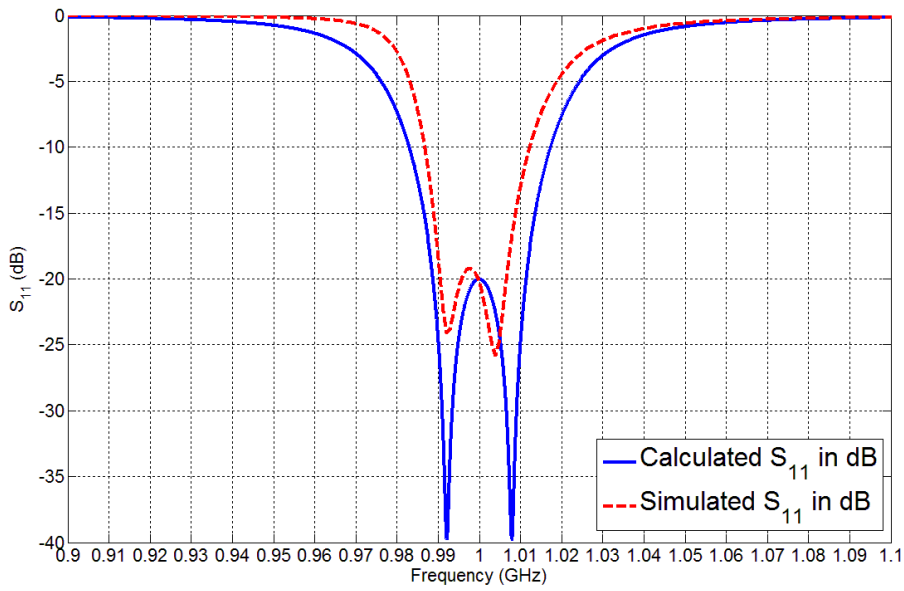

Figure 4.13 Calculated and simulated response of S_{11} of 2nd order dipole antenna-filter.

4.3.3 Fabrication and Measurement

The 2nd order dipole antenna-filter has been fabricated based on the physical dimensions in Figure 4.12. Figure 4.14 shows a photograph of the fabricated 2nd order dipole antenna-filter. The position of the second dipole has been altered slightly to achieve the desired response. The measured S_{11} is compared with the simulated S_{11} as shown in Figure 4.15. The measured S_{11} shows the good agreement with the simulation. The measured passband bandwidth of S_{11} at -20 dB is 20 MHz whereas the simulated passband bandwidth is 16 MHz.

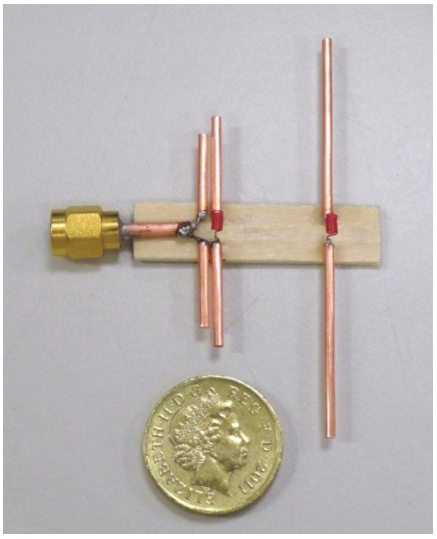

Figure 4.14 Photograph of the fabricated 2nd order dipole antenna-filter.

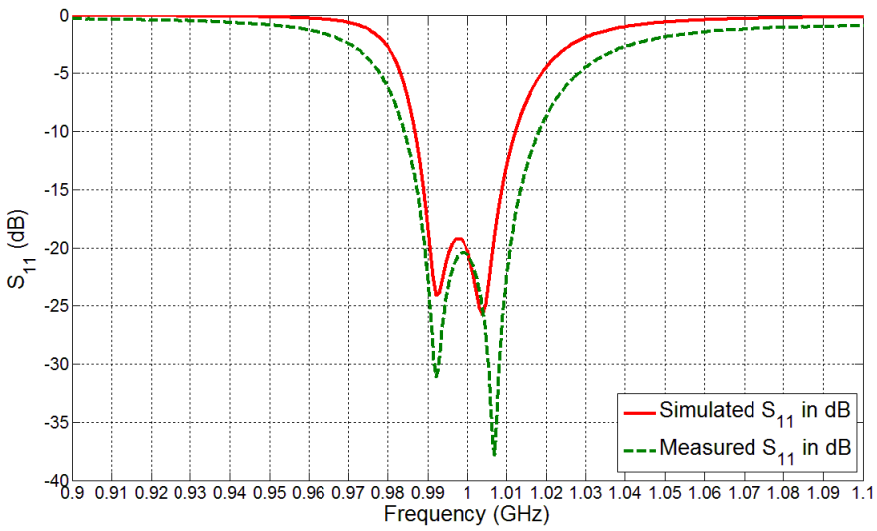

Figure 4.15 Simulated and measured S_{11} of 2nd order dipole antenna filter.

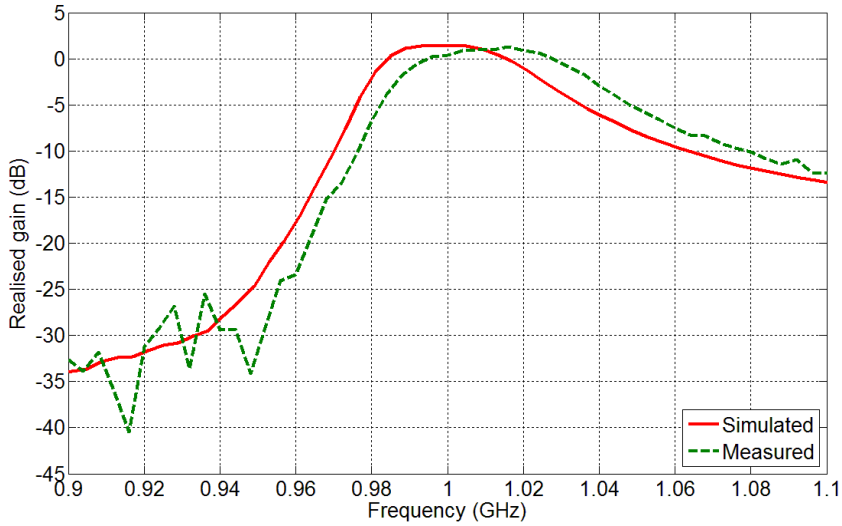

Figure 4.16 Simulated and measured realised gain of 2nd order dipole antenna filter.

Figure 4.16 shows the measured realised gain response of the two-resonator antenna-filter compared with the simulation. The measurement and simulation results are in good agreement. The maximum measured realised gain is 1.5 dB whereas the maximum simulated realised gain is 1.7 dB. The 2nd order dipole antenna-filter has the maximum cross-polarisation levels in H-plane at 1 GHz shown in Figure 4.17(b) that are -7 dB in the simulation and -12.35 dB in the measurement, whereas the maximum cross-polarisation levels in E-plane at 1 GHz shown in Figure 4.17(e) are -14 dB in the simulation and -14.72 dB in the measurement. The 3 dB beamwidth in the E-plane is 84 degrees according to simulation and it is 76 degrees in the measurement. It is smaller than the 1st order antenna-filters by about 4 degrees in simulation and 5 degrees in measurement. The 3 dB beamwidth in H-plane is larger than in E-plane as about 246 degrees in the simulation and 250 degrees in the measurement. This is because its radiation pattern is similar to an omnidirectional pattern. The antenna-filter can be designed being narrower the 3 dB beamwidth for H-plane since it has more elements like an Uda-Yagi antenna. The performance of the 2nd order dipole antenna-filter is summarised and presented in Table 4.1.

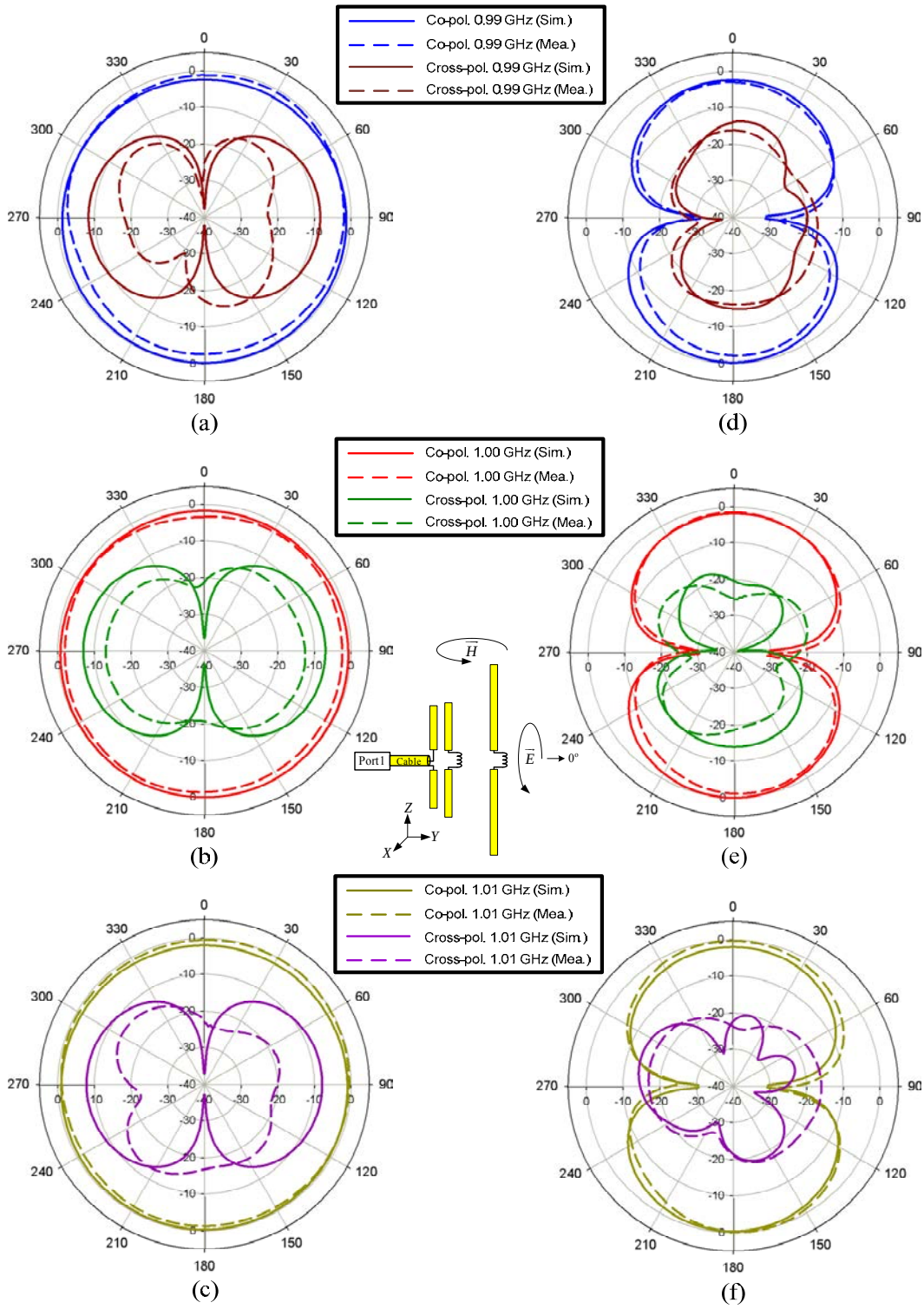

Figure 4.17 Normalised simulated and measured radiation patterns of 2nd order dipole antenna filter at 0.99 GHz, 1 GHz, 1.01 GHz for H (XY) plane (a, b, c) and E (YZ) plane (d, e, f). (Radial units are dB. Circumferential scale is θ in degrees.)

Table 4.1 Summary of the 2nd order dipole antenna-filter performance

Parameters	Frequency (GHz)	3 dB Beamwidth (deg.)		Back lobe level (dB)		Cross-polarisation level (dB)	
		Sim.	Mea.	Sim.	Mea.	Sim.	Mea.
H-plane	0.99	300	308	-2.46	-1.80	-8.42	-14.00
	1.00	330	326	-1.86	-1.87	-7.00	-12.35
	1.01	310	320	-2.02	-1.96	-7.88	-12.9
E-plane	0.99	78	72	-2.46	-3.076	-13.65	-14.96
	1.00	84	76	-1.86	-1.55	-14.00	-14.72
	1.01	80	74	-2.02	-2.04	-13.79	-15.94

4.4 Three-Resonator Dipole Antenna-Filter

4.4.1 Antenna-Filter Design

This section presents the design of a 3rd order antenna-filter using dipole antennas based on the coupling matrix, similar to the design in Section 4.3. Figure 4.18 shows the topology of three-coupled resonator antenna-filter; the input is port 1 and the radiation is from all three resonators.

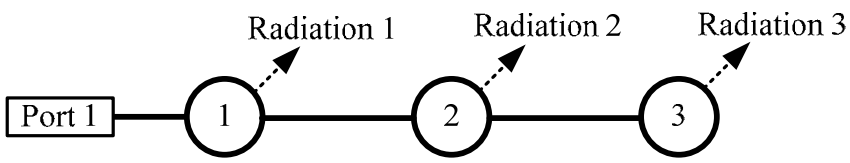

Figure 4.18 Topology of designed three-resonator dipole antenna filter.

The coupling matrix equation of the topology shown in Figure 4.18 can be expressed as

$$[A]=[q_e]+[q_u]+p[U]-j[m]$$

$$[A]=\begin{bmatrix} \frac{1}{q_e}+\frac{1}{q_{u1}} & 0 & 0 \\ 0 & \frac{1}{q_{u2}} & 0 \\ 0 & 0 & \frac{1}{q_{u3}} \end{bmatrix}+p\begin{bmatrix} 1 & 0 & 0 \\ 0 & 1 & 0 \\ 0 & 0 & 1 \end{bmatrix}-j\begin{bmatrix} 0 & m_{12} & 0 \\ m_{12} & 0 & m_{23} \\ 0 & m_{23} & 0 \end{bmatrix}$$

$$=\begin{bmatrix} \frac{1}{q_e}+\frac{1}{q_{u1}}+p & -jm_{12} & 0 \\ -jm_{12} & \frac{1}{q_{u2}}+p & -jm_{23} \\ 0 & -jm_{23} & \frac{1}{q_{u3}}+p \end{bmatrix} \tag{4.14}$$

where $q_{e1} = FBW \cdot Q_{e1}$ is the normalised external quality factor of the input resonator.

$q_{ui} = FBW \cdot Q_{ui}$ is the normalised unloaded quality factor of the resonator i; i =1, 2, 3.

$m_{12} = M_{12}/FBW$ is the normalised coupling coefficient between the resonator 1 and the resonator 2.

$m_{23} = M_{23}/FBW$ is the normalised coupling coefficient between the resonator 2 and the resonator 3.

$p = \frac{j}{FBW}\left(\frac{f}{f_0}-\frac{f_0}{f}\right)$ is the complex frequency variable.

The 3rd order antenna-filter is initially designed with a return loss (L_R) of 20 dB and a fractional bandwidth of 2% (FBW = 0.02) at the centre frequency (f_0) of 1 GHz. The g-values for 3rd order Chebyshev lowpass prototype filter with a return loss of 20 dB (or

passband ripple L_{Ar} = 0.04321) are chosen. The g-values are calculated using the equation (2.21) as g_0 =1.0, g_1 = 0.8516, g_2 = 1.1032, g_3 = 0.8516 and g_4 = 1.0.

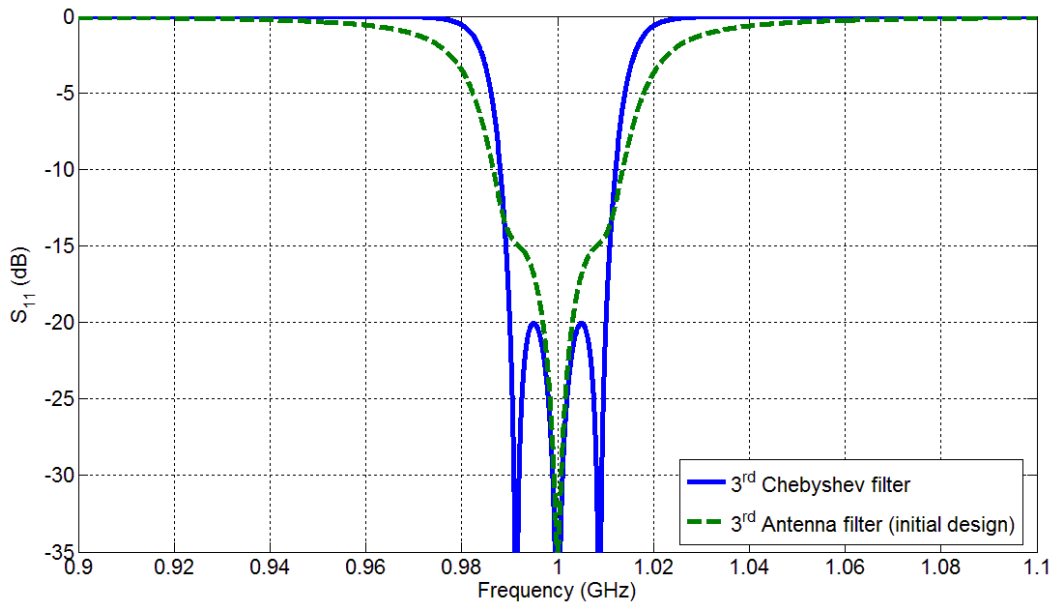

Figure 4.19 Comparison of calculated responses of 3rd Chebyshev filter and initial responses of 3rd order antenna-filter.

The antenna-filer is initially designed using equation (4.14) to be similar to the design of 2nd antenna-filter, in Section 4.3. The initial designed values are given as Q_{u1} = Q_{u2} = 112, Q_{u3} = Q_{e1} = 42.58 and M_{12} = M_{23} = 0.02063. Figure 4.19 shows the calculated initial response of the antenna-filter compared with the ideal response of 3rd order Chebyshev filter. The initial response of S_{11} does not match with the Chebyshev response and only shows one pole due to additional losses of resonators defined by Q_u that are included in this calculation. The response of the designed 3rd order antenna-filter can be further improved by adjusting the value of the coupling coefficient M_{23}. Figure 4.20 shows the curve of max value of S_{11} ($S_{11,max}$) within the passband against the M_{23} value. This curve is used to estimate the required S_{11} level at the passband frequency. This can be found by reducing the value of M_{23} to meet

the $S_{11,max}$ value of -20 dB. This calculated value of M_{23} is found to be 0.017 which corresponded to the $S_{11,max}$ of -20 dB, as depicted in Figure 4.20. The final response is plotted and compared with the initial response, as shown in Figure 4.21. The final curve shows a three-pole filter response with the passband and a return loss S_{11} of 20 dB as corresponding to the specifications.

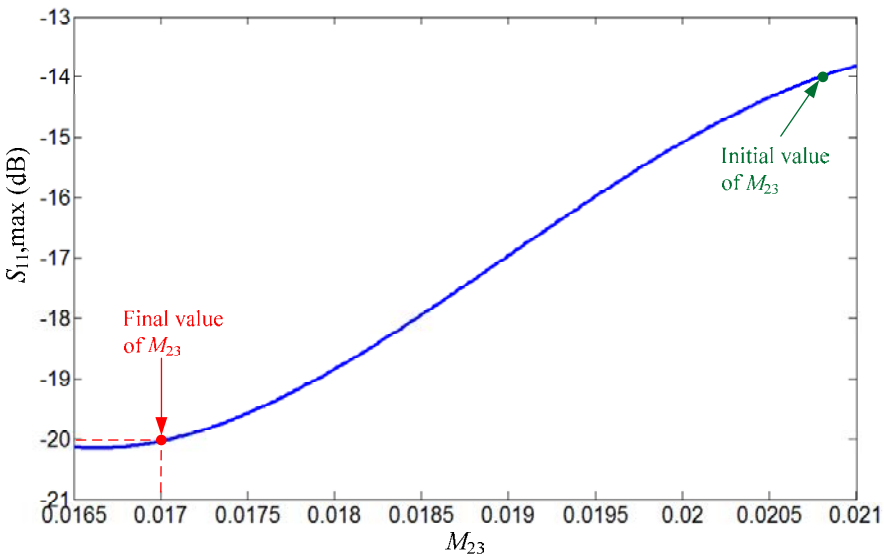

Figure 4.20 Max value of S_{11} ($S_{11,max}$) within the passband obtained from the calculation of coupling matrix for different values of M_{23}.

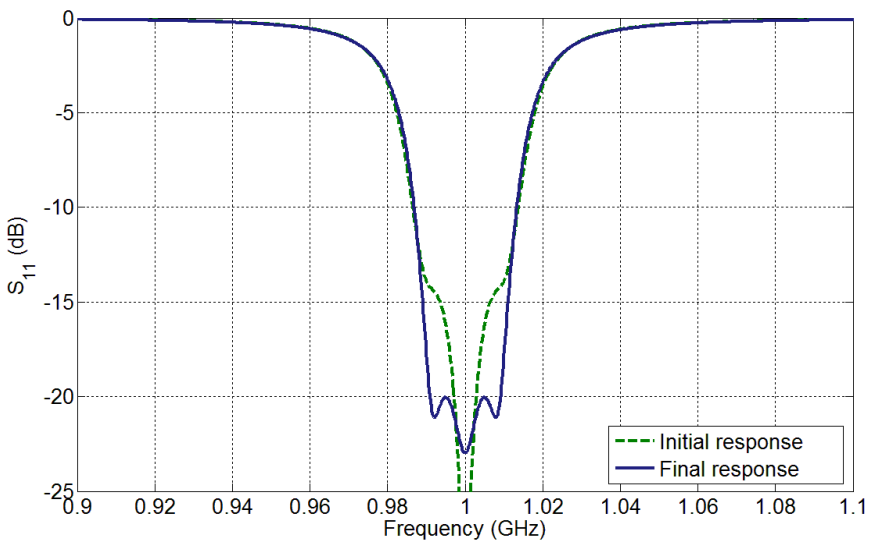

Figure 4.21 Initial and final responses of S_{11} in dB calculated from the coupling matrix.

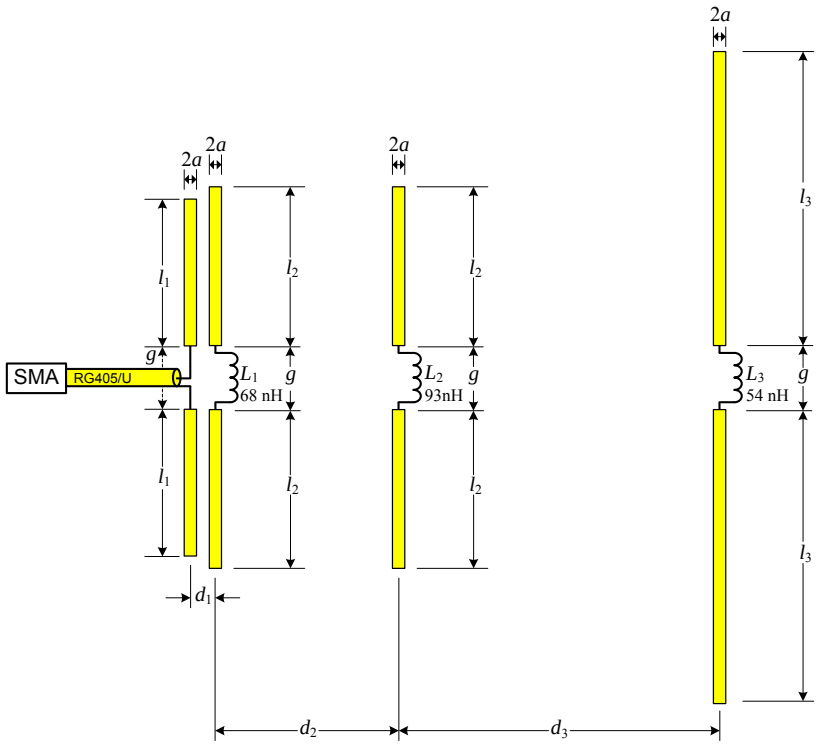

Figure 4.22 Geometry of 3rd order dipole antenna filter and all dimensions are a = 0.75 mm, g = 5 mm, l_1 = 14.6 mm, l_2 = 17 mm, l_3 = 29.45 mm, d_1 =2.5 mm, d_2 = 19.8 mm, d_3 = 30.8 mm.

4.4.2 Calculation and Simulation Results

Figure 4.22 shows the completed structure of the 3rd order dipole antenna-filter. All of the dimensions shown in Figure 4.22 have been defined and correspond to the calculated design parameters. The length of the 3rd resonator is longer than the others because that length can ensure Q_{u3} that is equal to Q_{e1} value for this design. The simulated response of the return loss S_{11} is compared with that obtained through calculation, as shown in Figure 4.23. The simulation and calculation results are in reasonable agreement. The simulated passband S_{11} level is about -17.5 dB whereas the calculation is -20 dB. The difference between simulation and calculation occurs as a result of additional losses included in the designed structure and may affect the response.

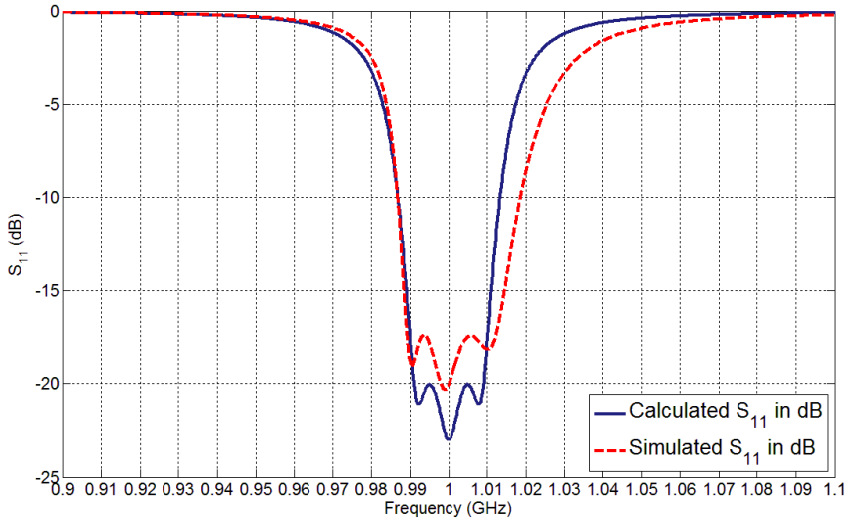

Figure 4.23 Calculated and simulated response of S_{11} of 3rd order dipole antenna filter.

4.4.3 Fabrication and Measurement

The 3rd order dipole antenna-filter has been fabricated based on the physical dimensions given in Figure 4.22. Figure 4.24 shows a photograph of the fabricated 3rd order dipole antenna-filter. The device has been tuned with a small movement in the position of the third dipole to achieve the desired response. The measured S_{11} is compared with the simulated S_{11} as shown in Figure 4.25. The three-pole antenna filter was measured to have the S_{11} response with the passband bandwidth that is slightly larger than the simulation.

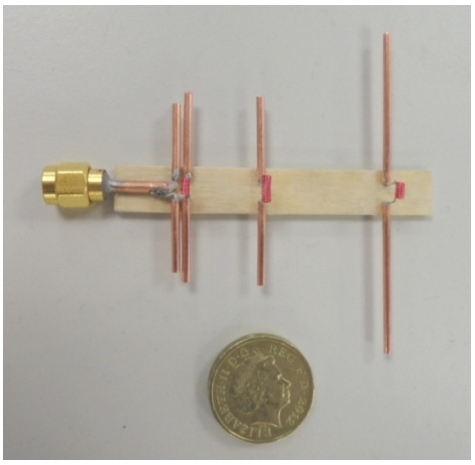

Figure 4.24 The photograph of the fabricated 3rd order dipole antenna filter.

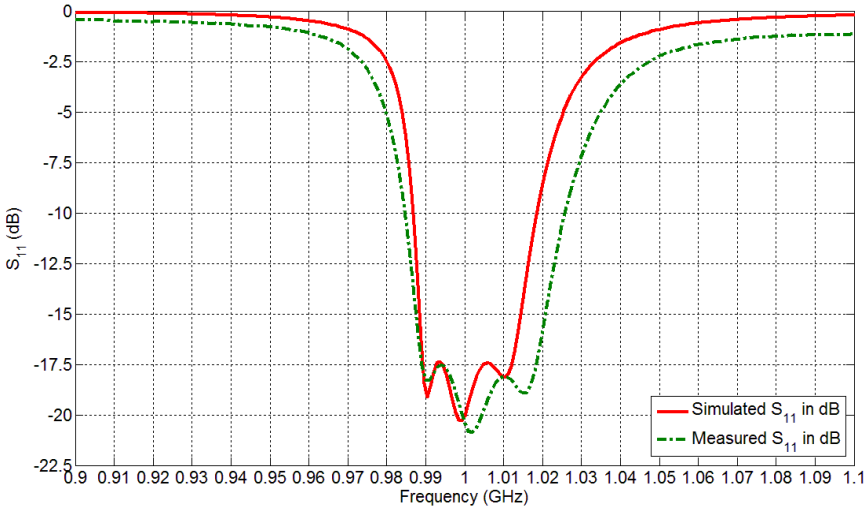

Figure 4.25 Simulated and measured S_{11} response of 3rd order dipole antenna filter.

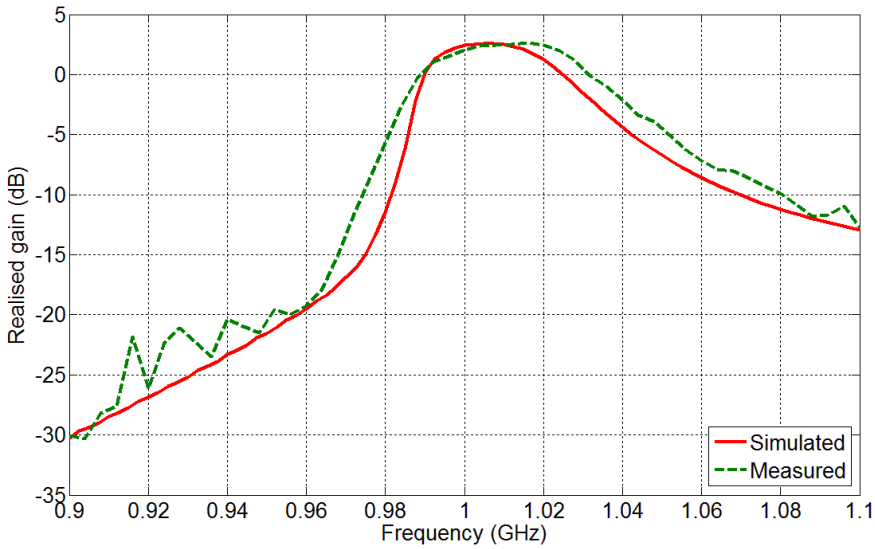

Figure 4.26 Simulated and measured realised gain of 3rd order dipole antenna filter.

The realised gain response of three-pole antenna filter was measured and compared with the simulation, as shown in Figure 4.26. The measured results are in good agreement with the simulations. The maximum measured realised gain is 2.6 dB whereas simulated value is 2.56 dB. The response shape of realised gain shows the filtering response that is similar to the bandpass filter.

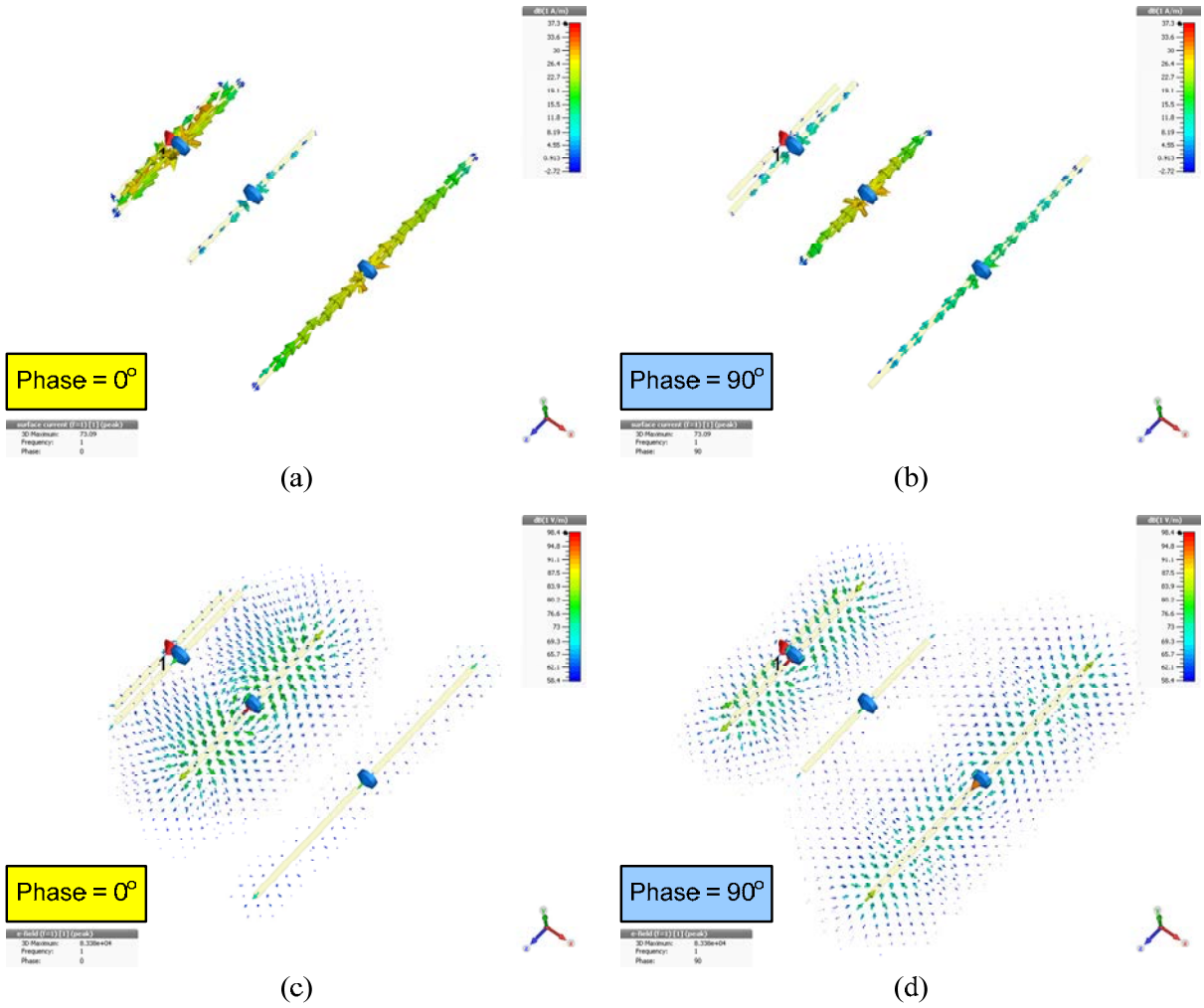

Figure 4.27 The simulated results of 3rd order dipole antenna-filter at 1 GHz shown in three-dimensions (3D) for the surface current (a, b) and the E-field propagation (c, d).

The directional radiation pattern of the dipole antenna-filter can be identified by looking at the current distribution and E-field propagation at the centre frequency f_0 of 1 GHz obtained using CST simulation software [3]. The simulated currents on the structure of 3rd order dipole antenna-filter at 1 GHz are shown in Figure 4.27(a) for the phase of 0° and 4.27(b) for the phase of 90°. The simulated E-field propagations at 1 GHz are represented as the voltage surrounding the structure and are shown in Figure 4.27(c) for the phase of 0° and 4.27(d) for the phase of 90°. Looking at the current at phase = 0° in Figure 4.27(a), it can be seen that the

maximum amplitude of current distribution occurs at the middle of the back-side of the structure where is a feed or a driven element. Also, the current at the feed is higher than the current amplitude occurred at the front-side where it is the third dipole element. However, the third element is longer than the feed and performs as similar to a reflector of an end-fire Yagi-Uda dipole array. This can be verified based on the impedance of a reflector element that represents the inductive using CST simulation software [3]. Looking at the phase = 0°, the current surrounding on the third element shown in Figure 4.27(a) is high, whereas the voltage surrounding the third element shown in Figure 4.27(c) is low. On the other hands, at the phase = 90°, the current on the third element shown in Figure 4.27(b) is low, whereas the voltage surrounding the third element shown in Figure 4.27(d) is high. The results show that the current on the third element lags the voltage induced on the third element in 90 degrees, which its impedance represents the inductive as similar to a reflector element of an end-fire Yagi-Uda dipole array. In addition, the radiated power (P_r) is related to the maximum current (I_m) excited on the structure corresponding to an equation [6]; $P_r = |I_m|^2/R_r$. Thus, the main directional radiation pattern will be occurred at the back-side of this structure where is the maximum current I_m occurred, as shown in Figure 4.28. It can be concluded that the main directional radiation pattern of the 3rd order dipole antenna-filter goes to the back-side (at $\theta = 180^o$), because (i) the third dipole element serves as the reflector and (ii) the maximum amplitude of the current on the structure occurs at the feed or the back-side of the structure. Thus, the radiation pattern of this design is not the omnidirectional like a single dipole but it is more similar to an end-fire Yagi-Uda dipole array. Also, the structure of the antenna-filter has three-radiation elements arraying as similar to an end-fire Yagi-Uda dipole array.

The measured radiation patterns at frequencies within the passband are in good agreement with the simulation, as shown in Figure 4.29. The 3rd order dipole antenna-filter has the maximum cross-polarisation levels in H-plane at 1 GHz shown in Figure 4.29(b) that are -13 dB in the simulation and -13.31 dB in the measurement, whereas the maximum cross-polarisation levels in E-plane at 1 GHz shown in Figure 4.29(e) are -14 dB in the simulation and -20.44 dB in the measurement. The 3 dB beamwidth at 1 GHz, in the E-plane, is 78 degrees according to simulation and 74 degrees in the measurement. It is smaller than the 2nd order antenna-filters by about 6 degrees in simulation and 2 degrees in measurement. The performance of the 3rd order dipole antenna-filter is summarised and presented in Table 4.2.

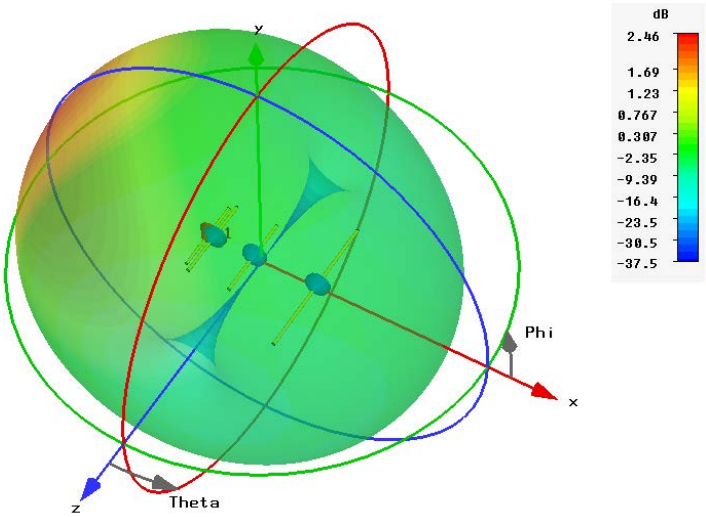

Figure 4.28 The simulated radiation pattern of 3rd order dipole antenna-filter at 1 GHz in three-dimensions (3D).

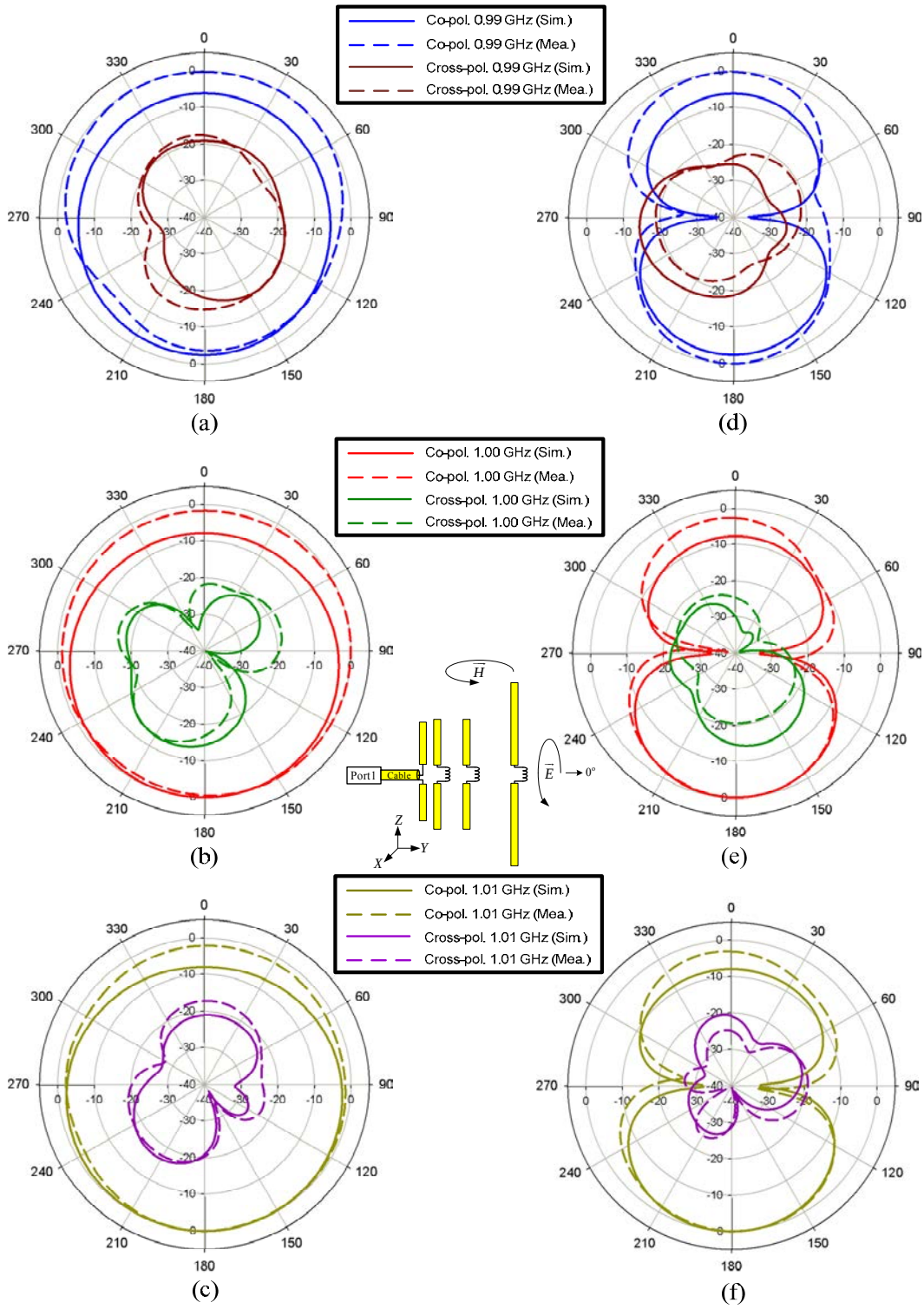

Figure 4.29 Normalised simulated and measured radiation patterns of 3rd order dipole antenna filter at 0.99 GHz, 1 GHz, 1.01 GHz for H (XY) plane (a, b, c) and E (YZ) plane (d, e, f). (Radial units are dB. Circumferential scale is θ in degrees.)

Table 4.2 Summary of the 3rd order dipole antenna-filter performance

Parameters	**Frequency (GHz)**	**3 dB Beamwidth (deg.)**		**Back lobe level (dB)**		**Cross-polarisation level (dB)**	
		Sim.	Mea.	Sim.	Mea.	Sim.	Mea.
H-plane	0.99	164	195	-6.32	-1.20	-15.32	-14.57
	1.00	164	194	-7.81	-1.91	-13.00	-13.31
	1.01	162	192	-7.96	-2.13	-16.38	-17.18
E-plane	0.99	76	66	-6.32	-1.20	-14.09	-18.87
	1.00	78	74	-7.81	-2.84	-14.00	-20.44
	1.01	82	86	-7.96	-3.14	-20.18	-19.00

The directivity, radiation and total efficiencies of dipole antenna-filters are obtained from the simulation and are used to compare their performances. These three parameters are related to the realised gain responses of dipole antenna-filters which will be shown below. The simulated directivity versus frequency of three dipole antenna-filters is shown in Figure 4.30. The simulated directivity of 3rd order dipole antenna-filter at the centre frequency (f_0) of 1 GHz has the highest value comparing with 2nd and 1st order dipole antenna-filters by about 2.2 dBi and 2.9 dBi, respectively. The simulated radiation and total efficiencies are used to describe the radiation performance of antenna-filters and are shown in Figure 4.31 and 4.32, respectively. It can be observed that the 3rd order dipole antenna filter exhibits good stop-band suppression comparing with others for both radiation and total efficiencies. However, the radiation efficiency at 1 GHz for the 3rd order dipole antenna-filter is lower than the 2nd order

dipole antenna-filter as 17.34 %, but it is higher than the 1st order dipole antenna-filter as 3.72%. Similarly, the total efficiency at 1 GHz for the 3rd order dipole antenna-filter is lower than the 2nd order dipole antenna-filter as 16.64 %, but it is higher than the 1st order dipole antenna-filter as 31.59%. Although the antenna efficiencies of the 3rd order dipole antenna-filter is not higher than the 2nd order dipole antenna-filter, but its realised gain is higher than 2nd order dipole antenna-filter in the passband. This is because the directivity of the 3rd order dipole antenna-filter is higher than the directivity of the 2nd order dipole antenna-filter in the passband bandwidth of interest. It is noted that the realised gain is usually obtained from the sum of total antenna efficiency and antenna directivity in the unit of decibel (dB). This can be seen the realised gain responses of three dipole antenna-filters obtained from simulation and measurement, as shown in Figure 4.33.

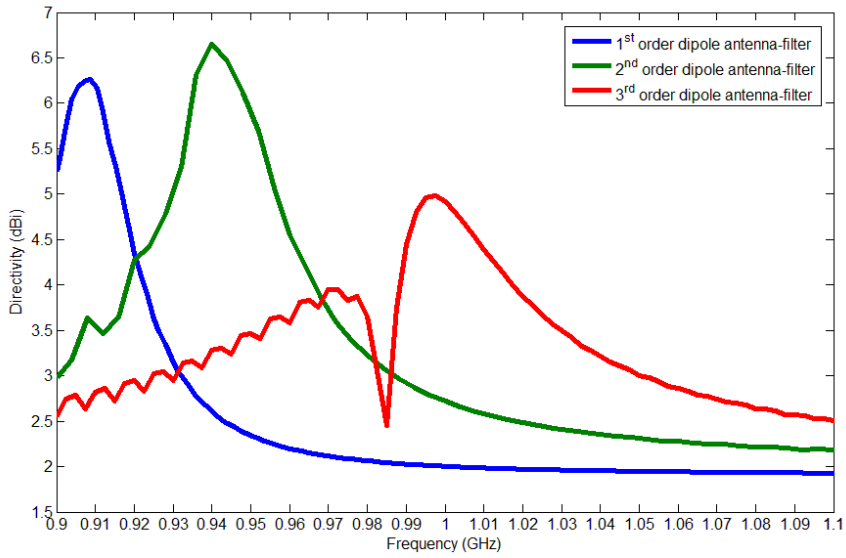

Figure 4.30 Simulated directivity versus frequency of three dipole antenna-filters.

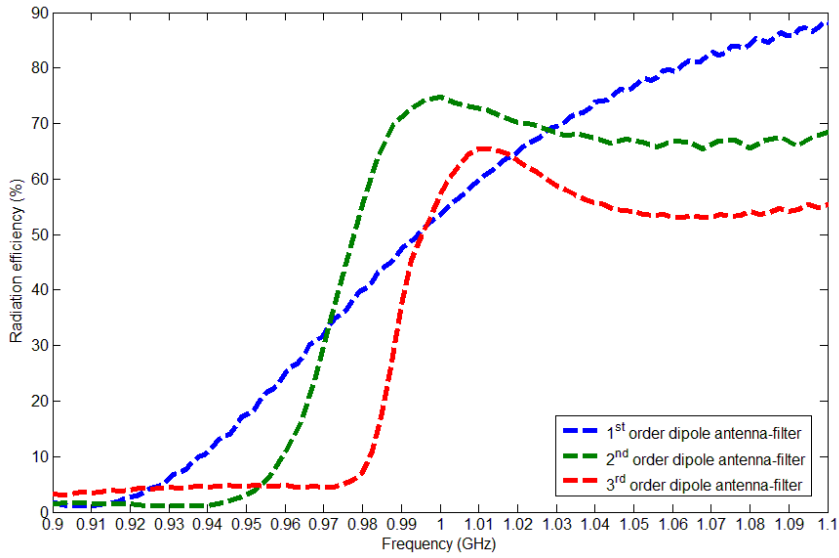

Figure 4.31 Simulated radiation efficiency versus frequency of three dipole antenna-filters.

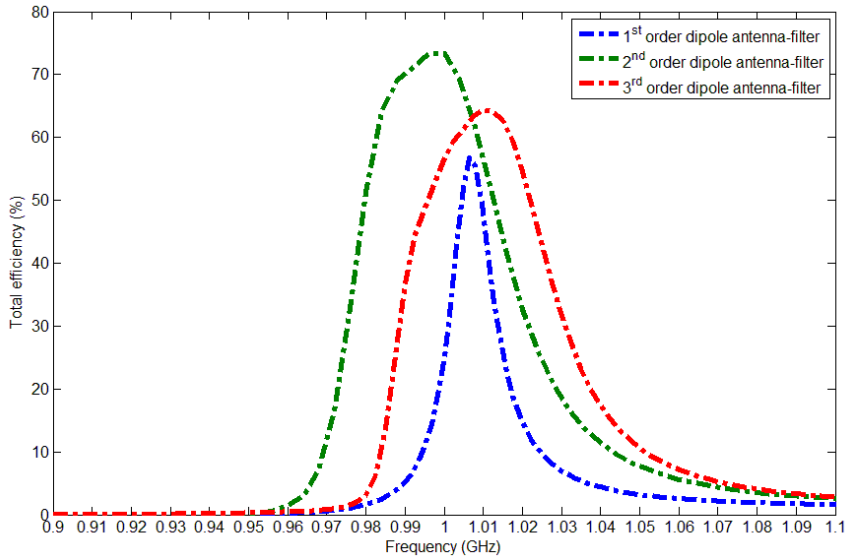

Figure 4.32 Simulated total efficiency versus frequency of three dipole antenna-filters.

The simulated realised gain of the 3rd order dipole antenna-filter observed in the passband is higher than 1st and 2nd order dipole antenna-filters as 3.31 dB and 1.56 dB, respectively, whereas the measured result is higher than 1st and 2nd order dipole antenna-filters as 3.63 dB and 1.24 dB, respectively. The simulated stopband rejection of the 3rd order dipole antenna-filter is estimated at the out-of-band of the realised gain response and is higher than 1st and 2nd

order dipole antenna-filters as about 3.38 dB and 1.39 dB, respectively, whereas the measured result is higher than 1st and 2nd order dipole antenna-filters as about 3.73 dB and 0.76 dB, respectively. The results of 3rd order dipole antenna-filter show good filtering performance for the realised gain that is better than 1st and 2nd order dipole antenna-filters as expected. The performance of three-dipole antenna-filters is summarised and shown in Table 4.3.

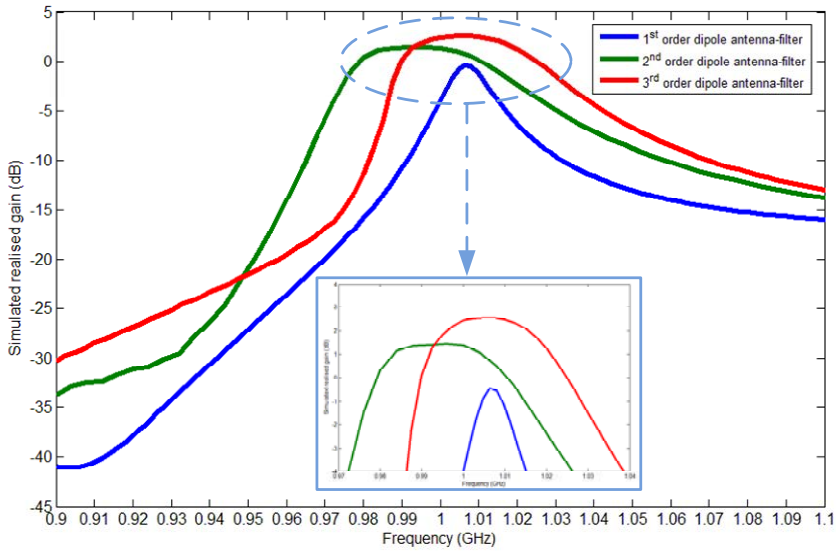

(a)

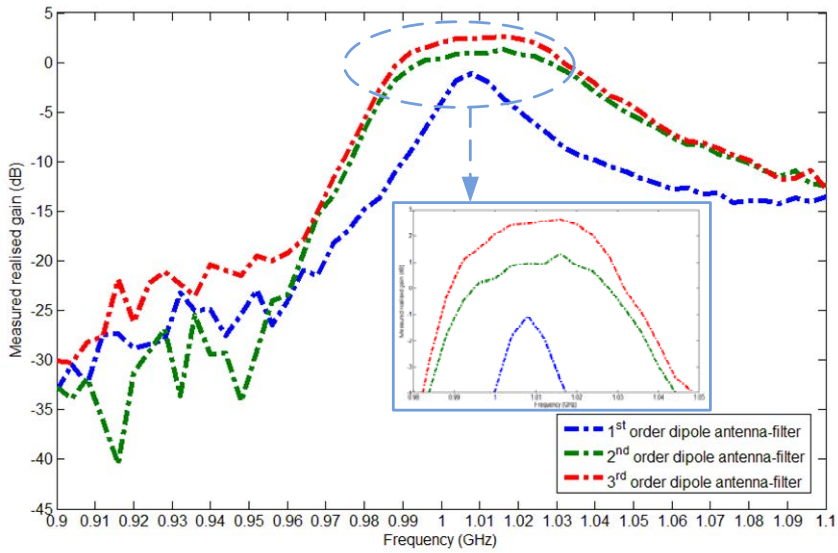

(b)

Figure 4.33 Realised gain responses of three dipole antenna-filters obtained from (a) simulation. (b) measurement.

Table 4.3 Summary of three dipole antenna-filter performance.

Component	**Passband return loss S_{11} (dB)**		**Passband realised gain (dB)**		**Stopband rejection (dB)**	
	Sim.	Mea.	Sim.	Mea.	Sim.	Mea.
1st order dipole antenna-filter	-26.84	-26.25	-0.75	-1.09	9.22	8.75
2nd order dipole antenna-filter	-19.18	-20.39	1.00	1.30	11.21	11.72
3rd order dipole antenna-filter	-17.36	-17.51	2.56	2.54	12.60	12.48

The performance improvement of the designed 3rd order dipole antenna-filter can be verified by comparing with a single dipole antenna. This dipole antenna-filter has better performance in comparison with a single dipole operating at the same frequency. The length l_d of the dipole is 140 mm, whereas the longest length l of the antenna-filter (resonator 3) is 64 mm. Figure 4.34 shows the comparison between the simulated realised gain of the dipole antenna-filter and the single dipole antenna. It is shown that the gain of the antenna-filter is 0.37 dB higher than that of the gain of the dipole. The response of antenna-filter shows the filtering response with the improvement of out-of-band suppression. This can be further improved by increasing the number of resonator used (i.e. dipoles with inductors).

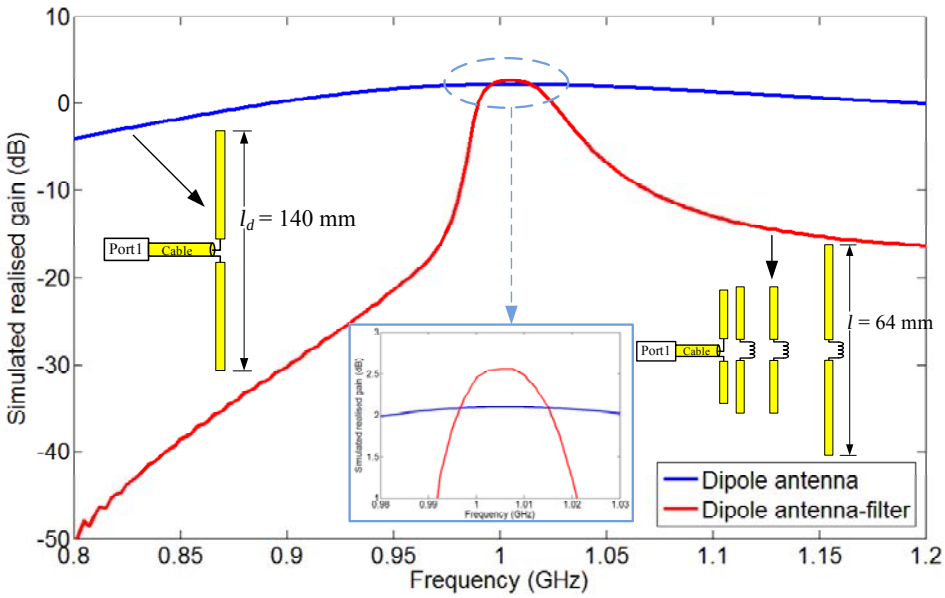

Figure 4.34 Comparison of simulated realised gain between single dipole antenna and 3rd order dipole antenna-filter.

4.5 Conclusions

The coupling matrix for the one-port component has been used to design and optimise the filtering responses of three dipole antenna-filter components. The design approaches show the progression of antenna-filters in order to understand the design principle based on the coupled-resonator filter theory. The performance of the 3rd order dipole antenna-filter shows the improvement in the realised gain compared with the single dipole antenna, and the size is also smaller. The realised gain response shows the filtering response with good stop-band rejection and a flat in that passband. The structure of 3rd order dipole antenna-filter is similar to an end fire Yagi-Uda dipole array and exhibits the main directional radiation pattern at $\theta = 180^{o}$. This is because the last element served as the reflector and also the maximum current occurred at the feed. Three proposed dipole antenna-filters have small sizes, are light in weight and are suitable to use in wireless communication system.

References

[1] Hong J. S. and Lancaster M. J. Microstrip Filters for RF/Microwave Applications. New York, USA: John Wiley & Sons; 2001.

[2] Cameron R. J., Kudsia C. M. And Mansour R. R. Microwave Filters for Communication Systems: Fundamental, Design, and Applications. New Jersey, USA: John Wiley & Sons; 2007.

[3] Computer Simulation Technology (CST), Microwave Studio [Internet]. 2014 Available from URL: http://www.cst.com.

[4] Lancaster M. J. Passive Microwave Device Applications of High-Temperature Superconductors. Cambridge, UK: Cambridge University Press; 1997.

[5] Kraus J. D. and Marhefka R. J. Antennas For All Applications. 3rd ed. New York, USA: McGraw-Hill; 2003.

[6] Balanis C. A. Antenna Theory Analysis and Design. 3rd ed. New Jersey, USA: John Wiley & Sons; 2005.

Chapter 5

Waveguide Antenna-Filters

5.1 Introduction

Chapter 4 presented design methodology for a one-port dipole antenna-filter. This methodology involved using the coupling matrix for lossy resonator circuits, to optimise return loss (S_{11}) of low Q_u resonators. In general, all resonators in the filter circuit require a high unloaded quality factor in order to improve the passband frequency response [1]. For example, a rectangular waveguide cavity resonator can provide high unloaded quality factor. The structure of a rectangular cavity [2] when enclosed has low energy loss in the resonator. The design is simple and can be utilised to combine with other waveguide components such as waveguide aperture antennas. This chapter presents three design approaches for X-band waveguide aperture antennas which are integrated with the rectangular waveguide cavity resonators. Figure 5.1(a) shows a diagram of the first design. The concept is to replace the last resonator of the filter circuit with an antenna. In this case, the antenna can serve simultaneously in as one of the resonators of the filter and a radiator. In addition, the approach shown in Figure 5.1 (b) is called an *antenna power divider*. The principle of the filter design is used here to combine the bandpass filter, the power divider and two-antenna array into a single component. The third approach shown in Figure 5.1 (c), which involved integrating with a pair of bandpass filters for splitting two frequency bands and is named an *antenna-diplexer*. The three design approaches presented here may be of interest in the reduction of sizes in comparison with the conventional designs. Coupling matrix synthesis is employed for all three-designs. The three design approaches, mentioned above, have been fabricated. They

are a 5-resonator antenna-filter, a 3-resonator power divider, and a 3-resonator antenna-diplexer. These three components are designed to operate at X-band frequencies using waveguide technology. They have been fabricated and measured.

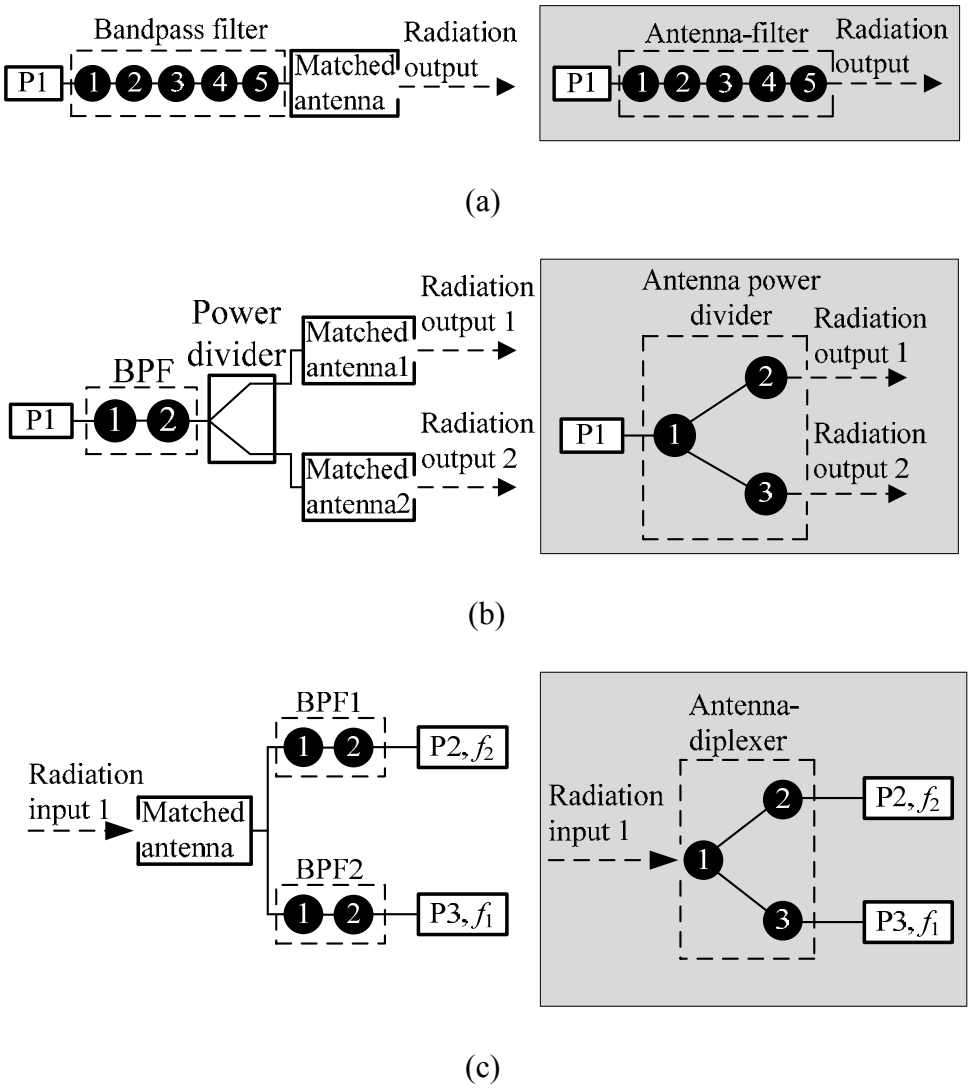

Figure 5.1 Block diagrams comparing the new approach (diagrams on the right) to that of conventional antenna (on the left): (a) Antenna-filter (b) Antenna power divider (c) Antenna-diplexer.

In this chapter, Section 5.2 presents the overview of the rectangular waveguide cavity. Section 5.3 presents the design of the waveguide aperture antenna. Section 5.4 describes the methodology for extracting the coupling coefficient extraction from the physical structure of waveguide components. The coupling matrix synthesis is presented in Section 5.5. The design, simulation, fabrication and measurement of the X-band 5-resonator antenna-filter, the X-band 3-resonator antenna power divider and the X-band 3-resonator antenna diplexer are discussed in Section 5.6, Section 5.7 and Section 5.8, respectively. A conclusion is given in Section 5.9.

5.2. Quality Factors of Cavity Resonators

The cavity resonator design has been described in Chapter 2. The total quality factor of a cavity resonator coupled to an external circuit can be expressed using the loaded quality factor (Q_l), which may be defined as [3]

$$\frac{1}{Q_l} = \frac{1}{Q_e} + \frac{1}{Q_u} \tag{5.1}$$

where Q_e is the external quality factor associated with the external coupling at the input port.

Q_u is the unloaded quality factor associated with losses in the resonator.

The total Q_u of the cavity resonator may be defined by adding these losses together as follows [3]

$$\frac{1}{Q_u} = \frac{1}{Q_c} + \frac{1}{Q_d} + \frac{1}{Q_r} \tag{5.2}$$

where Q_c, Q_d and Q_r are the conductor, dielectric and radiation quality factors, respectively.

For an air-filled waveguide cavity resonator, the resonator has an enclosed structure covered with conducting material and no dielectric material within the cavity walls. It implies that the

total Q_u of the cavity resonator only considers the conductor quality factor (Q_c). The Q_c of the rectangular waveguide cavity resonator for TE_{101} mode is defined as [2]

$$Q_c = \frac{\left(k_{101} a \cdot d\right)^3 b \cdot \eta}{2\pi^2 R_s \left(2a^3 b + 2bd^3 + a^3 d + ad^3\right)} \tag{5.3}$$

where $\eta = \sqrt{\mu / \varepsilon}$ is the wave impedance.

$\mu = \mu_r \cdot \mu_0$ is the permeability (H/m).

μ_r is the relative permeability of a material.

$\mu_0 = 4\pi$ x 10^{-7} H/m is the permeability of free space.

$\varepsilon = \varepsilon_r \cdot \varepsilon_0$ is the permittivity (F/m).

ε_r is the relative permittivity of a material.

$\varepsilon_0 = 8.854$ x 10^{-12} F/m is the permittivity of free space.

R_s is the surface resistance of the conducting wall is given by [2]

$$R_s = \sqrt{\frac{\omega\mu}{2\sigma}} \tag{5.4}$$

where $\omega = 2\pi f$ is the angular frequency (rad/sec).

σ is the conductivity of materials (S/m).

For example, the copper cavity in [4] has a surface resistance R_s = 0.022 Ω and a conductor quality factor Q_c = 12,700. The cavity size was $a = b = d$ = 3 cm, that corresponds to the resonant frequency of 7,070 MHz.

5.2.1 Extraction of External Quality Factor from Physical Structure

This section presents the methodology for extraction of the external quality factor from the physical structure of a rectangular waveguide cavity, using CST simulation software [5].

In this work, the WR-90 waveguide is employed to design a resonant cavity circuit. The initial dimension of the WR-90 waveguide cavity resonator has been defined, as described in Chapter 2. The geometry of the cavity resonator coupled to the input/output ports is shown in Figure 5.2.

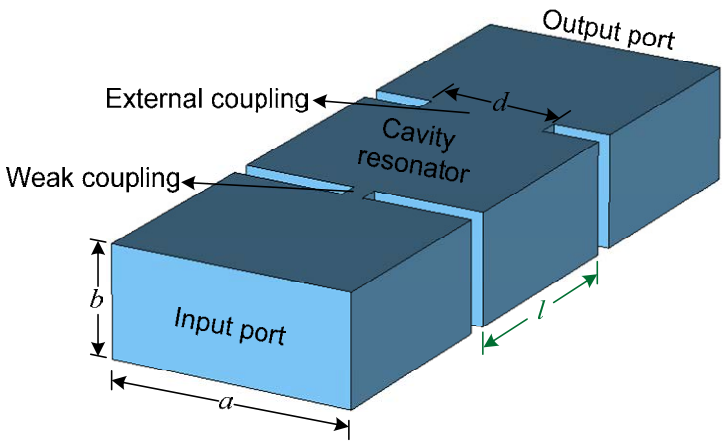

Figure 5.2 Geometry of a cavity resonator coupled to the input/output ports. a = 22.86 mm, b = 10.16 mm, l = 19.88 mm.

The waveguide cavity structure, shown in Figure 5.2, has been made in the CST simulation software [5]; the blue part is the vacuum, which is covered with a perfect electrical conducting material (PEC). This material is a lossless material, which is no conductor loss considered in the resonator. The input port needs to be weakly coupled to the cavity through a small aperture of an inductive iris [6] for this approach to work. The inductive iris is located between the cavity and the output port. The aperture d can be adjusted in order to change the value of Q_e. The thickness of the iris is selected as 2 mm. The external quality factor Q_e can be obtained from the simulated magnitude of S_{21} response using a formula [1], given as

$$Q_e = \frac{f_0}{\Delta f_{3dB}} \tag{5.5}$$

where f_0 is the centre frequency of the loaded resonator, $\Delta f_{3dB} = f_2 - f_1$ is the 3 dB bandwidth, f_1 and f_2 are frequency points in the 3 dB bandwidth as indicated in Figure 5.3.

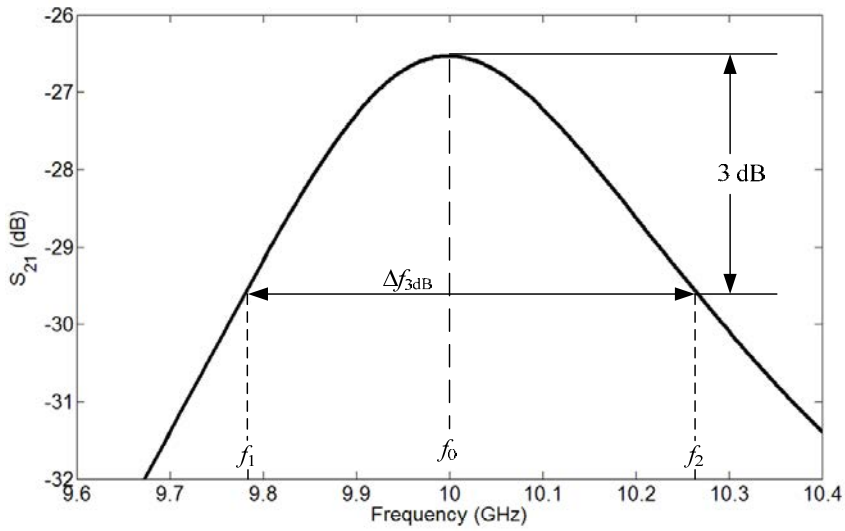

Figure 5.3 The simulated magnitude of S_{21} response of the structure in Figure 5.4. In this case $Q_e = 20.96$.

The simulated structure, shown in Figure 5.2, is a prototype structure used to obtain the Q_e values for different values of d. This is achieved using from the simulated S_{21} response using the equation (5.5). Here l has been adjusted to keep the centre frequency of 10 GHz. The Q_e and l values for different values of d are plotted in Figure 5.4. This plotted Q_e graph will be utilised in the design of the antenna-filter in Section 5.6.

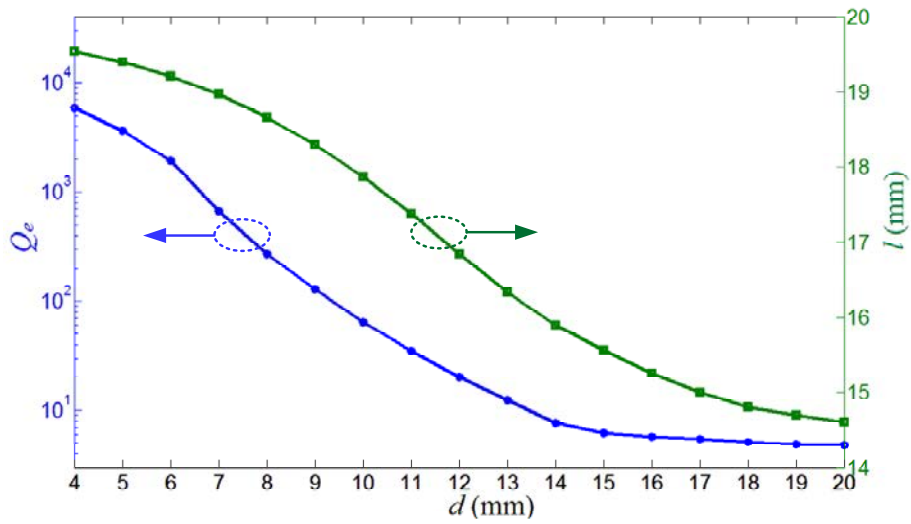

Figure 5.4 Q_e and l values of the waveguide cavity resonator obtained from the simulated S_{21} response with a centre frequency of 10 GHz for different values of d.

5.3 Waveguide Aperture Antennas

This section presents a design for a waveguide aperture antenna which utilises the inductive irises. The structure of a single resonator waveguide aperture antenna is represented, as depicted in Figure 5.5. Here Q_e and Q_r are the quality factors associated with the external coupling at the input port and the radiation resistance. The total Q_l for the waveguide aperture antenna can be defined as

$$\frac{1}{Q_l} = \frac{1}{Q_e} + \frac{1}{Q_r} \tag{5.6}$$

In the simulation, the antenna structure has been made from a PEC material. The resonator antenna is weakly coupled to the input port with an inductive iris. The coupling coefficient between the resonator and the external circuit is determined using the formula in [3], given as

$$\beta = \frac{P_e}{P_0} = \frac{Q_u}{Q_e} \tag{5.7}$$

where β is the coupling coefficient between the resonator and the external circuit.

P_e is the average power loss from the resonator to the external circuit.

P_0 is the average power loss in the resonator.

Following equation (5.7), weak coupling means the value of coupling coefficient can be approximated to be zero $(\beta \cong 0)$ leading to a Q_e value of infinity. Thus, equation (5.6) can be approximated as $Q_l = Q_r$.

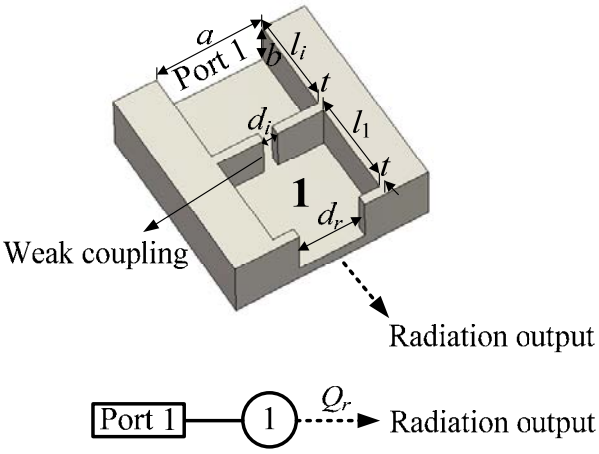

Figure 5.5 The structure of a waveguide aperture antenna with top cover removed. a = 22.86, b = 10.16, d_i = 3, l_i = 20 and t = 2. Unit: mm.

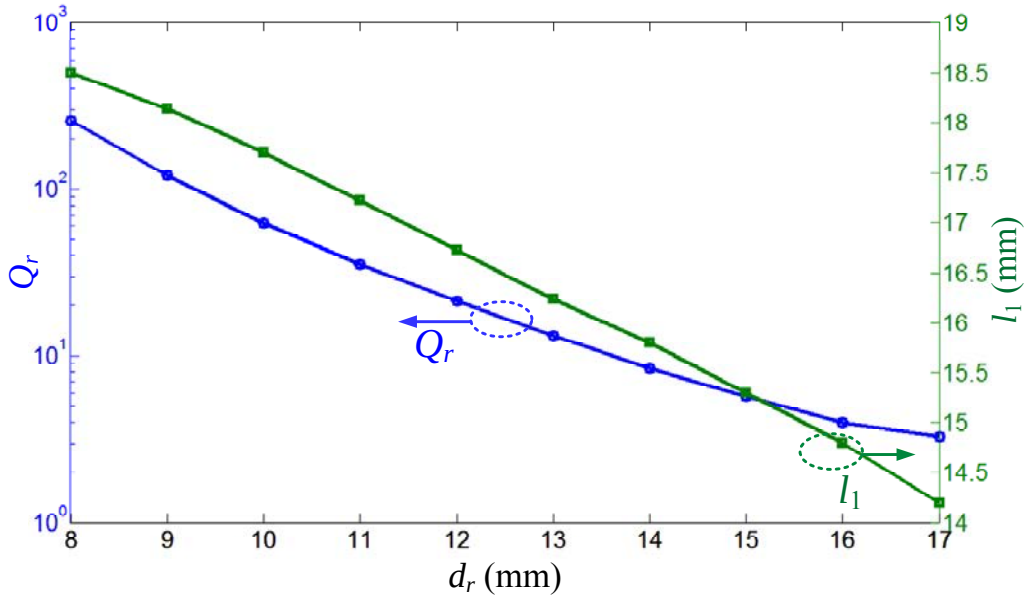

Figure 5.6 The Q_r and l_1 values of a waveguide aperture antenna obtained from the simulated S_{11} response with a resonant frequency of 10 GHz for different values of d_r.

The antenna structure shown in Figure 5.5 is utilised to obtain the Q_r value using CST simulation software [5]. The Q_r value is extracted from the simulated response of S_{11} magnitude using a Q-calculation for a one-port component [3]. The antenna structure, shown in Figure 5.5 can be designed to increase the value of Q_r by reducing d_r. Here l_1 has been

adjusted to keep the centre frequency at 10 GHz. The value of Q_r is obtained from CST simulation [5]. A curve of Q_r values versus d_r is plotted in Figure 5.8. Q_r will be employed in the design of the antenna-filters, in Section 5.6. Specifically, it will be used to define the physical aperture dimensions to match the Q_e of the filter with the Q_r of the design.

5.4 Coupling Coefficient Extraction from Physical Structure

This section presents the methodology for extraction of the coupling coefficient from the physical structure incorporating two-coupled cavities. This is achieved using the CST simulation software [5]. Figure 5.7 shows an example of the waveguide structure utilised to extract the coupling coefficient (M). The structure represents two cavity resonators coupled together with an inductive iris. The input and output ports are weakly coupled to the cavity resonator with inductive irises having a small aperture size.

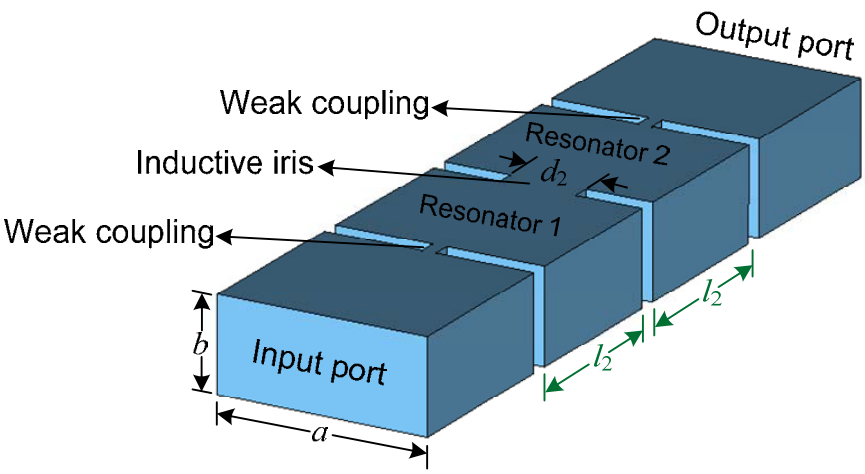

Figure 5.7 The simulated structure of two-coupled waveguide cavity resonators. a = 22.86 mm, b = 10.16 mm.

The coupling coefficient can be obtained from the simulated response of S_{21} magnitude using a formula for a synchronously tuned coupled resonator from [1] as

$$M = \frac{f_{p2}^2 - f_{p1}^2}{f_{p2}^2 + f_{p1}^2} \tag{5.8}$$

where M is the coupling coefficient, f_{p2} is the higher resonant peak of S_{21} and f_{p1} is the lower resonant peak of S_{21}, as indicated in Figure 5.8.

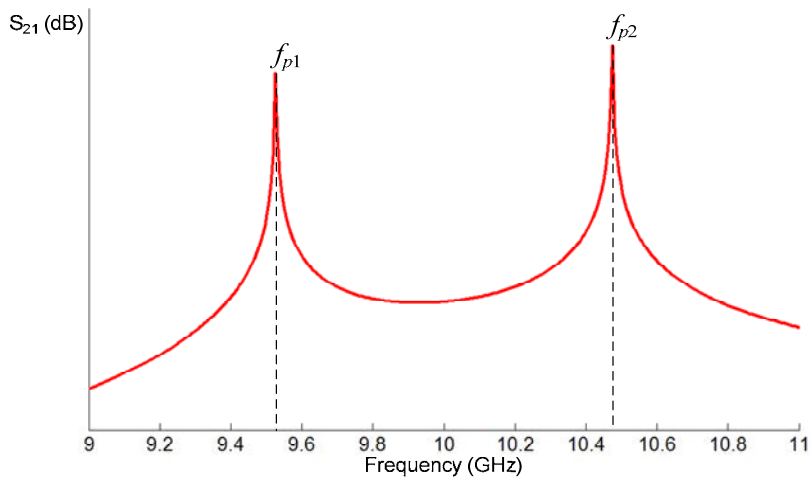

Figure 5.8 The simulated magnitude of S_{21} for the structure shown in Figure 5.7. The coupling coefficient here is $M = 0.0942$.

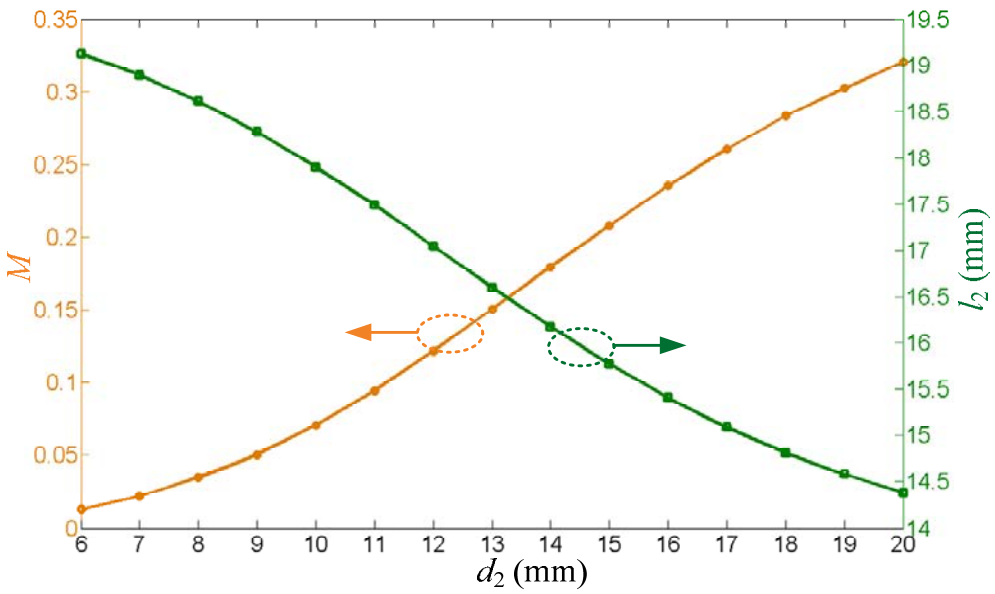

Figure 5.9 M and l_2 values of the two-coupled waveguide cavity resonators obtained from the simulated S_{21} response with a centre frequency of 10 GHz for different values of d_2.

The simulated structure, shown in Figure 5.7, can be utilised to obtain the M values for different values of d_2 from the simulated S_{21} response using equation (5.8). Here l_2 has been adjusted to keep the centre frequency of 10 GHz. The M and l_2 values for different values of d_2 are plotted in Figure 5.9. The graph showing M will be utilised in the design of antenna-filter, in Section 5.6.

The self-coupling coefficient M_{ii} is related to the self-resonant frequency of the resonator i in a filter. For the case of asynchronous tuning, it is defined by [7]

$$M_{ii} = 2\left(\frac{f_{0i}^2 - f_0^2}{f_{0i}^2 + f_0^2}\right) \tag{5.9}$$

where f_{0i} is the resonant frequency of the resonator i and f_0 is the desired centre frequency. Equation (5.9) can be used to extracting the self-coupling coefficient M_{ii} from the waveguide structure for the design of an antenna-diplexer, in Section 5.8.

5.5 Coupling Matrix Synthesis for Multiple Port Antenna-Filters

In this work, the coupling matrix of the antenna-filter circuit is chosen for the design. It is used in a similar way to the coupled-resonator two-port filter circuits [1] and Chapter 2. Here the radiation inputs/outputs of proposed antenna-filters are considered as the input/output ports of the equivalent filter. Matrix [A] can be expressed as [8]

$$[A] = [q] + p[U] - j[m] \tag{5.10}$$

where [U] is the n x n unit matrix, p is the complex frequency variable i.e. $p = (j/FBW)(f/f_0 - f_0/f)$, f_0 is the centre frequency and FBW is the fractional bandwidth, [q] is an n x n matrix with all entries zero, except for $q_{ii} = 1/q_{ei}$ for the input/output ports and $q_{ii} = 1/q_{ri}$ for the

radiation inputs/outputs, i stands for the index of the resonator connected to input/output ports and radiation inputs/outputs, q_{ei} is the normalised external quality factor of the resonators at the input/output ports (i.e. $q_{ei} = FBW \cdot Q_{ei}$), q_{ri} is the normalised radiation quality factor of the antennas at the radiation inputs/outputs (i.e. $q_{ri} = FBW \cdot Q_{ri}$). Both Q_{ei} and Q_{ri} are the external quality factor at the input/output ports and the radiation quality factors at the radiation inputs/outputs. They are calculated from the normalised quality factors q_{ei} and q_{ri} by

$$Q_{ei} = \frac{q_{ei}}{FBW} \tag{5.11}$$

and

$$Q_{ri} = \frac{q_{ri}}{FBW} \tag{5.12}$$

These Q_{ei} and Q_{ri} values are utilised as the Q_e and Q_r values extracted from the physical dimensions of the waveguide structure in order to realise the waveguide device. Also, $[m]$ is the normalised coupling matrix whose elements are the normalised coupling coefficient between resonator i and j (i.e. $m_{ij} = M_{ij}/FBW$) and the self-couplings $m_{ii} = M_{ii}/FBW$. Here M_{ij} is the coupling coefficient between resonator i and j, M_{ii} is the self-coupling coefficient of resonator i. Both M_{ij} and M_{ii} are calculated from the normalised coupling coefficients m_{ij} and m_{ii} by

$$M_{ij} = FBW \cdot m_{ij} \tag{5.13}$$

and

$$M_{ii} = FBW \cdot m_{ii} \tag{5.14}$$

These M_{ij} and M_{ii} values are utilised as the M and M_{ii} values extracted from the physical dimensions of the waveguide structure in order to realise the waveguide device.

Assuming that we have a 3-port circuit, the *S*-parameters, for the coupling topology shown in Figure 5.1(b) and 5.1(c), can be derived from the matrix [*A*] in (5.10) as,

$$S_{ii} = \pm\left(1 - \frac{2}{q_{ei}}[A]_{ii}^{-1}\right) \tag{5.15}$$

$$S_{23} = \frac{2}{\sqrt{q_{e2} \cdot q_{e3}}}[A]_{23}^{-1} \tag{5.16}$$

where S_{ii} is the reflection coefficient at the input/output waveguide port *i*, S_{23} is the isolation of the proposed antenna-diplexer between waveguide port 2 and port 3, q_{ei} is the normalised external quality factor of resonator *i*, q_{e2} is the normalised external quality factor of resonator 2 and q_{e3} is the normalised external quality factor of resonator 3. In the case where one port is a radiation port. S_{21} and S_{31} are related to the frequency response of the gain, but are not considered here. A more generalised equation for three-port network, based on more than 3 resonators, is given in [8]. This multi-port matrix is used in Section 5.7 and 5.8.

5.6 X-Band 5-Resonator Waveguide Antenna-Filter

5.6.1 Waveguide Antenna-Filter Design

This section presents the design of a 5-resonator waveguide aperture antenna-filter. The coupling model of a 5-resonator waveguide antenna-filter is designed as an in-line topology, as shown in Figure 5.10. The antenna-filter is designed to have a 2% fractional bandwidth (*FBW* = 0.02) at the centre frequency f_0 of 10 GHz. A fifth-order Chebyshev lowpass prototype with a return loss of -20 dB is chosen. The coupling coefficients, external and radiation quality factors of the proposed design are calculated from the normalised conventional design equation (2.50) presented in Chapter 2; as in the matrix form,

$$[m]=\begin{bmatrix} 0 & 0.866 & 0 & 0 & 0 \\ 0.866 & 0 & 0.636 & 0 & 0 \\ 0 & 0.636 & 0 & 0.636 & 0 \\ 0 & 0 & 0.636 & 0 & 0.866 \\ 0 & 0 & 0 & 0.866 & 0 \end{bmatrix}$$

$q_{e1} = q_{r5} = 0.9714$

The calculated response of the S_{11} can be calculated from the values of $[m]$, q_{e1} and q_{r5}, using equation (5.15), the result is shown in Figure 5.11.

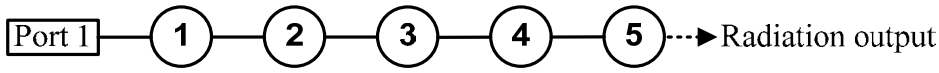

Figure 5.10 Topology of the designed waveguide antenna-filter.

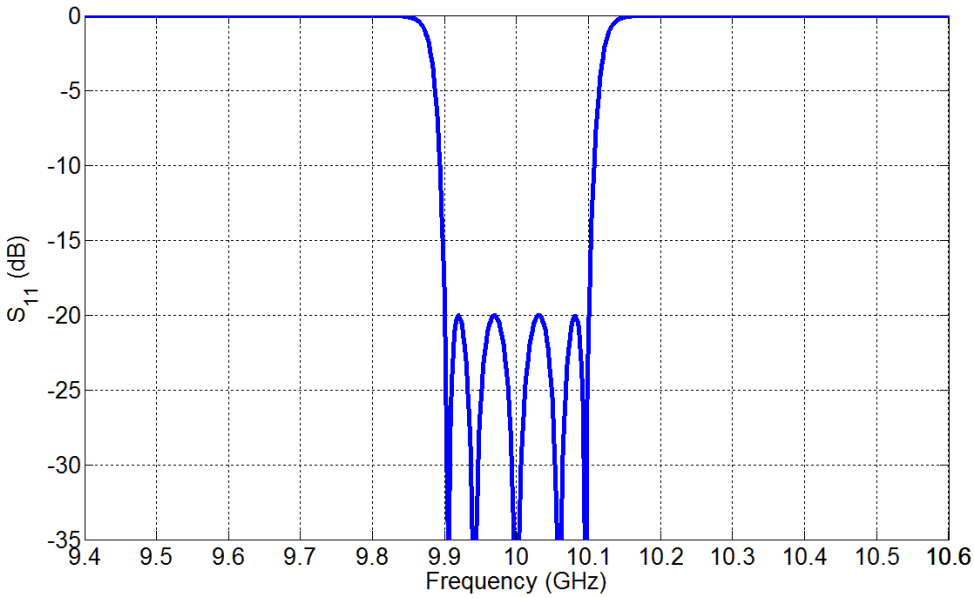

Figure 5.11 S_{11} in dB for the designed waveguide antenna-filter calculated from the coupling matrix.

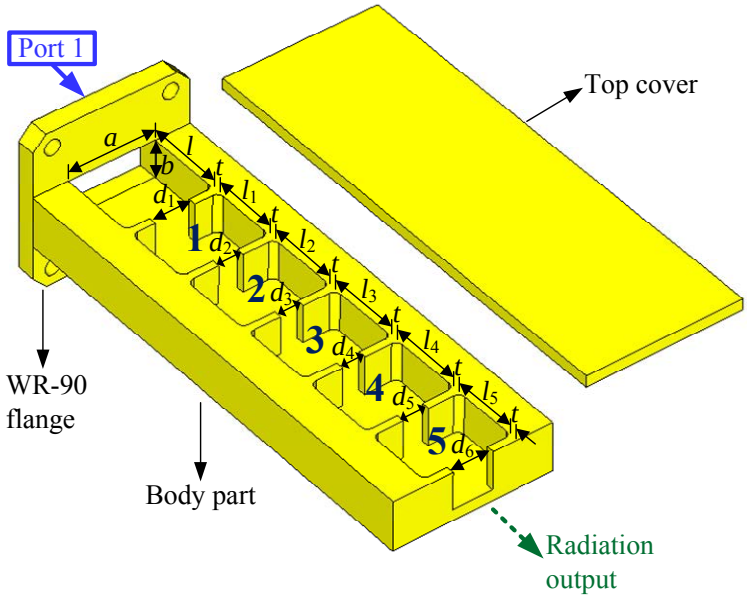

Figure 5.12 The three-dimensional schematic of the X-band 5-resonator antenna-filter.

Figure 5.12 shows the layout of the antenna-filter in three-dimensions. The antenna-filter has a direct-coupled resonator structure. The waveguide structure is designed for manufacturing using a CNC milling machine. All of the inside corners are rounded with a radius of 1.6 mm. These corners have only a minor effect on the performance of the antenna-filter. In order to define the physical dimensions of the waveguide structure, the coupling coefficient, the external quality factor and the radiation quality factor are calculated for FBW = 0.02 using equations (5.11) to (5.14) and found to be $M_{12} = M_{45} = 0.01732$, $M_{23} = M_{34} = 0.01272$, $Q_{e1} = Q_{r5} = 48.57$. These values will be utilised to find the initial physical dimensions of the waveguide structure as described in Section 5.2, 5.3 and 5.4, respectively. The whole waveguide structure of the antenna-filter is initially designed to have these initial physical dimensions. The simulated S_{11} response of the initial structure, is shown in Figure 5.13. The response can be improved by optimising the waveguide structure using the optimiser in the CST software package [5]. Starting from the initial response, the waveguide antenna-filter has been optimised to meet goals related to the passband performance (i.e. S_{11} <= -20 dB from 9.9

GHz to 10.1 GHz). This involved varying the length of cavity and antenna, the width of the coupling irises and the width of the aperture. The final simulated S_{11} response is shown in Figure 5.14. All dimensions of the optimised structure corresponding to the parameters shown in Figure 5.12 are: a = 22.86, b = 10.16, d_1 = 10.38, d_2= 6.42, d_3 = 5.84, d_4 = 5.84, d_5 = 6.52, d_6 = 10.49, l = 20, l_1 = 17.13, l_2 = 18.7, l_3 = 18.84, l_4 = 18.7, l_5 = 16.87, t = 2 (Unit: mm).

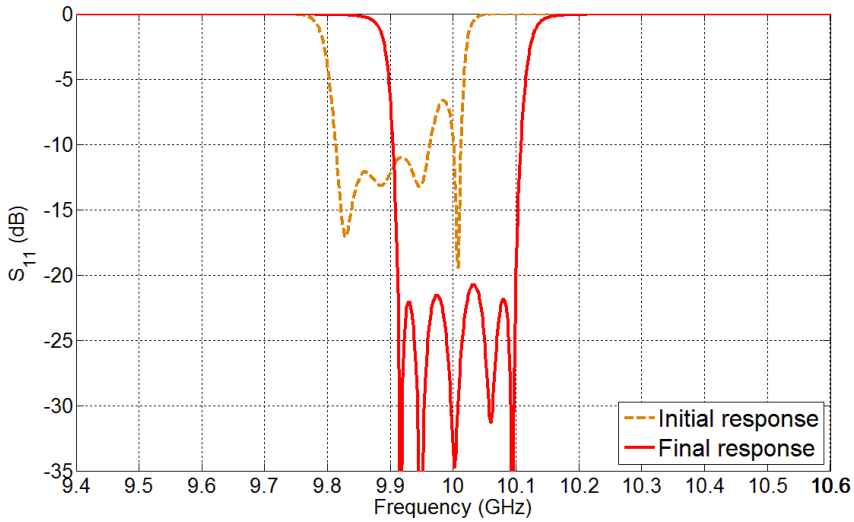

Figure 5.13 Simulated initial and final response of the X-band 5-resonator antenna-filter.

The simulated return loss (S_{11}) of the antenna-filter, compared with the response calculated from the coupling matrix, is shown in Figure 5.14. They are in good agreement.

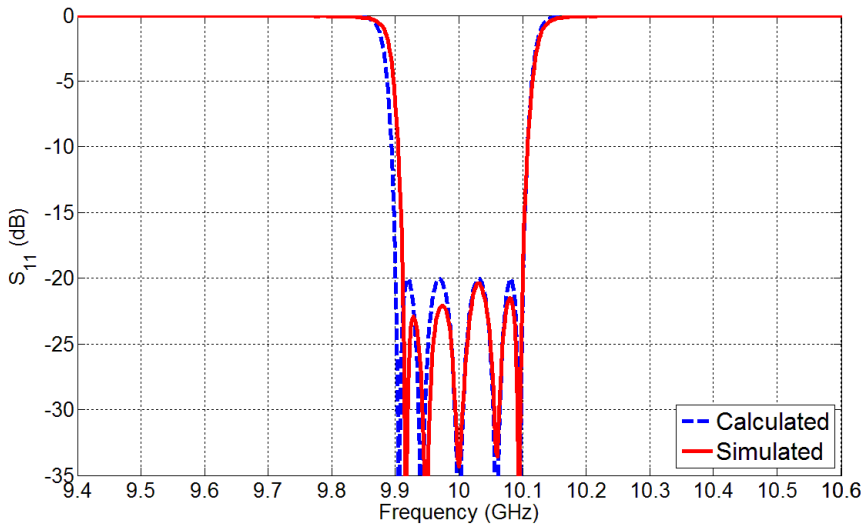

Figure 5.14 The S_{11} response of the X-band 5-resonator antenna-filter from coupling matrix (a dashed line) and simulation (a solid line).

5.6.2 Fabrication and Measurement

The X-band 5-resonator antenna-filter has been fabricated from aluminum alloy 5083 (RS components) using a CNC milling machine. Figure 5.15 shows a photograph of the antenna-filter. The simulated and measured return loss of antenna-filter, depicted in Figure 5.16(a), shows good agreement. The measurement shows that the passband has a maximum return loss of -18.6 dB.

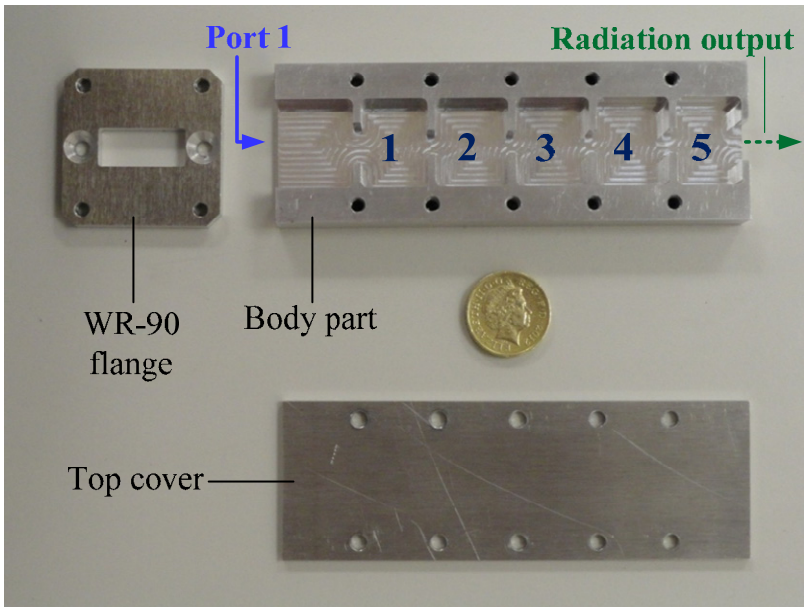

Figure 5.15 Photograph of the fabricated antenna-filter.

The antenna-filter has been measured inside an anechoic chamber using an HP8722D vector network analyzer (VNA) and an X-band horn antenna (1624 from Flann Microwave Company, a reference antenna) to obtain the frequency response of the realised gain. The measured realised gain is compared with the simulation results as shown in Figure 5.16(b). The antenna-filter is found to have a passband gain of about 5.7 dB, and measured stopband rejection is about 55.7 dB. The simulated total efficiency versus frequency of antenna-filter is plotted in Figure 5.17. It can be seen that the total efficiency exhibits very good filtering performances, and similar to the 5th order bandpass filter of the actual device. The total

efficiency in the passband (9.9 to 10.1 GHz) is about 70%, while the maximum efficiency is occurred at the centre frequency (10 GHz) as about 93.83%. The results shows very high antenna efficiency occurred around the passband corresponding to the realised gain response of antenna-filter.

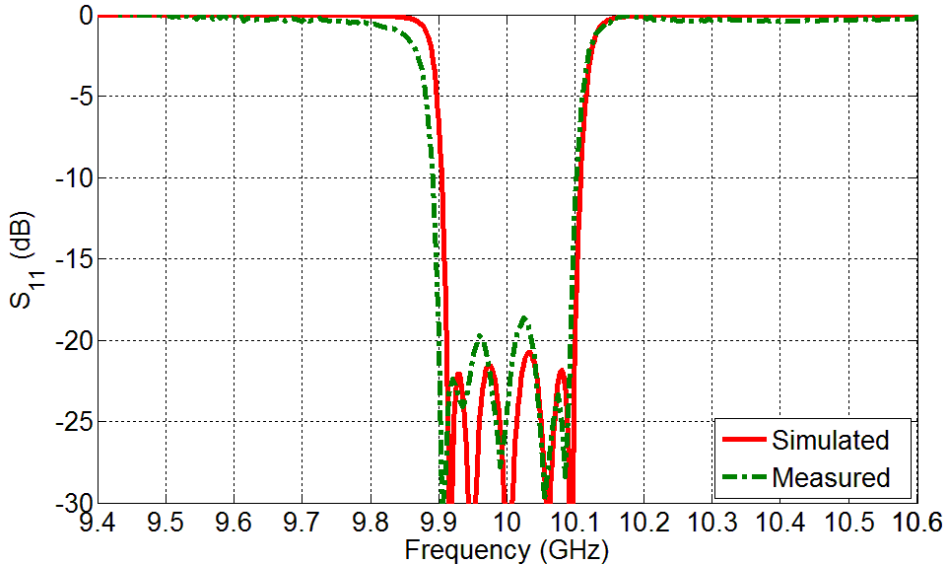

(a)

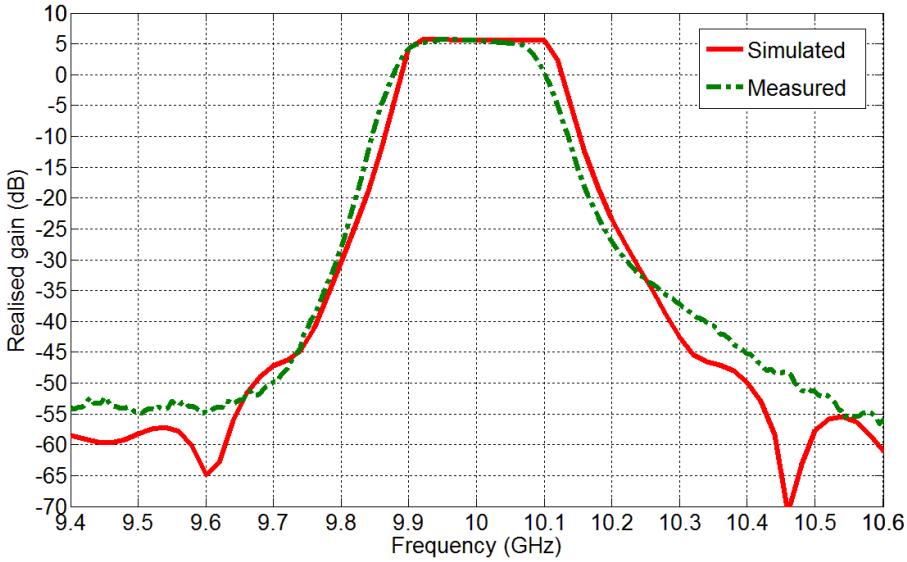

(b)

Figure 5.16 Simulated and measured results for the X-band 5-resonator antenna-filter. (a) Return loss S_{11} (b) Realised gain.

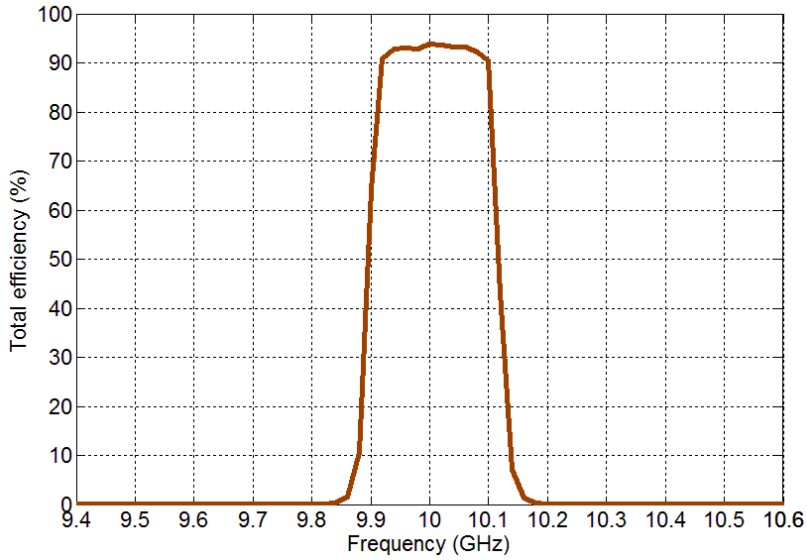

Figure 5.17 Simulated total efficiency for the X-band 5-resonator antenna-filter.

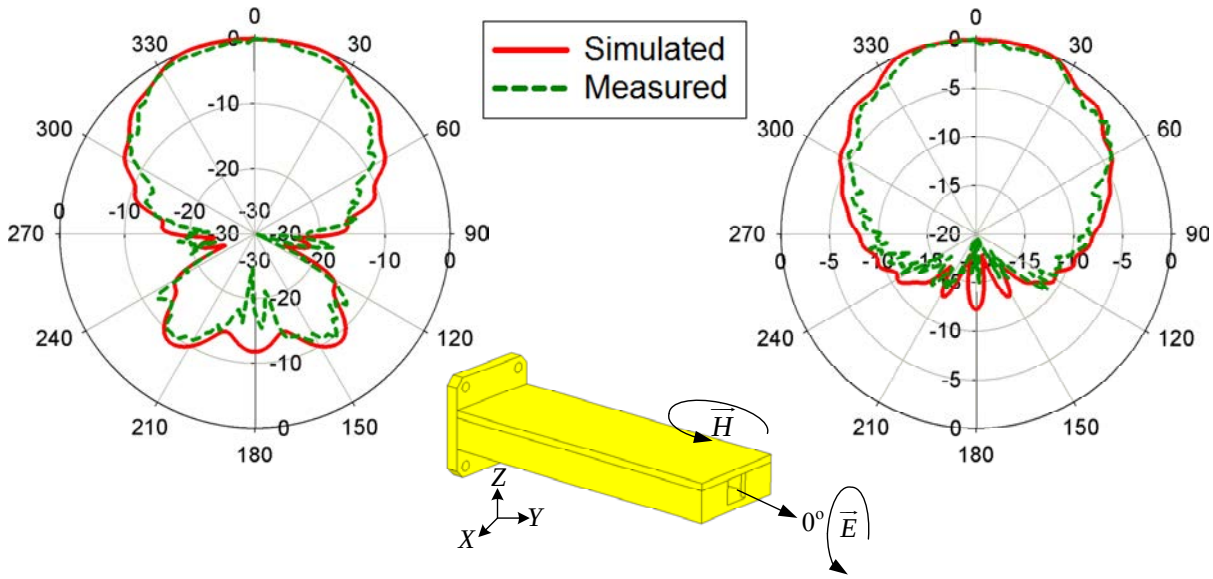

(a) (b)

Figure 5.18 Normalised simulated and measured radiation patterns for the antenna-filter at 10 GHz in co-polarisation: (a) H (XY) plane. (b) E (YZ) plane. (Radial units are dB. Circumferential scale is θ in degrees.)

The simulated and measured radiation patterns of the antenna-filter are shown in Figure 5.18. It can be seen that the antenna-filter exhibits good agreement in terms of radiation pattern in H and E-plane orientation. The cross polarisation levels in H-plane are below -50 dB in the measurements and below -80 dB in the simulations, as shown in Table 5.1. The performance of the antenna-filter is summarised and presented in Table 5.1. The results show flat response in the passband gain, good out-of-band rejection and low levels of cross-polarisation.

Table 5.1 Summary of the antenna-filter performance

Parameters	**Frequency (GHz)**	**3 dB Beamwidth (deg.)**		**Side lobe level (dB)**		**Cross-polarisation level (dB)**	
		Sim.	Mea.	Sim.	Mea.	Sim.	Mea.
H-plane	10	85	72	-8.7	-9.59	-80	-50
E-plane	10	99	96	-9.5	-9.95	-81	-49.8

5.7 X-Band 3-Resonator Antenna Power Divider

5.7.1 Waveguide Antenna Power Divider Design

This section presents the design of a 3-resonator antenna power divider. This circuit includes power division as well as basic filtering functionally whilst using two of the three resonators as a two-element array. This allows the antenna array feature in order to improve the directional radiation characteristics with integrated filter. The topology of a designed three-resonator antenna power divider is shown in Figure 5.19.

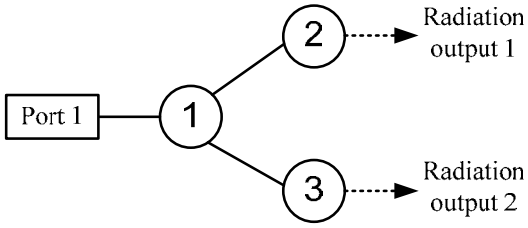

Figure 5.19 Topology of the designed waveguide antenna power divider.

The antenna power divider is designed to have 2% fractional bandwidth (FBW = 0.02) at the centre frequency f_0 of 10 GHz and a passband return loss of -20 dB. A gradient-based local optimisation algorithm [8] has been utilised here to get the coupling matrix. The optimised normalised coupling coefficients, external and radiation quality factors are:

$$[m] = \begin{bmatrix} 0 & 1.175 & 1.175 \\ 1.175 & 0 & 0 \\ 1.175 & 0 & 0 \end{bmatrix}$$

$$q_{e1} = q_{r2} = q_{r3} = 0.6648$$

The calculated response of the S_{11} from the values of $[m]$, q_{e1}, q_{r2} and q_{r3} using the equation (5.15) is shown in Figure 5.20. The coupling coefficients and the external quality factors are computed for FBW = 0.02 and found to be $M_{12} = M_{13} = 0.0235$, $Q_{e1} = Q_{r2} = Q_{r3} = 33.24$. These values will then be utilised for defining the physical dimensions of the waveguide structure using a procedure similar to that described in Section 5.6.1.

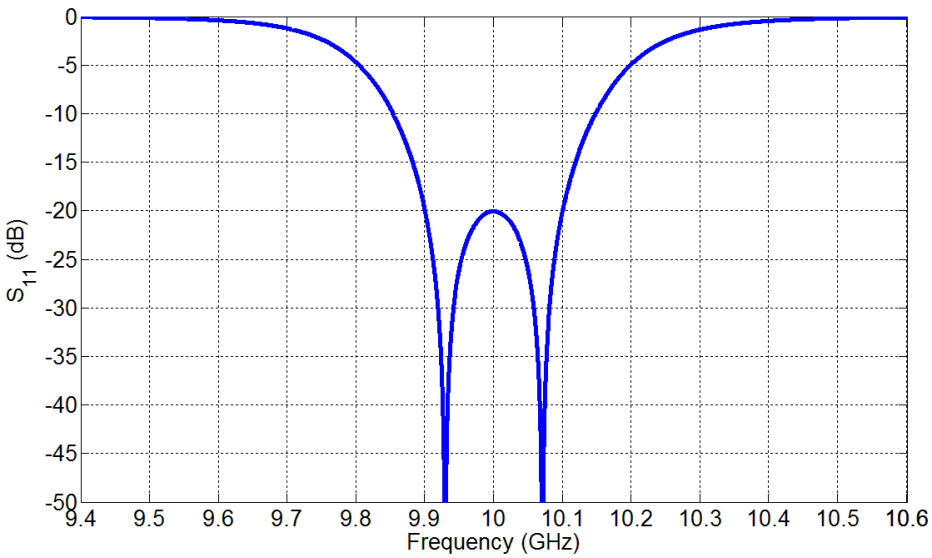

Figure 5.20 The calculated response of S_{11} in dB of the designed waveguide antenna power divider from the coupling matrix.

The 3D structure of the X-band 3-resonator antenna power divider is illustrated in Figure 5.21, it has one waveguide port and two-apertures separated by $\lambda_0/2$ (15 mm) forming a simple array. The waveguide structure, shown in Figure 5.21 is equivalent to the coupling topology of the three-resonator power divider, discussed in [8]. The implementation of the antenna power divider has again been designed based on X-band waveguide with an inductive iris. The physical dimensions of the waveguide antenna-diplexer have been initially defined and optimised in a similar way to that presented in Section 5.6.1. All dimensions of the optimised structure corresponding to the parameters shown in Figure 5.20 are: a = 22.86, b = 10.16, d_1 = 11.32, d_2 = d_3 = 9.4, d_4 = d_5 = 11.32, l = 20, l_1 = 15.6, l_2 = l_3 = 17.5, t = 2 (Unit: mm). All of the inside corners are rounded with a radius of 1.6 mm. The simulated return loss S_{11} for the proposed antenna power divider is in good agreement with the calculated response, as shown in Figure 5.22. The realised gain and radiation patterns will be discussed in Section 5.7.2.

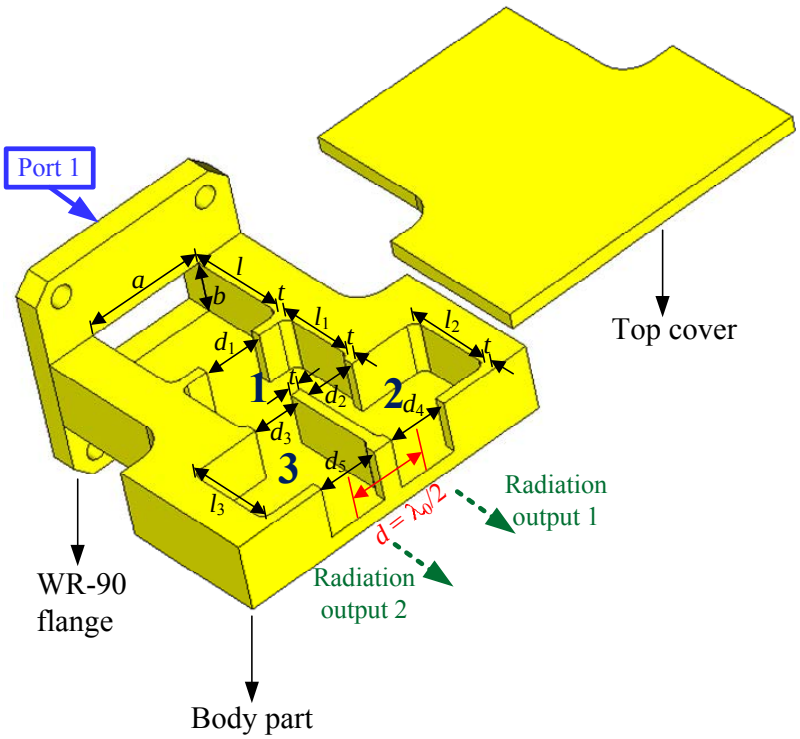

Figure 5.21 X-band 3-resonator antenna power divider.

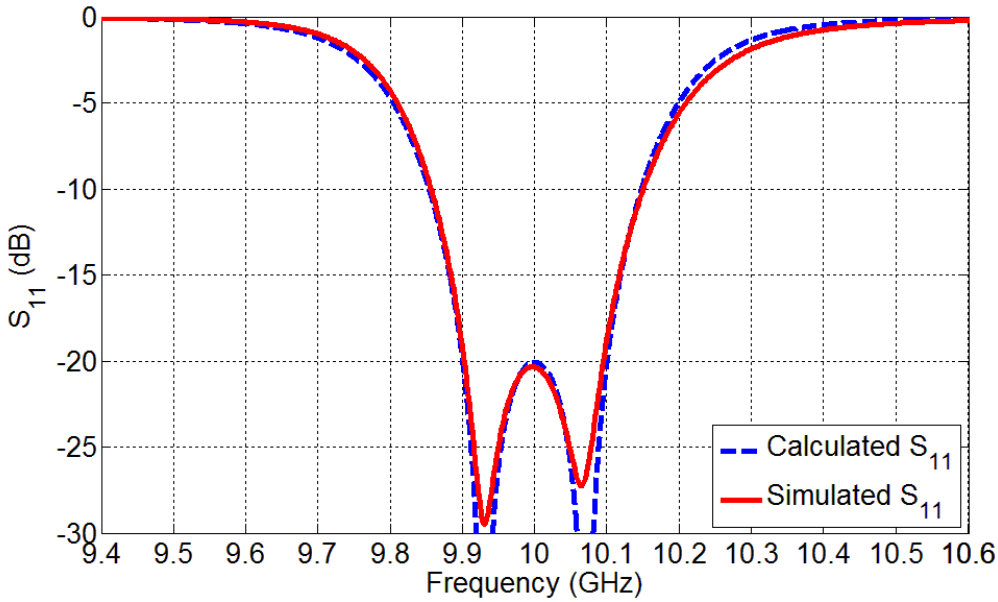

Figure 5.22 S_{11} of the X-band 3-resonator antenna power divider derived from the coupling matrix (dashed lines) and CST simulation (solid lines).

5.7.2 Fabrication and Measurement

The X-band 3-resonator antenna power divider is also made from aluminum alloy and a photograph of it is shown in Figure 5.23. The simulated and measured return loss curves are depicted in Figure 5.24(a). The measured response is in good agreement with the simulated response. The measurement shows a maximum return loss of -21.5 dB with a passband bandwidth of 202 MHz, whereas the expected maximum return loss obtained from CST simulations is -20 dB with a passband bandwidth of 200 MHz.

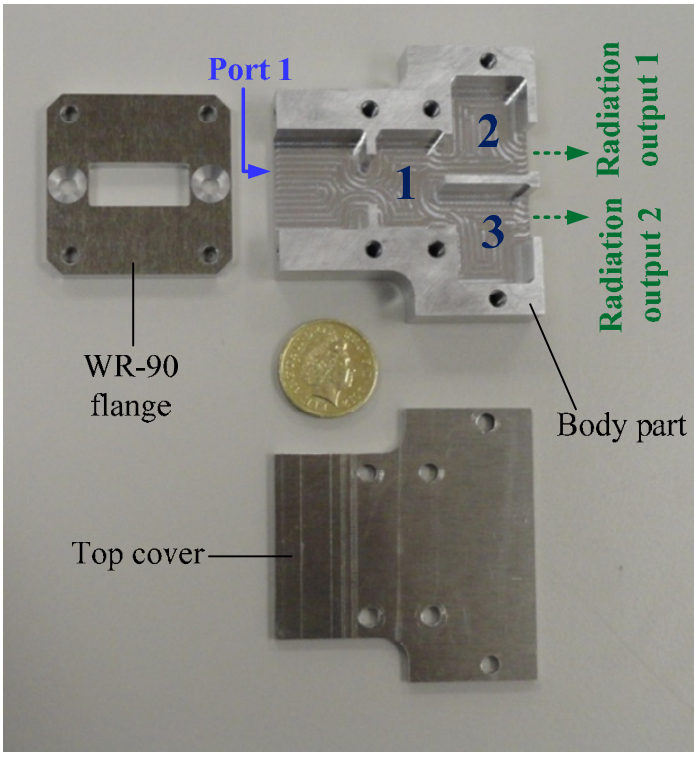

Figure 5.23 Photograph of the fabricated antenna power divider.

Figure 5.24(b) shows the measured realised gain, which exhibits good agreement with the simulation. It can be seen that a measured passband gain is about 8.9 dB, which is 3.2dB more than that of the single aperture antenna-filter presented in Section 5.6.2. The measured stopband rejection is about 14 dB. The simulated total efficiency versus frequency of antenna power divider is plotted in Figure 5.25. The total efficiency in the passband (9.9 to 10.1 GHz) is about 97.2% which is higher than the antenna-filter as 27.2%, while the efficieny at the centre frequency (10 GHz) is slightly dropped from the maximum efficiency of 98.4% as about 1.27%. The results show very high antenna efficiency around the passband corresponding to the realised gain response. However, this antenna power divider dose not exhibit the good responses of realised gain and total efficiency as well as the 5th order antenna-filter, because this design has a lower filter order (2nd order filter).

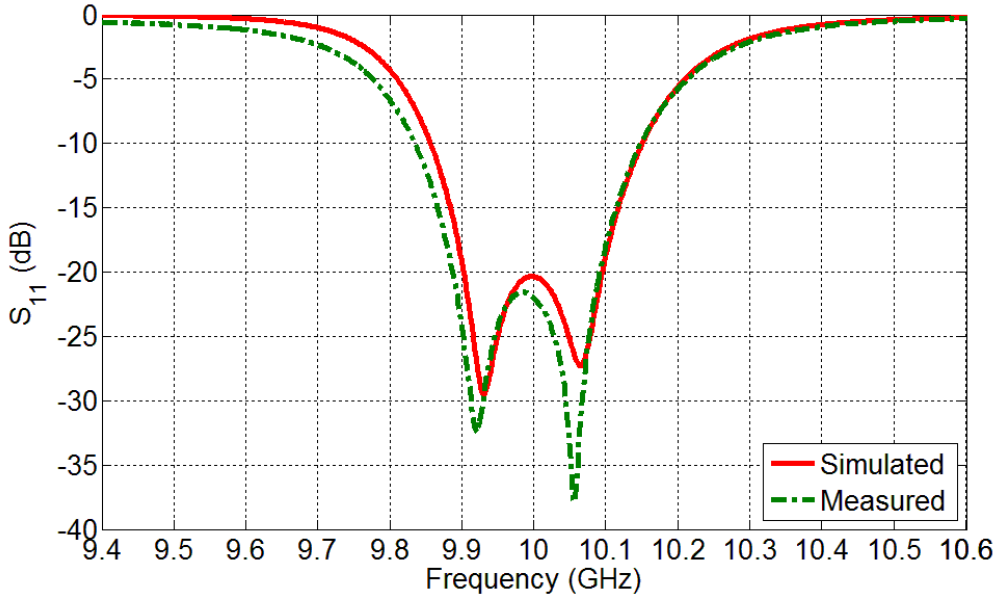

(a)

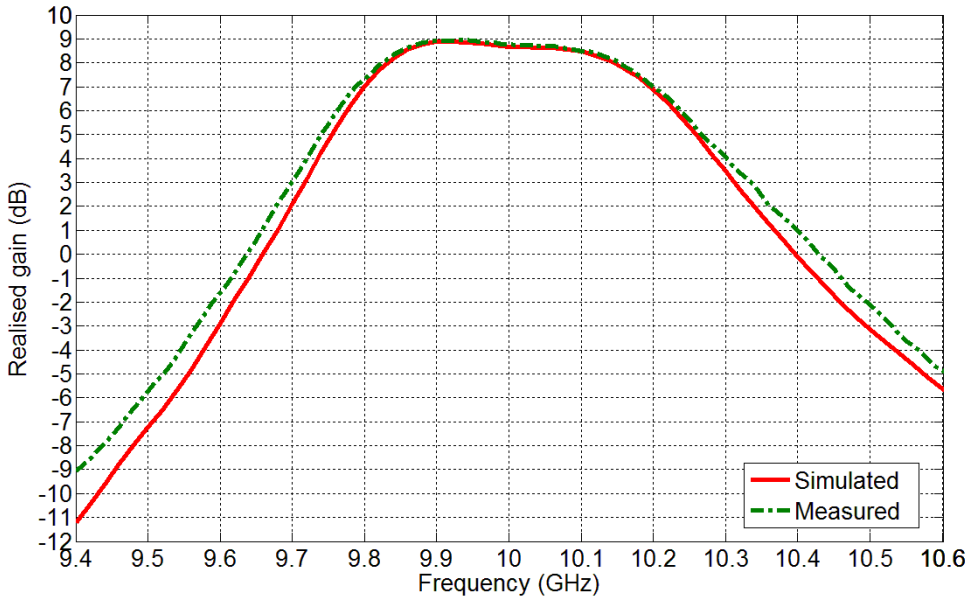

(b)

Figure 5.24 Simulated and measured results for the X-band 3-resonator antenna power divider. (a) Return loss S_{11} (b) Realised gain.

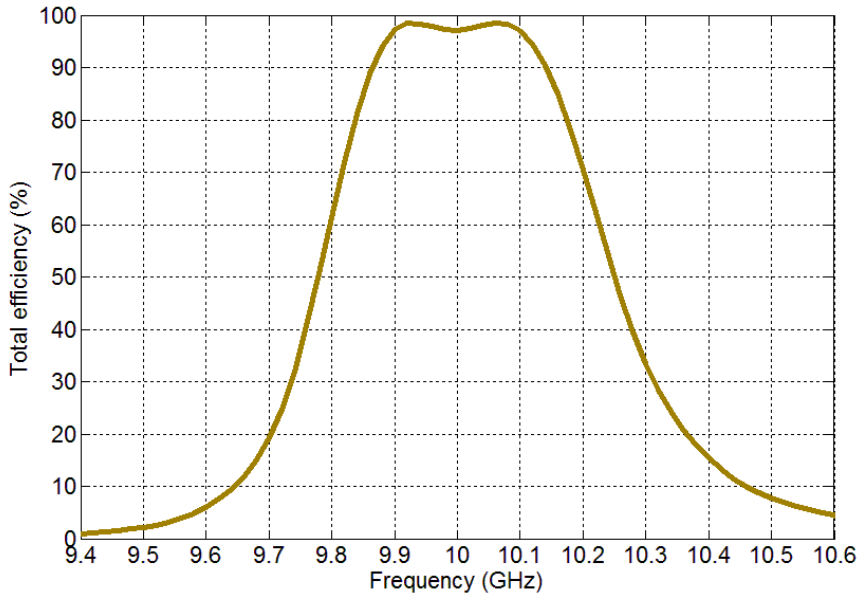

Figure 5.25 Simulated total efficiency for the X-band 3-resonator antenna power divider.

The simulated and measured radiation patterns for the antenna power divider are shown in Figure 5.26. It can be seen that the antenna power divider exhibits good radiation pattern shape in H and E plane orientations. The cross polarisation levels are measured in the H-plane as -49.2 dB and in the E-plane as -48.9 dB, whereas the simulated levels in H-plane are -59.7 dB and -67.9 dB for the E-plane. The performance of the antenna power divider is summarised in Table 5.2. As expected, the antenna power divider has better performance compared to the 5-resonator aperture antenna-filter in terms of higher passband gain, and narrower 3dB beamwidth.

Table 5.2 Summary of the antenna power divider performance

Parameters	**Frequency (GHz)**	**3 dB Beamwidth (deg.)**		**Side lobe level (dB)**		**Cross-polarisation level (dB)**	
		Sim.	Mea.	Sim.	Mea.	Sim.	Mea.
H-plane	10	52	51	-14.4	-15.14	-59.7	-49.2
E-plane	10	74.4	68	-10.5	-10.88	-67.9	-48.9

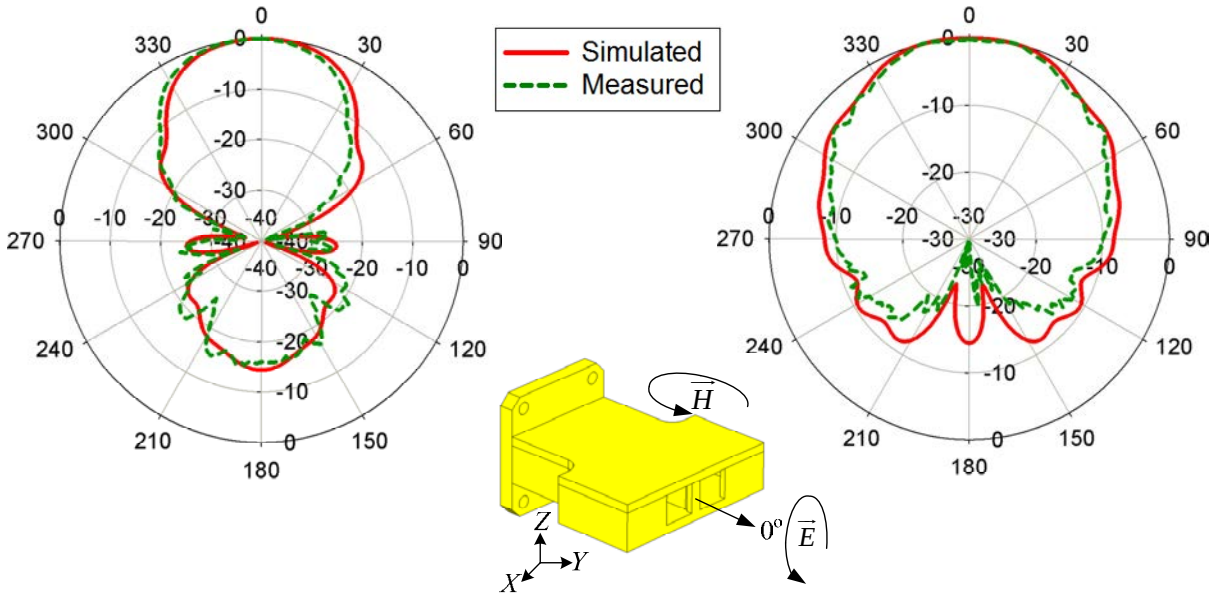

(a) (b)

Figure 5.26 Normalised simulated and measured radiation patterns for the antenna power divider at 10 GHz in co-polarisation: (a) H (XY) plane. (b) E (YZ) plane. (Radial units are dB. Circumferential scale is θ in degrees.)

5.8 X-Band 3-Resonator Antenna-Diplexer

5.8.1 Waveguide Antenna-Diplexer Design

Both of the previous designs operated in a single frequency band. This work presents an additional new component where the waveguide aperture antenna is designed to work at two frequency bands in a similar fashion to a diplexer. This component is an antenna-diplexer. The proposed design can be employed as a receiving component for separating two-frequency channels as would a conventional diplexer circuit, placed after the receiving antenna. The passband centre frequency is 9.93 GHz for channel 1 and 10.07 GHz for channel 2; the bandwidth of each channel is 0.1 GHz. The overall fractional bandwidth (two passbands and an intervening stop band) is 2.4% (FBW = 0.024). This design has a return loss of -20 dB and

uses 2 poles for each channel. Figure 5.27 shows the topology of the designed antenna-diplexer represented, as a three port device.

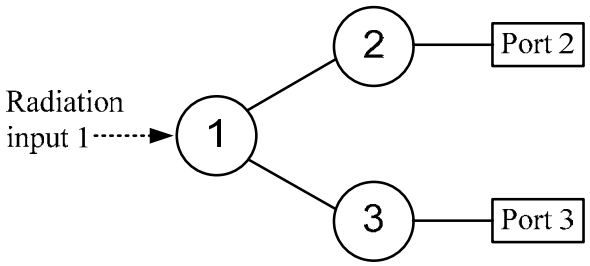

Figure 5.27 Topology of the designed waveguide antenna diplexer.

The coupling matrix of this antenna-diplexer has been optimised using the gradient-based local optimisation algorithm [8]. The optimised results give the normalised coupling coefficients, and external and radiation quality factors as:

$$[m] = \begin{bmatrix} 0 & 0.835 & 0.835 \\ 0.835 & 0.446 & 0 \\ 0.835 & 0 & -0.446 \end{bmatrix}$$

$q_{r1} = 1.944$, $q_{e2} = q_{e3} = 1.468$

The S-parameter response obtained using the values of $[m]$, q_{r1}, q_{e2} and q_{e3} using equations (5.15) and (5.16) are shown in Figure 5.28. The coupling coefficients and the external quality factors are computed for $FBW = 0.024$ and found to be $M_{22} = 0.0107$, $M_{33} = -0.0107$, $M_{12} = M_{13} = 0.02$, $Q_{r2} = 81$, $Q_{e2} = Q_{e3} = 61.17$.

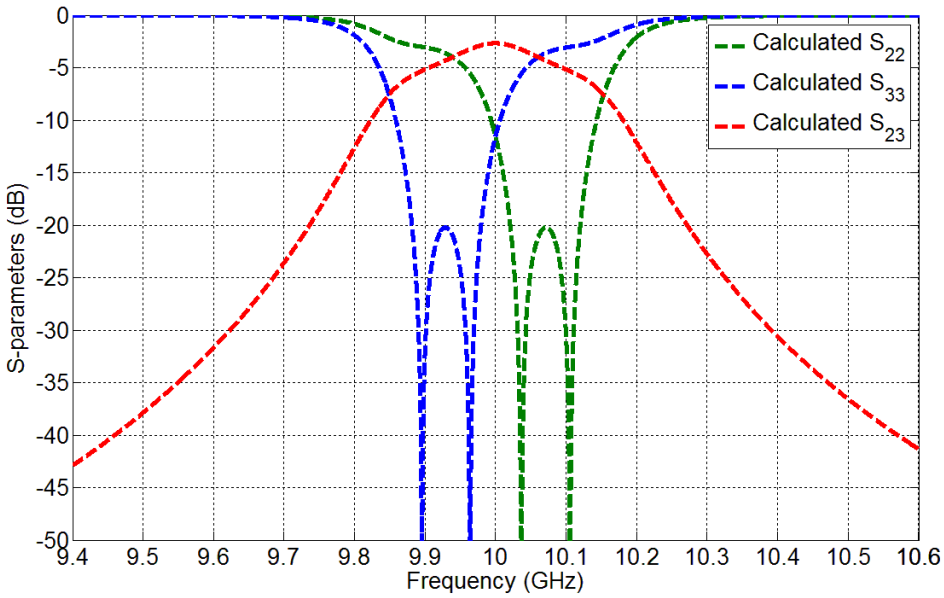

Figure 5.28 The *S*-parameters in dB for the designed waveguide antenna diplexer calculated from the coupling matrix.

The three dimensional structure of the X-band 3-resonator antenna-diplexer is illustrated in Figure 5.29. It is a three-port component including one antenna port. The proposed antenna-diplexer has been designed using an inductively coupled waveguide cavity resonator. The physical dimensions of the waveguide antenna-diplexer have been obtained using the designed parameters (i.e. the actual values of M, Q_e and Q_r) and is optimised using the procedure presented in Section 5.6.1. All dimensions of the optimised structure corresponding to the parameters shown in Figure 5.27 are a = 22.86, b = 10.16, d_1 = 9.9, d_2 = 9.35, d_3 = 9.39, d_4 = 11.84, d_5 = 12.08, l = 20, l_1 = 16.14, l_2 = 16.84, l_3 = 17.16, l_4 = 20.32, t = 2 (Unit: mm). All of the inside corners are rounded with a radius of 1.6 mm. The simulated *S*-parameters for the proposed antenna-diplexer are compared with the calculated response obtained from the coupling matrix and are seen to be in good agreement, as shown in Figure 5.30. It should be noted that the above antenna-diplexer exhibits poor isolation performance between two output ports. This work aims to show the principles of the methods by which this

isolation can be improved by utilising more resonators or by separating the operating frequency bands.

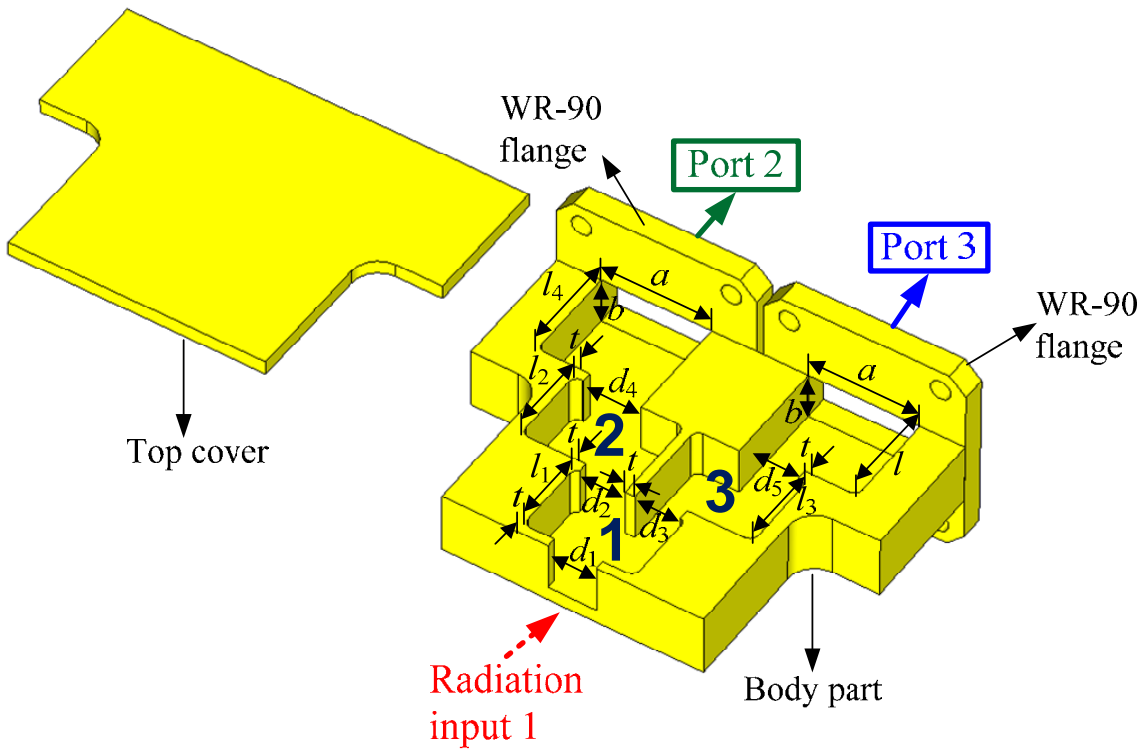

Figure 5.29 X-band 3-resonator antenna-diplexer.

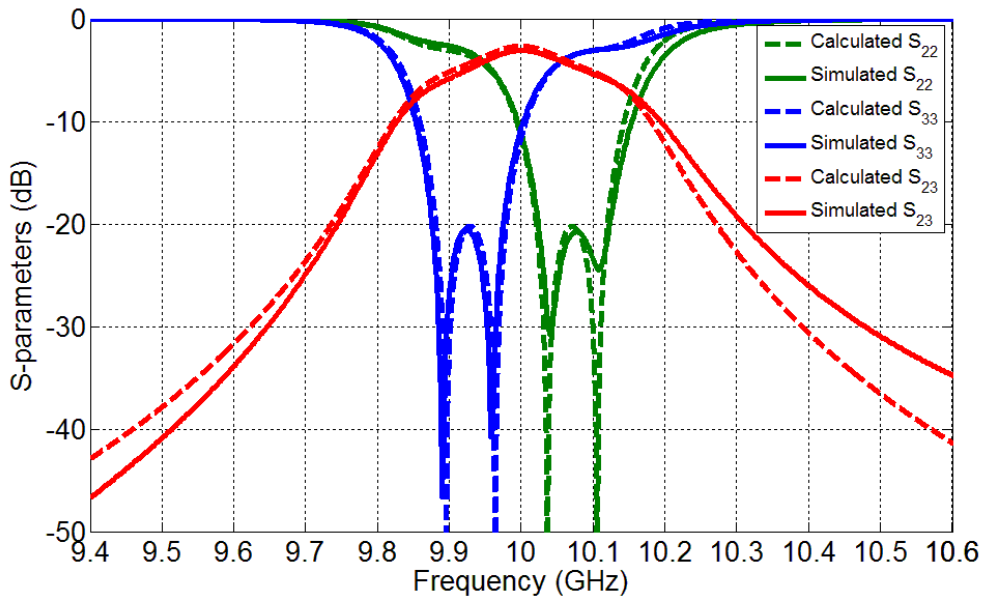

Figure 5.30 *S*-parameter responses of the X-band 3-resonator antenna-diplexer obtained from the coupling matrix (dashed lines) and simulation (solid lines).

5.8.2 Fabrication and Measurement

The X-band 3-resonator antenna-diplexer is made from aluminum alloy and is shown in Figure 5.31. The simulated and measured *S*-parameters of the antenna-diplexer are depicted in Figure 5.32(a). The measured response is in excellent agreement with the simulated response. The measurement shows that the passband of channel 1 has maximum return loss of -20.1 dB, whereas for channel 2 it is -21.0 dB. The isolation between the centre frequencies of two bands is measured to be 5.2 dB.

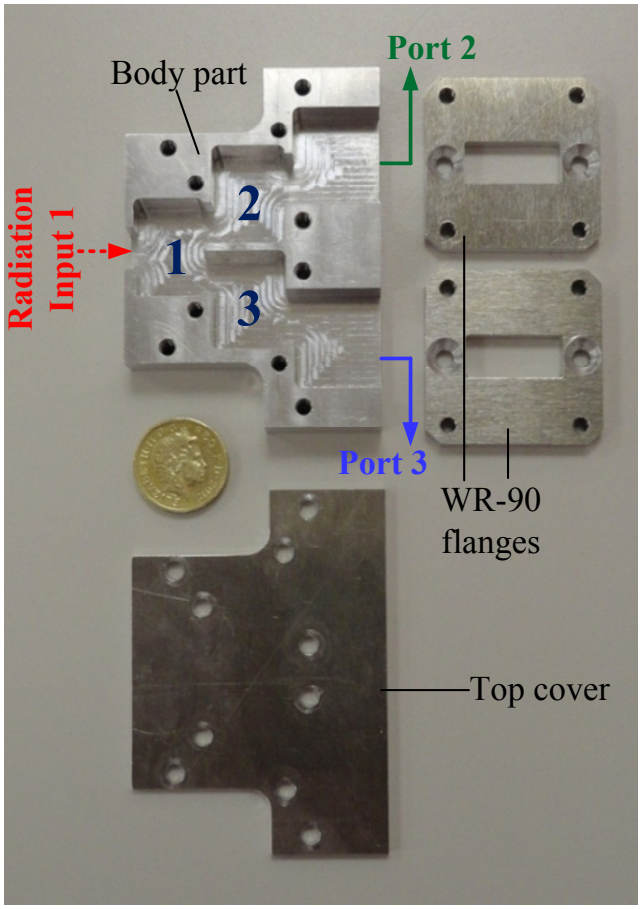

Figure 5.31 Photograph of the fabricated antenna-diplexer.

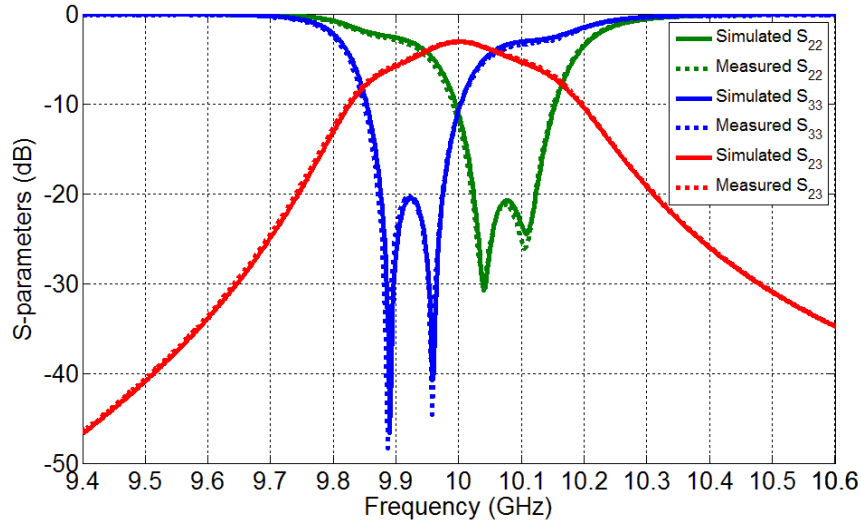

(a)

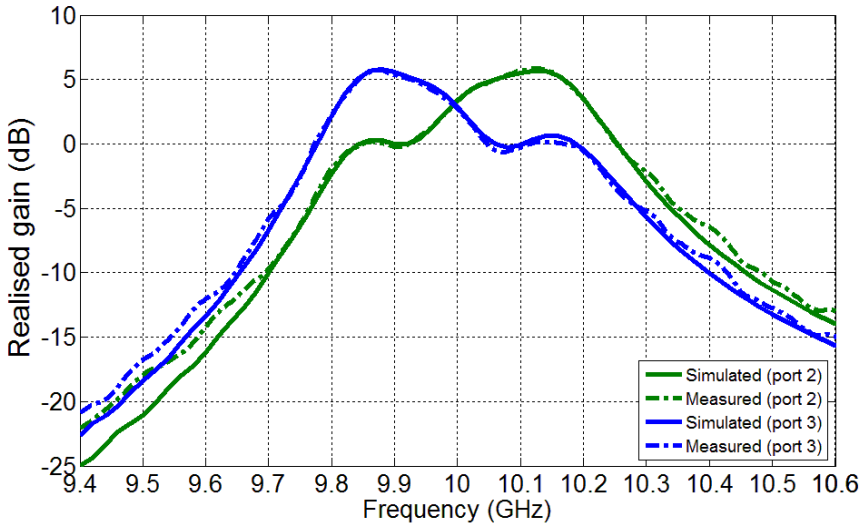

(b)

Figure 5.32 Simulated and measured results of the antenna-diplexer. (a) *S*-parameters. (b) Realised gain.

The realised gain for each channel of the antenna-diplexer has been measured comparing with the simulation results, as shown in Figure 5.32(b). The passband of channel 1 has a measured maximum gain of 6.25 dB at 9.88 GHz, whereas the passband of channel 2 has a measured maximum gain of 6.1 dB at 10.12 GHz. The stopband rejection of each channel was measured and is about 21 dB. The total efficiency versus frequency of antenna-

diplexer is plotted with the simulation results, as shown in Figure 5.33. The passband of channel 1 has a maximum total efficiency of 74.3% at 9.88 GHz, whereas the passband of channel 2 has a maximum total efficiency of 71.38% dB at 10.12 GHz. The results show the corresponding maximum realised gains with the maximum total efficiency at the same frequency of each channel. However, the total efficiency and realised gain of antenna-diplexer does not achieve better than previous designs. It can be achievable the good performance since the number of antenna is increased with the antenna array design technique.

It should be noted that the results of Figure 5.32(a) show that on port 2, 20% of received energy at the centre frequency goes to port 3 and vice versa. This work aims to show the principle of the design method and this leaking of received energy between two output ports can be improved by utilising more resonators and/or separating the bands.

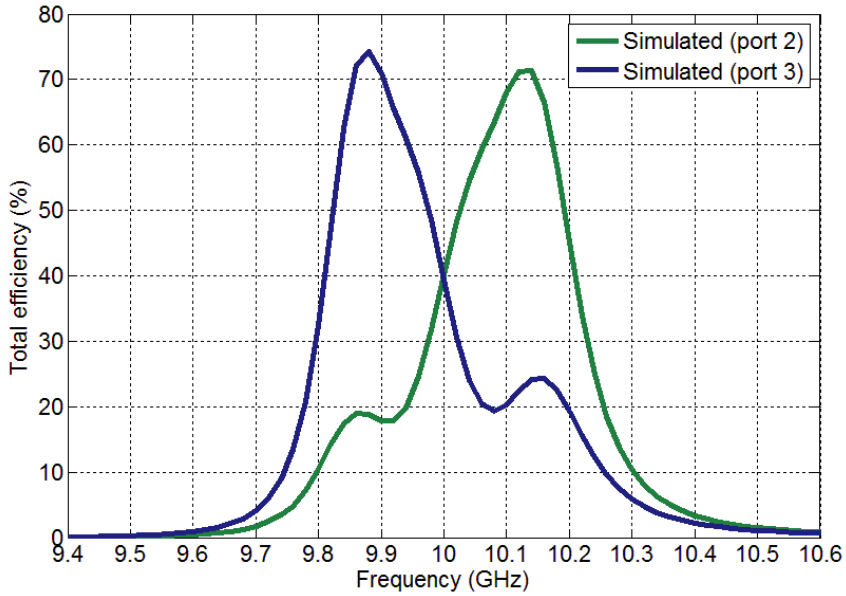

Figure 5.33 Simulated total efficiency for the X-band 3-resonator antenna-diplexer.

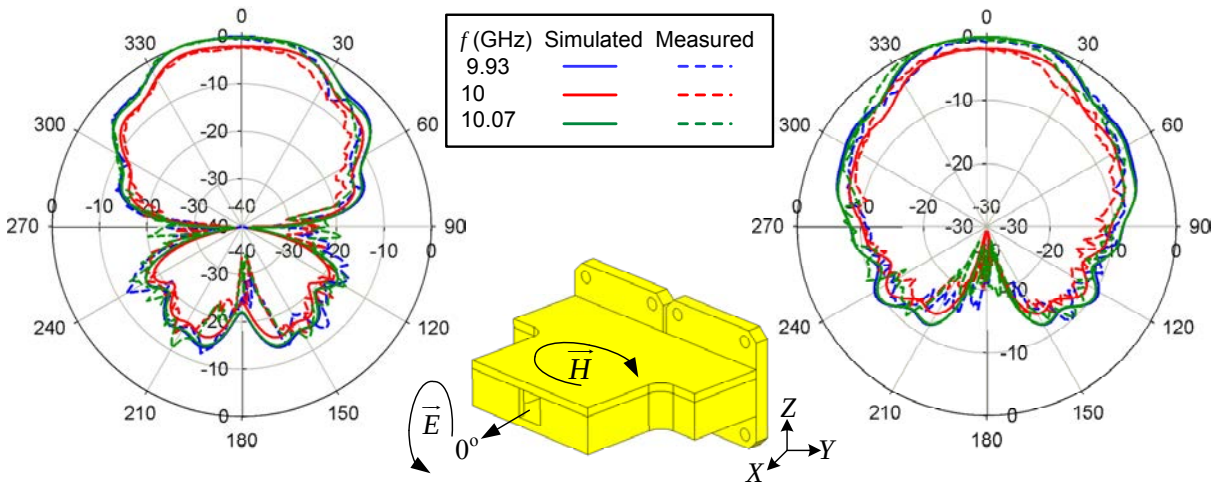

(a) (b)

Figure 5.34 Normalised simulated and measured radiation patterns of the antenna-diplexer in co-polarisation at the middle band frequency and two passband centre frequencies for each channels: (a) H (XY) plane. (b) E (XZ) plane. (Radial units are dB. Circumferential scale is θ in degrees.)

The simulated and measured radiation patterns of the antenna-diplexer are compared at the centre frequencies of each channel and are shown in Figure 5.34. It can be seen that the antenna-diplexer exhibits good radiation pattern shape in H and E-planes. The radiation pattern level measured at 10 GHz is lower than the measured maximum level by about 3 dB, which corresponds to the gain results at 10 GHz, depicted in Figure 5.32(b). The measured cross polarisation levels are below 49 dB, whereas the simulated cross polarisation levels are below 72 dB. The performance of the antenna diplexer is summarised and presented in Table 5.3.

Table 5.3 Summary of the antenna-diplexer performance

Parameters	**Frequency (GHz)**	**3 dB Beamwidth (deg.)**		**Side lobe level (dB)**		**Cross-polarisation level (dB)**	
		Sim.	Mea.	Sim.	Mea.	Sim.	Mea.
H-plane	9.93	62.7	58	-4.8	-4.64	-72.2	-46.1
	10	63.7	60	-4.9	-4.9	-72.9	-49.6
	10.07	64.9	57	-5.1	-4.46	-74.9	-45.5
E-plane	9.93	66.3	73	-4.1	-4.4	-72.2	-48.8
	10	68.5	64	-4.2	-5.24	-73	-51.1
	10.07	70.7	70	-4.3	-4.67	-74.8	-48.8

5.9 Conclusions

The multiport coupling matrix has been used to demonstrate three components which utilise the resonant properties of antennas for filtering. The coupling matrix approach is general and can be used for any waveguide aperture antenna. The approach can, in principle, be executed using a larger number of radiations and/or filtering elements to configure complex functionality whilst minimising the weight and volume of the component. The bandwidth of the antenna-filters is limited by the radiation Q of the radiating resonator(s), however this can be adjusted by altering the aperture size, in the examples given here.

A prototype for the X-band 5 resonator antenna-filter was built. There is good agreement between the measurement and simulation results pertaining to the return loss and radiation pattern shapes. An X-band 3 resonator antenna power divider is designed in order to

improve antenna gain with compact size and is suitable for use in a transmitter. An X-band 3 resonator antenna-diplexer is designed for use in a receiver where it could be utilised as a frequency splitter with compact size. The measurement results for this and the antenna-diplexer agree very well with simulations. These proposed components have compact sizes, light weights and small number of front-end microwave components, and as such they are suitable for use of modern communication systems

References

[1] Hong J. S. and Lancaster M. J. Microstrip Filters for RF/Microwave Applications. New York, USA: John Wiley & Sons; 2001.

[2] Pozar D. M. Microwave Engineering. 3rd ed. USA: John Wiley & Sons; 2005.

[3] Lancaster M. J. Passive Microwave Device Applications of High-Temperature Superconductors. Cambridge, UK: Cambridge University Press; 1997.

[4] Collin R. E. Foundation for Microwave Engineering. 2nd ed. USA: John Wiley & Sons; 2011.

[5] Computer Simulation Technology (CST), Microwave Studio [Internet]. 2014 Available from URL: http://www.cst.com.

[6] Matthaei G. L., Young L., Jones E.M.T. Microwave Filters, Impedance-matching Networks and Coupling Structures. North Bergen, NJ, USA: Artech House, 1980.

[7] Talal F. Skaik, Synthesis of Coupled Resonator Circuits with Multiple Outputs using Coupling Matrix Optimization, PhD thesis, University of Birmingham, UK, 2011.

[8] Skaik T., Lancaster M. J., and Huang F. Synthesis of multiple output coupled resonator microwave circuits using coupling matrix optimization. IET J. Microw., Antennas, Propag. 2011 Jun.; 5(9): 1081–1088.

Chapter 6

Conclusions and Future Work

6.1 Conclusions

This thesis presented new design techniques for antenna-filters involving use of coupling matrix synthesis. The approach is applied to dipole and waveguide structures. The work has been divided into three main parts: two port dipole antenna-filter, one port dipole antenna-filter and waveguide antenna-filter.

The objective of the work presented in Chapter 3 was to design a coupled resonator filter using antennas in order to help understand the antenna. In this work the antenna is treated as a resonator within a filter circuit. A dipole antenna is selected as the resonator type in this work. The structure of this antenna is simple and suited for designing the resonator. The antennas can be arrayed to form an in-line structure which is suitable for design the two-port coupled-resonator filter. The coupling matrix has been utilised to obtain the filter response of the two-port dipole antenna-filter from specifications resulting in the design parameters (quality factors and coupling coefficient). However, any loss in the filter needs to be considered which consist of radiation, material and inductor loss. These losses are associated with the low Q_u value of the resonators which causes. The insertion loss of the two-port dipole antenna-filter is 3.1 dB in simulation and is 3.4 dB in measurement, which are in good agreement with the calculation obtained using the method in [1] which is about 3.5 dB. The proposed antenna-filter in Chapter 3 is a two-port device and has similar in structure which is a conventional dipole antenna array. The design method used for two-port filter in Chapter 3 can be utilised to design a one-port dipole antenna-filter presented in Chapter 4.

The work presented in Chapter 4 aimed to integrate the dipole antenna into a filter circuit replacing the second port with a radiation port. All resonators in this antenna-filter are dipole antennas integrated with inductors and can also be radiating elements. The work in Chapter 4 has started looking at a 1st order antenna-filter for a clear understanding of the concept of antenna and filter integration. The design of the 1st order dipole antenna-filter used the coupling matrix synthesis to optimise the filter response with the optimised design parameters (Q_{e1} and Q_{u1}). The 1st order antenna-filter adjusts the Q_{e1} and Q_{u1} values by changing the position between a feed and a resonator antenna. The realised gain response of the 1st order antenna-filter has showed the similar shape of 1st order bandpass filter. The poor realised gain for this design can be improved when the number of antenna elements is increased as presented in 2nd and 3rd order designs. The 2nd order antenna-filter design is based on the design concept of the antenna-filter work in the filter literature by assuming the Q_u value of the last resonator is the same Q_e value of the input resonator to preserve the filter characteristic. The design can be achieved with the optimised Q_e value for this design as described in Section 4.2.1. The measurement and simulation results showed in good agreement. The realised gain of the 3rd order antenna-filter showed the filtering response with good agreement between simulation and measurement. The work in Chapter4 has been achieved following the principle theory of antenna and filter and the coupling matrix synthesis for the antenna-filter component. This design method can be applicable in the coupled resonator antenna-filter for different topologies, one of which is presented in Chapter 5.

The third part in Chapter 5 presented three design approaches of antenna-filters using a waveguide structure [2]. All approaches have utilised waveguide aperture antennas as resonators. A 5-resonator antenna-filter is the first design of this work and has an in-line coupling topology with one input electrical port and one output is the radiation. The designed

waveguide antenna-filter is higher order than the dipole antenna-filter in Chapter 4. This can improve the filtering response for the realised gain (flat in the passband and high suppression in the stopband). A coupling matrix optimisation technique [3] has been utilised in the second and third design approaches to find the optimum values for the coupling coefficient, the external quality factor and the radiation quality factor corresponding to the desired specifications. The second design has developed a two-antenna array integrated with the coupled resonator power divider [3]. The aim of this work was to improve the antenna performances (i.e. realised gain and radiation pattern) using a two-antenna array which included the filtering function. The third component is a three-port component that works in two different frequencies. This is to integrate the antenna into the coupled resonator diplexer for reducing the number of components in the front-ends and also to reduce the circuit size. The degradation of isolation between output ports (S_{23}) occurred due to the small number of resonators in the circuit. This can be improved by increasing the number of resonators in future designs.

6.2 Future work

The work on antenna-filters based on the coupled resonator filter theory can be further developed to design antenna-filters with a larger number of resonators with different coupling topologies by using the coupling matrix optimisation technique [3]. The coupling structure with the cross coupling between resonators can be applicable to the future design for controlling the transmission zeros of the gain response. Figure 6.1 shows topology example of 4-resonator antenna-filter with cross coupling; where black circles represent resonators, solid lines represent couplings and a dashed line represents a cross coupling.

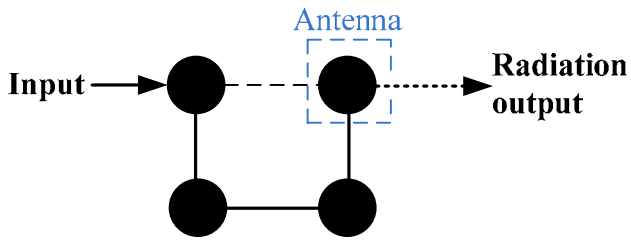

Figure 6.1 A topology example of 4-resonator antenna-filter with cross coupling.

The technique can be applicable to the coupling between antenna elements considered as the cross coupling in the designed coupling structure for reducing the number of resonators in the circuit. The cross coupling technique can generate the transmission zero in the gain response of antenna-filters which can improve the selectivity of antenna-filters as well as cutting out unwanted signals at specific frequencies. The antenna power divider can be further improved with increasing the number of antenna elements and keeping the half wavelength spacing. Figure 6.2 shows a tree topology example of 15-resonator antenna power divider. The coupling structure of this further design can improve the filter response using the coupling matrix optimisation. Also the technique can improve the antenna performances such as high gain, narrow beamwidth and low side lobe level. The principle of antenna-diplexer design can be further modified for the integration design of antenna and multiplexer. The coupling topology model for this future work may be designed in the similar way of the coupled resonator multiplexer in [4]. Figure 6.3 shows a tree topology example of 15-resonator antenna-multiplexer. More work is required in controlling the radiation patterns of the structures. This may focus on the design of *N*-element antenna arrays integrated with filters for the future designs.

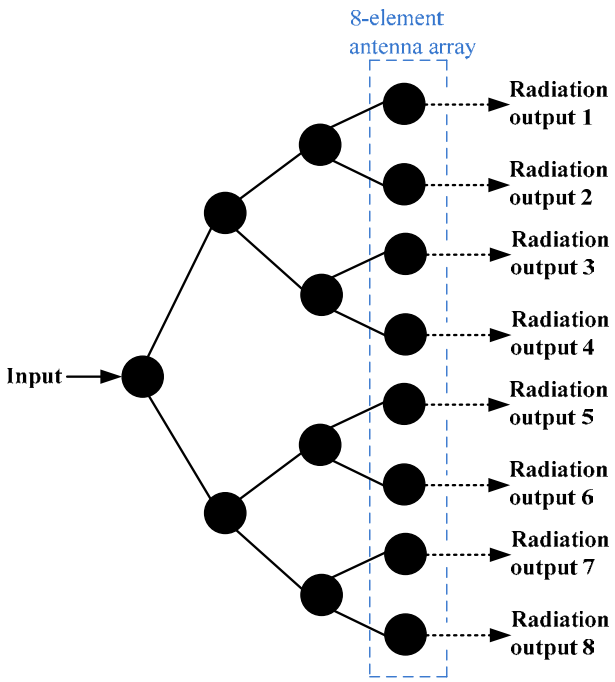

Figure 6.2 A tree topology example of 15-resonator antenna power divider. [4]

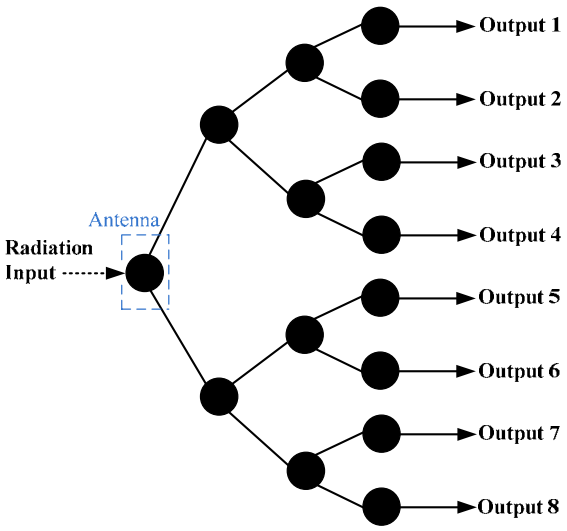

Figure 6.3 A tree topology example of 15-resonator antenna-multiplexer. [4]

References

[1] Hong J. S. and Lancaster M. J. Microstrip Filters for RF/Microwave Applications. New York, USA: John Wiley & Sons; 2001.

[2] Pozar D. M. Microwave Engineering. 3rd ed. USA: John Wiley & Sons; 2005.

[3] Skaik T., Lancaster M. J., and Huang F. Synthesis of multiple output coupled resonator microwave circuits using coupling matrix optimization. IET J. Microw., Antennas, Propag. 2011 Jun.; 5(9): 1081–1088.

[4] Shang X., Wang Y., Xia W., Lancaster M. J. Novel Multiplexer Topologies Based on All-Resonator Structures. IEEE Trans. Microw. Theory Tech. 2013 Nov.; 61(11): 3838–3845.

APPENDIX A

Q calculation method for the one-port component

This appendix presents a *Q* calculation method for a one-port component. For example, an antenna is the one-port component in the work of this thesis. The method is useful to obtain *Q*-factors for the antenna in this thesis. A diagram of one-port component coupled to an external source is shown in Figure A.1(a). When the component is coupled to the external source, the circuit will behave as a resonant circuit with a coupling circuit in a case of resonant mode, as shown in Figure A.1(b). In this case, quality factors of this component can be extracted from the reflection coefficient (S_{11}).

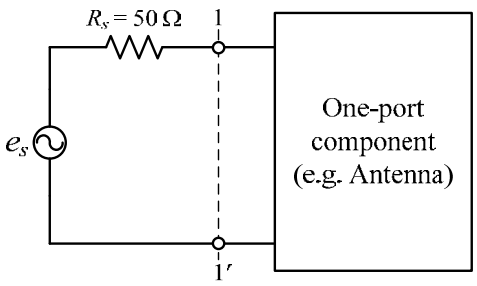

(a)

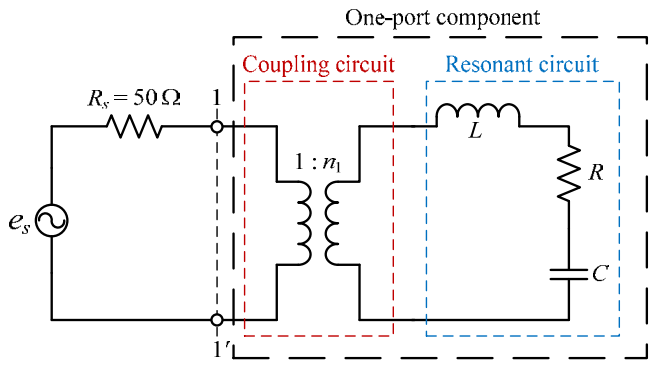

(b)

Figure A.1 (a) A one-port component coupled to an external source (b) Equivalent circuit of a component for one-port measurements [1].

The derived equation of reflection coefficient S_{11} from the circuit shown in Figure A.1(b) is given by [1]

$$S_{11}(f) = \frac{S_{11}(f_0) + j\frac{Q_u}{1+\beta}\Delta(f)}{1 + j\frac{Q_u}{1+\beta}\Delta(f)} \tag{A.1}$$

where Q_u is the unloaded quality factor.

$$\Delta(f) = 1 - \frac{f_0^2}{f^2} \tag{A.2}$$

f is the frequency variable (Hz)

f_0 is the centre frequency (Hz).

$$\beta = \frac{1 \pm |S_{11}(f_0)|}{1 \mp |S_{11}(f_0)|} \text{ is the coupling coefficient} \tag{A.3}$$

The β may be three-coupled modes which are considered from the smith chart as shown in Figure A.2.

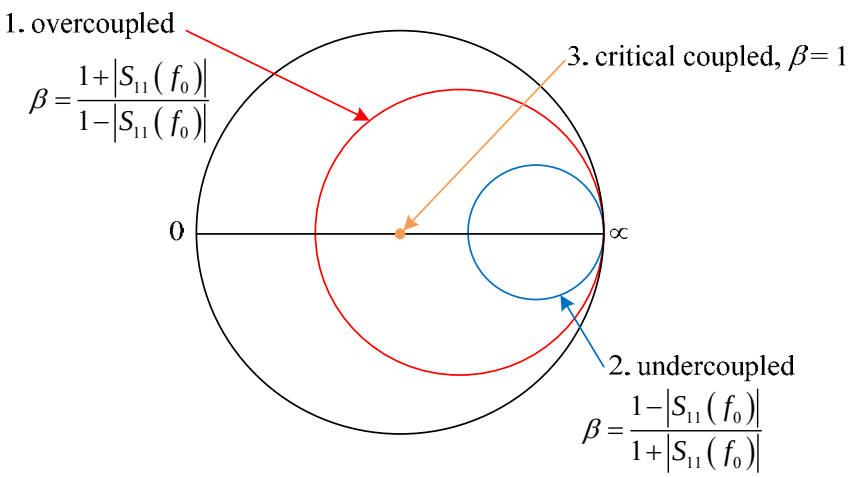

Figure A.2 A Smith chart of two resonant circuits; one is overcoupled, two is undercoupled and three is critical coupled [1].

The quality factors of the component can be calculated from the magnitude of reflection coefficient ($|S_{11}(f)|$) using the equation (A.1) which is rearranged as [1]

$$Q_{ui} = \frac{1}{|\Delta(f)|}\left[\frac{|S_{11}(f)|^2(1+\beta)^2-(1-\beta)^2}{1-|S_{11}(f)|^2}\right]^{\frac{1}{2}} \tag{A.4}$$

$$Q_{ua} = \frac{Q_{u1}+Q_{u2}+\cdots+Q_{un}}{n} \tag{A.5}$$

$$Q_e = Q_{ua}\frac{P_0}{P_e} = \frac{Q_{ua}}{\beta} \tag{A.6}$$

and

$$Q_l = \frac{Q_{ua}}{1+\beta} \tag{A.7}$$

where Q_{ui} , $i = 1, 2, ...,n$ is the unloaded quality factor obtained from different frequencies in the passband excepted for the centre frequency f_0.

Q_{ua} is the average unloaded quality factor.

Q_e is the external quality factor.

Q_l is the loaded quality factor.

This method can be used to extract Q-factors for the one-port component from the EM simulation software. Here an half-wavelength dipole antenna made from a copper material is an example for this Q calculation method. The dipole antenna is designed and made in the CST simulation software, as shown in Figure A.3.

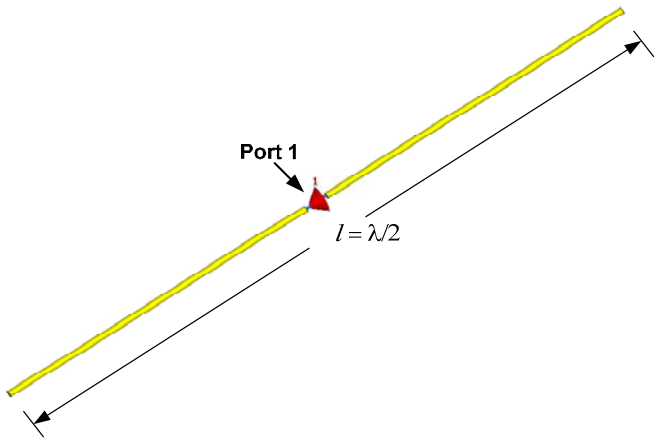

Figure A.3 A simulated structure of an half-wavelength dipole antenna.

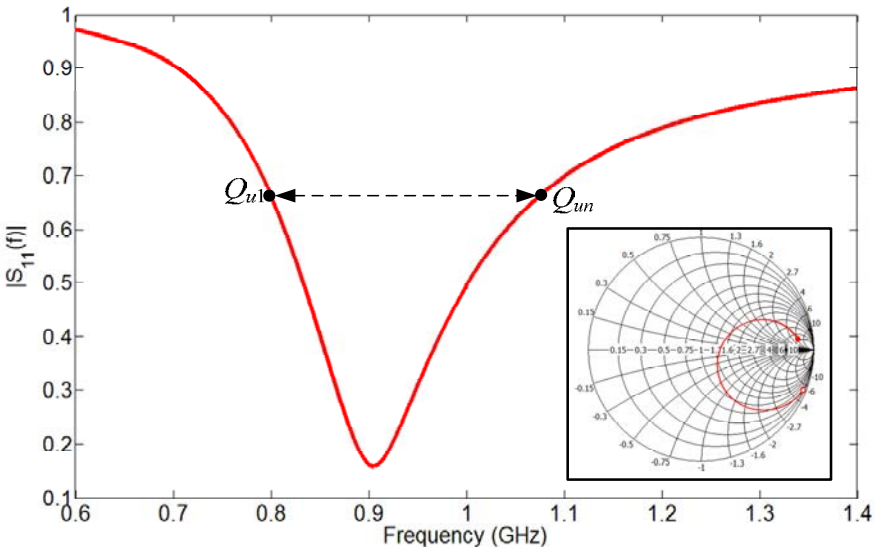

Figure A.4 The simulated $|S_{11}(f)|$ of an half-wavelength dipole antenna.

The antenna has been simulated to obtain the response of S_{11} magnitude ($|S_{11}(f)|$). The simulated response of $|S_{11}(f)|$ is shown in Figure A.4. The coupling coefficient β of this example can be found from a simulated smith chart shown in the inset of Figure A.4. This coupling coefficient represents as the undercoupled (the circle is smaller than one) and is calculated from the magnitude of $S_{11}(f_0)$ at the centre frequency of 0.9 GHz using an equation

(A.3). The calculated β value using the equation (A.3) is 0.725. The Q-factors are calculated from different values of $|S_{11}(f)|$ around half magnitude (0.15-0.65) of $|S_{11}(f)|$ within the passband frequency (0.8 GHz–1.1 GHz) using equations (A.4) to (A.7). The calculated results of average Q-factors are Q_{ua} = 5.26, Q_e = 7.25 and Q_l = 3.04. This is shown a calculation example of the method and will be utilised in the work of this thesis. The method can be used to obtain the radiation quality factor (Q_r) for different antenna structure when the antenna is made from a perfect electric conductor (PEC) material which considers the total $Q_u = Q_r$. This has been described in Chapter 5.

References

[1] Lancaster M. J. Passive Microwave Device Applications of High-Temperature Superconductors. Cambridge, UK: Cambridge University Press; 1997.

APPENDIX B

Publications

Nugoolcharoenlap E., Shang X., Lancaster M. and Huang F., "Design of Waveguide Aperture Antenna-Filters using Coupling Matrix Theory" Submitted to Transaction on Microwave Theory and Techniques on 5th Dec. 2014.

Submitted to MTT

Design of Waveguide Aperture Antenna-Filters using Coupling Matrix Theory

Ekasit Nugoolcharoenlap, Xiaobang Shang, *Member, IEEE*, Michael J. Lancaster, *Senior Member, IEEE*, and Frederick Huang

***Abstract*—This paper presents a novel design approach for antennas which include filtering functionality (antenna-filter). The approach follows the well established coupled-resonator filter design theory, for which each resonator can not only be used as a filter element but also as a radiator. Three antennas are demonstrated which have additional functions as a bandpass filter, a filtering power divider and a diplexer. These antennas are designed at X-band using waveguide technology, fabricated from Aluminum alloy and measured. The measured results have an excellent agreement with the simulations.**

***Index Terms*—Waveguide aperture antenna, Antenna-filter, Antenna power divider, Antenna-diplexer.**

I. Introduction

Antennas and filters are essential components of RF receivers/transmitters. In the pursuit of miniaturization and improved performance, there is a growing interest in combining the antenna and filter into a single component. We will call this component an *antenna-filter*. This is achievable with resonant antenna elements where the antenna can serve as one of the resonators of the filter, in addition to the original role as a radiation element [1]. This allows the design of the antenna (with integrated filters) by following the conventional coupled-resonator filter theory [2]. In principle all resonators of the filter can be used as radiating elements, but here just the last resonator of the filter is replaced with an antenna. The filtering function is retained as long as the antenna has a resonant frequency the same as the filter and a radiation quality factor that equals to external quality factor of the filter.

A diagram of an antenna filter is depicted in Fig. 1(a). This approach has been investigated extensively, such as the work demonstrated using strip-line filter [3] and waveguide filter [4], [5]. In addition, the filter designs have been implemented on the various printed antennas for size reduction like the inverted-L antenna [6], the Γ-shaped antenna [7], [8] and the patch antenna [9]–[13]. An approach of a single slot-antenna integrated with filters was presented in [14] and implemented on the X-band waveguide with good filter response. Another

Manuscript received …….. This work was supported by the U.K. Engineering and Physical Science Research Council (EPSRC) under contract EP/H029656/1.

Ekasit Nugoolcharoenlap, Xiaobang Shang, Michael J. Lancaster and Frederick Huang are with School of Electronics, Electrical and Systems Engineering, the University of Birmingham, B15 2TT, U.K. (e-mail: ekasit.n@gmail.com).

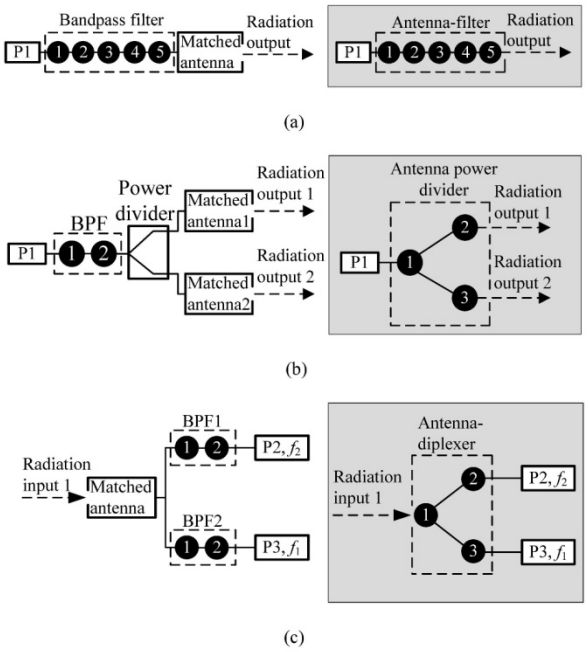

Fig. 1. Block diagrams comparing the new approach (diagrams on the right) to conventional antenna design (on the left): (a) antenna-filter (b) antenna power divider (c) antenna-diplexer.

approach of the slot antenna-filter was implemented on the substrate integrated wave guide (SIW) structure and presented in [15]. This approach is based on synthesis of equivalent circuit, which is able to provide accurate bandwidth with well-shaped passband response. The radiation pattern of this slot-antenna with integrated filter exhibited a large beamwidth and a low back lobe level. Although these antennas have been designed using basic filter design principles, none use the coupling matrix approach which has significant advantages as will be seen below.

A waveguide aperture antenna can be designed with narrow beamwidth and low side lobe level. Such an antenna was used in the design of antenna-filter implemented in an evanescent waveguide [16]–[18] with a large bandwidth. The substrate integrated waveguide (SIW) structure can also be used in an aperture antenna with integrated cavity filter as presented in [19]. To improve antenna gain and beamwidth simultaneously with the size reduction, an antenna array design [20] is

interesting. The antenna array can be incorporated in the antenna-filter. Examples are four-slot antenna arrays integrated with cavity filters [21], four-patch antenna arrays integrated with power dividers and filters [22] and Yagi antenna combined with a high Q-resonator [23]. The approach presented in this paper using the coupling matrix allows the integration of a power divider and two aperture antennas. This integrated design of antenna arrays using a power divider with the filtering function is named here as an *antenna power divider*.

In addition, it is possible to design an antenna with multi-band responses, the coupling matrix approach presented here can also be utilized for this propose. This is named here as an *antenna-diplexer*. A diagram of an antenna-diplexer is depicted in Fig. 1(c). Previously a dual-band antenna has been designed with an integrated diplexer and presented in [24]. The approach exhibited a new combined component for a transceiver of a wireless LAN system with compact size and good filter performance. In [25], a microstrip patch antenna was designed and combined with two bandpass filters as a single module.

This paper presents three new designs of X-band waveguide aperture antennas as the single modules using the coupling matrix. They are a 5-resonator antenna-filter, a 3-resonator antenna power divider and a 3-resonator antenna diplexer. All these antennas are designed using the coupling matrix which allows a comprehensive design and a good understanding of the principles of antenna-filters.

This paper is organized as follows. The waveguide aperture antenna design is discussed in Section II and includes the coupling matrix synthesis utilized for obtaining the initial values of the design. The results are compared with theory and simulation and discussed in Section III. The fabrication and measurements of the three proposed design are discussed in Section IV, and a conclusion is given in Section V.

II. WAVEGUIDE APERTURE ANTENNA DESIGN

In this section, a design of waveguide aperture antenna which the utilises inductive irises [26] to control the external (Q_e) and radiation (Q_r) quality factors is discussed. Here Q_e and Q_r are the quality factors associated with the external coupling at the input port and the radiation resistance. The structure of the single resonator waveguide aperture antenna-filter can be represented as depicted in the inset of Fig. 2.

In Fig. 2 the value of Q_r is obtained from the simulated S_{11} using a Q-calculation for a one-port component using the technique in [27]. The antenna structure shown in the inset of Fig. 2 can be designed to increase the value of Q_r by reducing d_r. Here l_1 has been adjusted to keep the center frequency at 10 GHz. The value of Q_r is obtained from CST simulation [28] when there is a weak coupling structure at the input i.e. when d_1 is small. The Q_r values versus d_r is plotted in Fig. 2. This Q_r will be employed in the design of the antenna-filters in Section III for defining the physical aperture dimensions to match Q_e of the filter with the radiation Q of the design.

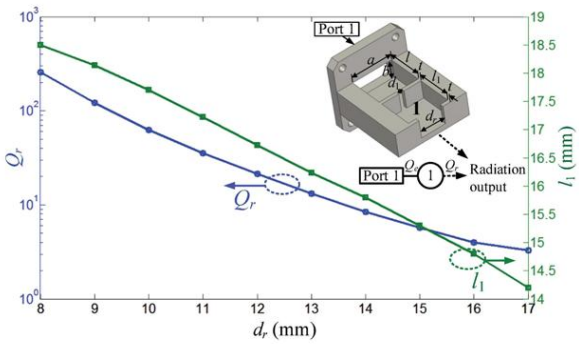

Fig. 2. Q_r and l_1 values of a waveguide aperture antenna obtained from the simulated S_{11} response with a resonant frequency of 10 GHz for different values of d_r. a = 22.86, b = 10.16, d_1 = 3, l = 20 and t = 2. Unit: mm.

III. COUPLING MATRIX AND STRUCTURE DESIGN

In this work, the coupling matrix of the antenna-filter circuit is chosen for the design. It is used in a similar way to the coupled-resonator filter circuits [2] but here we consider the radiation inputs/outputs as the input/output ports of the equivalent filter. A matrix $[A]$ can be expressed as [2]

$$[A] = [q] + p[U] - j[m] \tag{1}$$

where $[U]$ is the $n \times n$ unit matrix, p is the complex frequency variable i.e. $p = (j/FBW)(f/f_0 - f_0/f)$, f_0 is the center frequency and FBW is the fractional bandwidth, $[q]$ is an $n \times n$ matrix with all entries zero, except for $q_{ii} = 1/(FBW \cdot Q_{ei})$ for the input/output ports and $q_{ii} = 1/(FBW \cdot Q_{ri})$ for the radiation inputs/outputs, i stands for the index of the resonator connected to input/output ports and radiation inputs/outputs, Q_{ei} is the external quality factor of the resonators at the input/output waveguide ports, Q_{ri} is the radiation quality factor of the antennas at the radiation inputs/outputs. Note here we have unusually defined the coupling matrix for multiple ports rather than for a conventional two port filter [2]. Also, $[m]$ is the normalized coupling matrix whose elements are the normalized coupling coefficient between resonator i and j. Here we can also define for later $m_{ij} = M_{ij}/FBW$ and the self-couplings $m_{ii} = M_{ii}/FBW$, M_{ij} is the coupling coefficient between resonator i and j, M_{ii} is the self-coupling coefficient of resonator i.

The S-parameters, assuming now a 3-port circuit, for the coupling topology shown in Fig. 1(b) and 1(c), can be derived from the matrix $[A]$ in (1) as,

$$S_{ii} = \pm\left(1 - \frac{2}{q_{ei}}[A]_{ii}^{-1}\right) \tag{2}$$

$$S_{23} = \frac{2}{\sqrt{q_{e2} \cdot q_{e3}}}[A]_{23}^{-1} \tag{3}$$

where S_{ii} is the reflection coefficient at the input/output waveguide port i, S_{23} is the isolation of the proposed antenna-diplexer between waveguide port 2 and port 3, q_{e2} is the scaled external quality factor of resonator 2 and q_{e3} is the scaled

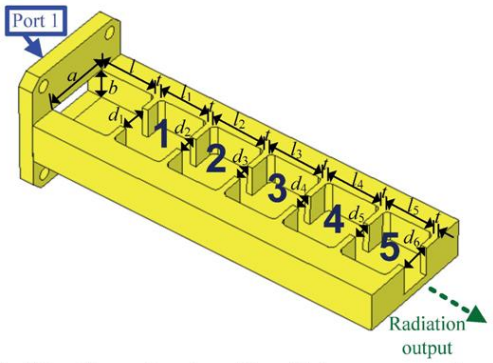

Fig. 3. X-band 5-resonator antenna-filter with top cover removed. a = 22.86, b = 10.16, d_1 = 10.38, d_2= 6.42, d_3 = 5.84, d_4 = 5.84, d_5 = 6.52, d_6 = 10.49, l = 20, l_1 = 17.13, l_2 = 18.7, l_3 = 18.84, l_4 = 18.7, l_5 = 16.87, t = 2. Unit: mm. All the inside vertical edges have the same radius of 1.6 mm.

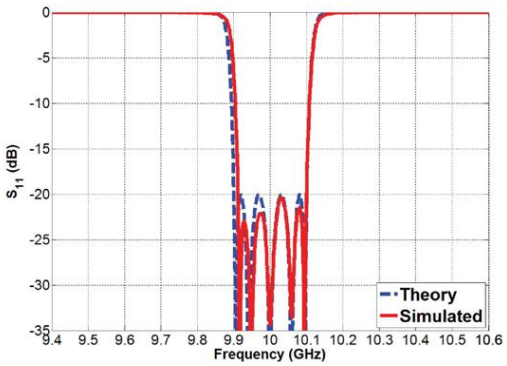

Fig. 4. S_{11} response of an X-band 5-resonator antenna-filter from coupling matrix (dashed lines) and simulation (solid lines).

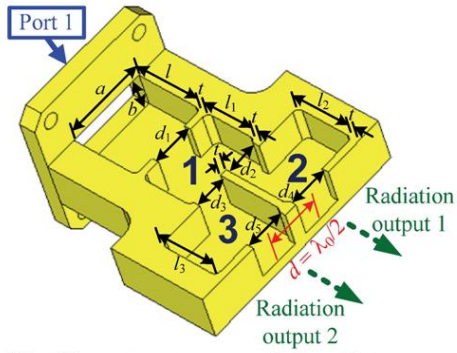

Fig. 5. X-band 3-resonator antenna power divider with top cover removed. a = 22.86, b = 10.16, d_1 = 11.32, d_2 = d_3 = 9.4, d_4 = d_5 = 11.32, l = 20, l_1 = 15.6, l_2 = l_3 = 17.5, t = 2. Unit: mm. All the inside vertical edges have the same radius of 1.6 mm.

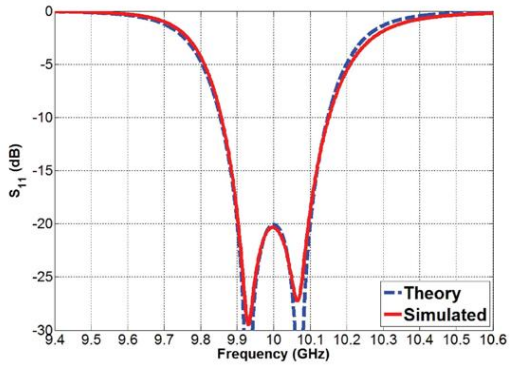

Fig. 6. S_{11} of the X-band 3-resonator antenna power divider derived from the coupling matrix (dashed lines) and electromagnetic simulation (solid lines).

external quality factor of resonator 3. In the case where one port is a radiation port, the S_{21} and S_{31} are related to the frequency response of the gain but not considered here. A more generalized equation for three-port network based on more than 3 resonators is given in [29].

A. X-band 5-resonator antenna-filter

This section presents the design of a 5-resonator aperture antenna-filter. It has an in-line topology, as illustrated in Fig. 3. The antenna-filter is designed to have a 2% fractional bandwidth (FBW = 0.02) at the center frequency f_0 of 10 GHz. A fifth-order Chebyshev lowpass prototype with a return loss of 20 dB is chosen. The coupling coefficients, external and radiation quality factors of the proposed design are calculated from the normalized conventional design equations in [2], as $m_{1,2} = m_{4,5} = 0.866$, $m_{2,3} = m_{3,4} = 0.636$, $q_{e1} = q_{r5} = 0.9714$.

The proposed waveguide antenna-filter has been designed based on the X-band waveguide with the inductive iris. The design of the iris sizes are done by using standard techniques [2]. The simulated return loss of the antenna-filter compared with the theoretical response calculated from the coupling matrix is shown in Fig. 4. They are in good agreement.

B. X-band 3-resonator antenna power divider

This section presents the design of a 3rd order antenna power divider. Such a circuit includes power division as well as basic filtering functionally whilst using two of the three resonators as radiators. This allows beam forming with integrated filtering.

The structure of the X-band 3-resonator antenna power divider is illustrated in Fig. 5, it has one electrical port and two-apertures separated by $\lambda_0/2$ (15 mm) forming a simple array. The waveguide structure shown in Fig. 5 is equivalent to a coupling topology of the three-resonator power divider, as discussed in [29]. The design of antenna power divider is to have 2% fractional bandwidth (FBW = 0.02) at the center frequency f_0 of 10 GHz and a passband return loss of 20 dB. A gradient-based local optimization algorithm [29] has been utilized here to get the coupling matrix. The optimized normalized coupling coefficients, external and radiation quality factors are: $m_{1,2} = m_{1,3} = 1.175$, $q_{e1} = q_{r2} = q_{r3} = 0.6648$.

The implementation of the antenna power divider has again been designed based on X-band waveguide with an inductive iris. The simulated return loss S_{11} for the proposed antenna power divider has a good agreement with that of the theory, as shown in Fig. 6. Radiation patterns will be discussed in section IV.

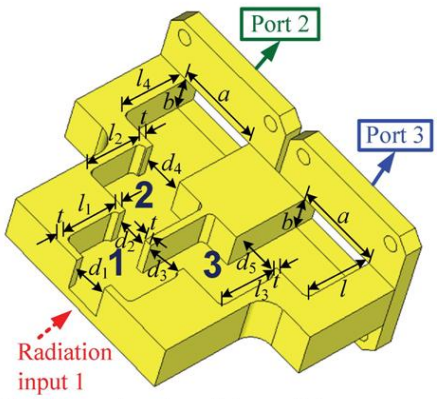

Fig. 7. X-band 3-resonator antenna-diplexer with top cover removed. a = 22.86, b = 10.16, d_1 = 9.9, d_2 = 9.35, d_3 = 9.39, d_4 = 11.84, d_5 = 12.08, l = 20, l_1 = 16.14, l_2 = 16.84, l_3 = 17.16, l_4 = 20.32, t = 2. Unit: mm. All the inside vertical edges have the same radius of 1.6 mm.

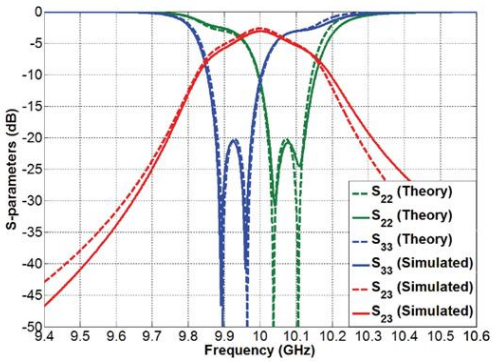

Fig. 8. S-parameter responses of the X-band 3-resonator antenna-diplexer from coupling matrix (dashed lines) and simulation (solid lines).

C. X-band 3-resonator antenna-diplexer

Both the previous designs operated in a single frequency band. This work presents an additional new component where the waveguide aperture antenna is designed to work at two bands in a similar fashion to a diplexer; we call this an *antenna-diplexer*. The proposed design can be employed as a receiving component for separating two-frequency channels as would a conventional diplexer circuit placed after the receiving antenna. The three dimensional structure of the X-band 3-resonator antenna-diplexer is illustrated in Fig. 7, it is a three-port component including one antenna port. The waveguide structure shown in Fig. 7 can be represented with a coupling matrix with three-resonators and three ports. This example is designed to be centered at 10 GHz, and the passband center frequency is 9.93 GHz for channel 1 and 10.07 GHz for channel 2; the bandwidth of each channel is 0.1 GHz. The overall fractional bandwidth (two passbands and an intervening stop band) is 2.4% (FBW = 0.024). This design has a return loss of 20 dB with 2 poles for each channel. The coupling matrix of this antenna-diplexer has been optimized using the gradient-based local optimization algorithm [29].

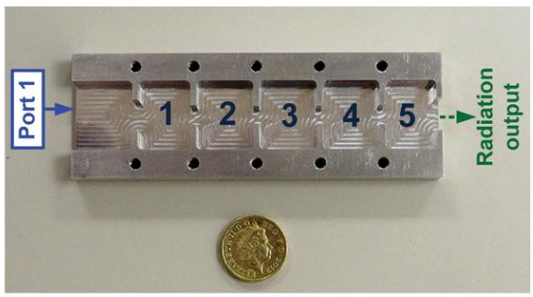

Fig. 9. Photograph of the fabricated antenna-filter with top cover removed.

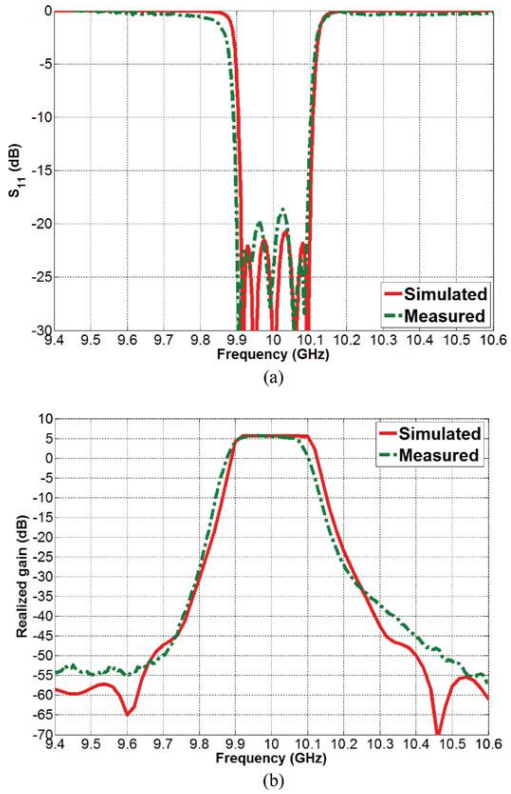

Fig. 10. Simulated and measured results of the X-band 5-resonator antenna-filter. (a) Return loss S_{11} (b) Realized gain.

The optimized results give the normalized coupling coefficients, external and radiation quality factors of $m_{2,2}$ = 0.446, $m_{3,3}$ = -0.446, $m_{1,2} = m_{1,3}$ = 0.835, q_{r1} = 1.944, $q_{e2} = q_{e3}$ = 1.468.

The proposed antenna-diplexer has been designed using inductively coupled waveguide cavity resonators. The simulated S-parameters for the proposed antenna-diplexer are compared with the calculated response obtained from the coupling matrix and have good agreement, as shown in Fig. 8. It should be noted that the above antenna-diplexer shows poor isolation performance between two output ports. In this paper we are aiming to show the principles of the methods and this isolation can be improved by utilizing more resonators.

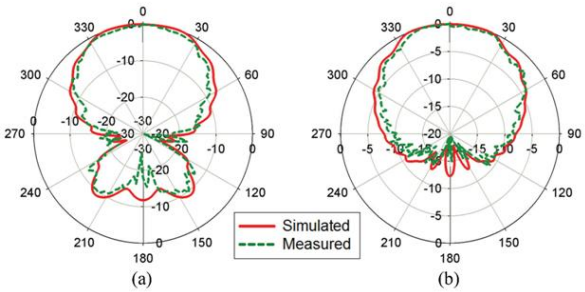

Fig. 11. Normalized simulated and measured radiation patterns of the antenna-filter: (a) *H*-plane co-polarization at 10 GHz (b) *E*-plane co-polarization at 10 GHz.

TABLE I.
Summary of the Antenna-Filter Performance

Parameters	Frequency (GHz)	3 dB Beamwidth (deg.)		Side lobe level (dB)		Cross-polarization level (dB)	
		Sim.	Mea.	Sim.	Mea.	Sim.	Mea.
H-plane	10	85	72	-8.7	-9.59	-80	-50
E-plane	10	99	96	-9.5	-9.95	-81	-49.8

IV. Fabrication and Measurements

A. X-band 5-resonator antenna-filter

The X-band 5-resonator antenna-filter has been fabricated from aluminum alloy 5083 (RS components) using a CNC milling machine. Fig. 9 shows a photograph of the filter. The simulated and measured return loss of antenna-filter depicted in Fig. 10(a) shows good agreement. The measurement shows that the passband has a maximum return loss of 18.6 dB.

The antenna-filter has been measured inside an anechoic chamber to obtain the realized gain and is plotted and compared with the simulation results as shown in Fig. 10(b). It can be seen that the antenna-filter is found to have a passband gain of about 5.7 dB, and measured stopband rejection is about 55.7 dB. The simulated and measured radiation patterns of the antenna-filter are shown in Fig. 11.

It can be seen that the antenna-filter exhibits good agreement in terms of radiation pattern in H and E plane orientation. The cross polarization levels in H-plane are below -50 dB in the measurements and below -80 dB in the simulations as shown in Table I. The performance of the antenna-filter is summarized and presented in Table I.

The results show flat response in the passband gain, good out-of-band rejection and low levels of cross-polarization.

B. X-band 3-resonator antenna power divider

The X-band 3-resonator antenna power divider is also made from aluminum alloy and a photograph of it is shown in Fig. 12. The simulated and measured return loss is depicted in Fig. 13(a). The measured response is in good agreement with the simulated response. The measurement shows a maximum return loss of 21.5 dB with the passband bandwidth of 202 MHz, whereas the expected maximum return loss obtained

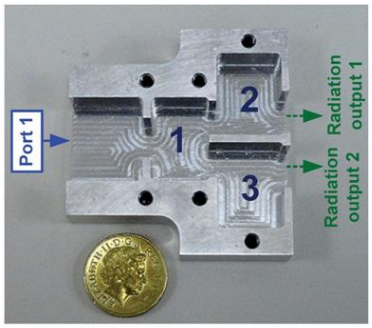

Fig. 12. Photograph of the fabricated antenna power divider with top cover removed.

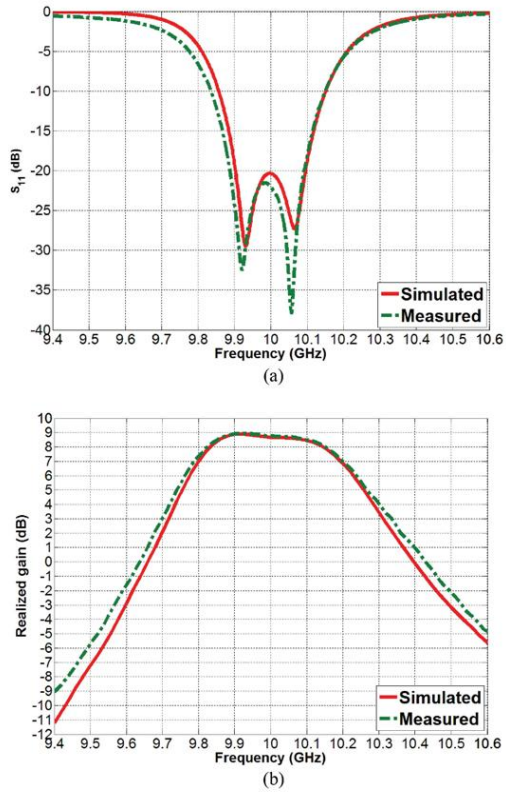

Fig. 13. Simulated and measured results of the X-band 3-resonator antenna power divider. (a) Return loss S_{11} (b) Realized gain.

from CST simulations is -20 dB with the passband bandwidth of 200 MHz.

Fig. 13(b) shows the measured realized gain, which exhibits excellent agreement with the simulation. It can be seen that a measured passband gain is about 8.9 dB, which is 3.2dB more than the single aperture antenna-filter device. The measured stopband rejection is about 14 dB.

The simulated and measured radiation patterns of the antenna power divider are shown in Fig. 14. It can be seen that the antenna power divider exhibits good-shaped radiation pattern in H and E plane orientation. The cross polarization

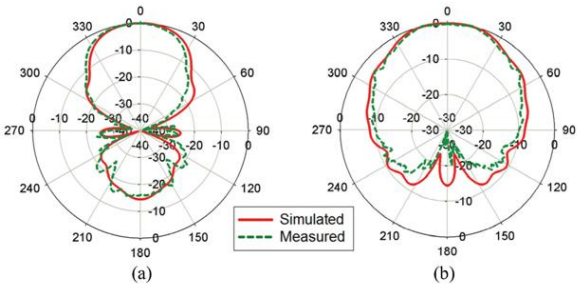

Fig. 14. Normalized simulated and measured radiation patterns of the antenna power divider: (a) *H*-plane co-polarization at 10 GHz (b) *E*-plane co-polarization at 10 GHz.

TABLE II.
Summary of the Antenna power divider Performance

Parameters	Frequency (GHz)	3 dB Beamwidth (deg.)		Side lobe level (dB)		Cross-polarization level (dB)	
		Sim.	Mea.	Sim.	Mea.	Sim.	Mea.
H-plane	10	52	51	-14.4	-15.14	-59.7	-49.2
E-plane	10	74.4	68	-10.5	-10.88	-67.9	-48.9

levels are measured in H-plane as -49.2 dB and E-plane is -48.9 dB, whereas the simulated in H-plane is -59.7 dB and E-plane is -67.9 dB. The performance of the antenna power divider is summarized in Table II.

As expected, the antenna power divider has better performance compared to the 5-resonator aperture antenna-filter in terms of higher passband gain, and narrower 3dB beamwidth.

C. X-band 3-resonator antenna-diplexer

The X-band 3-resonator antenna-diplexer is made from aluminum alloy and is shown in Fig. 15. The simulated and measured *S*-parameters of antenna-diplexer are depicted in Fig. 16(a). The measured response is in excellent agreement with the simulated response. The measurement shows that the passband of channel 1 has maximum return loss of 20.1 dB, whereas for channel 2 it is 21.0 dB. The isolation between the center frequencies of two bands is measured to be 5.2 dB.

The antenna-diplexer realized gain of each channel is plotted with the simulation results in Fig. 16(b). The passband of channel 1 has a measured maximum gain of 6.25 dB at 9.88 GHz, whereas the passband of channel 2 has a measured maximum gain of 6.1 dB at 10.12 GHz. The stopband rejection of each channel is measured and is about 21 dB.

It should be noted that the results of Fig. 16 show the 20% of received energy at the center frequency of the port 2 goes to the port 3 and vice versa. This paper aims to show the principle of the method and this leaking received energy between two output ports can be improved by utilizing more resonators.

The simulated and measured radiation patterns of the antenna-diplexer are compared at the center frequencies of each channel and are shown in Fig. 17. It can be seen that the antenna-diplexer exhibits good-shaped radiation pattern in H and E plane orientation.

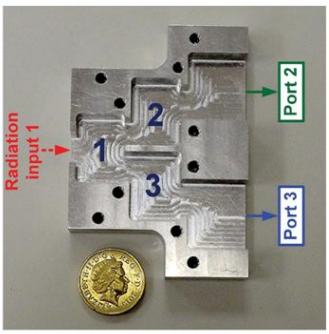

Fig. 15. Photograph of the fabricated antenna-diplexer with top cover removed.

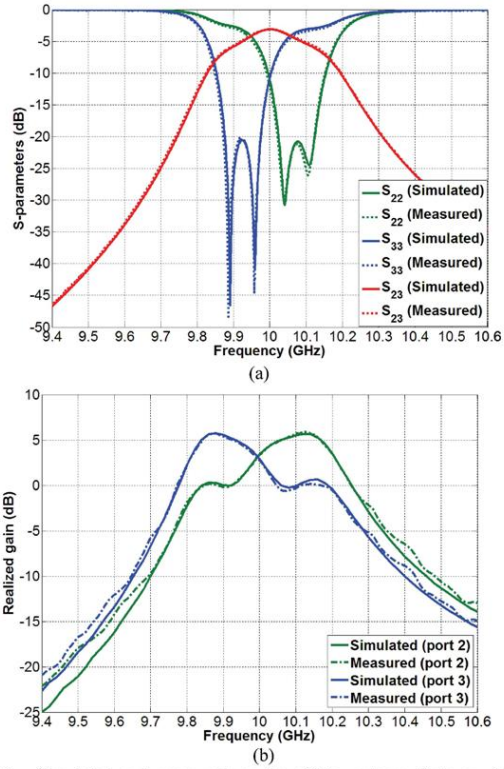

Fig. 16. Simulated and measured results of the antenna-diplexer. (a) *S*-parameters. (b) Realized gain.

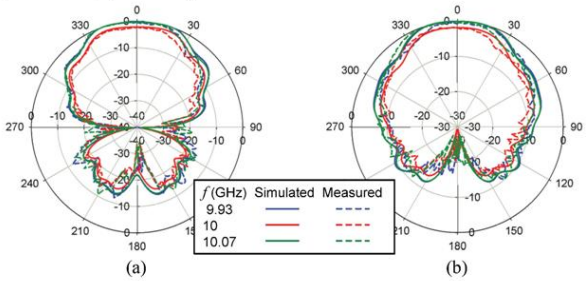

Fig. 17. Normalized simulated and measured radiation patterns of the antenna-diplexer: (a) *H*-plane co-polarization at the middle frequency and two frequencies at the peak gain (b) *E*-plane co-polarization at the middle frequency and two frequencies at the peak gain.

TABLE III.
Summary of the Antenna-Diplexer Performance

Parameters	Frequency (GHz)	3 dB Beamwidth (deg.)		Side lobe level (dB)		Cross-polarization level (dB)	
		Sim.	Mea.	Sim.	Mea.	Sim.	Mea.
H-plane	9.93	62.7	58	-4.8	-4.64	-72.2	-46.1
	10	63.7	60	-4.9	-4.9	-72.9	-49.6
	10.07	64.9	57	-5.1	-4.46	-74.9	-45.5
E-plane	9.93	66.3	73	-4.1	-4.4	-72.2	-48.8
	10	68.5	64	-4.2	-5.24	-73	-51.1
	10.07	70.7	70	-4.3	-4.67	-74.8	-48.8

The radiation pattern level measured at 10 GHz has lower than the measured maximum level by about 3 dB, as shown in the gain results depicted in Fig. 16(b). The measured cross polarization levels are below 49 dB, whereas the simulated cross polarization levels are below 72 dB. The performance of the antenna diplexer is summarized and presented in Table III.

V. Conclusion

The multiport coupling matrix has been used to demonstrate three components which utilize the resonant properties of antennas for filtering. The coupling matrix approach is general and can be used for any resonant antenna structure; it is not limited to waveguide aperture antennas. The approach can in principle encompass a larger number of radiation and/or filtering elements to configure complex functionality whilst minimizing the weight and volume of the components. Although not done here the coupling matrix can also take into account cross coupling between antenna elements in an array. The bandwidth of the antenna-filters has a limitation based on the radiation Q of the radiating resonator(s), however this can be adjusted by altering the aperture size in the examples. A challenge is to have more of the resonator elements in an antenna-filter as radiators to control the radiation pattern whilst still maintaining the required filtering.

The example of the X-band 5 resonator antenna-filter exhibited the good agreement with the measurement for the return loss and radiation pattern shapes as expected. The X-band 3 resonator power-divider is designed for a receiver and utilized as the frequency splitter with compact size. The measurement results for this and the antenna-diplexer agree very well with simulations. The proposed approach can then be of interest in the use of modern communication systems due to the reduction of the number of microwave front-end components.

Acknowledgment

The authors would like to thank Mr. W. Hay, University of Birmingham, Edgbaston, Birmingham, U.K., who fabricated the X-band waveguide components.

References

[1] K. Chang, R. A. York, P. S. Hall, T. Itoh, "Active integrated antennas," *IEEE Trans. Microw. Theory Techn.*, vol.50, no. 3, pp. 937–943, Mar. 2002.

[2] J. S. Hong and M. J. Lancaster, *Microstrip Filters for RF/Microwave Applications*. New York, NY, USA: Wiley, 2001.

[3] F. Queudet, I. Pele, B. Froppier, Y. Mahe, and S. Toutain, "Integration of pass-band filters in patch antennas," in *Proc. 32nd Eur. Microw. Conf.*, Sep. 23–26, 2002, pp. 685–688.

[4] G. Goussetis and D. Budimir, "Antenna filter for modern wireless systems," in *Proc. 32nd Eur. Microw. Conf.*, Sep. 23–26, 2002, pp. 1–3.

[5] M. Troubat, S. Bila, M. Thévenot, D. Baillargeat, T. Monédière, S. Verdeyme, and B. Jecko, "Mutual synthesis of combined microwave circuits applied to the design of a filter-antenna subsystem," *IEEE Trans. Microw. Theory Tech.*, vol. 55, no. 6, pp. 1182–1189, Jun. 2007.

[6] C.-T. Chuang and S.-J. Chung, "Synthesis and Design of a New Printed Filtering Antenna," *IEEE Trans. Antennas Propag.*, vol. 59, no. 3, pp. 1036-1042, Mar. 2011.

[7] W.-J. Wu, Y.-Z. Yin, S.-L. Zuo, Z.-Y. Zhang, J.-J. Xie, "A new compact filter-antenna for morden wireless communication systems," *IEEE Antennas Wireless Propag. Lett.*, vol. 10, pp. 1131–1134, Oct. 2011.

[8] C.-T. Chuang and S.-J. Chung, "A Compact Printed Filtering Antenna Using a Ground-Intruded Coupled Line Resonator," *IEEE Trans. on Antennas and Propag.*, vol.59, no.10, pp. 3630–3637, Oct. 2011.

[9] J. H. Zuo, X. W. Chen, G. R. Han, L. Li, and W.M. Zhang, "An integrated approach to RF antenna-filter co-design," *IEEE Antennas Wireless Propag. Lett.*, vol. 8, pp. 141–144, 2009.

[10] O.A. Nova, J.C. Bohorquez, N.M. Pena, G.E. Bridges, L. Shafai and C. Shafai, "Filter-Antenna Module Using Substrate Integrated Waveguide Cavities," *IEEE Antennas and Wireless Propag. Lett.*, vol. 10, pp. 59–62, 2011.

[11] C.-K. Lin and S.-J. Chung, "A Compact Filtering Microstrip Antenna with Quasi-Elliptic Broadside Antenna Gain Response," *IEEE Antennas and Wireless Propag. Lett.*, vol. 10, no., pp. 381–384, 2011.

[12] Y. Yusuf, H. Cheng, X. Gong, "Co-Designed substrate-Integrated Waveguide Filters with Patch Antennas," *IET J. Microw., Antennas, Propag.*, vol. 7, no. 7, pp. 493–501, May 2013.

[13] Y. Yusuf and X. Gong, "A vertical integration of high-Q filters with patch antennas with enhanced bandwidth and high efficiency," in *IEEE Int. Microwave Symp. Dig.*, Jun. 5–10, 2011, pp. 1–4.

[14] Y. Yang and M. Lancaster, "Waveguide slot antenna with integrated filters," presented at the ESA Workshop on Antennas for Space Applications, Noordwijk, Netherlands, Oct. 2010, pp. 48–54.

[15] Y. Yusuf and X. Gong, "Compact low-loss integration of high-Q 3-D filters and highly efficient slot antennas," *IEEE Trans. Microw. Theory Tech.*, vol. 59, no. 4, pp. 857–865, Apr. 2011.

[16] P. Ludlow and V. Fusco, "Reconfigurable small-aperture evanescent waveguide antenna," *IEEE Trans. Antennas Propag.*, vol. 59, no. 12, pp. 4815–4819, Dec. 2011.

[17] P. Ludlow, V. Fusco, G. Goussetis and D.E. Zelenchuk, "Applying Band-Pass Filter Techniques to the Design of Small-Aperture Evanescent-Mode Waveguide Antennas," *IEEE Trans. Antennas Propag.*, vol. 61, no. 1, pp. 134–142, Jan. 2013.

[18] P. Ludlow, V. Fusco, G. Goussetis and D. E. Zelenchuk, "Small Aperture Evanescent-mode waveguide antenna matched using distributed coupled resonators," *Electron. Lett.*, vol. 49, no. 9, pp. 580–581, Apr. 2013.

[19] Y. Yusuf, X. Gong, "Integration of three-dimensional high-Q filters with aperture antennas and bandwidth enhancement utilising surface waves," *IET J. Microw., Antennas, Propag.*, vol. 7, no. 7, pp. 468–475, May 2013.

[20] C. A. Balanis, *Antenna Theory Analysis and Design 3rd Ed.* New Jersey, NJ, USA: Wiley, 2005.

[21] H. T. Cheng, Y. Yusuf, and X. Gong, "Vertically integrated three-pole filter/antennas for array applications," *IEEE Antennas Wireless Propag. Lett.*, vol. 10, pp. 278–281, 2011.

[2] C.-K. Lin and S.-J. Chung, "A filtering microstrip antenna array," *IEEE Trans. Microw. Theory Tech.*, vol. 59, no. 11, pp. 2856–2863, Nov. 2011.

[3] Z. Wang, P. S. Hall, P. Gardner, "Yagi antenna with frequency domain filtering performance," in *IEEE Antennas & Propag. Soc. Int. Symp.*, Jul. 2012., pp. 1–2.

[4] V. Demir, C. P. Huang, A. Elsherbeni, "Novel Dual-Band WLAN Antennas with Integrated Band-Select Filter For 802.11 a/b/g WLAN Radios In Portable Devices," *Microw. & Opt. Technol. Lett.*, vol. 49, no. 8, pp. 1868–1872, Aug. 2007.

[5] D. Zayniyev, H. F. AbuTarboush, D. Budimir, "Microstrip Antenna Diplexers for Wireless Communications," in *Proc. 39th Eur. Microw. Conf.*, Sep. 29–Oct. 1, 2009, pp. 1508–1510.

[6] G. L. Matthaei, L. Young, E.M.T. Jones, *Microwave Filters, Impedance-matching Networks and Coupling Structures*. North Bergen, NJ, USA: Artech House, 1980.

[7] M. J. Lancaster, *Passive Microwave Device Applications of High-Temperature Superconductors*. Cambridge, UK: Cambridge Univ. Press, 1997.

[8] Computer Simulation Technology (CST), Microwave Studio, 2014 [Online]. Available: www.cst.com.

[9] T. Skaik, M. J. Lancaster, and F. Huang, "Synthesis of multiple output coupled resonator microwave circuits using coupling matrix optimization," *IET J. Microw., Antennas, Propag.*, vol. 5, no. 9, pp. 1081–1088, Jun. 2011.